2003

平成15年度

金沢医科大学

共同研究成果報告書

平成17年12月

金沢医科大学

はじめに

平成16年度は国立大学の法人化にみられる大学改革が急速に進み、成果主義、評価主義の厳しい時代が幕を開けました。金沢医科大学も平成16年度から大学院が改組され、医学部と総合医学研究所を含む全学的な教育・研究体制が構築されました。私たちの大学は、高度な学術研究を推進し、創造性豊かな優れた人材を育成する医育機関として一般社会から立派な評価を受け、その存在感を主張していますが、研究実績の評価と研究の活性化は本学存立の最優先課題であります。本研究助成事業は医学部と総合医学研究所あるいは学外の著名な研究者との共同研究を推進し、特徴ある独創的な研究を助成するために、大学院改組の前年である平成15年から新たに始まりました。研究期間を複数年として長期の展望を持たせ、大学院改組を見据えた医学研究の充実を目指します。

今回、学内公募で申請があった20件のうち3件が採択され、本報告書は平成15年度の研究成果をまとめたものであります。今後、ますます医学部と総合医学研究所あるいは学外の研究機関との共同研究が広がり、本研究助成事業が新しい研究の価値創造の源となることを願っております。

最後に、本報告書の取りまとめの労をとられた研究推進評価特別委員会および研究助成センター事務課の各位に感謝申し上げます。

平成17年12月

金沢医科大学
学長　山本　達

目　　次

１．研究課題名：循環ショックの病態生理の解明と治療法の共同開発（研究番号C2003-1）

２．キーワード：１）循環ショック（circulatory shock）
２）虚血再灌流（ischemia reperfusion）
３）肺水腫（pulmonary edema）
４）肝循環（hepatic circulation）
５）冠循環（coronary circulation）

３．研究代表者：芝本利重・医学部・教　授・生理機能制御学(生理学)
研究分担者：土田英昭・医学部・教　授・侵襲制御学(麻酔学)
佐久間　勉・医学部・教　授・呼吸機能治療学(呼吸器外科)
久保恵嗣・信州大学・医学部・教　授・第一内科学
大久保信司・医学部・助教授・循環制御学(循環器内科学)(現東京医科大学霞ヶ浦病院)
倉田康孝・医学部・助教授・生理機能制御学(生理学)

４．研究目的

循環ショックの病態は単に血圧低下にとどまらず、組織の微小循環障害から機能障害に発展する複雑な全身反応である。血行力学的に心原性ショックと非心原性ショックに大別され、前者は心臓ポンプ機能の失調による。一方、非心原性ショックの血圧低下とその臓器循環・機能障害の機序については十分には解明されてない。しかしながら、これらのショックに共通した病態として微小循環障害と虚血再灌流障害、それに基づく炎症反応としてのサイトカインをはじめとしたmediatorが病態形成に関わり多臓器不全を惹起し、肝臓では肝不全、肺では透過性亢進型肺水種であるARDS、心臓では冠不全、心不全にいたるものと考えられる。本研究の目的は心原性、出血性、アナフィラキシィー、敗血症による循環ショックの血圧低下機序とそれによる臓器循環障害の病態生理を肝循環、肺循環、冠循環に注目してwhole animal、臓器、細胞、遺伝子レベルからの多面的アプローチにより明らかにすることである。

５．研究計画

(課題 1) ラットとモルモットの肝アナフィラキシィーモデルを確立し、血管収縮部位同定と肝内血液動態を解明する。さらに、責任物質と責任細胞について、Kupffer cell と肥満細胞の関与を遺伝子改変ラットを用いて検討する。また、一酸化窒素と一酸化炭素の肝アナフィラキシィー反応に及ぼす影響を解明する（芝本・土田担当)。

(課題 2) ラットで脱血ショックモデル、誤嚥性肺傷害モデル、虚血再潅流傷害モデルを作成し、ショック時の肺胞上皮細胞の Na^+ channel、Cl^- channel、Na ポンプ、β受容体間のシグナル伝達に関し研究する（佐久間担当)。

(課題３）血小板活性化因子、アンギオテンシン、カテコールアミンのモルモット単離心室筋のイオンチャネル電流への作用をパッチクランプ法及びシミュレーション法で検討し、虚血・再灌流不整脈誘発性を実験的・理論的に検討する（倉田担当)。

(課題４）心筋を一定の条件で短時間の虚血に暴露すると、その心筋の虚血性細胞壊死が起こりにくくなる現象である虚血プレコンディショニング(ischemic preconditioning)の機序について心筋細胞膜のオピオイド受容体の心筋梗塞巣ならびにアポトーシスに対する関与を検討する。また、ラット冠動脈狭窄心不全モデルを用いて炎症サイトカイン（iNOS, eNOS, IL-1β, IL-5, IL-6, NFκB, γIFN, TNF）およびANP、ならびにBNP、VEGFの発現をRT-PCRにより検討する。(大久保担当)

６．研究成果

1) モルモット肝アナフィラキシィーは後類洞血管を有意に収縮させ、肝鬱血を来たす。一酸化窒素は肝血管収縮を緩和するが、一酸化炭素には修飾作用がないことを明らかにした。
2) ラットのアナフィラキシィーショックにおける肝血管収縮の役割を解明した。
3) 肝類洞抵抗測定法を摘出灌流肝臓で確立し、ショックの代償機構であるノルエピネフリンの肝血管収縮部位を解明した。
4) アナフィラキシー伝達物質のヒスタミン、血小板活性化因子、トロンボキサンのラットとモルモットの肝血管への作用を明らかにした。
5) モルモット肝アナフィラキシィー時の一酸化窒素の産生にはズリ応力依存性と非依存性の様式があり、作用する肝血管分節が異なることを明らかにした。
6) マウス肝血管アナフィラキシー解明の前段階として、その肝血管の特性とアナフィラキシーショックと心原性ショック時放出されるヒスタミンとノルエピネフリンの作用を明らかにした。
7) ラット肺を用いてUTPが肺胞水分クリアランスを亢進すること、β交感神経刺激薬の効果を促進すること、その作用はクロライドチャンネルを介することを明らかにした。
8) ラット肺を用いて選択的α_1−, β_1−, β_2−, β_3−交感神経刺激薬が肺胞水分クリアランスを亢進させることを報告した。ただし、α_1−, β_1−, β_2−交感神経刺激薬は選択的受容体を介するが、β_3−交感神経刺激薬はβ_2−受容体を介することが示唆される成績を得た。
9) ラット肺及びヒト切除肺の肺胞内カテコールアミンの吸収は、エピネフリンに比しノルエピネフリンの吸収速度がまさる。ノルエピネフリンの吸収にはβ受容体は関与しないが、Naチャネルが関与することを明らかにした。
10) 虚血再灌流後の致死的心筋障害やアポトーシス発現にデルタオピオイド受容体が重要な役割を演じており、虚血プレコンディショニングやモルヒネによるデルタオピオイド受容体活性化が、再灌流障害を減少させることを明らかにした。
11) 洞結節自動能とその異常（洞性不整脈）の発現が分岐現象の一種であり、主にL型Ca^{2+}チャネルと遅延整流K^+チャネル電流に起因することを理論的に推察した。
12) アンギオテンシンⅡがタイプ１受容体とPKC活性化を介してラット心室筋持続性外向きK^+電流を抑制することを解明した。

７．研究の考察・反省

各研究課題において当初の計画された一部は達成されたものと考える。研究課題が多すぎたために来年度へ持ち越したものもある。しかしながら、研究遂行中に新たに企画立案され急遽、遂行されたものもあるので全体としては活発な研究活動が行われたものと考える。引き続き、予定された研究計画を遂行する。

８．研究発表

Kurata Y, Hisatome I, Imanishi S, Shibamoto T. Roles of L-type Ca^{2+} and delayed-rectifier K^+ currents in sinoatrial node pacemaking: insights from stability and bifurcation analyses of a mathematical model. Am J Physiol Heart Circ Physiol 2003 ; 285: H2804-H2819. (MLDB)

Kamikado C, Shibamoto T, Hongo M, Koyama S. Effects of Hct and norepinephrine on segmental vascular resistance distribution in isolated perfused rat livers. Am J Physiol Heart Circ Physiol 2004; 286:H121-H130. (MLDB)

Ruan Z, Shibamoto T, Shimo T, Tsuchida H, Koizumi T, Nishio M. NO, but not CO, attenuates anaphylaxis-induced postsinusoidal contraction and congestion in guinea pig liver. Am J Physiol Regul Integr Comp Physiol 2004; 286:R94-R100. (MLDB)

Shibamoto T, Narushima M, Ling YQ, Shimo T, Tsuchida H, Kurata Y, Ogura T. Different hepatic vascular response to noradrenaline and histamine between guinea pig and rat. Acta Physiol Scand 2004; 180:255-263. (MLDB)

Okubo S, Tanabe Y, Takeda K, Kitayama M, Kanemitsu S, Kukreja RC, Takekoshi N. Ischemic preconditioning and morphine attenuate myocardial apoptosis and infarction after ischemia-reperfusion in rabbits: role of delta-opioid receptor. Am J Physiol Heart Circ Physiol 2004; 287:H1786-H1791. (MLDB)

Matsuda H, Kurata Y, Imanishi S, Sato R, Shibamoto T. Effects of Angiotensin II on sustained outward currents in rat ventricular myocytes. Pflugers Arch 2004; 448:54-62. (MLDB)

Ruan Z, Shibamoto T, Shimo T, Koizumi T, Tsuchida H, Kurata Y, Ogura T, Kubo K. Effects of platelet-activating factor and thromboxane A_2 on isolated perfused-guinea pig liver. Prostaglandins Other Lipid Mediators 2004; 73:73-85. (MLDB)

Sakuma T, Gu X, Sugita M, Sagawa M, Sakuda M, Toga H. Uridine 5'-triphosphate stimulates alveolar fluid clearance in the isolated rat lungs. J Pharmacol Sci 2004; 95: 420-425. (MLDB)

Gu X, Sugita M, Sagawa M, Sakuda M, Osanai K, Toga H, Sakuma T. Effects of α_1-, β_1-, β_2-, β_3-adrenergic agonists on alveolar fluid clearance in isolated rat lungs. J Kanazawa Med Univ 2004; 29: 91-96.

Shibamoto T, Ruan Z, Cui S, Kurata Y, Koizumi T, Kubo K. Anaphylactic hepatic venoconstriction is attenuated by nitric oxide released via shear stress-dependent and -independent mechanisms in Guinea pig. Clin Exp Pharmacol Physiol 2005; 32:288-293. (MLDB)

Sakuma T, Gu X, Sugita M, Sagawa M, Sakuda M, Toga H. Catecholamine clearance from alveolar spaces of rat and human lungs. Respiration 2005; 72: 189-196. (MLDB)

Shibamoto T, Cui S, Ruan Z, Kurata Y. Effects of norepinephrine and histamine on vascular resistance in isolated perfused mouse liver. Jpn J Physiol 2005; 55: 143-148. (MLDB)

Shibamoto T, Cui S, Ruan Z, Liu W, Takano H, Kurata Y. Hepatic venoconstriction is involved in anaphylactic hypotension in rats. Am J Physiol Heart Circ Physiol 2005; 289: H1436-1441. (MLDB)

芝本利重, 上門千哲, 倉田康孝. 血管閉塞法による肝微小血管圧の測定とその応用. 循環制御 2004; 25:146-157.

Am J Physiol Heart Circ Physiol 286: H121–H130, 2004.
First published August 28, 2003; 10.1152/ajpheart.01136.2002.

Effects of Hct and norepinephrine on segmental vascular resistance distribution in isolated perfused rat livers

Chiaki Kamikado,[1] Toshishige Shibamoto,[4] Minoru Hongo,[3] and Shozo Koyama[2]

[1]*First Department of Surgery, Kagoshima University School of Medicine, Kagoshima 890-8520;* [2]*Division 2, Department of Physiology, Shinshu University School of Medicine;* [3]*Department of Cardiovascular Medicine, Shinshu University School of Health Sciences, Matsumoto 390-8621; and* [4]*Division 2, Department of Physiology, Kanazawa Medical University, Uchinada 920-0293, Japan*

Submitted 26 December 2002; accepted in final form 21 August 2003

Kamikado, Chiaki, Toshishige Shibamoto, Minoru Hongo, and Shozo Koyama. Effects of Hct and norepinephrine on segmental vascular resistance distribution in isolated perfused rat livers. *Am J Physiol Heart Circ Physiol* 286: H121–H130, 2004. First published August 28, 2003; 10.1152/ajpheart.01136.2002.—We studied the effects of blood hematocrit (Hct), blood flow, or norepinephrine on segmental vascular resistances in isolated portally perfused rat livers. Total portal hepatic venous resistance (R_t) was assigned to the portal (R_{pv}), sinusoidal (R_{sinus}), and hepatic venous (R_{hv}) resistances using the portal occlusion (P_{po}) and the hepatic venous occlusion (P_{hvo}) pressures that were obtained during occlusion of the respective line. Four levels of Hct (30%, 20%, 10%, and 0%) were studied. R_{pv} comprises 44% of R_t, 37% of R_{sinus}, and 19% of R_{hv} in livers perfused at 30% Hct and portal venous pressure of 9.1 cmH_2O. As Hct increased at a given blood flow, all three segmental vascular resistances of R_{pv}, R_{sinus}, and R_{hv} increased at flow >15 ml/min. As blood flow increased at a given Hct, only R_{sinus} increased without changes in R_{pv} or R_{hv}. Norepinephrine increased predominantly R_{pv}, and, to a smaller extent, R_{sinus}, but it did not affect R_{hv}. Finally, we estimated P_{po} and P_{hvo} from the double occlusion maneuver, which occluded simultaneously both the portal and hepatic venous lines. The regression line analysis revealed that P_{po} and P_{hvo} were identical with those measured by double occlusion. In conclusion, changes in blood Hct affect all three segmental vascular resistances, whereas changes in blood flow affect R_{sinus}, but not R_{pv} or R_{hv}. Norepinephrine increases mainly presinusoidal resistance. P_{po} and P_{hvo} can be obtained by the double occlusion method in isolated perfused rat livers.

blood viscosity; hepatic circulation; hepatic vascular occlusion methods

LIVER AND LUNG circulation is analogous (19). Both the pulmonary artery and the portal vein are unique in their ability to carry large flows of venous blood under low hydrostatic pressures. The pulmonary arterioles and the portal venules have a similar anatomy (19). The vascular arrangement of the hepatic units is analogous to that of the lung in that both lobules have a central inflow (pulmonary artery and portal vein) and a peripheral outflow (pulmonary vein and hepatic vein) (18). In addition, embryologically, the tracheo-bronchial tree and the biliary ductal system originate from the gut.

The longitudinal distribution of pulmonary vascular resistance has been extensively studied using vascular occlusion techniques, and the pulmonary vasculature can be represented by a simple hydrodynamic model consisting of three segments in series, each with a characteristic resistance and compliance (10, 12). The middle segment, which contains the capillaries, has relatively low resistance and high compliance, and the other two segments have relatively low compliance and high resistance. The pulmonary arterial and venous occlusion technique (9–11) allows partitioning of the pulmonary vasculature into these three segments. Theoretically, if the flow is stopped across one segment, the pressure gradient across that segments becomes zero, and the total pressure gradient would decrease accordingly. In other words, the rapid changes in pulmonary arterial pressure and pulmonary venous pressure with inflow and outflow occlusion, respectively, represent the pressure drops across the arterial and venous relatively indistensible vessels (10). The total arteriovenous pressure difference minus the sum of these two pressure drops gives the pressure drop across the vessels in the middle that are much more distensible. Although hepatic circulation is analogous to pulmonary circulation in several aspects, as described above, no investigations have been performed to adopt this inflow and outflow occlusion technique to partition the hepatic vasculature into the three segments.

The responsiveness of the hepatic longitudinal vascular segments differs depending on vasoactive agents (3, 23, 24). The differences in the response of these vascular segments to a variety of stimuli are, in part, due to the intrinsic vasomotor properties of the blood vessels as well as their passive viscoelastic properties. In addition, the microrheological behavior of blood may vary in the segments of the hepatic vasculature. Blood apparent viscosity has been shown to change depending on the different size vessels in the systemic circulation (13, 14). As blood vessels decrease in diameter between 300 and 30 μm, blood apparent viscosity decreases due to Fahraeus-Lindqvist effect (1, 6). Hematocrit (Hct) is an important determinant of blood viscosity and can affect resistance to blood flow in the circulation (4, 17). In the liver, little is known about the effect of changes in blood Hct on the longitudinal distribution of vascular resistance. Thus we examined the effect of different Hct on the longitudinal vascular resistance distribution in the rat liver.

Norepinephrine constricts predominantly the presinusoidal vessels over the postsinusoidal vessels of hepatic veins (3, 15, 22, 24). Maass-Moreno and Rothe (15), by using the double-lumen catheter inserted through the caval wall into hepatic vein in anesthetized dogs, reported that an infusion of norepinephrine caused a large increase in portal venous pressure but little change in pressure gradient from the large hepatic vein to vena cava. However, the side port of the catheter that was used to

Address for reprint requests and other correspondence: T. Shibamoto, Dept. of Physiology, Division 2, Kanazawa Medical Univ., Uchinada 920-0293, Japan (E-mail: shibamo@kanazawa-med.ac.jp).

The costs of publication of this article were defrayed in part by the payment of page charges. The article must therefore be hereby marked "*advertisement*" in accordance with 18 U.S.C. Section 1734 solely to indicate this fact.

measure the hepatic venous pressure was far downstream from the hepatic venules. Their subsequent study (22), which used the micropuncture method, revealed that norepinephrine caused significant increases in microhepatic venous (venule) pressure and the resistance between the sinusoids and the vena cava. However, a more detailed investigation on the constrictive site of norepinephrine has not been reported.

Recently, Hakim et al. (11) showed that the double occlusion conducted in isolated perfused lungs can be analyzed to provide three segments without performing the single occlusion of pulmonary arterial or venous occlusion independently. We examined whether resistance of the three segments of portal-hepatic venous vessels can be determined by one double occlusion maneuver lasting 3 to 4 s in isolated perfused rat livers. This approach has the advantage of being able to partition the vasculature into three segments when the vasculature is not in a steady state.

The first purpose of this study was to obtain the segmental resistances of portal veins and middle and hepatic veins by using both the portal (inflow) and hepatic venous (outflow) occlusion techniques in isolated rat livers perfused via the portal vein with the hepatic artery ligation. In the liver, the highest compliant and most distensible segment of the middle segment, which could be obtained by the present vascular occlusion methods, corresponds to the sinusoidal bed, but not the small portal and hepatic veins, because the sinusoids are the locus of the high compliance in the liver (2, 8). This is based on the evidence that the sinusoids comprise the majority of the vasculature of the liver and that the vascular compliance of the liver is ~10 times higher than that of the body as a whole (2). Thus one of the most important purposes of the present study is to measure the resistance of the middle segment of the sinusoids. The second purpose was to describe the effects of Hct and blood flow on the distribution of vascular resistance. The third goal was to determine the effect of norepinephrine on the vascular resistance distribution. The final purpose of the present study was to determine whether one double occlusion technique could provide portal or hepatic venous occlusion pressure, either of which was obtained individually by occlusion of the corresponding vessel.

MATERIALS AND METHODS

Isolated liver preparation. Twenty-nine male Sprague-Dawley rats weighing 270–370 g [328 ± 32 g (SD)] were anesthetized with pentobarbital sodium (50 mg/kg iv) and mechanically ventilated with room air. The experiments conducted in the present study were approved by the Animal Research Committee of Shinshu University School of Medicine. A catheter was placed in the right carotid artery. After a laparotomy was performed, the hepatic artery was ligated. Before the cannulation of the portal vein, the perfusion circuit was filled with diluted blood of a donor rat, as described below. At 5 min after the injection of 500 units of heparin into the carotid artery, the portal vein was cannulated with a stainless cannula (1.3 mm ID, 2.1 mm OD) and then portal perfusion started. The rat was rapidly bled through the carotid arterial catheter just before the portal cannulation. After thoracotomy, the supradiaphragmatic portion of the inferior vena cava (IVC) was cannulated with a stainless cannula (2.1 mm ID, 3.0 mm OD), and the IVC above the renal veins was ligated. The perfused liver was then transferred to a weighing pan, which was suspended from an electric balance (model LF-6, Murakami Koki; Osaka, Japan), and the initial wet liver weight [8.8 ± 1.1 g (SD)] was recorded.

The perfusing blood was obtained by exanguination of an intact donor rat that was anesthetized and heparinized, and this blood was diluted with 5% bovine serum albumin (Fraction V powder-A2153, Sigma) in a Krebs solution composed of (in mM) 118 NaCl, 5.9 KCl, 1.2 $MgSO_4$, 2.5 $CaCl_2$, 1.2 NaH_2PO_4, 25.5 $NaHCO_3$, and 5.6 glucose at the following Hct levels: 30% (n = 8), 20% (n = 7), 10% (n = 8), and 0% (n = 6). The blood (50 ml) was recirculated at a constant flow rate using a Masterflex pump through a heat exchanger and a bubble trap in the portal line. The perfusing blood in the reservoir was continuously bubbled with 95% O_2-5% CO_2 at 37°C. The portal (P_{pv}) and hepatic venous (P_{hv}) pressures were continuously measured with pressure transducers (Gould) attached to a sidearm placed just proximal to the perfusion cannula. The zero reference was set to the level of the hepatic hilus. The flow rate and height of the venous reservoir could be adjusted independently to maintain P_{hv} at 0 to1 cmH_2O, with P_{pv} a dependent variable. The perfusion flow rate (Q) was measured with an electromagnetic flow meter (model MFV 1200, Nihonkohden), and the flow probe was positioned in the portal inflow line. To occlude the portal or hepatic venous line instantaneously for measurement of the portal occlusion pressure (P_{po}) or hepatic venous occlusion pressure (P_{hvo}), two solenoid valves were placed around the perfusion tubes upstream from the P_{pv} sidearm cannula and downstream from the P_{hv} sidearm cannula. The hemodynamic variables were continuously monitored and displayed on a thermal physiograph (model 8K23, NEC Sanei; Tokyo, Japan).

Measurement of P_{po} and P_{hvo} by single occlusion maneuver. When a steady state of a constant P_{pv} was reached, the single occlusion maneuver of portal or venous occlusion was performed, and the signals were sampled at 100 Hz and stored in a computer. Portal occlusion was accomplished for 3 s by closing the solenoid valve set in the portal line. Hepatic venous occlusion was accomplished for 1.5 s by closing the solenoid valve set in the hepatic venous line while inflow continued. Portal and hepatic venous pressure tracings were displayed and analyzed independently. An example of portal occlusion was shown in Fig. 1*A*. A stretch of data on P_{pv} between 0.3 and 1.8 s after portal occlusion for 3 s was fitted to a single exponential and extrapolated back to *time 0* (instant of occlusion). This extrapolated pressure was then used as P_{po}. An example of hepatic venous occlusion tracing was shown in Fig. 1*B*, and a stretch of data (0.3–1.0 s) on P_{hv} was fitted to a straight line and extrapolated back to *time 0* (instant of occlusion). This extrapolated pressure was used as P_{hvo}.

Estimation of P_{po} and P_{hvo} from double occlusion. We estimated P_{po} and P_{hvo} from the double occlusion tracing, as shown in Fig. 1*C*. Double occlusion was accomplished for 3 s by closing both of the inflow and outflow valves simultaneously. P_{pv} during double occlusion was analyzed to determine P_{po} in the same manner as the portal occlusion maneuver. The stretch of P_{pv} data between 0.3 and 1.8 s was selected and fitted to a monoexponential. The fitted curve was extrapolated back to the time of occlusion, and the *time 0* pressure was designated as the double occlusion-derived P_{po} ($P_{po\text{-}do}$). Likewise, data between 0.3 and 1.8 s on P_{hv} tracing during double occlusion were fitted to an exponential and extrapolated back to the time of occlusion. This *time 0* pressure was designated as the double occlusion-derived P_{hvo} ($P_{hvo\text{-}do}$).

Experimental protocol. Hepatic hemodynamic parameters were observed for at least 30 min after the start of perfusion until an isogravimetric state (no weight gain or loss) was obtained by adjusting flow rate and the height of the reservoir at a P_{hv} of 0 to 1 cmH_2O, and at a highest Q. After this baseline measurement, the flow rate was increased or decreased by 5 ml/min ranging from 5 to 40 ml/min with keeping P_{hv} constant at 0 to1 cmH_2O. At each steady state of a given flow rate, all three occlusion maneuvers of portal occlusion, hepatic venous occlusion, and double occlusion were performed at a random order. The flow rate was then returned to 25 ml/min for the 30% Hct group, 30 ml/min for the 20% Hct group, 35 ml/min for the 10% Hct group, and 40 ml/min for the 0% Hct group. After stabilization of vascular pressures, the effect of two doses of norepinephrine on the

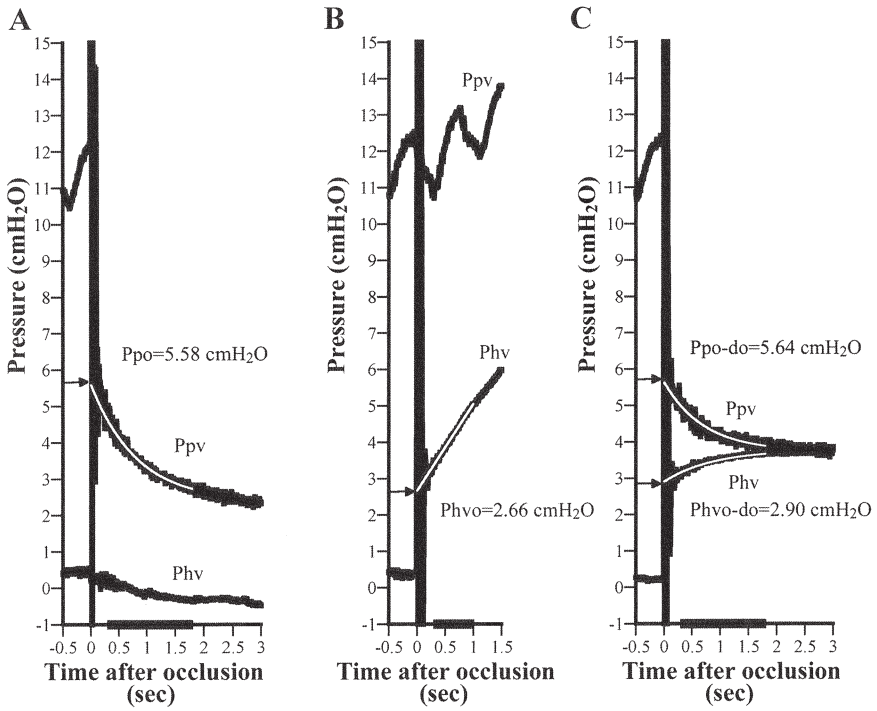

Fig. 1. A representative recording of portal venous pressure (P_{pv}) and hepatic venous pressure (P_{hv}) during the portal (*A*), hepatic venous (*B*), and double occlusion (*C*) in isolated rat liver perfused at 25 ml/min with blood of 30% Hct. In *A*, a white line on the P_{pv} is the fitting curve, which was calculated using P_{pv} data of 0.3–1.8 s after portal occlusion, and this sampling time was represented by a thick bar on the time scale axis. The arrow indicates the portal occlusion pressure (P_{po}) of 5.58 cm. In *B*, the white line on the P_{hv} is the fitting line, which was calculated using P_{hv} data of 0.3–1.0 s after hepatic venous occlusion, and this sampling time was represented by a thick bar on the time scale axis. The arrow indicates the hepatic venous occlusion pressure (P_{hvo}) of 2.66 cmH_2O. In *C*, two white lines on the P_{pv} and P_{hv} are the fitting curves which were calculated using P_{pv} and P_{hv} data, respectively, of 0.3–1.8 s after double occlusion occlusion, and this sampling time was represented by a thick bar on the time scale axis. The arrows indicate double occlusion-derived P_{po} ($P_{po\text{-}do}$) of 5.64 cmH_2O and double occlusion-derived P_{hvo} ($P_{hvo\text{-}do}$) of 2.90 cmH_2O, respectively, and a thick bar on the time scale axis (0.3–1.8 s) indicates the sampling time for regression curves.

vascular resistance distribution was studied. Norepinephrine (Sigma) was infused continuously at the low dose of 1 μg/min into the portal vein until P_{pv} increased and stabilized. Under this steady state, portal, hepatic venous, and double occlusions were performed. The effect of the high dose of 10 μg/min was then examined in a similar manner.

Experiments in the present study were carried out in livers perfused with blood of 30%, 20%, 10%, and 0% Hct. In each preparation, the effect of only one fixed Hct was examined: the perfusate Hct was not changed throughout the experimental period, once the perfusion started at a given Hct. Blood flow rate was expressed as $ml \cdot min^{-1} \cdot 10$ g liver wt^{-1}, and the blood flow groups were assigned to eight groups from 5 ml/min (2.5–7.5 $ml \cdot min^{-1} \cdot 10$ g liver wt^{-1}) to 40 ml/min (37.5–42.5 $ml \cdot min^{-1} \cdot 10$ g liver wt^{-1}) group.

For determination of hepatic segmental vascular resistances, the total portal-hepatic venous (R_t), and portal venous (R_{pv}), sinusoidal (R_{sinus}), and hepatic venous (R_{hv}) resistances were calculated as follows

$$R_t = (P_{pv} - P_{hv})/Q \quad (1)$$

$$R_{pv} = (P_{pv} - P_{po})/Q \quad (2)$$

$$R_{sinus} = (P_{po} - P_{hvo})/Q \quad (3)$$

$$R_{hv} = (P_{hvo} - P_{hv})/Q \quad (4)$$

For calculation of these segmental vascular resistances, we adopted the mean value of P_{pv} for 5 s before the initial vascular occlusion maneuver as the P_{pv} in the equations. The P_{pv} before the subsequent occlusion maneuver did not differ by 0.2 cmH_2O from the P_{pv} of the initial occlusion maneuver.

Statistics. All results are expressed as the means ± SD, unless mentioned otherwise. Comparisons of a given variable between the groups were performed using analysis of variance, followed by Bonferroni's test. A P value <0.05 was considered significant. For the correlation between P_{po} and $P_{po\text{-}do}$ or between P_{hvo} and $P_{hvo\text{-}do}$, least-square linear regression analysis was used. Statistical significance of correlation of the linear regression was tested with analysis of variance. A paired Student's *t*-test was used to compare the mean pressures obtained with the single occlusion method and the double occlusion method.

RESULTS

Effects of blood flow rate on hepatic vascular pressures and resistances. Figure 2, *left*, shows the mean data of hepatic vascular pressures, including P_{po} and P_{hvo} obtained from analysis of tracings of portal occlusion and hepatic venous occlusion, respectively, in different Hct groups. For example, in the Hct 30% and 15 ml/min group, where the livers were perfused with blood of the highest Hct of 30% at 15.6 ± 1.6 $ml \cdot min^{-1} \cdot 10$ g liver wt^{-1}, P_{pv} was 9.1 ± 1.4 cmH_2O, which was similar to the P_{pv} levels observed in in vivo rats (3), P_{po} 5.3 ± 1.1 cmH_2O, P_{hvo} 2.0 ± 0.4 cmH_2O, and P_{hv} 0.4 ± 0.11 cmH_2O. On the basis of these data, the calculated segmental vascular resistances of R_{pv}, R_{sinus}, and R_{hv} were 0.251 ± 0.044, 0.212 ± 0.071, and 0.105 ± 0.022 $cmH_2O \cdot ml^{-1} \cdot min \cdot 10$ g liver wt^{-1}, respectively, as shown in Fig. 2, *left*. This indicates that R_{pv} comprises 44% of R_t, 37% of R_{sinus}, and 19% R_{hv} in livers perfused with blood of 30% Hct at the physiological portal pressure.

Within each Hct group, when the flow rate increased at a constant outflow pressure of P_{hv}, P_{pv} and P_{hvo} increased, whereas P_{po} did not changed significantly, as shown in Fig. 2, *left*. This results in the flow-dependent increases in both P_{pv}-to-P_{po} and P_{hvo}-to-P_{hv} gradients, and the flow-dependent decreases in the P_{po}-to-P_{hvo} gradients. On the basis of these pressure gradient changes, R_{sinus} decreased, and either R_{pv} or R_{hv} did not change when the blood flow increased within each Hct group, as shown in the right panel of Fig. 2. Actually, R_{sinus} at 30% Hct comprised 60 ± 12% of R_t in the minimal flow group of 5 ml/min, 41 ± 11% in 10 ml/min, 36 ± 11% in 20 ml/min, 28 ± 8% in 15 ml/min, and 25 ± 6% in 25 ml/min. An interesting finding was that the sensitivity of the inflow pressure of P_{pv} to changes in flow rate was low: in the 30% Hct groups, only a twofold increase in P_{pv} from 6 to 12 cmH_2O was observed as blood flow was increased fivefold from 5 to 25

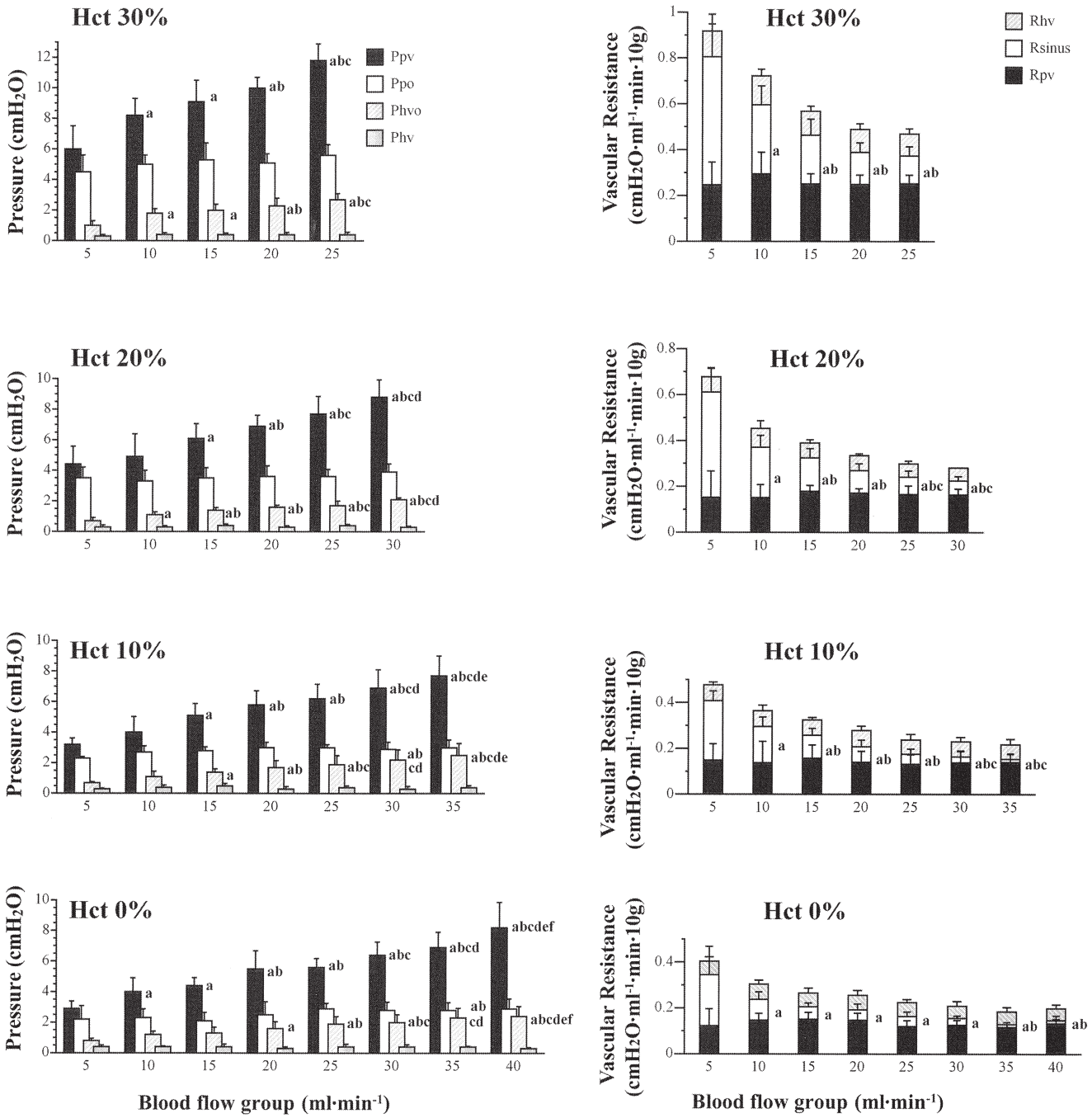

Fig. 2. *Left*, summary of P_{pv}, P_{po}, P_{hvo}, and hepatic venous pressure (P_{hv}) of isolated rat livers perfused with blood of 30%, 20%, 10%, and 0% Hct in the blood flow groups. *Right*, summary of segmental hepatic vascular resistances of portal venous (R_{pv}), sinusoidal (R_{sinus}) and hepatic venous resistance (R_{hv}) of isolated rat livers perfused with blood of Hct 30%, 20%, 10%, and 0% in the blood flow groups. Values are means ± SD; $^{a}P < 0.05$ vs. 5 ml/min group; $^{b}P < 0.05$ vs. 10 ml/min group; $^{c}P < 0.05$ vs. 15 ml/min group; $^{d}P < 0.05$ vs. 20 ml/min group; $^{e}P < 0.05$ vs. 25 ml/min group; and $^{f}P < 0.05$ vs. 30 ml/min group.

ml/min. Representative recordings of hepatic vascular pressures in various flow rates of a liver perfused with 30% Hct were shown in Fig. 3. P_{pv} and P_{hv} in this figure were not recorded at same time, but recorded during portal occlusion and during hepatic venous occlusion, respectively, and were compositely shown in the same frame at each blood flow rate.

Effects of Hct on hepatic vascular pressures and resistances. Figure 4 shows the hepatic vascular pressures (*left panel*) and segmental vascular resistances (*right panel*), as a function of perfusate Hct. At all blood flow rates studied, P_{pv}, P_{po}, and P_{hvo} were significantly greater in 30% Hct groups than those in 20% Hct groups. Thus increases in Hct from 20% to 30% resulted in significant increases in all three segmental resistances of R_{pv}, R_{sinus}, and R_{hv} at blood flow >15 ml/min. However, at the low blood flow of 5 and 10 ml/min, only R_{sinus} did not change significantly whereas R_{pv} and R_{hv} significantly increased as Hct increased from 20% to 30%. All three segmental vascular resistances of any blood flow became significantly greater at

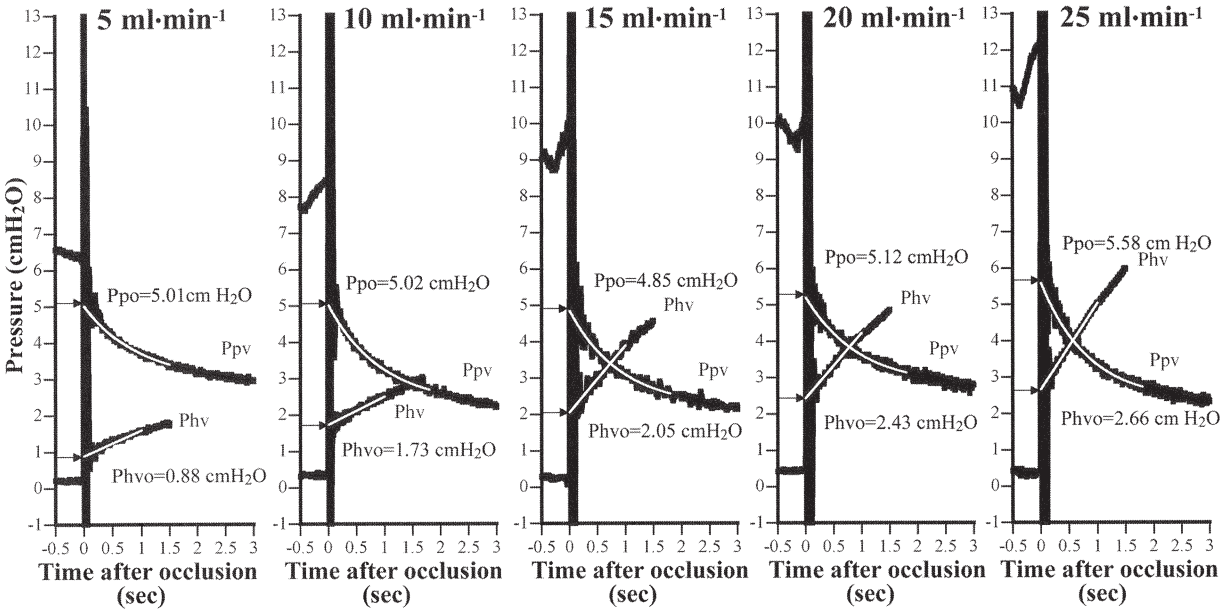

Fig. 3. Representative recordings of an isolated liver perfused with blood of 30% hematocrit (Hct) at various flow rates. P_{pv} during portal occlusion and the P_{hv} during hepatic venous occlusion were successively recorded at separate times but were compositely shown in the same frame at each blood flow rate. White lines indicate the fitting curves for P_{pv} and P_{hv} after portal and hepatic venous occlusion, respectively. The top and bottom arrows indicate P_{po} and P_{hvo}, respectively.

30% Hct than at 10% Hct and 0%. Figure 5 shows representative recordings of livers perfused with blood of different Hct at the same blood flow of 25 ml/min. P_{pv} and P_{hv} in this figure were not recorded at same time but were compositely shown in the same frame at each blood Hct, as shown in Fig. 3.

Effects of norepinephrine infusion on the hepatic vascular resistance distribution at various Hct and flow rates. Figure 6 shows the summary of the hepatic segmental vascular resistances in response to norepinephrine at the four levels of Hct. Although the basal levels of segmental vascular resistances differed depending on Hct, the trends of the response of segmental vessels to norepinephrine were similar; R_{hv} did not change significantly, whereas R_{pv} and R_{sinus} increased dose and Hct dependently. Actually, an infusion of 1 μg/min norepinephrine caused a 1.5- to 1.7-fold increase in R_{pv} and a 1.7- to 2.4-fold increase in R_{sinus} and caused no significant changes in R_{hv} among any Hct groups studied. Furthermore, the higher dose of 10 μg/min norepinephrine caused a 2.5-fold increase in R_{pv} and a 3.1- to 4.4-fold increase in R_{sinus} and again caused no significant changes in R_{hv}.

Estimation of P_{po} and P_{hvo} by the double occlusion maneuver. Figure 1 shows a representative recording during portal occlusion, hepatic venous occlusion, and double occlusion in an isolated rat liver perfused with blood of 30% Hct at 25 ml/min. P_{po} and P_{hvo} obtained via portal occlusion and hepatic venous occlusion, respectively, were almost identical with the pressures obtained by analysis of the tracings of P_{pv} and P_{hv} during the double occlusion maneuver. The agreement between the two methods was tested using all data obtained from both normal livers and livers with vasoconstriction induced by norepinephrine, where P_{pv} ranged from 2.25 to 36.58 cmH_2O. Actually 235 paired measurements of P_{hvo} and $P_{hvo\text{-}do}$, and 225 paired measurements of P_{po} and $P_{po\text{-}do}$ were analyzed. The agreement between these two methods was evaluated in two different ways. First, the mean values of each pressure with the two methods were compared using a simple Student's *t*-test. There were no significant differences between P_{po} and $P_{po\text{-}do}$, and between P_{hvo} and $P_{hvo\text{-}do}$ under all conditions studied. The agreement between the two methods was further tested by using regression analysis. Regression line equations for P_{po} versus $P_{po\text{-}do}$, and for P_{hvo} versus $P_{hvo\text{-}do}$ are given in Fig. 7, *A* and *B*, respectively. There were strong positive relationships for P_{po} and $P_{po\text{-}do}$ ($r > 0.99$). The slope for P_{po} (1.009 ± 0.009, $P = 0.99$) and the *y*-intercept (-0.021 ± 0.042 cmH_2O, $P = 0.612$), statistically, did not differ from the median slope and zero, respectively. Likewise, concerning the regression lines for P_{hvo} versus $P_{hvo\text{-}do}$, the slope for P_{hvo} (0.996 ± 0.013, $P = 0.62$) and the *y*-intercept (0.009 ± 0.031 cmH_2O, $P = 0.775$), statistically, did not differ from the median slope and zero, respectively (Fig. 7).

DISCUSSION

The present study determined the three segmental vascular resistances of isolated portally perfused rat livers by using both portal (inflow) and hepatic venous (outflow) occlusion techniques. When outflow from the liver was suddenly occluded while inflow continued at a constant rate, there was a virtually instantaneous increase in outflow pressure of P_{hv}, after which outflow pressure rose more gradually. This initial increase in P_{hv} was designated as P_{hvo}. Inflow occlusion at a constant outflow pressure caused a nearly instantaneous drop in inflow pressure of P_{pv}, followed by a more gradual decline. This initial decreased P_{pv} was designated as P_{po}. The sudden increase in P_{hv} on outflow occlusion and the sudden decrease in P_{pv} on inflow occlusion can be interpreted to result from cessation of flow across resistances provided by relatively noncompliant vessels on the hepatic venous and portal ends of the vasculature, respectively, as observed in isolated lungs (10). With the use of P_{po} and P_{hvo}, the total hepatic vascular

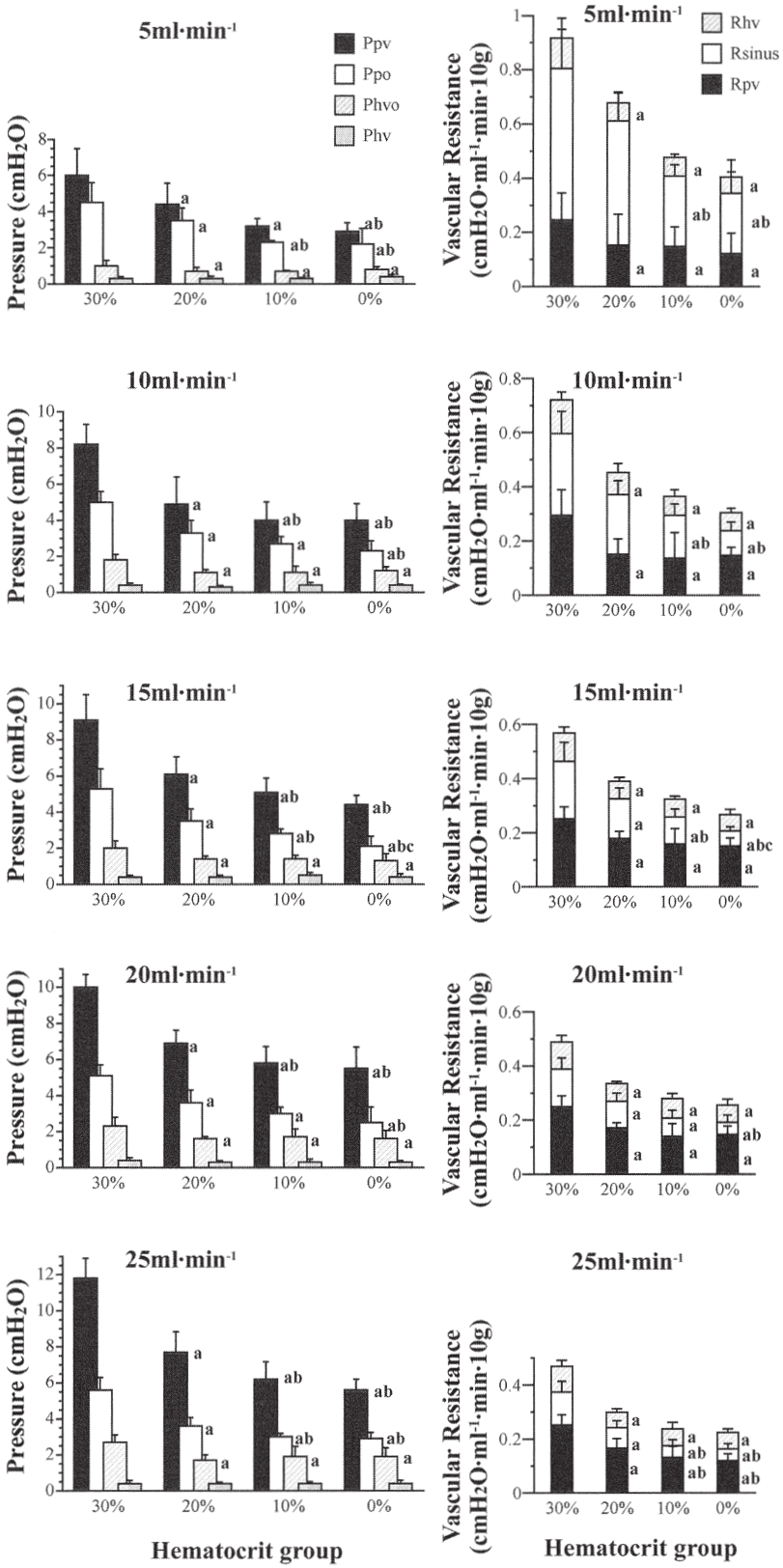

Fig. 4. *Left*, summary of hepatic P_{pv}, P_{po}, P_{hvo}, and P_{hv} pressures of isolated rat livers perfused at various flow rates in the different Hct groups. *Right*, summary of segmental hepatic R_{pv}, R_{sinus}, and R_{hv} resistances of isolated rat livers perfused at various flow rates in the different Hct groups. Values are means ± SD; $^{a}P < 0.05$ vs. Hct 30% group; $^{b}P < 0.05$ vs. Hct 20% group; $^{c}P < 0.05$ vs. Hct 10% group.

pressure gradient of P_{pv}-to-P_{hv} was divided into three pressure gradients of P_{pv}-to-P_{po}, P_{po}-to-P_{hvo}, and P_{hvo}-to-P_{hv}, which may correspond to the segmental vascular resistances of the relatively less compliant portal veins (R_{pv}), a middle compliant compartment of sinusoids (R_{sinus}), and the relatively less compliant hepatic veins (R_{hv}).

One of the major findings of the present study was that R_{pv} comprises 44% of R_t, and R_{sinus} 37%, and R_{hv} 19% in livers

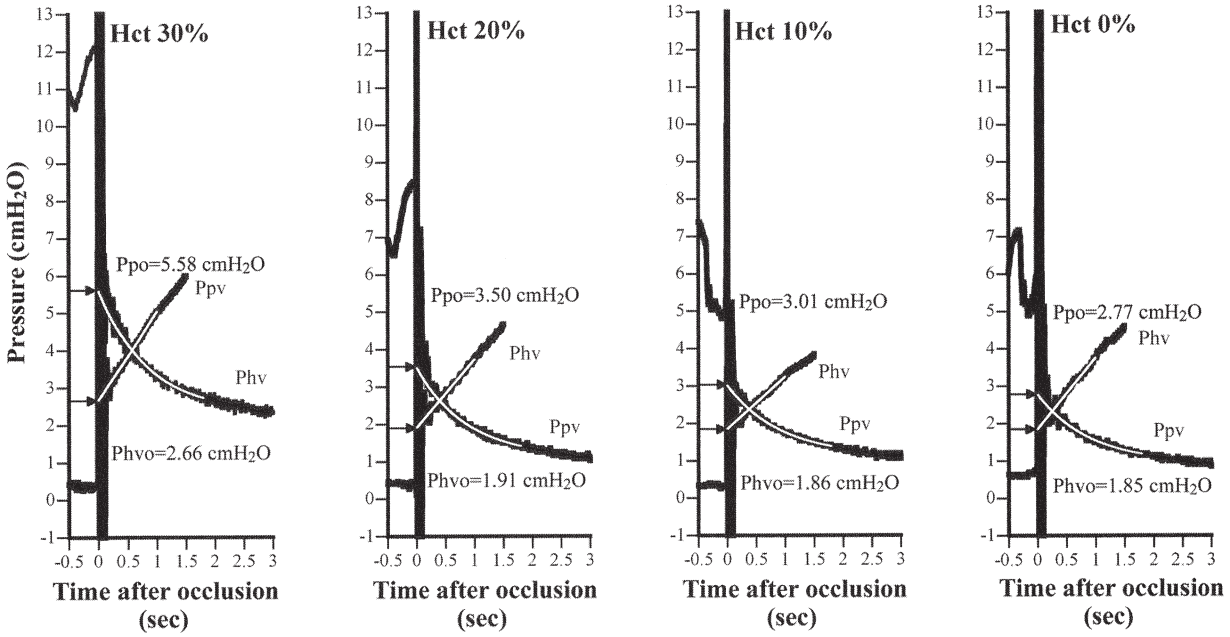

Fig. 5. Representative recordings of P_{pv} and P_{hv} in isolated livers perfused with blood of different Hct at the same blood flow rate of 25 ml/min. In each panel, P_{pv} during portal occlusion and P_{hv} during hepatic venous occlusion were recorded successively at separate times but were compositely shown in the same frame. White lines indicate the fitting curves for P_{pv} and P_{hv} after portal and hepatic venous occlusion, respectively. The top and bottom arrows indicate the P_{po} and the P_{hvo}, respectively.

perfused with 30% Hct at physiological P_{pv} of 9.1 cmH_2O. This finding indicates that almost one-half of R_t occurs in the presinusoidal vessels, one-third in the hepatic sinusoids, and only one-fifth of R_t in the postsinusoidal vessels in rat livers. These results on hepatic vascular resistance distribution are consistent with the findings from the hepatic micropuncture study (3, 16). Bohlen et al. (3), by puncturing surface hepatic venules (10–30 μm diameter), into which two adjacent acini drained, with servo-null micropipettes, reported that hepatic venule pressure was 5.1 ± 1.0 mmHg, and P_{pv} and vena caval pressure averaged 8.0 ± 1.4 and 3.4 ± 0.9 mmHg, respectively, indicating that the hepatic venule to vena caval pressure gradient comprised as small as 37% of the total P_{pv}-to-vena caval pressure gradient. Maass-Moreno and Rothe (16) demonstrated much more definitively that the P_{pv}-to-portal venule gradient comprises 53% of the total P_{pv}-to-P_{hv} gradient, the portal venule-to-hepatic venule gradient, which may correspond to R_{sinus} of the present study, 25%, and the hepatic venule-to-P_{hv} gradient, which may correspond to R_{hv}, 22%.

Flow rates and hepatic segmental vascular resistances. It is well known that an increase in blood flow decreases vascular resistance in systemic circulation. The flow dependence of vascular resistance was also observed in isolated perfused rat livers of the present study. As shown in Fig. 3, when the flow rate at any given Hct was increased at a constant P_{hv}, R_t decreased. This decrease in R_t was ascribed exclusively to a decrease in R_{sinus} but not in R_{hv} or R_{pv}. The mechanism for this decrease in R_{sinus} may be mainly due to microvascular distension and recruitment.

An interesting finding was that the sensitivity of inflow pressure of P_{pv} to changes in flow rate is low: in the 30% Hct groups, only a twofold increase in P_{pv} from 6 to 12 cmH_2O was

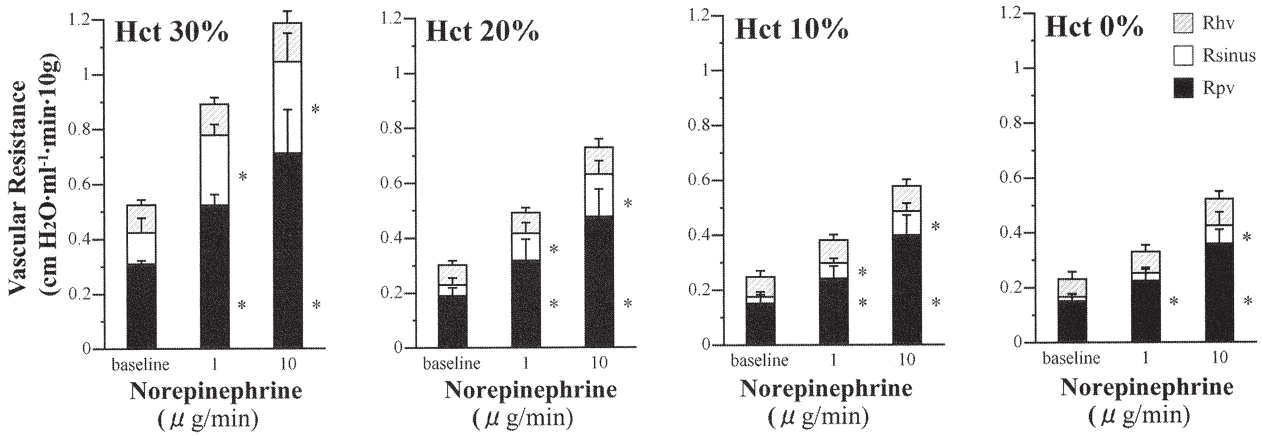

Fig. 6. Effects of norepinephrine on R_{pv}, R_{sinus}, and R_{hv} of isolated rat livers perfused with blood of 30%, 20%, 10%, and 0% Hct. Values are means ± SD. *$P < 0.05$ vs. baseline.

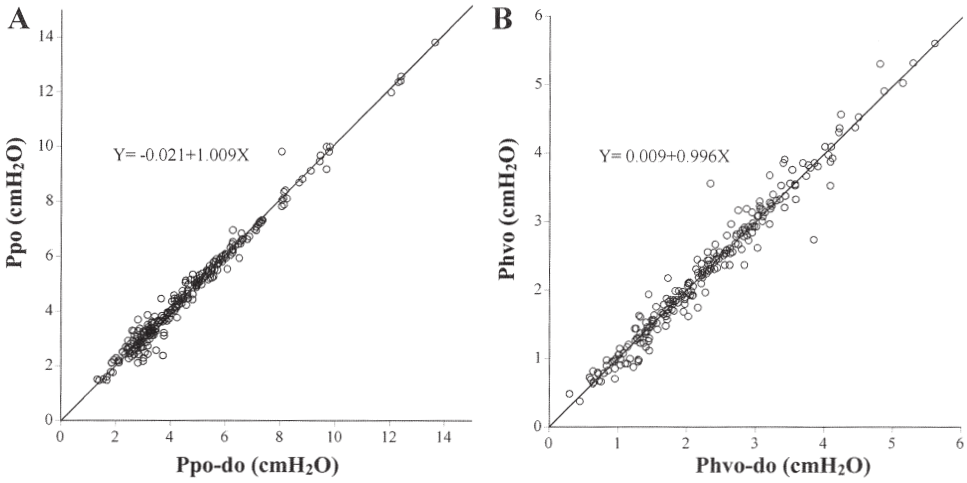

Fig. 7. Relationship between P_{po} and $P_{po\text{-}do}$ (*A*) and between P_{hvo} and $P_{hvo\text{-}do}$ (*B*). The line of identity is drawn. The equation for linear regression is also shown.

observed as the flow is increased fivefold from 5 to 25 ml/min. This small increase in P_{pv}, hence R_t, in response to increased blood flow is ascribed to minimal changes in the pressure gradient of the sinusoids, that is P_{po}-to-P_{hvo} gradient. This indicates that hepatic sinusoids could accept more blood flow without greatly elevating P_{pv} probably through sinusoidal distension and recruitment.

Hct changes and hepatic segmental vascular resistances. In the present study, an increase in Hct from 0% to 30% resulted in a significant increase in R_t. This increase in R_t seems to be due to increases in all three segments of R_{pv}, R_{sinus}, and R_{hv}, as shown in Fig. 4. However, as perfusate Hct increased from 20% to 30% at low flow rate of 5 and 10 ml/min, R_{pv} and R_{hv} significantly increased, whereas R_{sinus} did not change significantly. This lack of change in R_{sinus} may be ascribed to the Fahraeus effect, where Fahraeus and Lindqvist (6) first demonstrated that, as tube diameter is reduced <300 μm, the apparent viscosity of red blood cell suspensions decreases as a result of an actual decrease in small tube Hct. In the systemic microcirculation, in vivo studies indicate that the Hct starts decreasing in vessels with diameters <70 μm and reaches a value in the capillaries of $<25\%$ of the systemic Hct (14). If this finding of the systemic circulation could be applied to the hepatic circulation, the changes in the perfusate Hct, hence the perfusate viscosity, would be so small in hepatic sinusoids due to the Fahraeus effect, compared with the large portal and hepatic veins, then the sinusoidal resistance may not change significantly.

In contrast, at blood flow >15 ml/min, R_{sinus} also increased as perfusate Hct increased from 20% to 30%. This seems to be contradictory to the Fahraeus effect. A possible explanation may be related to an increase in sinusoidal Hct due to rapid transcapillary fluid shifts, which could be caused by an increase in blood flow, hence the microvascular pressures (2). At a high blood flow rate, the microvascular pressures between P_{po} and P_{hvo} are high enough to cause enhanced transvascular cell-free perfusate filtration at the sinusoids, whose endothelium is not continuous and extremely leaky (8). During passage of blood through the sinusoids at high sinusoidal pressure, the apparent Hct might have increased due to enhanced transsinusoidal filtration. This possible increasing Hct effect might have counteract the decreasing Hct effect of the Fahraeus effect, resulting in an increase in R_{sinus} at high flow rate. However, we did not measure the difference in Hct between inflow and outflow blood. Further careful study is required in this respect.

Effect of norepinephrine on hepatic segmental vascular resistances. The present study shows that norepinephrine increased primarily R_{pv} and, to the lesser extent, R_{sinus}, whereas it did not affect R_{hv}. The absence of vasoreactivity to norepinephrine in the large hepatic veins is also reported in in vivo rats. Bohlen et al. (3) showed that an infusion of norepinephrine 2.9 ± 1.3 μg·min^{-1}·kg^{-1} caused a significant increase in P_{pv} by 2.96 ± 1.00 mmHg but no change in hepatic venule pressure (-0.22 ± 1.26 mmHg) with the decrease in portal flow rate 88% of the control. This finding suggests that the large hepatic veins distal to the hepatic venules do not respond to norepinephrine, and this is consistent with the present study. However, their subsequent study revealed that norepinephrine caused significant increases in the hepatic venule pressure and the resistance between the sinusoids and the vena cava in rabbits (22). The discrepancy might be ascribed to the species difference between rat and rabbit.

An interesting finding of the present study is that norepinephrine increased significantly the sinusoidal resistance. This suggests that norepinephrine causes sinusoidal constriction. Reilly et al. (20) reported that the small but significant decrease in sinusoidal diameter was observed when α-adrenergic receptors were stimulated. Although sinusoids do not contain smooth muscle cells, hepatic stellate cells, which are contractile and located around the sinusoidal endothelial cells, might reduce the diameter of sinusoids if it could contract in response to norepinephrine (25). However, there is no evidence that norepinephrine or α-adrenergic agonist contracts stellate cells (21). Zhang et al. (28), using intravital microscopy, measured the diameter of sinusoids in isolated perfused rat livers. They found no changes in sinusoidal hemodynamics in response to phenylephrine, α-adrenergic agonist, although the portal pressure increases. In addition, although activated stellate cells clearly exhibit enhanced contractility, the degree of contractility of normal stellate cells remains controversial (5, 21). Another possible mechanism for the norepinephrine-induced increase in R_{sinus} may be due to contraction of vascular smooth muscle. Anatomic studies show that in rat livers, presinusoidal vessels of preterminal portal venules as small as 40 μm diameter contain a significant amount of smooth muscle (5).

Thus the middle segment in the present study might contain the portal venules.

Estimation of P_{po} and P_{hvo} by double occlusion maneuver. We have shown that P_{po} and P_{hvo} obtained via the single-occlusion technique of portal occlusion and hepatic venous occlusion, respectively, were identical with $P_{po\text{-}do}$ and $P_{hvo\text{-}do}$ that were obtained by the double occlusion maneuver. The agreement between the two methods was verified in the wide range of P_{pv} from 2.25 to 36.58 cmH_2O. There were strong positive relationships between P_{po} and $P_{po\text{-}do}$, and between P_{hvo} and $P_{hvo\text{-}do}$. More importantly, the slope and *y*-intercept of their regression lines, statistically, did not differ from the median slope and zero, respectively.

The shortcoming of portal occlusion and hepatic venous occlusion techniques is that measurement should be done during steady state to obtain the segmental vascular resistance distribution because each technique cannot be done simultaneously. When two occlusions are being performed, it is necessary to wait for the pressure to return to a steady value before the next occlusion can be performed. This may cause problems because vascular constriction is not always stable. This problem is totally solved by one double occlusion technique. The double occlusion technique makes it possible to measure P_{po} and P_{hvo} during an unsteady state, when hepatic vascular pressures are changing in response to experimental maneuvers such as a bolus injection of vasoactive substances.

Limitation of present study. There are limitations of the current experiment. The first is related to the lack of hepatic artery flow and a good source of oxygen, especially in the groups with a Hct of 0% and 10%. However, even in the perfused livers with 0% Hct, perfusate Po_2 could attain as high as 300 mmHg by bubbling the perfusate with 95% O_2-5% CO_2, as revealed by our previous study (26). Another criticism is that the tying off of the hepatic artery could be influencing the compliance and resistance characteristics of hepatic circulation, especially the middle vascular segment. However, we do not think that the ligation of hepatic artery influenced critically determination of P_{po} and P_{hvo}. An anatomic study revealed that the hepatic artery does not directly supply the sinusoids and that its primary vascular beds are formed not in the parenchymal but the stromal compartment, such as peribiliary vascular plexus, portal tract interstitium, portal vein vasocasorum, hepatic capsule, and central-sublobular-hepatic vaso vasorum (5). The final confluence of the hepatic artery occurs at the first third of the sinusoids and terminal portal venules (27). We assume that the ligated hepatic artery should be collapsed with closed ends because of absence of blood flow, and therefore they could not influence the vascular resistance of the overall portal to hepatic veins. The ligated hepatic arterial end might serve as a capacitor of the sinusoids and possibly affect the compliance of the sinusoids, only when the sinusoidal pressure could exceed the pressure high enough to open this collapsed flow-deficient blind sac. However, even if the compliance of the sinusoids could increase, these might not affect measurement of P_{po} and P_{hvo} because these pressures are primarily determined by the characteristics of the noncompliant portal and hepatic venous segments, in which the hepatic artery does not substantially terminate.

Finally, the vascular occlusion technique estimates microvascular pressure in relationship to a point of high vascular compliance (10). The boundary of the middle vascular segment could not be known anatomically in the present study. However, the literature about the microstructure of the liver and Greenway and Lautt (8) showed that the sinusoids comprise the majority of the vasculature of the liver and that sinusoids, not the small portal and hepatic veins, are the locus of the high compliance. Thus we believe that the compliant middle vascular segment of the present study corresponds to the sinusoids. In contrast, the micropuncture technique provides a direct measurement of vascular pressures within anatomically defined vessels although it is limited to the measurement of the surface vessels. In isolated lungs, micropuncture and occlusion technique was applied in the same preparations. It is reported that the inflow occlusion pressure or pulmonary arterial occlusion pressure was slightly higher than the micropipette pressure of 50–80 μm diameter arterioles and that the venous occlusion pressure was slightly lower than the micropipette pressure of 20–50 μm diameter venules (7, 9). Further study is required in which micropuncture and vascular occlusion techniques are applied simultaneously in the same liver preparation to identify the hepatic vessels corresponding to vascular occlusion pressures.

In summary, we provided the hepatic vascular occlusion methods in isolated perfused rat livers to measure P_{po} and P_{hvo}, which enabled us to assign the portal hepatic R_t to the portal R_{pv}, R_{sinus}, and R_{hv}. It was demonstrated that R_{pv} comprises 44% of R_t, 37% R_{sinus}, and 19% R_{hv} in livers perfused at physiological P_{pv} and 30% Hct. We determined the effect of changes in blood Hct or blood flow rate on segmental vascular resistance distribution. As Hct increased at a given blood flow, all three segmental vascular resistances of R_{pv}, R_{sinus}, and R_{hv} increased at flow >15 ml/min. Because blood flow increased at a given Hct, either R_{pv} or R_{hv} did not change, but only R_{sinus} decreased presumably due to distension or recruitment of sinusoids. We also determined the preferential vasoconstrictive site induced by norepinephrine. Norepinephrine increased predominantly R_{pv} over R_{sinus}, but it did not affect R_{hv}. Finally, we demonstrated that P_{po} and P_{hvo} can be obtained by the double occlusion method in isolated perfused rat livers.

GRANTS

This work was supported by Collaborative Research Grant C2003-1 from Kanazawa Medical University and Grant-in-Aid No. 15591665 for Scientific Research from the Ministry of Education, Culture, Sports, Sciences and Technology of Japan.

REFERENCES

1. **Barbee JH and Cokelet GR.** The Fahraeus effect. *Microvasc Res* 3: 6–16, 1971.
2. **Bennett TD and Rothe CF.** Hepatic capacitance responses to changes in flow and hepatic venous pressure in dogs. *Am J Physiol Heart Circ Physiol* 240: H18–H28, 1981.
3. **Bohlen HG, Maass-Moreno R, and Rothe CF.** Hepatic venular pressures of rats, dogs, and rabbits. *Am J Physiol Gastrointest Liver Physiol* 261: G539–G547, 1991.
4. **Cokelet GR.** Blood rheology interpreted through the flow properties of the red cell. In: *Microcirculation*, edited by Grayson J and Zingg W. New York: Plenum, 1976, vol. 1, p. 9–32.
5. **Ekataksin W and Kaneda K.** Liver microvascular architecture: an insight into the pathophysiology of portal hypertension. *Semin Liver Dis* 19: 359–382, 1999.
6. **Fahraeus R and Lindqvist R.** The viscosity of the blood in narrow capillary tubes. *Am J Physiol* 96: 562–568, 1931.
7. **Fike CD, Gordon JB, and Kaplowitz MR.** Micropipette and vascular occlusion pressures in isolated lungs of newborn lambs. *J Appl Physiol* 75: 1854–1860, 1993.

8. **Greenway CV and Lautt WW.** Hepatic circulation. In: *Handbook of Physiology. The Gastrointestinal System. Motility & Circulation.* Bethesda, MD: Am. Physiol. Soc, 1989, sect. 6, vol. I, pt. 2, chapt. 41, p. 1519–1564.
9. **Hakim TS and Kelly S.** Occlusion pressure vs. micropipette pressures in the pulmonary circulation. *J Appl Physiol* 67: 1277–1285, 1989.
10. **Hakim TS, Michel RP, and Chang HK.** Partitioning of pulmonary vascular resistance in dogs by arterial and venous occlusion. *J Appl Physiol* 52: 710–715, 1982.
11. **Hakim TS, Sugimori K, and Ferrario L.** Analysis of the double occlusion which provides four pressure gradients. *Eur Respir J* 9: 2578–2583, 1996.
12. **Linehan JH, Dawson CA, and Rickaby DA.** Distribution of vascular resistance and compliance in a dog lung lobe. *J Appl Physiol* 53: 158–168, 1982.
13. **Lipowsky HH and Zweifach BW.** Methods for the simultaneous measurement of pressure differentials and flow in single unbranched vessels of the microcirculation for rheological studies. *Microvasc Res* 14: 345–361, 1977.
14. **Lipowsky HH, Usami S, and Chien S.** In vivo measurements of "apparent viscosity" and microvessel hematocrit in the mesentery of the cat. *Microvasc Res* 19: 297–319, 1980.
15. **Maass-Moreno R and Rothe CF.** Contribution of the large hepatic veins to postsinusoidal vascular resistance. *Am J Physiol Gastrointest Liver Physiol* 262: G14–G22, 1992.
16. **Maass-Moreno R and Rothe CF.** Distribution of pressure gradients along hepatic vasculature. *Am J Physiol Heart Circ Physiol* 272: H2826–H2832, 1997.
17. **Michel RP.** Arteries and veins of the normal dog lung: qualitative and quantitative structural differences. *Am J Anat* 164: 227–241, 1982.
18. **Rapport AM, Borowy CT, Lougheed WM, and Lotto WN.** Subdivision of hexagonal liver lobules into a structural and functional unit. *Anat Rec* 119: 11–27, 1954.
19. **Reeves JT, Leathers JE, and Boatright C.** Microradiography of the rabbit's hepatic microcirculation. The similarity of the hepatic portal and pulmonary arterial circulations. *Anat Rec* 154: 103–119, 1966.
20. **Reilly FD, McCuskey RS, and Cilento EV.** Hepatic microvascular regulatory mechanisms. I. Adrenergic mechanisms. *Microvasc Res* 21: 103–116, 1981.
21. **Rockey DC.** Hepatic blood flow regulation by stellate cells in normal and injured liver. *Semin Liver Dis* 21: 337–349, 2001.
22. **Rothe CF and Maass-Moreno R.** Hepatic venular resistance responses to norepinephrine, isoproterenol, adenosine, histamine, and ACh in rabbits. *Am J Physiol Heart Circ Physiol* 274: H777–H785, 1998.
23. **Shibamoto T, Wang HG, Miyahara T, Tanaka S, Haniu H, and Koyama S.** Pre-sinusoidal vessels predominantly contract in response to norepinephrine, histamine, and KCl in rabbit liver. *J Appl Physiol* 87: 1404–1412, 1999.
24. **Shibamoto T, Wang HG, Tanaka S, and Koyama S.** Hepatic capillary pressure is estimated using triple vascular occlusion method in isolated canine liver. *Am J Physiol Regul Integr Comp Physiol* 271: R1130–R1141, 1996.
25. **Wake K.** Presinusoidal stellate cells (fat-storing cells, interstitial cells, lipocytes), their related structure in and around the live sinusoids, and vitamin A-storing cells in extrahepatic organs. *Int Rev Cytol* 66: 303–353, 1980.
26. **Wang HG, Shibamoto T, and Miyahara T.** Endothelin-1 selectively contracts portal vein through both ET_A and ET_B receptors in isolated rabbit liver. *Am J Physiol Gastrointest Liver Physiol* 273: G1036–G1043, 1997.
27. **Watanabe Y, Puschel GP, Gardemann A, and Jungermann K.** Presinusoidal and proximal intrasinusoidal confluence of hepatic artery and portal vein in rat liver: functional evidence by orthograde and retrograde bivascular perfusion. *Hepatology* 19: 1198–1207, 1994.
28. **Zhang JX, Pegoli W Jr, and Clemens MG.** Endothelin-1 induces direct constriction of hepatic sinusoids. *Am J Physiol Gastrointest Liver Physiol* 266: G624–G632, 1994.

Am J Physiol Regul Integr Comp Physiol 286: R94–R100, 2004.
First published October 2, 2003; 10.1152/ajpregu.00648.2002.

NO, but not CO, attenuates anaphylaxis-induced postsinusoidal contraction and congestion in guinea pig liver

Zonghai Ruan,[1,2] Toshishige Shibamoto,[1] Tomohiro Shimo,[1,3] Hideaki Tsuchida,[3] Tomonobu Koizumi,[2] and Matomo Nishio[4]

Division 2, Departments of [1]Physiology, [3]Anesthesiology, and [4]Pharmacology, Kanazawa Medical University, Uchinada 920-0293; and [2]First Department of Medicine, Shinshu University School of Medicine, Matsumoto 390-8621, Japan

Submitted 21 October 2002; accepted in final form 26 September 2003

Ruan, Zonghai, Toshishige Shibamoto, Tomohiro Shimo, Hideaki Tsuchida, Tomonobu Koizumi, and Matomo Nishio. NO, but not CO, attenuates anaphylaxis-induced postsinusoidal contraction and congestion in guinea pig liver. *Am J Physiol Regul Integr Comp Physiol* 286: R94–R100, 2004. First published October 2, 2003; 10.1152/ajpregu.00648.2002.—The pathophysiology of the hepatic vascular response to anaphylaxis in guinea pig is not known. We studied effects of anaphylaxis on hepatic vascular resistances and liver weight in isolated perfused livers derived from guinea pigs sensitized with ovalbumin. We also determined whether nitric oxide (NO) or carbon monoxide (CO) modulates the hepatic anaphylaxis. The livers were perfused portally and recirculatingly at constant flow with diluted blood. With the use of the double-occlusion technique to estimate the hepatic sinusoidal pressure (P_{do}), portal venous resistance (R_{pv}) and hepatic venous resistance (R_{hv}) were calculated. An antigen injection caused venoconstriction characterized by an increase in R_{pv} greater than R_{hv} and was accompanied by a large liver weight gain. Pretreatment with the NO synthase inhibitor N^G-nitro-L-arginine methyl ester, but not the heme oxygenase inhibitor zinc protoporphyrin IX, potentiated the antigen-induced venoconstriction by increasing both R_{pv} and R_{hv} (2.2- and 1.2-fold increase, respectively). In conclusion, anaphylaxis causes both pre- and postsinusoidal constriction in isolated guinea pig livers. However, the increases in postsinusoidal resistance and P_{do} cause hepatic congestion. Endogenously produced NO, but not CO, modulates these responses.

hepatic circulation; antigen; double occlusion pressure; hepatic vascular resistance

ANAPHYLAXIS IS AN immediate, type-1 hypersensitivity reaction that occurs after exposure of sensitized organisms and tissues to sensitizing antigen. The most common life-threatening feature of acute anaphylaxis is cardiovascular collapse and shock, although there are other life-threatening effects, including bronchospasm, angioedema, and pulmonary edema (24). Cardiovascular manifestation includes a rapid and precipitous decrease in systemic arterial pressure with a concomitant decrease in cardiac output (5). Anaphylactic hypotension is primarily caused by alterations in the systemic circulation that influence blood flow to the heart because left ventricular function is relatively well preserved during anaphylactic shock (5). Peripheral circulatory collapse is ascribed to hypovolemia, which results from a plasma volume loss. The latter could be the result of vasodilation with the peripheral pooling in large-capacity splanchnic venous beds and increased vascular permeability with a shift of intravascular fluid to the extravascular space.

In canine experimental models of anaphylactic shock, congestion of livers and the upstream splanchnic organs is important in the pathogenesis of circulatory collapse. Actually, eviscerated dogs did not develop anaphylactic shock (17). Enjeti et al. (5) reported that the severity of the anaphylactic shock could be decreased by occluding the descending aorta. Canine anaphylactic hepatic congestion is caused by constriction of postsinusoidal hepatic veins. Yamaguchi et al. (32), using the vascular occlusion method in isolated perfused livers derived from naturally sensitized dogs, demonstrated that selective postsinusoidal constriction occurs during hepatic anaphylaxis induced by injection of the *Ascaris suum* antigen in the perfusing blood. On the other hand, it has not been known so far whether in other species than dogs anaphylactic reaction causes constriction of postsinusoidal hepatic veins, resulting in hepatic congestion and pooling of circulating blood.

Nitric oxide (NO) is important in regulating blood flow by exerting vasodilatory actions in multiple vascular beds (19), including the hepatic circulation (18). With respect to the effects of NO on anaphylaxis, NO contributes to acute hypotension of anaphylaxis (20). NO also modulates anaphylaxis-induced changes in regional hemodynamics of coronary circulation (27) and pulmonary circulation (23) by serving as an endogenously released vasodilator. However, it has not been known whether NO modulates the change in hepatic hemodynamics during anaphylaxis.

In addition to NO, another endogenously generated gas, carbon monoxide (CO), may also exert local vasodilatory effects in the liver (6). It is reported that CO is continuously generated in livers and thereby contributes to maintenance of normal hepatic vascular tone (26). Moreover, CO is released in the hepatic circulation in response to various stressful stimuli (2, 3). However, there are no studies that determined the role of CO in the hepatic anaphylaxis.

To clarify the anaphylactic disturbance of hepatic circulation, we herein established anaphylactic models of isolated portally perfused guinea pig livers, in which the sinusoidal pressure was measured using the double-occlusion method (22, 32). The first purpose of the present study was to determine effects of anaphylaxis on hepatic vascular resistance distribution and liver weight changes. The second purpose was to determine, using an NO synthase inhibitor [N^G-nitro-L-arginine methyl ester (L-NAME)] and a specific inhibitor of CO-generating enzyme heme oxygenase (HO) [zinc protoporphyrin IX (ZnPP)], whether NO and/or CO modulates the hepatic anaphylaxis.

Address for reprint requests and other correspondence: T. Shibamoto, Dept. of Physiology, Division 2, Kanazawa Medical Univ., Uchinada 920-0293, Japan (E-mail: shibamo@kanazawa-med.ac.jp).

The costs of publication of this article were defrayed in part by the payment of page charges. The article must therefore be hereby marked "*advertisement*" in accordance with 18 U.S.C. Section 1734 solely to indicate this fact.

MATERIALS AND METHODS

Sensitization

Twenty-five male Hartley guinea pigs weighing 351 ± 31 (SD) g were used in this study. The experiments conducted in the present study were approved by the Animal Research Committee of Kanazawa Medical University. Guinea pigs were actively sensitized by the intraperitoneal injection of an emulsion made by mixing equal volumes of complete Freund's adjuvant (0.5 ml) with 1 mg ovalbumin (grade V; Sigma) dissolved in physiological saline (0.5 ml). The nonsensitized animals were injected with a mixture of complete Freund's adjuvant (0.5 ml) and physiological saline (0.5 ml) without ovalbumin.

Isolated Liver Preparation

After sensitization (2 wk), the animals were anesthetized with pentobarbital sodium (35 mg/kg ip) and mechanically ventilated with room air. A polyethylene tube was placed in the right carotid artery. After laparotomy, the cystic duct and the hepatic artery were ligated, and the bile duct was cannulated with the polyethylene tube (1.0 mm ID, 1.3 mm OD). At 5 min after intra-arterial heparinization (500 U/kg), 8–9 ml blood were withdrawn manually with a plastic syringe through the carotid arterial catheter. The intra-abdominal inferior vena cava (IVC) above the renal veins was ligated, and the portal vein was cannulated with a stainless cannula (2.1 mm ID, 3.0 mm OD) for portal perfusion. After thoracotomy, the supradiaphragmatic IVC was cannulated through a right atrium incision with the same size stainless cannula, and then portal perfusion was begun with the heparinized autologous blood that was diluted with 5% bovine albumin (Sigma) in Krebs solution (in mM: 118 NaCl, 5.9 KCl, 1.2 $MgSO_4$, 2.5 $CaCl_2$, 1.2 NaH_2PO_4, 25.5 $NaHCO_3$, and 5.6 glucose) at Hct of 8%. The liver was rapidly excised, suspended from an isometric transducer (TB-652T, Nihon-Kohden, Japan), and weighed continuously throughout the experimental period.

The sensitized and nonsensitized livers were perfused at a constant flow rate in a recirculating manner via the portal vein with blood that was pumped using a Masterflex roller pump from the venous reservoir through a heat exchanger (37°C). The recirculating blood volume was 40 ml. The height of the reservoir and the portal blood flow rate (Q) could be adjusted independently to maintain the portal and hepatic venous pressures at any desired level. The perfused blood was oxygenated in the venous reservoir by continuous bubbling with 95% O_2 and 5% CO_2. The portal venous (P_{pv}) and the hepatic venous (P_{hv}) pressures were measured using pressure transducers (TP-400T; Nihon-Kohden) attached by sidearm to the appropriate cannulas with the reference points at the hepatic hilus. To occlude inflow and outflow perfusion lines simultaneously for measurement of the double-occlusion pressure (P_{do}), two solenoid valves were placed in a position so that each sidearm cannula was between the corresponding solenoid valve and the liver. Portal Q was measured with an electromagnetic flowmeter (MFV 1200; Nihon-Kohden), and the flow probe was positioned in the inflow line. Bile was collected drop by drop in a small tube suspended from the force transducer (SB-1T; Nihon-Kohden). One bile drop yielded 0.027 g, and the time between drops was measured for determination of the bile flow rate (12). The hepatic vascular pressures, Q, liver weight, and bile weight were monitored continuously and displayed through a thermal physiograph (RMP-6008; Nihon-Kohden). Outputs were also digitized by the analog-digital converter at a sampling rate of 100 Hz. These digitized values were displayed and recorded using a personal computer for later determination of P_{do}.

Experimental Protocol

Hepatic hemodynamic parameters were observed for at least 20 min after the start of perfusion until an isogravimetric state (no weight gain or loss) was obtained by adjusting the flow rate and the height of the reservoir at a P_{hv} of 0–1 cmH_2O and at a Q of 36 ± 5 $ml \cdot min^{-1} \cdot 10$ g liver wt^{-1}. After the baseline measurements, the perfused livers excised from the sensitized animals were randomly assigned to one of the following three groups and that from the nonsensitized animals into the nonsensitized group.

The L-NAME group (n = 6). Before the injection of ovalbumin, L-NAME (100 μM) was administered in the reservoir. Ovalbumin (0.1 mg) was injected in the reservoir at 10 min after injection of L-NAME.

The ZnPP group (n = 6). Instead of L-NAME, ZnPP (10 μM) was administered in the reservoir, and ovalbumin (0.1 mg) was injected at 10 min after injection of ZnPP.

The sensitized group (n = 7). Ovalbumin (0.1 mg) was injected in the reservoir.

The nonsensitized group (n = 6). The livers were excised from the nonsensitized animals. Ovalbumin (0.1 mg) was injected in the reservoir.

The hepatic sinusoidal pressure was measured by the double-occlusion method (22, 32). Both the inflow and outflow lines were simultaneously and instantaneously occluded for 13 s using the solenoid valves, after which P_{pv} and P_{hv} rapidly equilibrated to a similar or identical pressure, which was P_{do}. Actually, P_{do} values were obtained from the digitized data of P_{pv} and P_{hv} using an original program (LIVER software; Biomedical Science, Kanazawa, Japan). In each experimental group, P_{do} was measured at baseline and 4-, 6-, 10-, and then at 10-min intervals for 120 min after an injection of ovalbumin.

The total portal-hepatic venous (R_t), portal or presinusoidal (R_{pv}), and hepatic venous or postsinusoidal (R_{hv}) resistances were calculated as follows

$$R_t = (P_{pv} - P_{hv})/Q \quad (1)$$

$$R_{pv} = (P_{pv} - P_{do})/Q \quad (2)$$

$$R_{hv} = (P_{do} - P_{hv})/Q \quad (3)$$

Statistics

All results are expressed as means ± SD. ANOVA followed by Bonferroni's test was used to test for significant differences. Differences were considered as statistically significant at P values <0.05.

RESULTS

Effect of antigen injection on hepatic hemodynamic variables, bile flow, and liver weight

The final wet liver weight measured immediately after experiment was 12 ± 2 g. The P_{do} at the baseline state of 25 perfused guinea pig livers was 3.5 ± 0.3 cmH_2O, with P_{pv} 7.3 ± 0.4 cmH_2O and P_{hv} 0.5 ± 0.3 cmH_2O at Q 36 ± 5 $ml \cdot min^{-1} \cdot 10$ g liver wt^{-1}. The calculated R_t was 0.19 ± 0.03 $cmH_2O \cdot ml^{-1} \cdot min^{-1} \cdot 10$ g liver wt^{-1}. The segmental vascular resistances of R_{pv} and R_{hv} were 0.11 ± 0.02 and 0.09 ± 0.02 $cmH_2O \cdot ml^{-1} \cdot min^{-1} \cdot 10$ g liver wt^{-1}, respectively, and the R_{hv}-to-R_t ratio was 0.44 ± 0.03. This indicates that 56% of the R_t of the isolated guinea pig livers exists in the portal venous side, which is similar to rabbit livers (15, 22).

Figure 1 shows a representative example of the response to ovalbumin. Within 1 min after antigen injection, venoconstriction occurred, as reflected by an increase in P_{pv}. P_{pv} increased from the baseline of 7.5 ± 0.5 cmH_2O to the peak of 22.6 ± 2.1 cmH_2O within 4–6 min after antigen. At the same time, the liver weight showed a gradual increase, reaching the peak of 2.4 ± 0.8 g/10 g liver wt at 10 min, as shown in Fig. 2. The

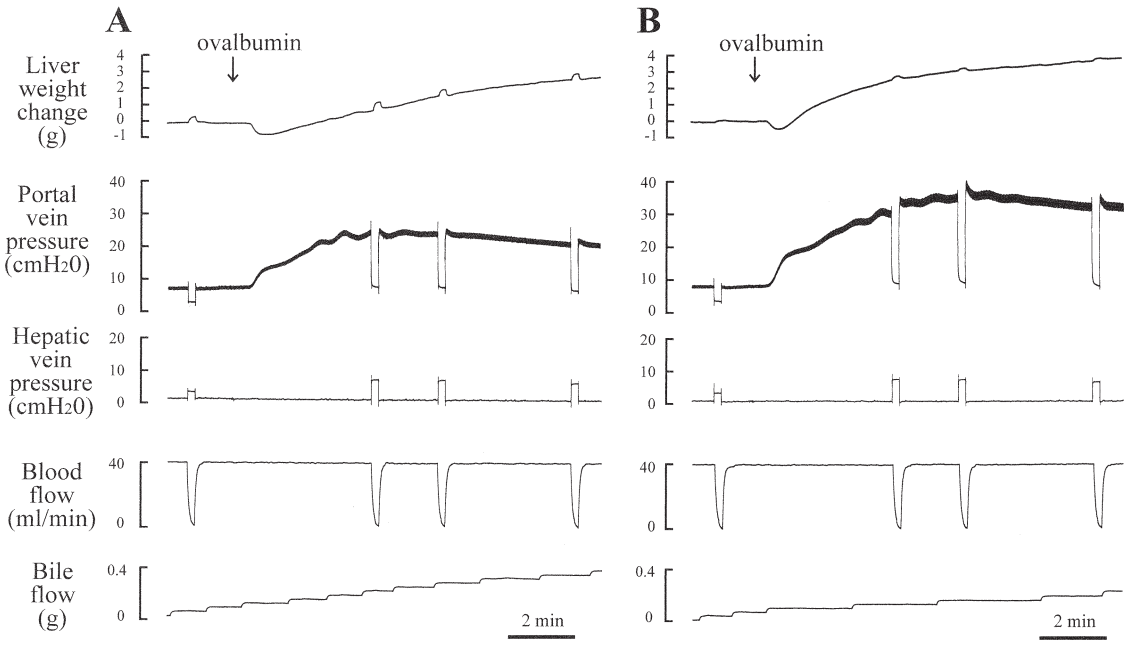

Fig. 1. Representative recording of the response to ovalbumin antigen of a guinea pig liver in the sensitized group (Sensitized; *A*) and the N^G-nitro-L-arginine methyl ester (L-NAME; *B*) group.

double-occlusion maneuver performed at 4 min after antigen revealed a higher P_{do} than the baseline value. P_{do} increased from a baseline value of 3.7 ± 0.3 to 7.9 ± 0.5 cmH_2O at 4 min after antigen, followed by a gradual return to the preinjection value, as shown in Fig. 2. At the maximal venoconstriction, the pressure gradient of P_{do} to P_{hv} was significantly increased from a baseline of 3.3 ± 0.3 to 7.4 ± 0.6 cmH_2O, indicating an increase in R_{hv}. However, the increase in the P_{pv}-to-P_{do} gradient from 3.8 ± 0.3 to 14.8 ± 2.1 cmH_2O after antigen was much greater than that in the P_{do}-to-P_{hv} gradient, indicating a greater increase in R_{pv} than R_{hv}. Concomitant with venoconstriction, bile flow decreased to 66 ± 11% of the basal flow rate, followed by a gradual recovery to 81 ± 10% at the end of the experimental period.

Figure 3 shows the time course of changes in R_t, R_{pv}, and R_{hv} after ovalbumin injection. R_t increased in the same time course as P_{pv} after antigen injection. R_t increased threefold from 0.21 ± 0.05 to 0.63 ± 0.10 $cmH_2O \cdot ml^{-1} \cdot min^{-1} \cdot 10$ g liver wt^{-1} at 4 min. After antigen injection, R_{pv} showed a 3.8-fold increase from the baseline of 0.11 ± 0.02 to the peak of 0.43 ± 0.07 $cmH_2O \cdot ml^{-1} \cdot min^{-1} \cdot 10$ g liver wt^{-1}, whereas R_{hv} showed only a 2.2-fold increase from 0.09 ± 0.02 to the peak of 0.21 ± 0.04 $cmH_2O \cdot ml^{-1} \cdot min^{-1} \cdot 10$ g liver wt^{-1}. The increase of R_{pv} was significantly greater than that of R_{hv}.

Effect of L-NAME and ZnPP on Basal Hepatic Circulation and Hepatic Anaphylaxis

Table 1 shows the summary data of hemodynamic variables at baseline and 10 min after administration of L-NAME or ZnPP. After injection of L-NAME, P_{pv}, but not P_{do}, increased significantly, resulting in a significant increase in R_{pv}, but not R_{hv}. Liver weight decreased only slightly but significantly after L-NAME. These findings indicate that L-NAME constricts primarily presinusoidal vessels and that endogenous NO dilates the portal veins rather than hepatic veins in basal states of isolated blood-perfused guinea pig liver. In contrast, administration of ZnPP, an inhibitor of HO, did not significantly change P_{pv}, suggesting that CO does not play a significant role in the maintenance of the basal vascular tone of isolated blood-perfused guinea pig livers.

Figure 1 shows a representative example of the response to ovalbumin antigen after pretreatment with L-NAME. P_{pv} increased markedly from the preantigen levels of 8.6 ± 0.6 to the peak of 40.7 ± 4.6 cmH_2O at 4–6 min after antigen. P_{do} also significantly increased after antigen (4.1 ± 0.4 vs. 9.5 ± 0.7 cmH_2O; preantigen vs. peak). The increase in the P_{pv}-to-P_{do} gradient was much larger than that in the P_{do}-to-P_{hv} gradient, suggesting that R_{pv} increased greater than R_{hv}. The liver weight increased markedly, reaching the peak of 4.6 ± 1.1 g/10 g liver wt at 10 min (Fig. 2).

The peak levels of R_t (1.15 ± 0.15 $cmH_2O \cdot ml^{-1} \cdot min^{-1} \cdot 10$ g liver wt^{-1}) in the L-NAME group were 1.8-fold greater than that in the sensitized group (0.64 ± 0.09 $cmH_2O \cdot ml^{-1} \cdot min^{-1} \cdot 10$ g liver wt^{-1}), as shown in Fig. 3. This indicates that the L-NAME pretreatment enhanced the anaphylaxis-induced increase in R_t. Although the pretreatment with L-NAME significantly augmented increases in both R_{pv} and R_{hv} after antigen, the increase in R_{pv} (2.2-fold) predominated over that in R_{hv} (1.2-fold). The increases in P_{do} after antigen were highest in the L-NAME groups among all groups studied (Fig. 2), which is consistent with the significant enhancement of R_{hv} after antigen. Liver weight gain in the L-NAME group was also highest among the groups shown in Fig. 2. In contrast, the ZnPP pretreatment did not affect the anaphylactic changes in any variables studied.

The basal bile flow rate was 0.04 ± 0.02 g·10 g liver $wt^{-1} \cdot min^{-1}$ (n = 25). The bile flow in the ZnPP group deceased to 65 ± 6% of the preantigen levels transiently as concurrent with venoconstriction, a finding similar to the sensitized group. In the L-NAME group, the bile flow rate

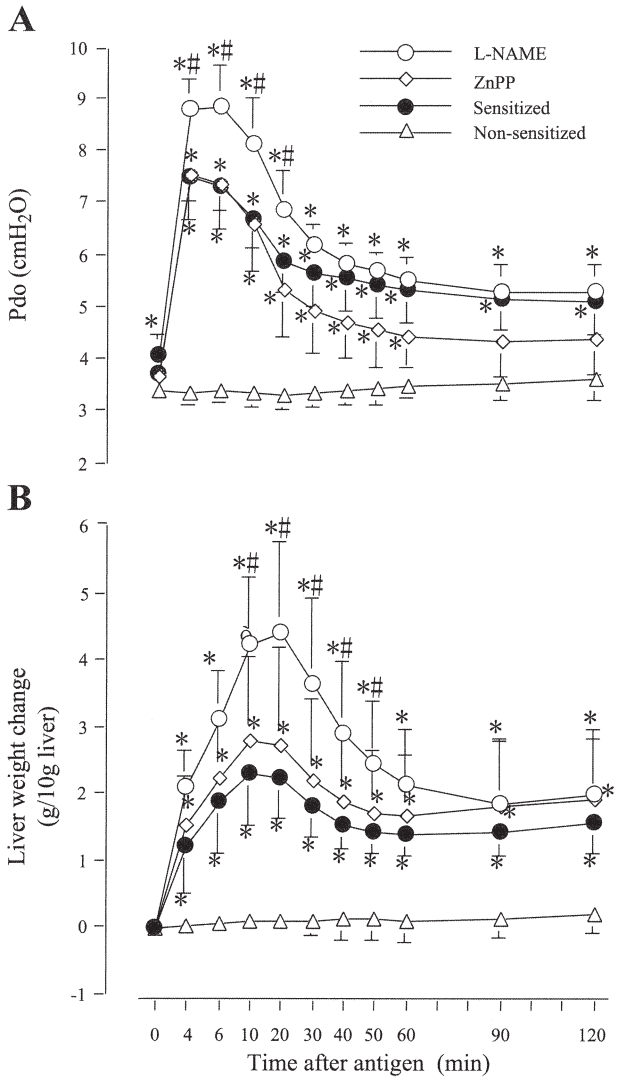

Fig. 2. Summary of the double-occlusion pressure (P_{do}; *A*) and liver weight changes (*B*) after antigen injection. Data are means ± SD. $P < 0.05$ vs. baseline (*) and vs. the sensitized group (#).

decreased markedly to 59 ± 15% of the preantigen levels within 6 min after antigen.

DISCUSSION

The main findings of the present study are that the anaphylactic reaction in isolated perfused guinea pig livers was characterized by increases in both of pre- and postsinusoidal resistances, accompanied by liver weight gain, and that L-NAME, but not ZnPP, augmented this anaphylaxis-induced venoconstriction and hepatic congestion.

It is well known that the hepatic vascular responses to anaphylaxis of rats (7) and dogs (31, 32) are characterized by constriction of the hepatic vessels. In dogs, anaphylactic constriction of the hepatic vessels is accompanied by severe hepatic congestion resulting from vigorous postsinusoidal contraction (32). We herein showed that the hepatic anaphylaxis of guinea pigs also causes venoconstriction and congestion. Furthermore, the double vascular occlusion technique revealed that both pre- and postsinusoidal vessels contracted in response to antigen, although the presinusoidal constriction was greater in magnitude than the postsinusoidal constriction. The significant postsinusoidal constriction, as reflected by an increase in

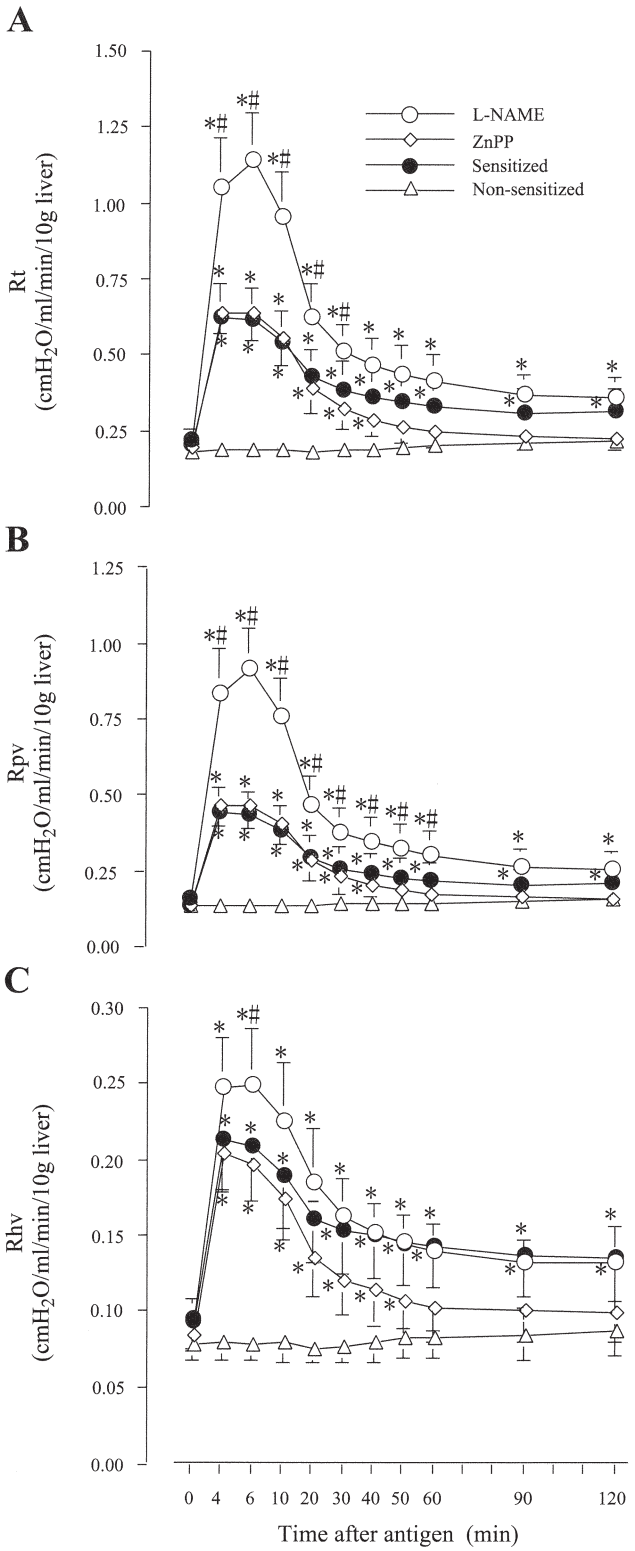

Fig. 3. Summary of total hepatic vascular (R_t; *A*), portal venous (R_{pv}; *B*), and hepatic venous (R_{hv}; *C*) resistances after antigen injection. Data are means ± SD. $P < 0.05$ vs. baseline (*) and vs. the sensitized group (#).

Table 1. *Basal hemodynamic variables in isolated perfused guinea pig livers of all groups studied*

	Nonsensitized Baseline (n = 6)	Sensitized Baseline (n = 7)	L-NAME (n = 6)		ZnPP (n = 6)	
			Baseline	After	Baseline	After
P_{pv}, cmH_2O	7.2±0.5	7.5±0.5	7.3±0.5	8.6±0.6*	7.3±0.3	7.7±0.5
P_{hv}, cmH_2O	0.5±0.2	0.4±0.1	0.6±0.2	0.8±0.3	0.5±0.2	0.6±0.3
P_{do}, cmH_2O	3.3±0.3	3.7±0.3	3.6±0.4	4.1±0.4	3.4±0.2	3.6±0.3
Blood flow, $ml \cdot min^{-1} \cdot 10\ g\ liver^{-1}$	36±4	35±5	36±3	36±3	35±3	35±3
R_t, $cmH_2O \cdot ml^{-1} \cdot min^{-1} \cdot 10\ g\ liver^{-1}$	0.18±0.04	0.21±0.05	0.19±0.02	0.23±0.03*	0.19±0.02	0.20±0.02
R_{pv}, $cmH_2O \cdot ml^{-1} \cdot min^{-1} \cdot 10g\ liver^{-1}$	0.11±0.03	0.11±0.02	0.10±0.01	0.13±0.02*	0.11±0.01	0.12±0.02
R_{hv}, $cmH_2O \cdot ml^{-1} \cdot min^{-1} \cdot 10\ g\ liver^{-1}$	0.08±0.02	0.10±0.02	0.09±0.01	0.10±0.01	0.08±0.01	0.08±0.01
Bile flow, $g \cdot min^{-1} \cdot 10\ g\ liver^{-1}$	0.03±0.01	0.03±0.01	0.03±0.01	0.02±0.01	0.03±0.01	0.02±0.01

Values are means ± SD; n, no. of animals. L-NAME, N^G-nitro-L-arginine methyl ester; ZnPP, zinc protoporphyrin IX; P_{pv}, P_{hv}, and P_{do}, portal venous, hepatic venous, and double-occlusion pressures, respectively; R_t, R_{pv}, and R_{hv}, total, portal venous, and hepatic venous resistance, respectively. All data were obtained before injection of ovalbumin. After data obtained 10 min after injection of L-NAME or ZnPP for the L-NAME or ZnPP groups, respectively. *$P < 0.05$ vs. baseline for the L-NAME and ZnPP groups.

P_{do}, may account for hepatic congestion, as evidenced by the profound liver weight gain. These findings may indicate that anaphylaxis-induced congestion of liver and upstream splanchnic organs could contribute to a decrease in circulating blood volume and thereby to anaphylactic hypotension in guinea pigs.

It has been shown that there is a species difference between dog and guinea pig in hepatic vessels that constrict preferentially during anaphylaxis; sensitized canine livers show selective postsinusoidal constriction (32), whereas sensitized guinea pig livers show predominant presinusoidal constriction. The mechanism by which such a species difference occurred is not known. However, canine postsinusoidal hepatic veins contain anatomically smooth muscle sphincters in hepatic sublobular veins (4) that could vigorously contract in response to various mediators of anaphylactic reaction, such as histamine (28), thromboxane A_2 (28), and platelet-activating factor (PAF; see Ref. 30). We speculate that receptors of these mediators might be localized predominantly in hepatic sublobular veins, which may account for anaphylaxis-induced selective postsinusoidal venoconstriction in canine livers. In guinea pig livers, the predominant presinusoidal constriction induced by anaphylaxis may be caused by these substances. However, effects of these vasoconstrictors on the segmental vascular resistances of guinea pig livers have not been currently known. In addition, the localization of smooth muscle sphincter is not known in guinea pig livers. Further study is required to identify the chemical mediators responsible for this hepatic anaphylactic venoconstriction.

We studied the modulating effects of NO on basal hepatic vascular tone in blood-perfused guinea pig livers. We found that L-NAME increased basal levels of R_{pv} but not R_{hv}. This finding indicates that endogenous basal production of NO may cause dilatation of primarily the portal side of the guinea pig hepatic vascular bed. These results contrast with the findings on the isolated rat livers perfused with a blood-free solution, in which inhibition of NO did not increase basal vascular tone (25). This discrepancy may be attributed to a difference in the mode of liver perfusion, especially the perfusate. We previously observed that L-NAME increased basal P_{pv} in the blood-perfused rat liver but not in blood-free perfused rat liver, although both rat livers were otherwise perfused in the same manner at a constant flow rate (unpublished observation). In blood-free perfused livers (25), compared with the blood-perfused livers, perfusate viscosity should be lower and thereby vascular resistance lower, which might generate only small shear stress and thus low levels of NO produced. This might account for a negligible role of NO in maintenance of basal vascular tone in blood-free perfused livers (25).

Synthesis of NO is stimulated during anaphylaxis (13). Indeed, inhibition of NO synthesis aggravates anaphylactic constriction of regional vasculature, such as coronary artery (27) and pulmonary circulation (23). We herein showed that NO inhibition pronounced hepatic anaphylactic venoconstriction. The exact mechanism for an activation of NO synthesis during hepatic anaphylaxis remains unclear. However, we assume that both effects of chemical mediators and shear stress could explain the increased NO production during hepatic anaphylaxis in this study. Indeed, most mediators of anaphylaxis, such as histamine (11, 14), leukotrienes (21), thromboxane A_2 (14), and PAF (8), all stimulate NO release from the vascular endothelium. Another possibility is related to venoconstriction-induced shear stress, which could generate NO from endothelium (10). In this respect, Macedo and Lautt (16) reported, using in situ cat liver administered norepinephrine, that L-NAME potentiated venoconstriction only under constant flow perfusion, where shear stress could increase, but not under constant pressure perfusion, where shear stress could not increase. In the present study, the hepatic perfusion flow was held constant during venoconstriction, and thus shear stress could have increased, resulting in increased NO release.

CO could serve as a vasodilator and is endogenously generated by hepatocytes via the constitutively expressed HO-2 (26). In the present study, inhibition of CO synthesis by ZnPP did not significantly alter either the basal hepatic vascular pressures or the anaphylactic hepatic venoconstriction, indicating that CO does not modulate hepatic circulation at basal levels or during anaphylaxis in isolated blood-perfused guinea pig livers. The former finding is not consistent with that on the isolated rat livers perfused with a blood-free solution, in which inhibition of CO increased basal vascular tone (25). No apparent action of CO on basal hepatic vascular tone in the present study might be attributed possibly to perfusate free Hb released through hemolysis. It is reported that oxyhemoglobin, oxygenated Hb, inhibits the action of CO (1, 9, 26, 29). The Masterflex roller pump used in the present study should have caused inevitable hemolysis, resulting in release of free Hb in the perfusate. This free Hb might have trapped CO, resulting in

prevention of the CO action. However, our preliminary study revealed that the perfusate Hb concentration measured at 10 min after baseline measurement, when effects of ZnPP on basal hepatic circulation were evaluated, was only 17.6 ± 4.4 mg/dl (2.6 ± 0.6 μM, $n = 7$). Moreover, at 120 min after antigen, the end of the experimental period, the perfusate Hb concentration (61.9 ± 12.6 mg/dl; 9.1 ± 1.9 μM) does not seem to reach the levels enough to inhibit the CO action, because the biological action of CO can be blocked by oxyhemoglobin at concentrations of 25–100 μM (1, 9, 26, 29). However, exact concentrations of Hb are not well known to exert inhibitory effects on CO action in the perfused guinea pig livers. We cannot exclude the possibility that hemolysis might affect the results of the present study.

No substantial effects of CO on hepatic anaphylactic venoconstriction contrast with recent reports that circulatory shock, such as endotoxemia (3) and hemorrhagic shock (2), induced HO-1 in the liver, which results in attenuation of the increased hepatic vascular resistance. It seems likely that CO might not modulate hepatic circulation if it could not be generated substantially by inducible HO-1 under stressful perturbations. In the present study, we only observed an acute short phase of anaphylaxis, in which HO-1 could not have been induced because it takes more than several hours to induce HO-1 after oxidative stress (2, 3).

In this study, liver weight gain was observed after antigen in all groups except the nonsensitized group. This weight gain might be caused by hepatic venoconstriction, as evidenced by a significant increase in R_{hv}. This postsinusoidal contraction could induce the upstream sinusoidal engorgement and increased extravascular fluid filtration caused by an increase in P_{do}, the sinusoidal hydrostatic pressure. In the L-NAME group, P_{do} after antigen increased to the highest levels among all groups, which indicates that the hepatic microvascular driving pressure for extravascular filtration was also highest. This assumption may account for the marked liver weight gain in the L-NAME group.

We found that the bile flow transiently decreased during hepatic anaphylaxis. The mechanism for this cholestasis is not known from the present study. This cholestasis could be caused by venoconstriction, which often causes the heterogeneous perfusion, resulting in partial anoxia and finally cholestasis. Actually reduced bile flow in the present study was dependent on venoconstriction in that in the L-NAME group where the antigen-induced increase in R_t was greatest among groups studied, the decrease in bile flow was also greatest. The direct effect of chemical mediators released during anaphylaxis on the bile-producing system might contribute to cholestasis in the present study.

The limitation of the present study is related to the use of a constant-flow portal perfusion with diluted, recirculating blood. Hepatic arterial perfusion with normally oxygenated blood would improve the metabolic milieu of the liver. With perfusion at prevailing arterial pressures, the large increase in R_{pv} would markedly reduce total hepatic blood flow and change the magnitude of the responses to NO. If the blood flow had not been constant, the 46% increase in liver weight with anaphylaxis and L-NAME would have been less. Another shortcoming is related to the perfusate, which included a foreign protein of bovine albumin for oncotic pressure control. However, the bovine albumin is routinely used as perfusate for a variety of isolated perfused organ studies. We believe that it might not substantially affect the results of the present study.

In summary, this study demonstrated that the hepatic vascular anaphylaxis in guinea pig isolated perfused liver is characterized by hepatic congestion caused by increases in postsinusoidal resistance (R_{hv}) and the sinusoidal pressure (P_{do}). The large increase in presinusoidal resistance (R_{pv}) is the primary cause of splanchnic bed congestion that leads to the serious reduction of circulating volume in anaphylactic shock. Finally, blocking NO, but not CO, increases basal tone and potentiates the anaphylaxis-induced hepatic congestion by acting mainly on the postsinusoidal vessels of guinea pig livers.

ACKNOWLEDGMENTS

We thank Dr. Keishi Kubo, Professor and Chairman of the First Department of Medicine, Shinshu University School of Medicine, for substantial suggestions and discussion on this study.

GRANTS

This research was supported by a Grant for Collaborative Research (C2003–1) and a Grant for Specially Promoted Research, from Kanazawa Medical University and Grant-in-Aid for Scientific Research No. 15591665 from the Ministry of Education, Culture, Sports, Sciences, and Technology of Japan.

REFERENCES

1. **Alkadhi KA, Al-Hijailan RS, Malik K, and Hogan YH.** Retrograde carbon monoxide is required for induction of long-term potentiation in rat superior cervical ganglion. *J Neurosci* 21: 3515–3520, 2001.
2. **Bauer M, Pannen BH, Bauer I, Herzog C, Wanner GA, Hanselmann R, Zhang JX, Clemens MG, and Larsen R.** Evidence for a functional link between stress response and vascular control in hepatic portal circulation. *Am J Physiol Gastrointest Liver Physiol* 271: G929–G935, 1996.
3. **Choi AM and Alam J.** Heme oxygenase-1: function, regulation and implication of a novel stress-inducible protein in oxidant-induced lung injury. *Am J Respir Cell Mol Biol* 15: 9–19, 1996.
4. **Ekataksin W and Kaneda K.** Liver microvascular architecture: an insight into the pathophysiology of portal hypertension. *Semin Liver Dis* 19: 359–382, 1999.
5. **Enjeti S, Bleecker ER, Smith PL, Rabson J, Permutt S, and Traystman RJ.** Hemodynamic mechanism in anaphylactic shock. *Circ Shock* 11: 297–309, 1983.
6. **Furchgott RF and Jothianandan D.** Endothelium-dependent and -independent vasodilation involving cyclic GMP: relaxation by nitric oxide, carbon monoxide and light. *Blood Vessels* 28: 52–61, 1991.
7. **Hines KL and Fisher RA.** Regulation of hepatic glycogenolysis and vasoconstriction during antigen-induced anaphylaxis. *Am J Physiol Gastrointest Liver Physiol* 262: G868–G877, 1992.
8. **Kamata K, Mori T, Shigenobu K, and Kasuya Y.** Endothelium-dependent vasodilator effects of platelet activating factor on rat resistance vessels. *Br J Pharmacol* 98: 1360–1364, 1989.
9. **Kyokane T, Norimizu S, Taniai H, Yamaguchi T, Takeoka S, Tsuchida E, Naito M, Nimura Y, Ishimura Y, and Suematsu M.** Carbon monoxide from heme catabolism protects against hepatobiliary dysfunction in endotoxin-treated rat liver. *Gastroenterology* 120: 1227–1240, 2001.
10. **Lamontagne D, Pohl U, and Busse R.** Mechanical deformation of vessel wall and shear stress determine the basal release of endothelium-derived relaxing factor in the intact rabbit coronary vascular bed. *Circ Res* 70: 123–130, 1992.
11. **Lamparter B, Gross SS, and Levi R.** Nitric oxide and the cardiovascular actions of histamine. *Agents Actions (Special Conference Issue)*: C187–C190, 1992.
12. **Ling Y-Q, Shibamoto T, Honda T, Kamikado C, Hironaka E, Hongo M, and Koyama S.** Increased sinusoidal pressure is associated with early liver weight gain in ischemia-reperfusion injury in isolated perfused rat liver. *J Surg Res* 88: 70–77, 2000.
13. **Levi R.** Cardiac anaphylaxis: models, mediators, mechanisms and clinical considerations. In: *Human Inflammatory Disease, Clinical Immunology*, edited by Marone G, Lichtenstein LM, Condorelli M, and Fauci AS. Toronto, Canada: Decker, 1988, p. 93–105.

14. **Levi R, Gross SS, Lamparter B, Fasehun OA, Aisaka K, Jaffe EA, Griffith OW, and Stuehr DJ.** Evidence that L-arginine is the biosynthetic precursor of vascular and cardiac nitric oxide. In: *Nitric Oxide from L-Arginine: A Bioregulatory System*, edited by Moncada S and Higgs EA. Amsterdam, Netherlands: Elsevier, 1990, p. 35–45.
15. **Maass-Moreno R and CF Rothe.** Distribution of pressure gradients along hepatic vasculature. *Am J Physiol Heart Circ Physiol* 272: H2826–H2832, 1997.
16. **Macedo MP and Lautt WW.** Shear-induced modulation of vasoconstriction in the hepatic artery and portal vein by nitric oxide. *Am J Physiol Gastrointest Liver Physiol* 274: G253–G260, 1998.
17. **Manwaring WH.** The physiological mechanism of anaphylactic shock. *Bull Johns Hopkins Hosp* 21: 275–277, 1910.
18. **Mittal M, Gupta TK, Lee F-Y, Sieber CC, and Groszmann RJ.** Nitric oxide modulates hepatic vascular tone in normal rat liver. *Am J Physiol Gastrointest Liver Physiol* 267: G416–G422, 1994.
19. **Moncada S, Palmer RM, and Higgs EA.** Nitric oxide: physiology, pathophysiology, and pharmacology. *Pharmacol Rev* 43: 109–142, 1991.
20. **Osada S, Ichiki H, Oku H, Ishiguro k, Kunimoto M, and Semma M.** Participation of nitric oxide in mouse anaphylactic hypotension. *Eur J Pharmacol* 252: 347–350, 1994.
21. **Sakuma I, Gross S, and Levi R.** Peptidoleukotrienes induce an endothelium-dependent relaxation of guinea pig main pulmonary artery and thoracic aorta. *Prostaglandins* 34: 685–696, 1987.
22. **Shibamoto T, Wang H-G, Miyahara T, Tanaka S, Haniu H, and Koyama S.** Pre-sinusoidal vessels predominantly contract in response to norepinephrine, histamine, and KCl in rabbit liver. *J Appl Physiol* 87: 1404–1412, 1999.
23. **Shibamoto T, Wang H-G, Tanaka S, Miyahara T, and Koyama S.** Participation of nitric oxide in the sympathetic response to anaphylactic hypotension in anesthetized dogs. *Neurosci Lett* 212: 99–102, 1996.
24. **Soreide E, Buxrud T, and Harboe S.** Severe anaphylactic reactions outside hospital: etiology, symptoms and treatment. *Acta Anaesthesiol Scand* 32: 339–442, 1988.
25. **Suematsu M, Goda N, Sano T, Kashiwagi S, Egawa T, Shinoda Y, and Ishimura Y.** Carbon monoxide: an endogenous modulator of sinusoidal tone in the perfused rat liver. *J Clin Invest* 96: 2431–2437, 1995.
26. **Suematsu M and Ishimura Y.** The heme oxygenase-carbon monoxide system: a regulator of hepatobiliary function. *Hepatology* 31: 3–6, 2000.
27. **Thelen KI, Dembinska-Kiec A, Pallapies D, Simmet T, and Peskar BA.** Effect of 3-morpholinosydnonimine (SIN-1) and N^G-nitro-L-arginine (NNA) on isolated perfused anaphylactic guinea-pig hearts. *Naunyn Schmiedebergs Arch Pharmacol* 345: 93–99, 1992.
28. **Urayama H, Shibamoto T, Wang HG, and Koyama S.** Thromboxane A2 analogue contracts predominantly the hepatic veins in isolated canine liver. *Prostaglandins* 52: 484–495, 1996.
29. **Vannacci A, Baronti R, Zagli G, Marzocca C, Pierpaoli S, Bani D, Passani MB, Mannaioni PF, and Masini E.** Carbon monoxide modulates the response of human basophils to FcεRI stimulation through the heme oxygenase pathway. *Eur J Pharmacol* 465: 289–297, 2003.
30. **Wang HG, Shibamoto T, and Koyama S.** Effect of platelet-activating factor on hepatic capillary pressure in isolated dog liver. *Prostaglandins Leukot Essent Fatty Acids* 57: 293–298, 1997.
31. **Weil R.** Studies in anaphylaxis. XXI. Anaphylaxis in dogs: a study of the liver in shock and peptone poisoning. *J Immunol* 2: 525–556, 1917.
32. **Yamaguchi Y, Shibamoto T, Hayashi T, Saeki Y, and Tanaka S.** Hepatic vascular response to anaphylaxis in isolated liver. *Am J Physiol Regul Integr Comp Physiol* 267: R268–R274, 1994.

Acta Physiol Scand 2004, 180, 255–263

Different hepatic vascular response to noradrenaline and histamine between guinea-pig and rat

T. Shibamoto,[1] M. Narushima,[2] Y.-Q. Ling,[3] T. Shimo,[1,4] H. Tsuchida,[4] Y. Kurata[1] and T. Ogura[1]

1 *Department of Physiology, Kanazawa Medical University, Uchinada, Japan*
2 *Department of Anaesthesiology, Tokyo Women's Medical University, School of Medicine, Kawadacho, Japan*
3 *Department of Surgery, Hebei Medical University, Hebei, China*
4 *Department of Anaesthesiology, Kanazawa Medical University, Uchinada, Japan*

Received 6 June 2003,
accepted 6 October 2003
Correspondence:
Dr T. Shibamoto, Department of Physiology, Division 2, Kanazawa Medical University, Uchinada 920-0293, Japan.

Abstract

Aim: Hepatic xenotransplantation from guinea-pig to rat has not been established. This failure is partly ascribed to differences in hepatic vascular characteristics between two species. However, the differences in hepatic vascular resistance distribution and responses to vasoconstrictors are not known. The present study was designed to determine basal levels of segmental vascular resistances and the responses to histamine and noradrenaline in isolated guinea-pig and rat livers.

Methods: The livers were haemoperfused (Hct 8.3%) via the portal vein at a constant flow. The sinusoidal pressure was measured by the double occlusion pressure, and was used to determine the pre- (R_{pre}) and post-sinusoidal (R_{post}) resistances.

Results: There was no significant difference in basal total hepatic vascular resistance (R_t) between two species, whereas R_{pre} in rat (69% of R_t) was significantly greater than that in guinea-pig (61% of R_t). The responses to noradrenaline were similar; R_{pre} increased in a greater magnitude than R_{post}, and liver weight was reduced. However, the noradrenaline-induced increase in R_t was greater in rats than in guinea-pigs. In contrast, histamine increased predominantly R_{post} over R_{pre}, and increased liver weight in guinea-pig, while it affected no haemodynamic variables in rat.

Conclusion: There exist species differences in the hepatic vasculature between rat and guinea-pig. Basal pre-sinusoidal resistance in rat is greater than that in guinea-pig. Although noradrenaline predominantly contracts pre-sinusoidal vessels in both species, histamine causes predominant post-sinusoidal vasoconstriction in guinea-pig liver, while it has no vasoactive effects on rat liver.

Keywords double occlusion pressure, guinea-pig, hepatic circulation, isolated perfused liver, rat, sinusoidal pressure, species difference, xenotransplantation.

Hepatic xenotransplantation from guinea-pig to rat was not successfully performed as reflected by poor graft reperfusion. One of the reasons for this failure could be ascribed to the differences in the characteristics and vasoreactivity of hepatic vessels between guinea-pigs and rats (Delriviere *et al.* 1998). Delriviere *et al.* (1998) proposed that the hypoperfusion might be related to anatomical and physiological differences between these two species, on the basis of the absence of hyperacute rejection in the graft liver as examined morphologically. They emphasized that guinea-pig portal vein branches have muscular walls susceptible to spasm, and portal blood flow is four times greater in guinea-pig than in rat because the guinea-pig intestine is both longer (two

times as long) and of greater diameter. However, further detail investigation has not been reported on the physiological differences in hepatic haemodynamics such as vascular resistance, its distribution and vascular responsiveness between guinea-pig and rat.

There are species differences in distribution of the hepatic vascular resistance. In canine livers, the pre-sinusoidal resistance comprises approximately 50% of the total liver vascular resistance (Yamaguchi *et al.* 1994), while it comprises 59% in rabbit livers (Wang *et al.* 1997b, Shibamoto *et al.* 1999), and more than 60% in rat livers (Bohlen *et al.* 1991, Ling *et al.* 2000). However, the basal hepatic vascular resistance distribution of guinea-pig liver is not known.

There are also species differences in the primary site of hepatic vasoconstriction. We have recently shown, using vascular occlusion methods for measurement of the hepatic sinusoidal pressure (Yamaguchi *et al.* 1994, Shibamoto *et al.* 1996), that the hepatic longitudinal vascular responsiveness differs depending on vasoconstrictive substances in isolated perfused canine livers (Yamaguchi *et al.* 1994, Shibamoto *et al.* 1996, Urayama *et al.* 1996, Wang *et al.* 1997a). Histamine (Shibamoto *et al.* 1996, Urayama *et al.* 1996) and the thromboxane A_2 analogue (Urayama *et al.* 1996) predominantly contract canine hepatic veins with resultant hepatic congestion, whereas noradrenaline constricts pre-sinusoidal vessels more vigorously than post-sinusoidal vessels with reduction of liver weight (Shibamoto *et al.* 1996). However, acetylcholine (Shibamoto *et al.* 1996) and platelet-activating factor (Wang *et al.* 1997a) constrict both of pre- and post-sinusoidal vessels in a similar magnitude. In contrast, in rabbit livers, pre-sinusoidal vessels predominantly contract in response to endothelin-1 (Wang *et al.* 1997b), noradrenaline, histamine and KCl (Shibamoto *et al.* 1999). However, effects of vasoconstrictors have not been determined on hepatic vascular resistance distribution in guinea-pig. In addition, only a limited number of studies reported the hepatic vascular responsiveness of rat liver (Bohlen *et al.* 1991). Currently there is no systematic study on the differences in the characteristics and vasoreactivity of hepatic vessels between guinea-pig and rat.

Therefore, we herein determined the basal hepatic vascular resistance distribution, and effects of histamine and noradrenaline on segmental vascular resistances in livers, which were isolated from weight-matched guinea-pigs and rats, and were perfused in the same manner. The reason for adopting these two substances as the vasoconstrictors in the present study was that noradrenaline (Bohlen *et al.* 1991, Shibamoto *et al.* 1996, Rothe & Maass-Moreno 1998, 2000) and histamine (Mahfouz & Geumei 1967, Lautt & Legare 1987, Shibamoto *et al.* 1996, Urayama *et al.* 1996, Rothe & Maass-Moreno 1998) predominantly constrict pre- and post-sinusoidal vessels, respectively, in canine and rabbit livers. In addition, histamine could be released during liver transplantation and thereby cause disturbance of hepatic circulation (Lorenz *et al.* 1973, Hansen *et al.* 1988).

Methods

Isolated liver preparation

The study protocol was approved by the Animal Research Committee of Kanazawa Medical University, Uchinada, Japan. Thirteen male Hartley guinea-pigs weighing 312 ± 5 g (SE) and 16 male Sprague–Dawley rats weighing 305 ± 5 g were anaesthetized with pentobarbital sodium (42 mg kg^{-1}, i.v.) and mechanically ventilated with room air. A polyethylene tube was placed in the right carotid artery. After laparotomy, the bile duct was cannulated with a polyethylene tube and the hepatic artery was ligated. At 5 min after intraarterial heparinization (500 U kg^{-1}), 6–8 mL of blood was withdrawn with a plastic syringe through the carotid arterial catheter. The intra-abdominal inferior vena cava (IVC) above the renal veins was ligated, and the portal vein was cannulated with a stainless cannula (2.1 mm ID, 3.0 mm OD for guinea-pig; 1.3 mm ID, 2.1 mm OD for rat) for portal perfusion. After thoracotomy, the supradiaphragmatic IVC was cannulated through a right atrial incision with the same size stainless cannula (2.1 mm ID, 3.0 mm OD), then portal perfusion was begun with the heparinized autologous blood diluted with 5% albumin-Krebs buffer (Hct 8.3%). The liver was rapidly excised, suspended from an electric balance and weighed.

The basic method for liver perfusion was described previously (Shibamoto *et al.* 1999). The liver was perfused at constant flow in a recirculating manner via the portal vein with blood that was pumped using a Masterflex pump from the venous reservoir through a heat exchanger (37 °C). The recirculating blood volume was 40 mL. The height of the reservoir and the blood flow rate could be adjusted independently to maintain the portal and hepatic venous pressures at any desired level. The perfused blood was oxygenated in the reservoir by continuous bubbling with 95% O_2 and 5% CO_2. The portal venous (P_{pv}) and the hepatic venous (P_{hv}) pressures were measured using pressure transducers with the reference points at the hepatic hilus. To measure the double occlusion pressure (P_{do}), two solenoid valves were placed around the perfusion tubes upstream from the P_{pv} sidearm cannula and downstream from the P_{hv} sidearm cannula (Shibamoto *et al.* 1999). Blood flow rate (Q) was measured with an electromagnetic flow meter, the probe of which was positioned in the inflow line. Bile was collected drop by drop in a small tube suspended from the force transducer. The time between drops was measured for

determination of the bile flow rate (Ling *et al.* 2000). The hepatic vascular pressures, blood flow, liver weight and bile flow were monitored continuously and displayed through a thermal physiograph.

Experimental protocol

The animals were randomly selected and used in terms of rat or guinea-pig. Hepatic haemodynamic parameters were observed for at least 20 min after start of perfusion during which an isogravimetric (no liver weight gain or loss) state was reached. After the baseline measurements, the perfused livers were challenged with either of histamine or noradrenaline. In the noradrenaline group (n = 7–12) 0.0068, 0.068, 0.68, 6.8 and 68 μg of noradrenaline (Bitartrate salt; Sigma, St Louis, MO, USA) were injected as a bolus into the portal line, and attained the final perfusate concentration of 0.001, 0.01, 0.1, 1 and 10 μM, respectively. In the histamine group (n = 5–7), 0.4, 4.4, 44.4 and 444 μg of histamine (Sigma) was injected as a bolus into the portal line, and attained the final perfusate concentration of 0.1, 1, 10 and 100 μM, respectively. In rat livers, the high dose of 4 and 40 mg (the final concentration of 1 and 10 mM, respectively) of histamine were also injected. The volume of each agent injected was adjusted to <1 mL. These drugs of noradrenaline and histamine were given in random order, and dose amounts were randomly assigned.

The hepatic sinusoidal pressure was measured by the double occlusion method (Yamaguchi *et al.* 1994, Shibamoto *et al.* 1999). Both the inflow and outflow lines were simultaneously and instantaneously occluded using the solenoid valves, after which P_{pv} and P_{hv} rapidly equilibrated to a similar or identical pressure, which was P_{do}. In each experimental group, P_{do} was measured at baseline and 1, 2, 3, 6,10, 20 and 30 min after an injection of each agent. When low doses of agents were injected, P_{do} was determined only at maximal vasoconstriction.

The total portal–hepatic venous (R_t), pre- (R_{pre}) and post-sinusoidal (R_{post}) resistances were calculated as follows:

$$R_t = (P_{pv} - P_{hv})/Q \quad (1)$$

$$R_{pre} = (P_{pv} - P_{do})/Q \quad (2)$$

$$R_{post} = (P_{do} - P_{hv})/Q \quad (3)$$

Statistics

All results are expressed as the mean ± SEM. Comparisons were made using Student's t-tests. A P-value <0.05 was considered significant.

Results

Comparison of basal haemodynamic variables

The initial wet liver weight was 10.2 ± 0.4 g for guinea-pigs and 8.4 ± 0.1 g for rats. Table 1 shows basal haemodynamic variables of isolated perfused rat and guinea-pig livers. Basal P_{pv} of 7.2 ± 0.3 cmH_2O for guinea-pigs at Q 35 ± 1 mL min^{-1} 10 g^{-1} liver weight was not significantly different from that of 7.3 ± 0.4 cmH_2O for rat at the almost same Q of 36 ± 2 mL min^{-1} 10 g^{-1} liver weight, resulting in no significant difference in basal R_t between two species. In contrast, basal P_{do}, 3.0 ± 0.04 cmH_2O, of guinea-pig was significantly greater than that of rat, 2.4 ± 0.12 cmH_2O. As a result, the segmental vascular resistance of R_{post} was significantly greater in guinea-pig than in rat (0.076 ± 0.004 vs. 0.061 ±0.008 cmH_2O mol^{-1} min^{-1} 10 g^{-1} liver weight). This is reflected by significantly greater values of the R_{post}-to-R_t ratio of guinea-pig, 0.39 ± 0.02, than that of rat,

Table 1 Basal haemodynamic variables of isolated perfused rat and guinea-pig livers

	Rat	Guinea-pig
Number of animals	16	13
Portal pressure (cmH_2O)	7.3 ± 0.4	7.2 ± 0.3
Hepatic venous pressure (cmH_2O)	0.3 ± 0.05	0.3 ± 0.04
Double occlusion pressure (cmH_2O)	2.4 ± 0.12	3.0 ± 0.04*
Portal flow rate (mL min^{-1} 10 g^{-1})	36 ± 2	35 ± 1
Total vascular resistance (cmH_2O mL^{-1} min^{-1} 10 g^{-1})	0.194 ± 0.015	0.196 ± 0.012
Pre-sinusoidal resistance (cmH_2O mL^{-1} min^{-1} 10 g^{-1})	0.133 ± 0.012	0.120 ± 0.009
Post-sinusoidal resistance (cmH_2O mL^{-1} min^{-1} 10 g^{-1})	0.061 ± 0.008	0.076 ± 0.004*
R_{post}-to-R_t ratio	0.31 ± 0.02	0.39 ± 0.02*

Values are given as mean ± SEM. *P < 0.05 vs. rat.

0.31 ± 0.02. The basal bile flow of guinea-pig (0.038 ± 0.004 g min^{-1}) was 2.7-fold greater than that of rat (0.014 ± 0.001 g min^{-1}).

Effects of noradrenaline and histamine on segmental vascular resistances and liver weight

The guinea-pig and rat livers showed qualitatively the same response to noradrenaline, as shown in Figures 1 and 2a. An injection of noradrenaline increased P_{pv}, which peaked 1 min and then gradually returned to the baseline levels within 40 min after injection. After noradrenaline injection, the sinusoidal pressure of P_{do} increased minimally but significantly, and the P_{pv}-to-P_{do} gradient increased in a greater magnitude than the P_{do}-to-P_{hv} gradient, a finding indicating that noradrenaline increased predominantly R_{pre}. Figure 3 shows the peak levels in R_{pre}, R_{post}, R_t, R_{post}-to-R_t ratio, weight change and bile flow after injection of noradrenaline. R_t increased in a dose-dependent manner at 0.1–10 μM, reaching the maximum level of 288 ± 11% of baseline for rat and 245 ± 10% for guinea-pig at 10 μM. The increase in R_{pre} of rat was significantly greater than that of guinea-pig at high concentrations. R_{post} also increased significantly but in a less magnitude than R_{pre}, and therefore the R_{post}-to-R_t ratio decreased dose-dependently to the minimum values of 65 ± 4% of baseline for rat and 71 ± 3% for guinea-pig at 10 μM. Immediately after noradrenaline injection, the liver weight was decreased and then gradually returned to

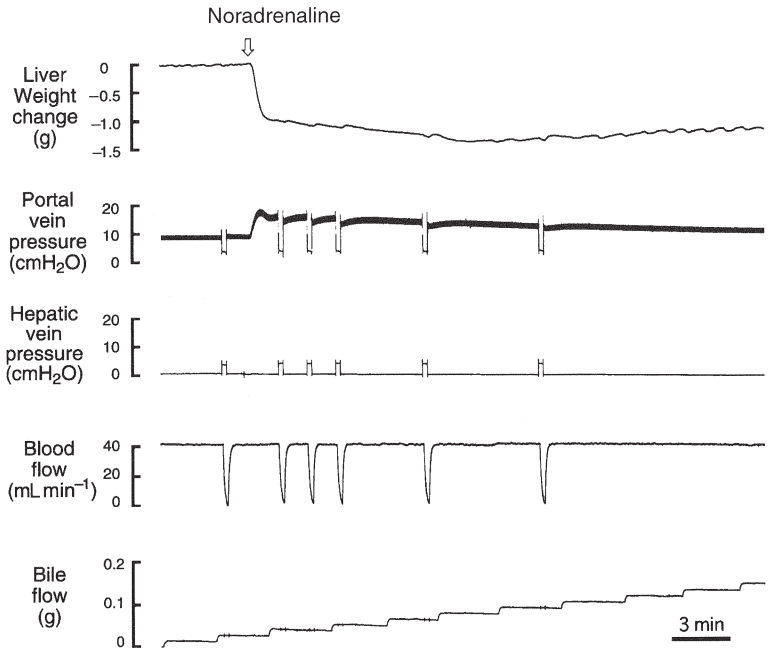

Figure 1 A representative recording of the response to noradrenaline at 1 μM of a rat liver.

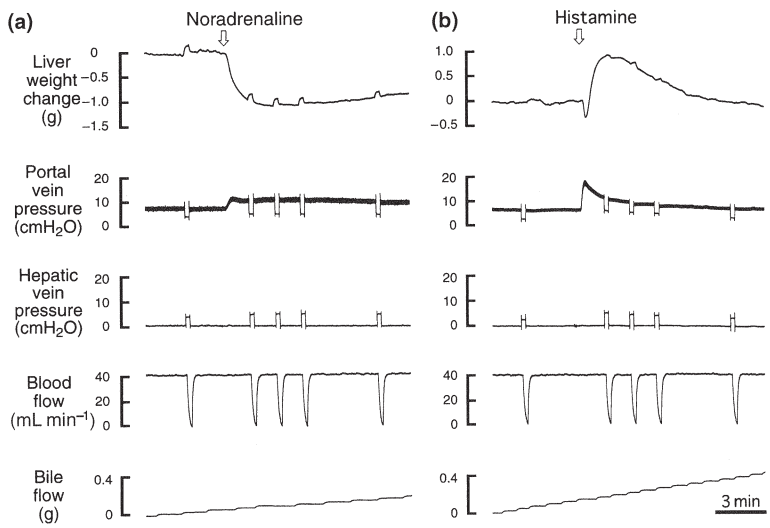

Figure 2 Representative recordings of the responses to noradrenaline at 1 μM (a) and histamine at 100 μM (b) of a guinea-pig liver.

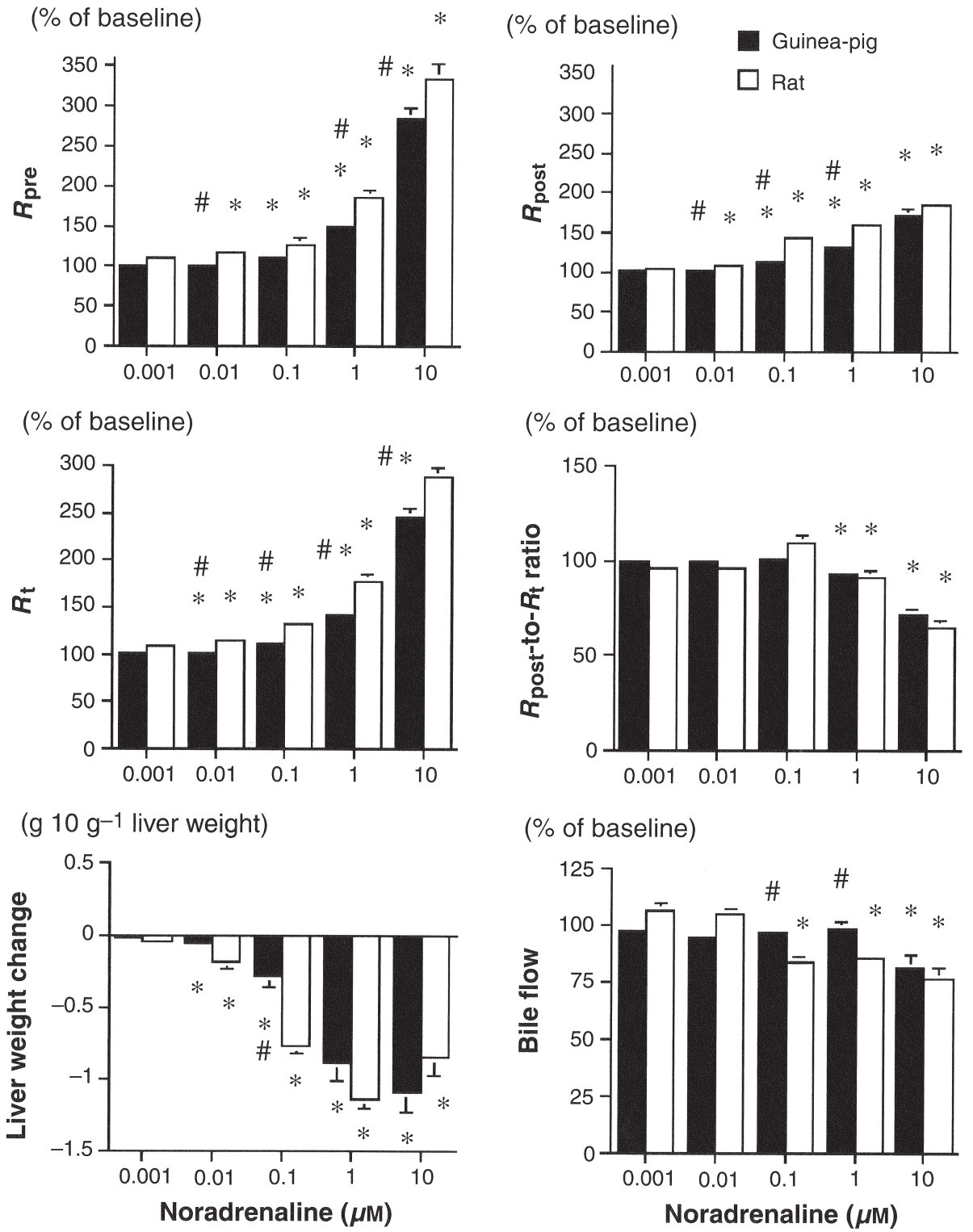

Figure 3 The peak changes in the total (R_t), pre- (R_{pre}) and post-sinusoidal (R_{post}) resistances, the R_{post}-to-R_t ratio, bile flow and liver weight change at 0.001–10 μM of noradrenaline as expressed by percentage of the baseline in guinea-pig and rat livers. Values are given as mean ± SEM. n = 5–7. $^{*}P < 0.05$ vs. the baseline. $^{\#}P < 0.05$ vs. rat.

the baseline, as shown in Figures 1 and 2a. In both species, the liver weight loss after injection of noradrenaline at 1 and 10 μM was approximately 1 g 10 g^{-1} liver weight. The bile flow rate decreased minimally but significantly at a high concentration of 10 μM noradrenaline in both species.

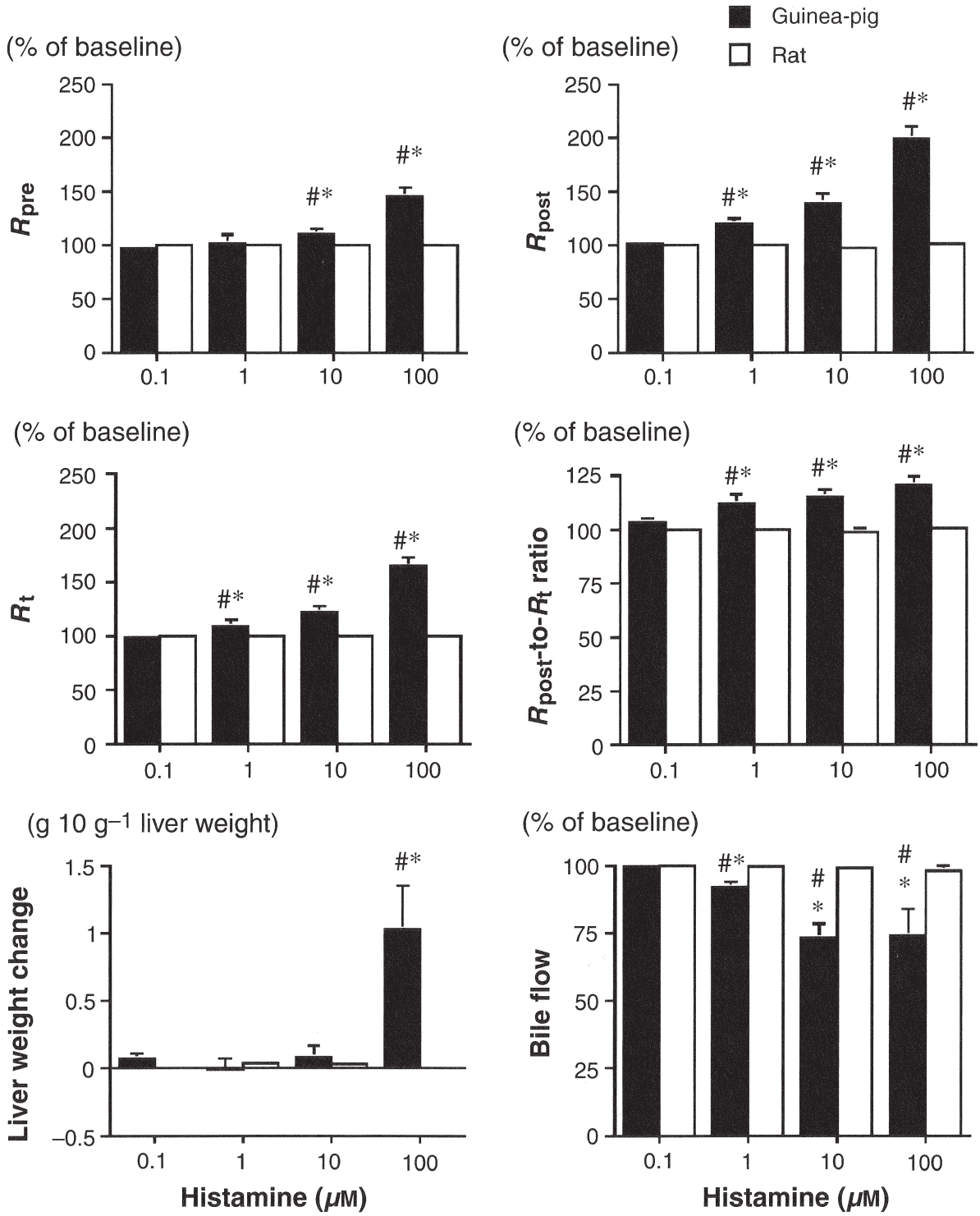

Figure 4 The peak changes in the total (R_t), pre- (R_{pre}) and post-sinusoidal (R_{post}) resistances, the R_{post}-to-R_t ratio, bile flow and liver weight change at 0.1–100 μM of histamine as expressed by percentage of the baseline in guinea-pig livers. The data of rat livers were obtained at 2 min after histamine. Values are given as mean ± SEM. n = 5–7. $^*P < 0.05$ vs. the baseline. $^{\#}P < 0.05$ vs. rat.

Histamine, in contrast to noradrenaline, caused quite different response between guinea-pig and rat. Rat livers showed no significant changes in hepatic haemodynamic variables when histamine at concentration up to 10 mM was used. The data of rat livers obtained 2 min after an injection of histamine (the final concentrations of 0.1–100 μM) were shown in Figure 4. In contrast, in guinea-pig livers, histamine at

concentrations 1–100 μM increased P_{pv} dose-dependently with a substantial increase in P_{do}. Figure 2b shows a response of a guinea-pig liver to histamine at 100 μM, in which P_{do} increased markedly in comparison with the noradrenaline-treated liver (Fig. 2a). This increase in P_{do} resulted in a greater increase in R_{post} than in R_{pre}, as shown in Figure 4. Actually, the R_{post}-to-R_t ratio significantly increased to 120 ± 4% at 100 μM histamine. After injection of histamine at 1 and 10 μM, the liver weight did not change significantly although hepatic vasoconstriction definitely occurred. At the maximum concentration of 100 μM histamine, predominant post-sinusoidal constriction caused hepatic congestion as reflected by liver weight gain by 1.0 ± 0.3 g 10 g^{-1} liver weight, as shown in Figure 2b. Concomitant with hepatic vasoconstriction, bile flow decreased transiently and slightly, but significantly, at histamine 10 and 100 μM.

Discussion

We found two major functional differences in hepatic vasculature between guinea-pig and rat. The first is that basal pre-sinusoidal resistance was more predominant in rat (69% of R_t) than in guinea-pig (61%) although R_t was almost the same. The second difference is related to the response to histamine: histamine caused predominant post-sinusoidal constriction with liver weight gain in guinea-pig, whereas it did not change hepatic haemodynamic variables in rats. In contrast, noradrenaline produced similar responses of predominant pre-sinusoidal constriction with liver weight loss in both species, although the magnitude of pre-sinusoidal constriction was greater in rat than in guinea-pig.

We have recently shown by measuring the sinusoidal pressure using the triple vascular occlusion method (Shibamoto *et al.* 1996) and the double occlusion method (Yamaguchi *et al.* 1994) in isolated canine livers, that R_{post} comprises approximately one-half of R_t. We subsequently demonstrated that 41% of R_t exists in post-sinusoidal vessels in isolated rabbit liver (Wang *et al.* 1997b, Shibamoto *et al.* 1999). This is in agreement with the study of Maass-Moreno & Rothe (1997), who reported that in intact rabbit livers the pressure gradient from the hepatic sinusoids averaged 41 ± 15% of the total P_{pv} to the abdominal vena caval pressure gradient. In the present study, we for the first time demonstrated that the basal hepatic vascular resistance distribution of guinea-pig liver was similar to that of rabbit livers in that R_{post} comprises 39% of R_t. With respect to rat liver, the present study also showed that R_{post} comprised only 31% of R_t. This marked predominance of pre-sinusoidal resistance over post-sinusoidal resistance was previously reported in *in vivo* rat (Bohlen *et al.* 1991) and in isolated rat livers perfused via both the portal vein and hepatic artery (Ling *et al.* 2000).

There are species differences in the hepatic vascular responsiveness. In dog livers, histamine predominantly contracts the post-sinusoidal vessels (Mahfouz & Geumei 1967, Lautt & Legare 1987, Shibamoto *et al.* 1996, Urayama *et al.* 1996), while noradrenaline primarily contracts the pre-sinusoidal vessels rather than the post-sinusoidal vessels (Bohlen *et al.* 1991, Shibamoto *et al.* 1996, Rothe & Maass-Moreno 1998). However, in rabbit livers, histamine, noradrenaline and endothelin-1 all selectively increases R_{pre} (Wang *et al.* 1997b, Shibamoto *et al.* 1999). In the present study, we found that the hepatic vascular responses of guinea-pig to histamine and noradrenaline are similar to those of dog: noradrenaline preferentially constricts the pre-sinusoid, while histamine the post-sinusoid. The difference in the vasoconstrictive site for histamine and noradrenaline might be ascribed, at least in part, to different distribution of functionally active receptors between the pre-sinusoidal vessels and the hepatic veins. In contrast, in the preset study, histamine did not change P_{pv} in rat livers. This is consistent with the findings of Noguchi & Plaa (1970), who reported that an injection of histamine (1–200 μg) had almost no effect on P_{pv} or flow rate of the isolated perfused SD rat livers, whereas the i.v. injection of histamine (1 μg) resulted in a drastic decrease in arterial blood pressure. Indeed, histamine (up to 10^{-4} M) did not contract isolated portal veins of male Wistar rats (Cohen & Wiley 1977, Hogestatt *et al.* 1986). The absence of vasoconstrictive response to histamine in rat liver may be due to lack of functional histamine receptor in rat hepatic vascular smooth muscles.

In the present study, the concentration of histamine required to produce significant hepatic vasoconstriction was 1 μM. The responsiveness of guinea-pig hepatic vessels to histamine seems to be weak in comparison with that to noradrenaline, as the lower concentration of 0.1 μM noradrenaline can induce significant hepatic vasoconstriction as shown in Figure 3. In addition, 100 μM histamine increased R_t only to 1.7-fold baseline, whereas the 10 times lower concentration of 10 μM noradrenaline increased R_t to 2.45-fold baseline. The similar phenomenon was observed in isolated rabbit livers (Shibamoto *et al.* 1999).

It is well known that noradrenaline causes a reduction in liver blood volume in cats (Greenway & Lautt 1972), dogs (Bennett *et al.* 1982, Shibamoto *et al.* 1996), and rabbits (Rothe & Maass-Moreno 1998, Shibamoto *et al.* 1999). In addition, Rothe and colleagues, using the micropipette servo-null pressure measurement technique, has recently demonstrated that the increase in pre-sinusoidal resistance is greater than that in the post-sinusoidal resistance in dogs (Bohlen

et al. 1991), rats (Bohlen *et al.* 1991), and rabbits (Rothe & Maass-Moreno 1998) during noradrenaline infusion. We added new evidence that the similar response to noradrenaline was observed in isolated guinea-pig and rat livers.

In the present study, a decrease in weight accompanied predominant pre-sinusoidal vessel constriction, when noradrenaline was injected in either guinea-pig or rat livers. The mechanism for this decrease in weight cannot be currently clarified. A reduction in unstressed volume of the hepatic venules or even sinusoids will explain the reduction in volume induced by noradrenaline (Greenway & Lautt 1989, Rothe 1993). Another possibility may be related to possible heterogeneous portal venule constriction. If there was heterogeneity in portal venule constriction among the hepatic lobules, that is, some vessels were closed and others open, the blood volume of sinusoids, that was distal to the closed portal venules, could be passively reduced due to a decrease in distending pressure of the sinusoids. Finally, in contrast to the aforementioned passive changes in liver volume, the possibility exists that there are contractile elements in the walls of the hepatic sinusoids that may be stimulated by noradrenaline and endothelin (Kawada *et al.* 1993, Ito *et al.* 1996, Rothe & Maass-Moreno 2000). Rothe & Maass-Moreno (2000) infused noradrenaline into *in vivo* rabbit, and found a decrease in liver volume although P_{pv} and hepatic venule pressure increased. This is a clear proof of an active response, and not a passive response to distending pressure. In contrast, the significant weight gain was observed in the isolated livers injected of the highest dose of histamine in the present study. The liver weight gain may be ascribed to an increase in hepatic intravascular volume due to sufficient vasoconstriction downstream from the compliant sinusoids. Increased extravascular fluid filtration caused by an increase in sinusoidal pressure, P_{do}, may also contribute to this weight gain (Bennett *et al.* 1982).

The present study provides the basic data on the differences in hepatic vessels between guinea-pig and rat, which might contribute to clarifying the mechanism for failure of hepatic xenotransplantation from guinea-pig to rat. Post-sinusoidal vessels of guinea-pig have responsiveness to histamine, and their constriction results in hepatic congestion. Actually, histamine could be released during liver transplantation and thereby lead to disturbance of liver transplantation (Lorenz *et al.* 1973, Hansen *et al.* 1988). We observe that other vasoconstrictors such as platelet-activating factor also cause guinea-pig post-sinusoidal constriction and congestion (unpublished observation). This oedematogenic property of transplanted guinea-pig liver might partly account for hypoperfusion as seen during xenotransplantation from guinea-pig to rat.

Conclusion

By measuring the hepatic sinusoidal pressure with the double occlusion method, we determined the basal vascular resistance distribution and effects of histamine and noradrenaline on the segmental vascular resistances in isolated guinea-pig and rat livers perfused with diluted blood in the same way. Although the basal R_t was found to be the same, the basal R_{post} comprises 39 and 31% of R_t in guinea-pig and rat livers, respectively. Noradrenaline predominantly increased the pre-sinusoidal vascular resistance with liver weight loss in both species. In contrast, histamine predominantly increased the post-sinusoidal resistance with liver weight gain in guinea-pig, but did not produce any significant changes in hepatic haemodynamics in rat livers. These differences in hepatic vascular responsiveness might at least in part lead to the difficulty of hepatic xenotransplantation between these two species.

This work was supported by a Grant for Collaborative Research from Kanazawa Medical University (C2003-1) and a Grant-in-Aid for Scientific Research from the Ministry of Education, Culture, Sports, Sciences and Technology of Japan (No. 15591665).

References

Bennett, T.D., MacAnespie, C.L. & Rothe, C.F. 1982. Active hepatic capacitance responses to neural and humoral stimuli in dogs. *Am J Physiol* **242**, H1000–H1009.

Bohlen, H.G., Maass-Moreno, R. & Rothe, C.F. 1991. Hepatic venular pressures of rats, dogs, and rabbits. *Am J Physiol* **261**, G539–G547.

Cohen, M.L. & Wiley, K.S. 1977. Comparison of arteries with longitudinal and circular venous muscle from the rat. *Am J Physiol* **232**, H131–H139.

Delriviere, L.D., Havaux, X., Gibbs, P. & Gianello, P.R. 1998. Basic anatomical and physiological differences between species should be considered when choosing combinations for use in models of hepatic xenotransplantation. An investigation of the guinea pig-to-rat combination. *Transplantation* **66**, 112–114.

Greenway, C.V. & Lautt, W.W. 1972. Effects of infusions of catecholamines, angiotensin, vasopressin and histamine on hepatic blood volume in the anesthetized cat. *Br J Pharmacol* **44**, 177–184.

Greenway, C.V. & Lautt, W.W. 1989. Hepatic circulation. In: S.G. Schultz, J.D. Wood & B.B. Rauner (eds) *Handbook of Physiology. The Gastrointestinal System. Motility and Circulation*, Section 6, Vol. 1, Part 2, Chapter 41, pp. 1519–1564. American Physiological Society, Bethesda, MD.

Hansen, C.P., Man, W.K., Kirkegaard, P., Jensen, S.L. & Boesby, S. 1988. Changes in plasma histamine during orthotopic liver transplantation in the pig. *Agents Actions* **23**, 348–350.

Hogestatt, E.D., Hammarstrom, L.E., Andersson, K.E. & Holmin, T. 1986. Contractile effects of various vasoactive

agents in small rat portal veins and hepatic arteries and the influence of sympathetic denervation on the noradrenaline response. *Acta Physiol Scand* **128**, 309–315.

Ito, Y., Katori M., Majima, M. & Kakita, A. 1996. Constriction of mouse hepatic venules and sinusoids by endothelins through ETb receptor subtype. *Int J Microcirc Clin Exp* **16**, 250–258.

Kawada, N., Tran-Thi, T., Klein, H. & Decker, K. 1993. The contraction of hepatic stellate (Ito) cells stimulated with vasoactive substances. Possible involvement of endothelin 1 and nitric oxide in the regulation of the sinusoidal tonus. *Eur J Biochem* **213**, 815–823.

Lautt, W.W. & Legare, D.J. 1987. Effect of histamine, norepinephrine, and nerves on vascular pressures in dog liver. *Am J Physiol* **252**, G472–G478.

Ling, Y.-Q., Shibamoto, T., Honda, T. *et al.* 2000. Increased sinusoidal pressure is associated with early liver weight gain in ischemia–reperfusion injury in isolated perfused rat liver. *J Surg Res* **88**, 70–77.

Lorenz, W., Hell, E., Boeckl, O. *et al.* 1973. Histamine release during orthotopic homologous liver transplantation in pigs. *Eur Surg Res* **5**, 11–20.

Maass-Moreno, R. & Rothe, C.F. 1997. Distribution of pressure gradients along hepatic vasculature. *Am J Physiol* **272**, H2826–H2832.

Mahfouz, M. & Geumei, A. 1967. Pharmacodynamic of intrahepatic circulation in shock. *Surgery* **61**, 755–762.

Noguchi, Y. & Plaa, G.L. 1970. Effect of acetylcholine, serotonin and histamine on the hemodynamics on the isolated perfused rat liver. *Arch Int Pharmacodyn* **188**, 312–319.

Rothe, C.F. 1993. Mean circulatory filling pressure: its meaning and measurement. *J Appl Physiol* **74**, 499–509.

Rothe, C.F. & Maass-Moreno, R. 1998. Hepatic venular resistance responses to norepinephrine, isoproterenol, adenosine, histamine, and ACh in rabbits. *Am J Physiol* **274**, H777–H785.

Rothe, C.F. & Maass-Moreno, R. 2000. Active and passive liver microvascular responses from angiotensin, endothelin, norepinephrine, and vasopressin. *Am J Physiol* **279**, H1147–H1156.

Shibamoto, T., Wang, H.-G., Tanaka, S. & Koyama, S. 1996. Hepatic capillary pressure is estimated using triple vascular occlusion method in isolated canine liver. *Am J Physiol* **271**, R1130–R1141.

Shibamoto, T., Wang, H.-G., Miyahara, T., Tanaka, S., Haniu, H. & Koyama, S. 1999. Presinusoidal vessels predominantly contract in response to norepinephrine, histamine, and KCl in rabbit liver. *J Appl Physiol* **87**, 1404–1412.

Urayama, H., Shibamoto, T., Wang, H.-G. & Koyama, S. 1996. Thromboxane A_2 analogue contracts predominantly the hepatic veins in isolated canine liver. *Prostaglandins* **52**, 483–495.

Wang, H.-G., Shibamoto, T. & Koyama, S. 1997a. The effect of platelet-activating factor on hepatic capillary pressure in isolated dog liver. *Prostaglandins Leukot Essent Fatty Acids* **57**, 293–298.

Wang, H.-G., Shibamoto, T. & Miyahara, T. 1997b. Endothelin-1 selectively contracts portal vein through ETA- and ETB-receptors in isolated rabbit liver. *Am J Physiol* **273**, G1036–G1043.

Yamaguchi, Y., Shibamoto, T., Hayashi, T., Saeki, Y. & Tanaka, S. 1994. Hepatic vascular response to anaphylaxis in isolated liver. *Am J Physiol* **267**, R268–R274.

Am J Physiol Heart Circ Physiol 287: H1786–H1791, 2004;
10.1152/ajpheart.01143.2003.

Ischemic preconditioning and morphine attenuate myocardial apoptosis and infarction after ischemia-reperfusion in rabbits: role of δ-opioid receptor

Shinji Okubo,[1] Yujirou Tanabe,[1] Kenji Takeda,[1] Michihiko Kitayama,[1] Seiyu Kanemitsu,[1] Rakesh C. Kukreja,[2] and Noboru Takekoshi[1]

[1]*Department of Cardiology, Kanazawa Medical University, Ishikawa 920-0293, Japan; and* [2]*Division of Cardiology, Department of Medicine, Virginia Commonwealth University Medical Center, Richmond, Virginia 23298*

Submitted 4 December 2003; accepted in final form 1 June 2004

Okubo, Shinji, Yujirou Tanabe, Kenji Takeda, Michihiko Kitayama, Seiyu Kanemitsu, Rakesh C. Kukreja, and Noboru Takekoshi. Ischemic preconditioning and morphine attenuate myocardial apoptosis and infarction after ischemia-reperfusion in rabbits: role of δ-opioid receptor. *Am J Physiol Heart Circ Physiol* 287: H1786–H1791, 2004; 10.1152/ajpheart.01143.2003.—We examined whether ischemic preconditioning (IPC) attenuates ischemia-reperfusion injury, in part, by decreasing apoptosis and whether the δ-opioid receptor (DOR) plays a pivotal role in the regulation of apoptosis. Rabbits were subjected to 30-min coronary artery occlusion (CAO) and 180 min of reperfusion. IPC was elicited with four cycles of 5-min ischemia and 10-min reperfusion before CAO. Morphine (0.3 mg/kg iv) was given 15 min before CAO. Naloxone (Nal; 10 mg/kg iv) and naltrindole (Nti; 10 mg/kg iv), the respective nonselective and selective DOR antagonists were given 10 min before either morphine or IPC. Infarct size (%risk area) was reduced from 46 ± 3.8 in control to 11.6 ± 1.0 in IPC and 19.5 ± 3.8 in the morphine group (means ± SE; $P < 0.001$ vs. control). Nal blocked the protective effects of IPC and morphine, as shown by the increase in infarct size to 38.6 ± 7.2 and 44.5 ± 1.8, respectively. Similarly, Nti blocked IPC and morphine-induced protection. The percentage of apoptotic cells (revealed by terminal deoxynucleotidyl transferase-mediated dUTP nick-end labeling assay) decreased in IPC (3.6 ± 1.9) and morphine groups (5.2 ± 1.2) compared with control group (12.4 ± 1.6; $P < 0.001$). Nti pretreatment increased apoptotic cells 11.2 ± 2.2% in IPC and 12.1 ± 0.8% in morphine groups. Nal failed to block inhibition of apoptosis in the IPC group (% of cells: 5.7 ± 1.3 vs. 3.6 ± 1.9 in IPC alone; $P > 0.05$). These results were also confirmed by nucleosomal DNA laddering pattern. We conclude that IPC reduces lethal injury, in part, by decreasing apoptosis after ischemia-reperfusion and activation of the DOR may play a crucial role in IPC or morphine-induced myocardial protection.

reperfusion injury

IT IS WELL KNOWN THAT APOPTOSIS plays an important role in the myocyte cell death after heart failure as well as ischemia-reperfusion (I/R). In vivo studies have demonstrated cardiomyocyte apoptosis during postnatal maturation (19), spontaneous hypertension in rats (14), rapid ventricular pacing (22), and microembolization-induced cardiac failure (35). Apoptosis has been documented in ischemic rat myocardium beginning 2 h after ischemia (18). In addition, extensive cardiomyocyte apoptosis was also observed in reperfused rabbit (12) and rat (3) hearts as well as in myocardial autopsy tissue death from acute myocardial infarction (17). Gottlieb et al. (12) and Fliss and Gattinger (5) showed that cell death during ischemia is mainly necrotic, whereas damage induced by reperfusion caused additional cell death principally through apoptosis.

Previous studies (2, 24, 30) have shown that ischemic preconditioning (IPC) markedly reduces necrosis in the heart. IPC also decreases internucleosomal DNA fragmentation in rat hearts in vivo, and there was a direct correlation between myocardial infarct size and DNA fragmentation after IPC (29). IPC has been shown to attenuate processing and activation of caspase-1 and caspase-3, and cleavage of poly(ADP-ribose) polymerase after prolonged ischemia and reperfusion in the heart (28). IPC is primarily mediated by activation of several triggers, including free radicals, adenosine, catecholamines, and bradykinin (reviewed in Ref. 26). In addition, studies from Gross's laboratory (13) have shown that opioids play an important role in IPC against myocardial infarction. The nonselective and selective opioid receptor antagonists, naloxone (Nal) and naltrindole (Nti), respectively, have been shown to completely block the infarct-limiting effect of IPC in rats (31), rabbits (21), and pigs (34). Similarly, the nonpeptide opioid agonist morphine mimicked IPC in the rat heart (32), which was abrogated by Nal, suggesting the role of opioid receptors in cardioprotection. Because opioid receptor signaling has been identified as the integral components of the cardioprotective effect of IPC (13), we hypothesized that this pathway may also regulate apoptosis during IPC. Accordingly, the major goal of this study was to show whether the inhibition of apoptosis and necrosis after IPC is mediated by activation of the δ-opioid receptor. A second goal was to show whether pharmacological preconditioning achieved by infusion of morphine also induces anti-apoptotic effect through δ-opioid receptor in the rabbit heart after I/R.

MATERIALS AND METHODS

All procedures were performed in conformance with the *Guide for the Care and Use of Laboratory Animals* (NIH Publication No. 85-23, Revised 1985).

Experimental groups and protocol. Ninety-two male New Zealand White rabbits (2.5–3.2 kg body wt) were used in this study. All rabbits underwent 30-min coronary artery occlusion (CAO) and 180 min of I/R, as shown in Fig. 1. The animals were randomized into the following eight groups: *1*) control ($n = 12$), in which no treatment was given; *2*) Nal control ($n = 10$), in which rabbits were treated with a nonspecific blocker of opioid receptor Nal (10 mg/kg iv) 10 min before I/R; *3*) Nti control ($n = 10$), where rabbits were treated with a selective blocker of the δ-opioid receptor Nti (10 mg/kg iv) 10 min before I/R; *4*) the preconditioning group (IPC; $n = 12$), where the IPC

Address for reprint requests and other correspondence: S. Okubo, Dept. of Cardiology, Kanazawa Medical Univ., 1-1 Daigaku, Uchinada, Kahoku, Ishikawa 920-0293, Japan (E-mail: shinkubo@kanazawa-med.ac.jp).

The costs of publication of this article were defrayed in part by the payment of page charges. The article must therefore be hereby marked "*advertisement*" in accordance with 18 U.S.C. Section 1734 solely to indicate this fact.

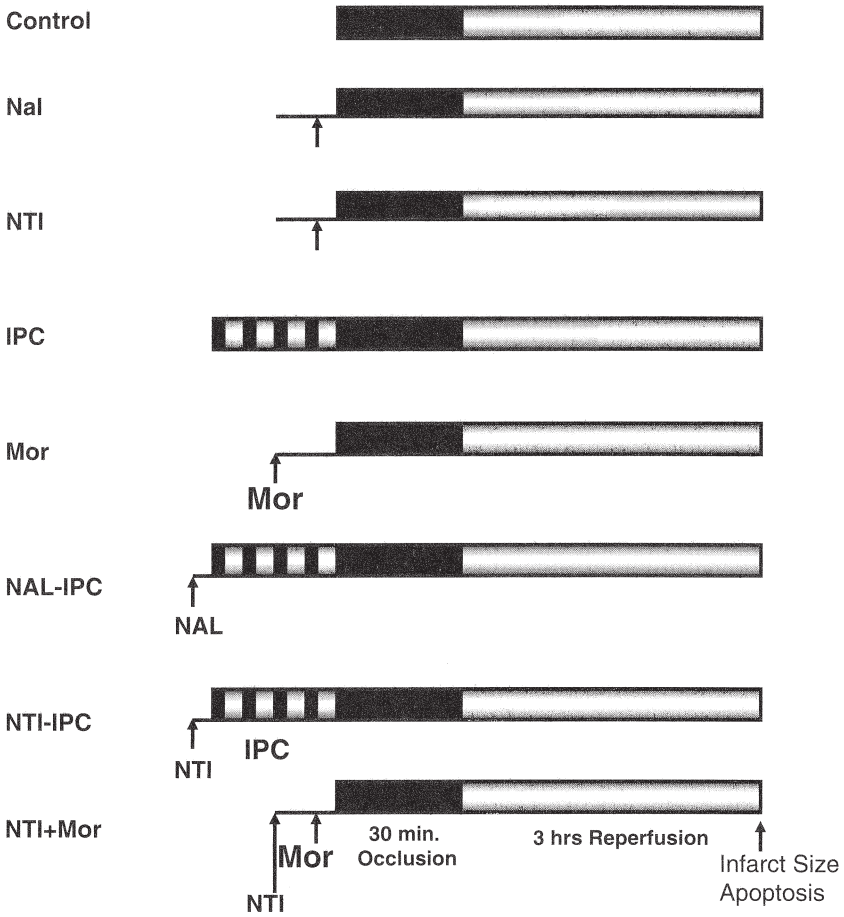

Fig. 1. Experimental protocol showing ischemic preconditioning (IPC), ischemia-reperfusion, and treatment schedules of morphine (Mor) and other inhibitors of opioid receptors. Nal, naloxone; Nti, naltrindole.

protocol consisted of four 5-min occlusions, each separated by 10-min reperfusion; *5*) morphine (Mor, 0.3 mg/kg, $n = 12$) was injected at a dose of 0.3 mg/kg iv 15 min before sustained ischemia; *6*) Nal+IPC ($n = 12$), where rabbits were treated with Nal (10 mg/kg iv) 10 min before IPC protocol (see *group 4*); *7*) Nti+IPC ($n = 12$), where animals were given Nti (10 mg/kg iv) 10 min before IPC; and *8*) Nti+Mor ($n = 12$). Nti (10 mg/kg iv) was given 10 min before morphine, which was injected (0.3 mg/kg iv) 15 min before sustained ischemia. In each group, four rabbits were used for evaluation of apoptosis.

Surgical preparation and measurement of infarct size. The rabbit model of the I/R protocol has been described previously (25, 27). After the animals were anesthetized with ketamine HCl (35 mg/kg) and xylazine (5 mg/kg), a left thoracotomy was performed to expose the heart. Myocardial ischemia was induced by occlusion of coronary artery, followed by reperfusion. At the end of each experiment, the coronary artery was reoccluded and 50% Unisperse blue dye solution was injected into the right jugular vein until the eyes turned blue. This was done to distinguish between perfused and nonperfused (risk area) regions of the myocardium. The animal was then euthanized and the heart was removed. The heart slices were incubated at room temperature for 20 min in 1% solution of triphenyltetrazolium chloride. After being stained, the infarct area (triphenyltetrazolium chloride negative) and risk area (area nonstained by Unisperse blue) were determined by computer morphometry with the use of Bioquant imaging software and the percentage of infarcted and risk areas were calculated.

Measurement of hemodynamics. The hemodynamic measurements included heart rate and mean arterial pressures. The rate-pressure product was determined as the product of the heart rate and peak arterial pressure. These parameters were continuously measured throughout the duration of the experimental protocol (Table 1).

In situ identification of nuclear DNA fragmentation. Four rabbits from each group were euthanized, and tissues were sampled from the ischemic area of the left ventricle. ApoAlert DNA fragmentation assay kit (Clontech) was used, which detects apoptosis-induced nuclear DNA fragmentation via a fluorescence assay. The assay is based on terminal deoxynucleotidyl transferase (TdT)-mediated dUTP nick-end labeling (TUNEL). After deparaffinization, the tissue sections were stained according to the manufacturer's instructions and nuclear DNA fragmentation was visualized. Apoptotic cells exhibited strong nuclear green fluorescence with a standard fluorescence filter set (520 ± 20 nm). All cells stained with propidium iodide exhibited strong red cytoplasmic fluorescence when viewed at >620 nm. The percentage of TUNEL-positive cardiomyocyte nuclei was determined using an eyepiece grid (×200 magnification). Five microscopic fields per section were selected from within the ischemic region. In each field, cells were counted and the percentage of apoptotic cardiomyocytes was calculated.

Genomic DNA extraction and agarose gel electrophoresis. For determination of genomic DNA fragmentation, hearts were rapidly removed after I/R and tissue samples from the ischemic region were homogenized. DNAs were isolated by lysis in digestion buffer (75 mM NaCl, 25 mM EDTA, 10 mM Tris, pH 8.0, 1% SDS, and 0.4 mg/ml freshly added proteinase K). After overnight digestion, DNAs were phenol/chloroform extracted, precipitated, spooled onto glass rods, dried, and dissolved in 10 mM Tris and 1 mM EDTA, pH 8.0, and quantified with the use of a spectrophotometer. For determination of DNA fragmentation, we used ApoAlert LM-PCR Ladder assay kit (Clontech) according to a previously described method (36). Briefly, 6 μg genomic DNA was mixed with 1 nmol 24 base pairs (bp) and 1 nmol 12-bp unphosphorylated oligonucleotides, annealed, and ligated. Ligations were stored at −20°C until PCR was performed. PCR reactions used ~150-ng

Table 1. *Hemodynamic data*

Group	Baseline	Occlusion	At Reperfusion	30 min After Reperfusion	3 h After Reperfusion
Heart rate, beats/min					
Control	176±9	179±6	176±6	174±12	170±11
Nal	167±8	160±8	156±7	167±8	160±5
Nti	170±8	174±9	167±5	174±7	172±5
IPC	182±9	188±9	178±6	172±8	173±5
Mor	188±10	185±7	187±7	187±3	180±11
Nal-PC	172±11	181±8	186±5	182±14	175±9
Nti-PC	176±8	186±9	189±8	185±11	182±10
Nti-Mor	172±13	176±10	179±11	173±15	168±11
Mean blood pressure, mmHg					
Control	99±7	89±10	91±8	87±5*	84±7*
Nal	101±8	95±5	93±11	96±10	93±5*
Nti	108±8	97±7	94±8	94±6	90±11*
IPC	94±11	87±12	91±12	86±11	85±9*
Mor	95±7	97±9	90±8	92±5	86±5*
Nal-PC	98±10	92±9	96±9	90±7	88±8*
Nti-PC	95±9	94±5	95±7	89±7	86±7
Nti-Mor	90±10	93±6	94±6	91±5	86±8
Rate pressure product, mmHg·ml^{-1}· min·1,000 g^{-1}					
Control	17.4±0.8	15.9±0.9	16.0±0.7	15.1±0.7*	14.3±0.8*
Nal	16.9±1.5	15.2±1.2	14.5±0.5	16.0±1.9	14.9±1.2*
Nti	18.3±1.9	16.9±1.1	15.7±0.5	16.3±1.4*	15.5±0.9*
IPC	17.1±1.3	16.4±1.1	16.2±0.8	14.8±0.9*	14.7±0.7*
Mor	17.9±1.5	17.9±0.8	16.8±2.1	17.2±0.6	15.5±1.1*
Nal-PC	16.9±1.4	16.7±1.2	17.9±1.6	16.4±1.3	15.1±1.4*
Nti-PC	16.7±0.9	17.5±0.7	17.9±1.3	16.5±0.5	15.6±0.6*
Nti-Mor	15.5±1.8	16.4±1.0	16.8±0.9	15.7±1.2	14.4±0.9*

Values are means ± SE. Nal, naloxone; Nti, naltrindole; IPC, ischemic preconditioning (PC); Mor, morphine. *$P < 0.05$ vs. baseline.

ligated DNA and used the 24-bp oligonucleotide as a primer. Samples were amplified for 25 cycles of PCR, and PCR products were analyzed by electrophoresis on 3% agarose gel (16).

Exclusion criteria. Animals were excluded from the study due to the following reasons: *1*) CAO did not produce adequate ischemia (the area at risk was <20% of the left ventricle); *2*) intractable ventricular fibrillation occurred during ischemia and/or reperfusion; and *3*) the animal died during the surgical procedure, so the protocol was not completed.

Statistical analysis. Values are expressed as means ± SE. The statistical significance was determined by ANOVA with repeated measurements. If a significant F value was found, Scheffé's test for multiple comparisons was used to identify differences among groups. Comparisons of means were made by using the Student's t-test for unpaired values. Statistical differences were considered significant if the P value was <0.05.

RESULTS

Infarct size. The risk areas ranged from 50% to 56% with no significant differences between all the groups (Fig. 2*A*; $P > 0.05$). These data suggest that changes in the size of infarcts observed between various groups in our experiments were not related to the percentage of area of the left ventricle occluded by our technique. Infarct size (expressed as a percentage of risk area) was 11.6 ± 1.0 in the IPC group and 19.5 ± 3.8 in the morphine-treated group, both of which were significantly lower compared with the infarct size of 46 ± 3.8 in the control group ($P < 0.001$, means ± SE; Fig. 2*B*). This reduction in infarct size by IPC was abolished by pretreatment with the nonselective opioid receptor antagonist Nal (38.6 ± 7.2%) and the δ-opioid-specific antagonist Nti (44.5 ± 1.8%). The infarct-limiting effect of morphine was also abolished by pretreatment with Nti (Nti+Mor: 49.3 ± 1.7% vs. 19.5 ± 3.8% for morphine; $P < 0.001$). Treatment of control rabbits with Nti or Nal had infarct size of 41.5 ± 3.6% and 42 ± 4.5%, respectively, which were not different compared with the infarct size in the untreated control group ($P > 0.05$).

Cardiomyocyte apoptosis. Figure 3*A* shows representative TUNEL-positive cardiomyocyte nuclei at ×200 and ×1,000

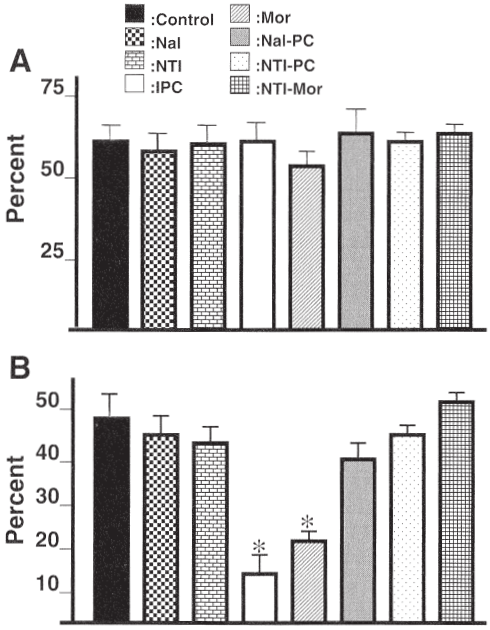

Fig. 2. Bar diagram showing risk area of the left ventricle (%LV; *A*) and infarct size (%risk area; *B*) for *groups 1–8*. See MATERIALS AND METHODS for a description of treatment groups. Results are means ± SE in 6–7 rabbits in each group (*$P < 0.001$).

magnifications. Quantitative analysis of DNA fragmentation was performed by using the TUNEL method at the single-cell level. The mean percentage of TUNEL-positive cardiomyocyte nuclei was 3.6 ± 1.9 in the IPC group, 5.2 ± 1.2 in the morphine group, which was significantly <12.4 ± 1.6, 12.9 ± 2.5, and 10.5 ± 1.9 of apoptotic cardiomyocytes in the control, Nal, and Nti-treated I/R hearts, respectively ($P < 0.001$; Fig. 3*B*). Nti pretreatment significantly increased TUNEL-positive cardiomyocytes in the IPC group (11.2 ± 2.2%) as well as the morphine-preconditioned group (12.1 ± 0.8%). Curiously, Nal failed to block the antiapoptotic effect of IPC, as shown by the percentage of apoptotic cells, which were 5.7 ± 1.3 in the Nal+IPC group and 5.2 ± 1.2 in the Nal+Mor-treated groups compared with the untreated control as well as Nal- and Nti-treated controls.

Genomic DNA fragmentation. For detection and qualitative evaluation of DNA fragmentation, we examined genomic DNA extracted from ischemic hearts that produced a typical "ladder" pattern. As shown in Fig. 4, ischemic left ventricular regions obtained from control, Nti-, and Nal-treated controls, Nti-pretreated IPC, and morphine groups subjected to I/R showed a typical DNA electrophoretic laddering pattern characterized by mononucleosomal and oligonucleosomal DNA fragmentation. However, DNA fragmentation (laddering pattern) was not observed in the tissue samples from animals in the IPC and Nal-treated preconditioned (IPC) as well as morphine-preconditioned rabbits showing protection from apoptosis.

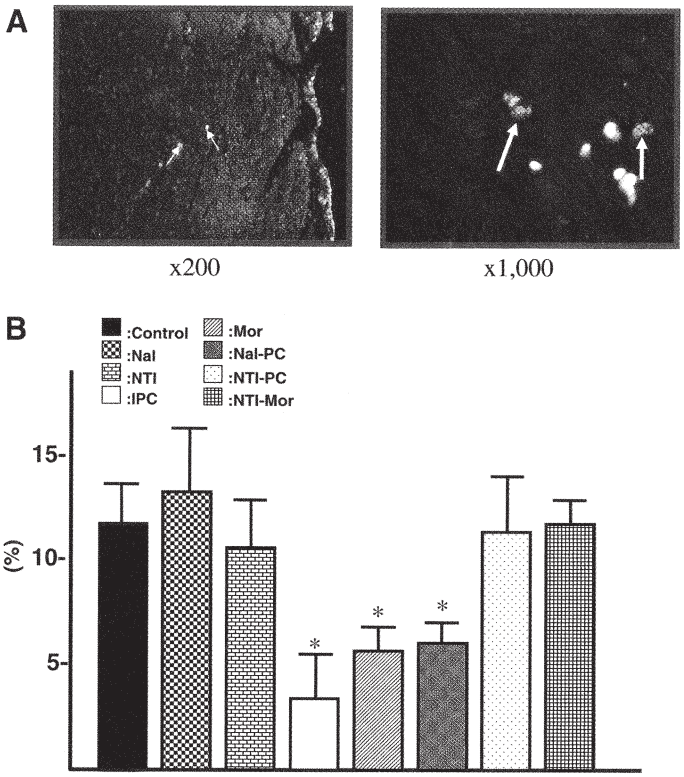

Fig. 3. *A*: light photomicrographs of heart sections from control group of rabbits subjected to 30 min of ischemia and 3 h of reperfusion. The bright green dots (indicated by arrows) correspond to a representative terminal deoxynucleotidyl transferase (TdT)-mediated dUTP nick-end labeling (TUNEL)-positive (fluorescent) nucleus. *B*: percentage of TUNEL-positive cells in heart cells. Data shown are means ± SE of four independent experiments quantified from five fields. The treatment groups and abbreviations are described in detail in MATERIALS AND METHODS. *$P < 0.001$.

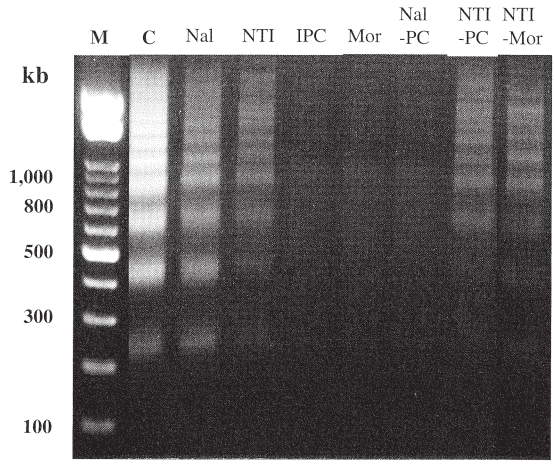

Fig. 4. Ligation-mediated PCR analysis of DNA from the ischemic zone. Genomic DNAs were prepared from various experimental groups, mixed with unphosphorylated oligonucleotides, annealed, and ligated. The DNA samples were amplified and PCR products were analyzed by electrophoresis on 3% agarose gel. The data shown are representative of 5 separate experiments. M, marker lane. The treatment abbreviations are same as in the experimental protocol and described in detail in MATERIALS AND METHODS.

Systemic hemodynamics. Heart rate, mean arterial blood pressure, and rate pressure product are shown in Table 1. Except as indicated, no significant differences in the baseline levels of these parameters were observed between each group. In addition, heart rate and mean arterial pressure remained reasonably stable throughout the reperfusion period, although these parameters decreased gradually at most of the data points in all the groups. Mean values were not significantly different between the groups at any time point for all the groups.

DISCUSSION

The major findings of this study are summarized as follows. First, the infarct-limiting effect of IPC and morphine is significantly blocked by Nal and Nti, the nonselective and selective δ-opioid inhibitor antagonists, respectively. Second, both IPC and morphine caused a significant decrease in the TUNEL-positive cardiomyocytes, inhibited the fragmentation of genomic DNA in the ischemic zone, and reduced infarct size compared with the control hearts. Third, Nti treatment before IPC and morphine reversed the anti-apoptotic and infarct-limiting effect of IPC and morphine. On the other hand, Nal failed to block the antiapoptotic effect of IPC as well as morphine. Both Nal and Nti had no effect on infarct size or apoptosis in the control rabbits subjected to I/R. The hemodynamics remained largely unchanged among the groups during the I/R protocol. For the first time, our results show an impressive anti-apoptotic effect of IPC, which is selectively mediated by δ-opioid receptor in the intact rabbit heart.

Many previous studies (12, 18) support the evidence that apoptosis may be the predominant form of ischemia-related cell death in the heart. Also, it has been shown that internucleosomal DNA fragmentation is restricted in the infarcted area after prolonged I/R in rat hearts in vivo. Both DNA fragmentation and infarct size were significantly decreased after prolonged ischemia and reperfusion in the preconditioned rat

hearts in vivo (29). Moreover, a direct correlation between myocardial infarct size and internucleosomal DNA fragmentations was reported (29). Consistent with these studies, our data also showed significant reduction of apoptotic cardiomyoctes after IPC in the ischemic zone, which was correlated with reduction of infarct size in the heart. An interesting observation in these studies is that selective δ-opioid receptor antagonist completely abolished the anti-apoptotic protection of IPC, suggesting an important role of this receptor in preventing cell death. Moreover, nonpeptide opioid, morphine also mimicked the cardioprotective effect of IPC, both in terms of infarct size reduction and attenuation of apoptosis. Morphine is considered a classic μ-opioid receptor agonist, although there is evidence that it also has important effects on the δ- and κ-opioid receptors and that cross-talk between μ- and δ-receptors can occur (4). The observation that morphine-mediated inhibition of apoptosis was also abolished by pretreatment with Nti further confirms the role of δ-opioid receptor in protecting against cardiomyocyte death. Interestingly, whereas Nal abolished the infarct-limiting effect of IPC, the drug failed to block anti-apoptotic effect of IPC or morphine. The reason for these discordant results remains unclear, but it is possible that Nal could selectively block the necrotic rather than the antiapoptotic pathway of acute IPC in the rabbit heart. Alternatively, perhaps different opioid receptors have opposing effects on apoptosis, thus blocking both by Nal may result in no significant effect.

Several previous studies by Gross and co-workers (see Ref. 13 for review) suggest the role of opioids in early IPC. These investigators demonstrated that the nonselective opioid receptor antagonist Nal completely antagonized the ability of IPC to reduce infarct size, whether administered before IPC stimulus or after the IPC stimulus just before the index ischemia. Subsequent studies by Gross's group showed that selective δ-1 antagonist 7-benzylidenenaltrexone blocked IPC-mediated protection in a dose-dependent fashion (33). Conversely, the selective δ-1 opioid receptor agonist TAN-67 produced a potent cardioprotective effect in chick embryonic myocytes, which was blocked by 7-benzylidenenaltrexone (15). In the present study, the dose of Nal or Nti (10 mg/kg) used in this study was higher compared with the one used in other studies used to block preconditioning (31, 32). However, none of these doses of the drugs had a significant effect on myocardial infarct size or apoptosis (in terms of TUNEL-positive nuclei or DNA fragmentation) compared with the nontreated control animals.

In the present study, we assessed apoptosis after a relatively short period of reperfusion (i.e., 3 h) by TUNEL and DNA fragmentation, which are known to measure the later stages of cell death. It has been reported (38) that the extent of necrosis peaks at 24 h of reperfusion, and remains constant thereafter. On the other hand, the appearance of apoptotic cells in the perinecrotic area progressively increases up to 72 h, suggesting that necrosis and apoptosis occur simultaneously during reperfusion, with a rapidly developing necrotic cell death during the early phase of reperfusion, followed by a slower appearance of apoptosis during the late phase of reperfusion. The number of apoptotic cells in the perinecrotic myocardium progressively increases during the extended period of reperfusion, which suggests the role of apoptosis in the development of infarction (39). Considering the reported delayed preconditioning effect of opioids (6), it would not be surprising if morphine or IPC also delay the extent of apoptosis in the survival animal models. This is an interesting question, which warrants investigations in the future.

It has been reported that the protective effect of opioids involves selective activation of signaling pathways, including PKC-δ (10), non-Src-dependent tyrosine kinase and ERK-1/2 (8, 9, 11). There are studies (7) that suggest the δ-1-opioid receptor reduced infarct size through the opening of mitochondrial ATP-sensitive K^+ channels, the proposed effectors of IPC. Moreover, the pharmacological opening of mitochondrial ATP-sensitive K^+ channels by diazoxide has been shown to preserve mitochondrial integrity and suppress the markers of apoptosis (1). It remains to be seen whether a similar signaling pathway also follows the δ-opioid receptor-mediated antiapoptotic effect of morphine and IPC. A recent study (20) showed that morphine protected against the death of primary rat neonatal astrocytes by nitric oxide and peroxynitrite. Pretreatment of astrocytes with phosphatidylinositol 3-kinase (PI3-kinase) inhibitors, including wortmannin and LY-294002, abrogated the effect of morphine on nitric oxide-induced cell death, indicating that the effects of morphine were, in part, mediated by PI3-kinase. It is possible that activation of δ-opioid receptor stimulation by IPC or morphine potentially activate the PI3-kinase pathway that may ultimately be responsible for the antiapoptotic effect of this receptor. There is currently no data in support of this contention, although the role of PI3-kinase in the acute phase of IPC against lethal ischemia-reperfusion injury has been well documented by recent published studies (23, 37).

In summary, our results provide the first direct evidence that both IPC and morphine attenuate cardiomycyte apoptosis through the activation of δ-opioid receptors. These observations raise the interesting possibility that novel agonists of δ-opioid receptors may be clinically useful in preventing cell death during I/R injury and heart failure and could potentially be used for treatment directed at these lethal disorders.

GRANTS

This work was supported in part by Collaborative Research Funding Grant C2003-1 from Kanazawa Medical University (to S. Okubo) and by National Heart, Lung, and Blood Institute Grants HL-51045 and HL-59469 (to R. C. Kukreja).

REFERENCES

1. **Akao M, Ohler A, O'Rourke B, and Marban E.** Mitochondrial ATP-sensitive potassium channels inhibit apoptosis induced by oxidative stress in cardiac cells. *Circ Res* 88: 1267–1275, 2001.
2. **Anderson BL, Berry RW, and Telser A.** A sodium dodecyl sulfate polyacrylamide gel electrophoresis system that separates peptides and proteins in the molecular weight range of 2,500 to 90,000. *Anal Biochem* 132: 365–375, 1983.
3. **Buerke M, Murohara T, Skurk C, Nuss C, Tomaselli K, and Lefer AM.** Cardioprotective effect of insulin-like growth factor I in myocardial ischemia followed by reperfusion. *Proc Natl Acad Sci USA* 92: 8031–8035, 1995.
4. **Ela C, Barg J, Vogel Z, Hasin Y, and Eilam Y.** Distinct components of morphine effects on cardiac myocytes are mediated by the κ- and δ-opioid receptors. *J Mol Cell Cardiol* 29: 711–720, 1997.
5. **Fliss H and Gattinger D.** Apoptosis in ischemic and reperfused rat myocardium. *Circ Res* 79: 949–956, 1996.
6. **Fryer RM, Hsu AK, Eells JT, Nagase H, and Gross GJ.** Opioid-induced second window of cardioprotection: potential role of mitochondrial K_{ATP} channels. *Circ Res* 84: 846–851, 1999.
7. **Fryer RM, Hsu AK, Nagase H, and Gross GJ.** Opioid-sensitive cardioprotection against myocardial infarction and arrhythmias: mitochondrial

versus sarcolemmal ATP-sensitive potassium channels. *J Pharmacol Exp Ther* 294: 451–457, 2000.

8. **Fryer RM, Pratt PF, Hsu AK, and Gross GJ.** Differential activation of extracellular signal regulated kinase isoforms in preconditioning and opioid-induced cardioprotection. *J Pharmacol Exp Ther* 296: 647–654, 2001.
9. **Fryer RM, Schultz JJ, Hsu AK, and Gross GJ.** Pretreatment with tyrosine kinase inhibitors partially attenuates ischemic preconditioning in rat hearts. *Am J Physiol Heart Circ Physiol* 275: H2009–H2015, 1998.
10. **Fryer RM, Wang Y, Hsu AK, and Gross GJ.** Essential activation of PKC-δ in opioid-initiated cardioprotection. *Am J Physiol Heart Circ Physiol* 280: H1346–H1353, 2001.
11. **Fryer RM, Wang Y, Hsu AK, Nagase H, and Gross GJ.** Dependence of δ_1-opioid receptor-induced cardioprotection on a tyrosine kinase-dependent but not a Src-dependent pathway. *J Pharmacol Exp Ther* 299: 477–482, 2001.
12. **Gottlieb RA, Burleson KO, Kloner RA, Babior BM, and Engler RL.** Reperfusion injury induces apoptosis in rabbit cardiomyocytes. *J Clin Invest* 94: 1621–1628, 1994.
13. **Gross GJ.** Role of opioids in acute and delayed preconditioning. *J Mol Cell Cardiol* 35: 709–718, 2003.
14. **Hamet P, Richard L, Dam TV, Teiger E, Orlov SN, Gaboury L, Gossard F, and Tremblay J.** Apoptosis in target organs of hypertension. *Hypertension* 26: 642–648, 1995.
15. **Huh J, Gross GJ, Nagase H, and Liang BT.** Protection of cardiac myocytes via δ_1-opioid receptors, protein kinase C, and mitochondrial K_{ATP} channels. *Am J Physiol Heart Circ Physiol* 280: H377–H383, 2001.
16. **Ito K.** DNA fragmentation of human infarcted myocardial cells demonstrated by the nick end labeling method and DNA agarose gel electrophoresis. *Am J Pathol* 146: 1325–1331, 1995.
17. **Itoh G, Tamura J, Suzuki M, Suzuki Y, Ikeda H, Koike M, Nomura M, Jie T, and Ito K.** DNA fragmentation of human infarcted myocardial cells demonstrated by the nick end labeling method and DNA agarose gel electrophoresis. *Am J Pathol* 146: 1325–1331, 1995.
18. **Kajstura J, Cheng W, Reiss K, Clark WA, Sonnenblick EH, Krajewski S, Reed JC, Olivetti G, and Anversa P.** Apoptotic and necrotic myocyte cell deaths are independent contributing variables of infarct size in rats. *Lab Invest* 74: 86–107, 1996.
19. **Kajstura J, Mansukhani M, Cheng W, Reiss K, Krajewski S, Reed JC, Quaini F, Sonnenblick EH, and Anversa P.** Programmed cell death and expression of the protooncogene bcl-2 in myocytes during postnatal maturation of the heart. *Exp Cell Res* 219: 110–121, 1995.
20. **Kim MS, Cheong YP, So HS, Lee KM, Kim TY, Oh J, Chung YT, Son Y, Kim BR, and Park R.** Protective effects of morphine in peroxynitrite-induced apoptosis of primary rat neonatal astrocytes: potential involvement of G protein and phosphatidylinositol 3-kinase (PI3-kinase). *Biochem Pharmacol* 61: 779–786, 2001.
21. **Kuzume K, Wolff RA, Amakawa K, Kuzume K, and Van Winkle DM.** Sustained exogenous administration of Met(5)-enkephalin protects against infarction in vivo. *Am J Physiol Heart Circ Physiol* 285: H2463–H2470, 2003.
22. **Liu Y, Cigola E, Cheng W, Kajstura J, Olivetti G, Hintze TH, and Anversa P.** Myocyte nuclear mitotic division and programmed myocyte cell death characterize the cardiac myopathy induced by rapid ventricular pacing in dogs. *Lab Invest* 73: 771–787, 1995.
23. **Mocanu MM, Bell RM, and Yellon DM.** PI3-kinase and not p42/p44 appears to be implicated in the protection conferred by ischemic preconditioning. *J Mol Cell Cardiol* 34: 661–668, 2002.
24. **Murry CE, Jennings RB, and Reimer KA.** Preconditioning with ischemia: a delay of lethal cell injury in ischemic myocardium. *Circulation* 74: 1124–1136, 1986.
25. **Okubo S, Bernardo NL, Elliott GT, Hess ML, and Kukreja RC.** Tyrosine kinase signaling in action potential shortening and expression of HSP72 in late preconditioning. *Am J Physiol Heart Circ Physiol* 279: H2269–H2276, 2000.
26. **Okubo S, Bernardo NL, Yoshida K, and Kukreja RC.** Myocardial preconditioning: basic concepts and potential mechanisms. *Mol Cell Biochem* 196: 3–12, 1999.
27. **Okubo S, Wildner O, Shah MR, Chelliah JC, Hess ML, and Kukreja RC.** Gene transfer of heat-shock protein 70 reduces infarct size in vivo after ischemia/reperfusion in the rabbit heart. *Circulation* 103: 877–881, 2001.
28. **Piot CA, Martini JF, Bui SK, and Wolfe CL.** Ischemic preconditioning attenuates ischemia/reperfusion-induced activation of caspases and subsequent cleavage of poly(ADP-ribose) polymerase in rat hearts in vivo. *Cardiovasc Res* 44: 536–542, 1999.
29. **Piot CA, Padmanaban D, Ursell PC, Sievers RE, and Wolfe CL.** Ischemic preconditioning decreases apoptosis in rat hearts in vivo. *Circulation* 96: 1598–1604, 1997.
30. **Schultz JEJ, Qian YZ, Gross GJ, and Kukreja RC.** The ischemia-selective K_{ATP} channel antagonist, 5-hydroxydecanoate, blocks ischemic preconditioning in the rat heart. *J Mol Cell Cardiol* 29: 1055–1060, 1997.
31. **Schultz JEJ, Rose E, Yao Z, and Gross GJ.** Evidence for involvement of opioid receptors in ischemic preconditioning in rat heart. *Am J Physiol Heart Circ Physiol* 268: H2157–H2161, 1995.
32. **Schultz JJ, Hsu A, and Gross GJ.** Ischemic preconditioning and morphine-induced cardioprotection involve the δ-opioid receptor in the intact rat heart. *J Mol Cell Cardiol* 29: 2187–2195, 1997.
33. **Schultz JJ, Hsu AK, and Gross GJ.** Ischemic preconditioning in the intact rat heart is mediated by δ_1- but not μ- or κ-opioid receptors. *Circulation* 97: 1282–1289, 1998.
34. **Schulz R, Gres P, and Heusch G.** Role of endogenous opioids in ischemic preconditioning but not in short-term hibernation in pigs. *Am J Physiol Heart Circ Physiol* 280: H2175–H2181, 2001.
35. **Sharov VG, Sabbah HN, Shimoyama H, Goussev AV, Lesch M, and Goldstein S.** Evidence of cardiocyte apoptosis in myocardium of dogs with chronic heart failure. *Am J Pathol* 148: 141–149, 1996.
36. **Staley K, Blaschke AJ, and Chun J.** Apoptosis DNA fragmentation is detected by a semiquantitative ligation-mediated PCR of blunt DNA ends. *Cell Death Differ* 4: 66–75, 1997.
37. **Tong H, Chen W, Steenbergen C, and Murphy E.** Ischemic preconditioning activates phosphatidylinositol-3-kinase upstream of protein kinase C. *Circ Res* 87: 309–315, 2000.
38. **Zhao ZQ, Nakamura M, Wang NP, Velez DA, Hewan-Lowe KO, Guyton RA, and Vinten-Johansen J.** Dynamic progression of contractile and endothelial dysfunction and infarct extension in the late phase of reperfusion. *J Surg Res* 94: 133–144, 2000.
39. **Zhao ZQ, Velez DA, Wang NP, Hewan-Lowe KO, Nakamura M, Guyton RA, and Vinten-Johansen J.** Progressively developed myocardial apoptotic cell death during late phase of reperfusion. *Apoptosis* 6: 279–290, 2001.

Pflugers Arch - Eur J Physiol (2004) 448: 54–62
DOI 10.1007/s00424-003-1217-6

ION CHANNELS, TRANSPORTERS

Hiroyuki Matsuda · Yasutaka Kurata · Sunao Imanishi · Ryoichi Sato · Toshishige Shibamoto

Effects of Angiotensin II on sustained outward currents in rat ventricular myocytes

Received: 8 October 2003 / Accepted: 12 November 2003 / Published online: 18 December 2003

Abstract We investigated the effects of angiotensin II (Ang II) on the sustained outward current (I_{sus}) and action potential of rat ventricular myocytes using the whole-cell patch-clamp technique. Ang II at 30 nM~3 μM inhibited I_{sus} with an IC_{50} of 240 nM, a Hill coefficient of 1.0 and maximum inhibition of 19.4%. Ang II-mediated inhibition of I_{sus} was voltage independent, was due to a decrease in the K^+ current and was abolished by the Ang II type-I (AT_1) receptor blocker, valsartan. The protein kinase C (PKC) inhibitors PKC19–36 or calphostin C, abolished Ang II-mediated inhibition of I_{sus}. In contrast, pretreatment with the protein kinase A (PKA) inhibitor PKA6–22 (100 μM) significantly enhanced the suppression of I_{sus} by 1 μM Ang II: (33.7±5.1% vs. control 17.1±2.3%). These results indicate that Ang II inhibits I_{sus} via the AT_1 receptor and activation of PKC. Ang II significantly prolonged action potential duration (APD) when the control APD was lengthened by a Ca^{2+} channel activator, BAY K8644. In myocytes with a relatively long APD, Ang II may prolong APD by inhibiting I_{sus}.

Keywords Angiotensin II · Sustained outward current · Angiotensin II type-1 receptor · Protein kinase C · Rat ventricular myocyte

Introduction

Although angiotensin II (Ang II) plays important physiological roles in vasoconstriction, aldosterone secretion, cell proliferation and regulation of water-electrolyte balance and blood pressure, it can also exert pathophysiological effects: previous studies have suggested that Ang II is involved in the development of various cardiovascular diseases such as hypertension, cardiac hypertrophy [4, 31], arteriosclerosis [8, 12] and arrhythmias. The arrhythmogenic effects of Ang II have been suggested by the following studies. First, Ang II enhances noradrenaline release and induces reperfusion arrhythmias under ischaemic conditions [30]. Second, direct activation of Ang II type-I (AT_1) receptor signalling decreases the conduction velocity in the ventricle of transgenic mice over-expressing AT_1 receptors [22] and third, ventricular arrhythmias occur far more frequently in wild-type than in AT_1 receptor knockout mice in ischaemia-reperfusion injury models [20]. Furthermore, several reports have shown therapeutic or preventive effects of angiotensin converting enzyme inhibitor (ACEI) and AT_1 receptor blockers (ARB) on ventricular arrhythmias [2, 24], supporting the arrhythmogenic effects of Ang II on the human ventricle. The ionic and subcellular mechanisms of the arrhythmogenic actions of Ang II are, however, unclear.

A possible ionic mechanism underlying cardiac arrhythmias is modulation of voltage-gated K^+ channel currents, which largely determine the action potential duration (APD) in mammalian cardiac myocytes [41]. K^+ channel dysfunctions may lead to ventricular arrhythmias such as torsades de pointes and ventricular fibrillation in acquired or inherited long-QT syndromes [42]. Ang II reportedly inhibits the slowly-activating delayed-rectifier K^+ current (I_{Ks}), while enhancing the rapidly-activating delayed-rectifier K^+ current (I_{Kr}) [11, 46]. In human atrial myocytes, however, the sustained outwards current (I_{sus}), rather than I_{Ks} or I_{Kr}, plays an important role in regulating APD [34]. The arrhythmogenic actions of Ang II may be, at least in part, attributable to the modulation of I_{sus}, although how Ang II modulates I_{sus} is not known. In this study, therefore, we investigated the effects of Ang II on I_{sus}, as well as on APD, in isolated rat ventricular myocytes using the whole-cell patch-clamp technique.

H. Matsuda · Y. Kurata (✉) · S. Imanishi · T. Shibamoto
Department of Physiology, Kanazawa Medical University,
1-1 Daigaku, Uchinada-machi, Kahoku-gun,
920-0293 Ishikawa, Japan
e-mail: yasu@kanazawa-med.ac.jp
Tel.: +81-76-2862211
Fax: +81-76-2868010

R. Sato
Department of Molecular Pharmacology and Biological Chemistry, Northwestern University Medical School,
Chicago, IL 60611-3008, USA

Ang II exerts the physiological and pathophysiological effects on ionic channels via the AT (AT_1 and AT_2) receptors, which belong to the G protein-coupled receptor superfamily and involve two classical signal transduction mechanisms, activation of phospholipase A_2, C and D via G_q proteins and inhibition of adenylate cyclase via G_i proteins [15]. Ang II may regulate the function of ion channels including cardiac K^+ channels by modulating protein kinases such as PKA and PKC [21, 36, 44]. We also determined, therefore, whether AT (AT_1 and AT_2) receptors and protein kinases are involved in the modulation of I_{sus} by Ang II. Our results indicate that Ang II inhibits I_{sus} via AT_1 receptors and activation of PKC.

Materials and methods

Isolation of rat ventricular myocytes

Single ventricular myocytes were isolated from male Wistar rats (150–200 g). The animals were anaesthetized with pentobarbitone sodium (40 mg kg^{-1} i.p.), the thoracic cavity opened and the heart excised quickly and suspended on a Langendorff perfusion apparatus. The isolated heart was perfused for 4 min with normal Tyrode solution, for 8 min with Ca^{2+}-free Tyrode solution and then for 12 min with the Ca^{2+}-free Tyrode solution containing collagenase (50 U ml^{-1}, Yakult, Tokyo, Japan). These procedures were performed at a constant perfusion rate (4 ml min^{-1}) and at 37°C. Finally, the heart was perfused for 8 min with a Kraftbrühe (KB) medium. Myocytes were dispersed by mechanical agitation and the isolated cells kept in KB medium at 4°C for at least 2 h before use in experiments.

Electrophysiological recordings

Myocytes were transferred to a small chamber (volume 0.2 ml) on the stage of an inverted microscope (Diaphot 300, Nikon, Tokyo, Japan). The chamber was perfused continuously at 1.5 ml min^{-1} and maintained at 37°C. We used only Ca^{2+}-tolerant rod-shaped cells with clear cross-striations and lacking any visible blebs on their surfaces. Currents were recorded using the whole-cell patch clamp technique [19]. All recordings were performed with an EPC-9 amplifier (Heka, Lambrecht, Germany) controlled by the manufacturer's software (Pulse, Heka) on a Power Macintosh G4 computer (Apple Computer, Cupertino, Calif., USA). Currents were filtered at 10 kHz. Patch electrodes were made of thin-walled glass capillaries (Kimax-51, Kimble, Vineland, N.J., USA) using a vertical puller (pp-83, Narishige, Tokyo, Japan). The pipette resistance was 1.5~2 MΩ, and the seal resistance was >10 GΩ.

First, we used ramp pulses ranging from −120 to +60 mV (18 mV s^{-1}) to estimate the effects of Ang II on both inward and outward currents. In rat ventricular myocytes there are three distinct outward K^+ currents activated by depolarization [37]: the rapidly activating and rapidly inactivating current (I_{to}) sensitive to 4-aminopyridine (4-AP), the rapidly activating and slowly inactivating current (I_k) sensitive to tetraethylammonium (TEA) and the rapidly activating, non-inactivating current (I_{sus}). In the present study, we focused on I_{sus}. To isolate I_{sus}, we used step pulses from a holding potential of −20 mV at which I_{to} and I_k, as well as the fast Na^+ current, are almost completely inactivated [6, 23]. Test pulses ranging from −30 to +50 mV (in 10-mV increments) were applied for 200 ms at a frequency of 0.2 Hz. The amplitude of I_{sus} was determined at the end of the 200-ms test pulses and normalized to the cell capacitance. Current data were accepted only when the series resistance had been stable throughout current recording. The series resistances just before the control and at the end of the recording were 5.3±0.3 and 5.4±0.3 MΩ, respectively (n=60). The voltage error due to the series resistances was estimated to be less than 5 mV, because the current amplitudes were usually less than 2 nA and the series resistance was compensated to 60–70%.

To examine the effects of Ang II on APD, we also recorded rat ventricular action potentials in the current-clamp mode. Action potentials were evoked by 6-ms stimuli (1 nA, 0.2 Hz). BAY K8644 (1 μM) was superfused before applications of Ang II to prolong the control APD and produce a plateau (phase 2) during which I_{sus} can be activated in rat ventricular action potentials.

Solutions and chemicals

The normal Tyrode solution used to isolate ventricular myocytes comprised (in mM): 135 NaCl, 4.0 KCl, 1.0 $MgCl_2$, 1.8 $CaCl_2$, 0.33 NaH_2PO_4, 10 glucose and 10 HEPES; pH was adjusted to 7.4 with NaOH. For whole-cell recordings of K^+ currents, we added 0.1 μM $CdCl_2$ to the Tyrode solution to suppress L-type Ca^{2+} currents. The internal solution in the patch electrode contained (mM) 20 KCl, 110 K-aspartate, 1 $MgCl_2$, 1 $CaCl_2$, 10 EGTA, 10 HEPES, 5 K_2ATP and 0.2 Na_2GTP; pH was adjusted to 7.2 with KOH (pCa 7.78). For experiments with K^+-free solutions, we substituted Cs^+ or Na^+ for K^+ in the external and internal solutions: CsCl for KCl, Cs-aspartate for K-aspartate and Na_2ATP for K_2ATP. The KB medium contained (mM) 90 KOH, 20 taurine, 70 glutamic acid, 10 glucose, 10 KH_2PO_4, 30 KCl, 1 $MgCl_2$, 10 HEPES and 0.5 EGTA; pH was adjusted to 7.3 with KOH. Ang II, PD 123,319, calphostin C, PKC fragment 19–36 (PKC19–36) and PKA fragment 6–22 (PKA6–22) were purchased from Sigma (St. Louis. Mo., USA). BAY K8644 was purchased from Wako (Osaka, Japan). Valsartan was a gift from Novartis (Tokyo, Japan).

Data analysis (curve fitting)

The concentration dependence of the Ang II-mediated block of I_{sus} was fitted with a Hill equation:

$$B_X = \frac{B_{max}}{1 + \left(\frac{IC_{50}}{X}\right)^n} \quad (1)$$

where B_X is the percentage block of I_{sus} at an Ang II concentration of X, with B_{max} being the maximal attainable block and IC_{50} and n the half-maximum inhibitory concentration of Ang II and the Hill coefficient, respectively. Curves were fitted using a non-linear, least-squares method.

Statistical analyses

Data are expressed as means±SEM. The significance of differences between means was established using Student's t-test, paired or unpaired as required. Differences were considered significant when $P<0.05$.

Results

Ang II inhibits I_{sus}

Figure 1A shows the effects of Ang II on inward and outward currents recorded during ramp pulses from −120 to +60 mV. Ang II (1 μM) reduced the outward currents at potentials positive to about −30 mV; no significant changes were observed in the inward current over

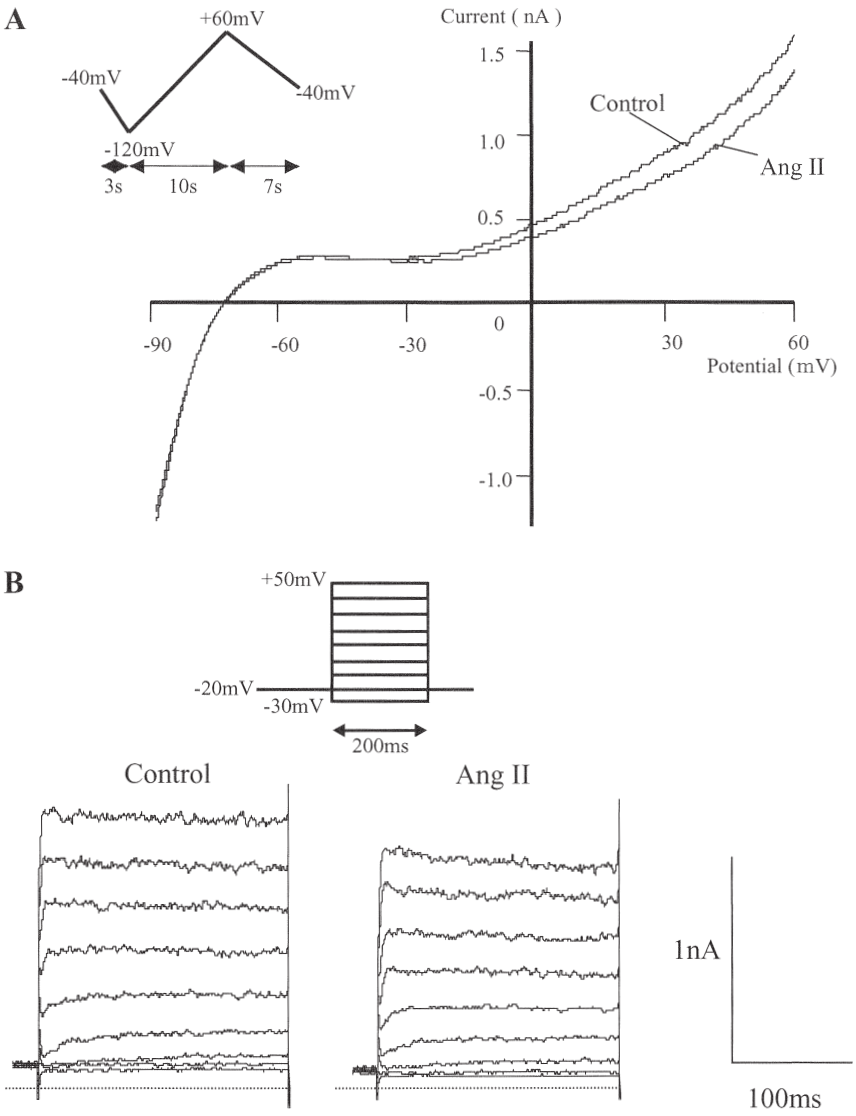

Fig. 1A, B Effects of angiotensin II (Ang II) on membrane currents in rat ventricular myocytes. **A** Inward and outward currents recorded with a ramp pulse from −90 to +60 mV (18 mV s^{-1}) before (*Control*) and 10 min after (*Ang II*) beginning the application of 1 μM Ang II. The ramp pulse protocol is shown in the *inset*. **B** Outward currents in response to 200-ms test pulses ranging from −30 to +50 mV (in 10-mV increments) were recorded at 0.2 Hz before (*Control*) and at 10 min after (*Ang II*) the application of 1 μM Ang II. The *horizontal broken lines* indicate zero current. The step pulse protocol is shown in the *inset*

potentials ranging from −120 mV to the reversal potential. Figure 1B shows the effects of Ang II on the I_{sus} family recorded with step-pulse depolarizations to test potentials of −30~+50 mV in 10-mV increments. At all test potentials, 1 μM Ang II inhibited I_{sus}, with a mean reduction of 17.1±2.3% (n=7) at +50 mV.

Time course of Ang II inhibition of I_{sus}

Figure 2 shows the time course of I_{sus} modulation by 1 μM Ang II. Control currents (before Ang II application) were recorded for 10~15 min after the formation of the whole-cell patch configuration; Ang II was applied only when amplitude of I_{sus} reached a steady state, i.e. when run down of I_{sus} was not apparent. The suppression of I_{sus} reached maximum at 5~10 min from the beginning of Ang II exposure and was reversed partially by washout of Ang II, although not completely reversed within 20 min.

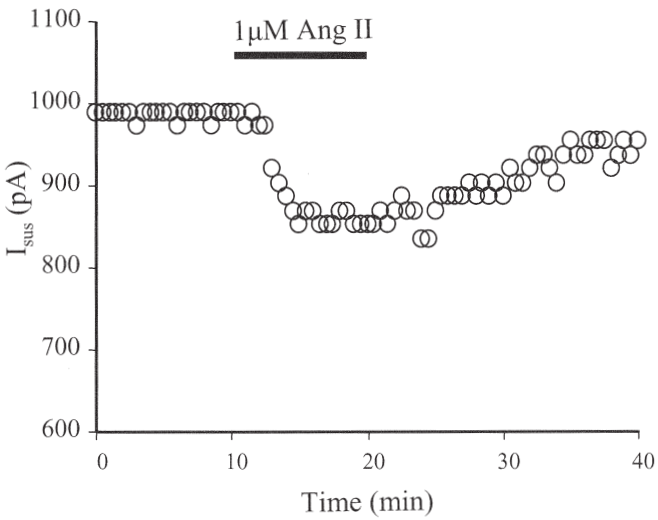

Fig. 2 Time course of the sustained outward current (I_{sus}) suppression during the application of 1 μM Ang II and recovery after the removal of Ang II. Depolarizing step pulses to +50 mV from a holding potential of −20 mV were applied for 200 ms every 30 s

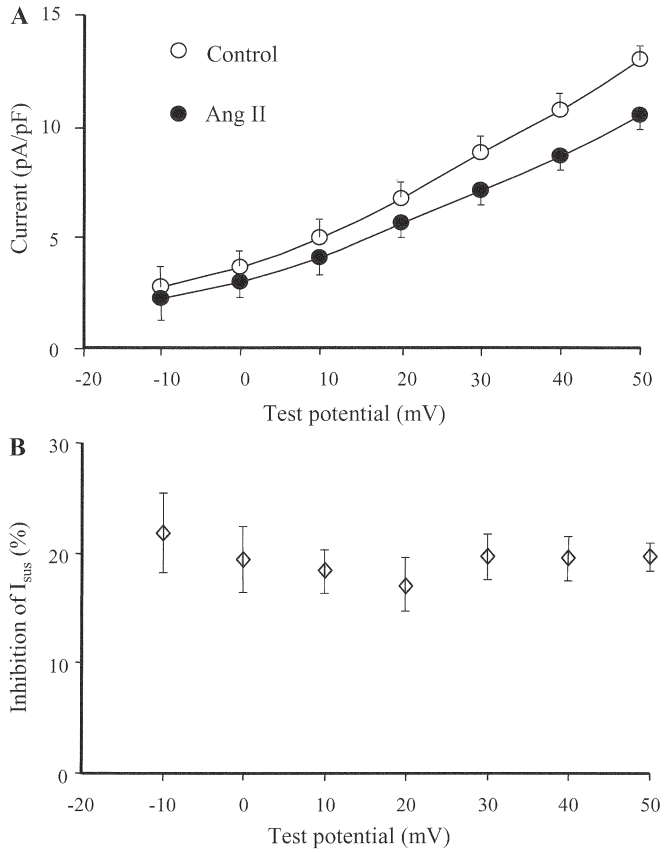

Fig. 3A, B Voltage dependence of Ang II inhibition of I_{sus}. **A** The amplitude of I_{sus} in the absence (*open circles*) and presence (*closed circles*) of 1 μM Ang II are plotted against the test potentials (n=5). **B** Percentage inhibition of I_{sus} at each test potential

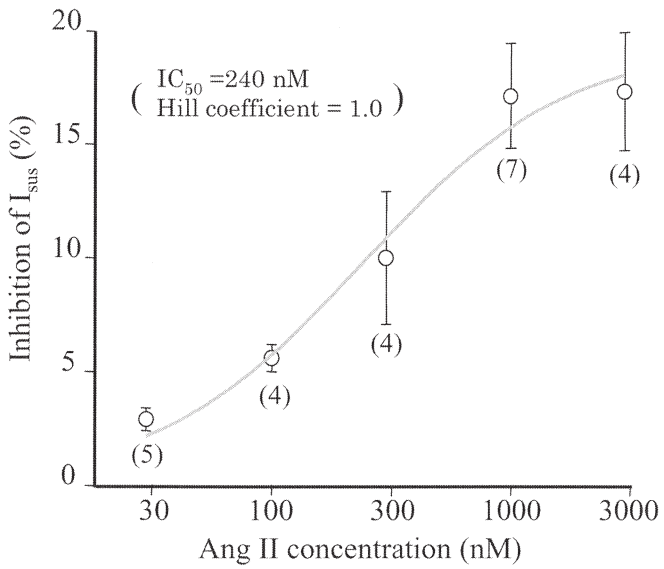

Fig. 4 Concentration dependence of Ang II inhibition of I_{sus}. The percentage inhibition of I_{sus} induced by 30 nM~3 μM Ang II is plotted against the concentrations of Ang II. The data for each concentration of Ang II were obtained from different cells. Means ±SEM; n (cells) in *parentheses*

Voltage dependence of Ang II inhibition of I_{sus}

To test whether the Ang II-induced block of I_{sus} is voltage dependent, the percentage inhibition of I_{sus} by 1 μM Ang II was determined for individual test pulses. As shown in Fig. 3, the degrees of the suppression of I_{sus} were nearly identical at all the test potentials. Thus, Ang II inhibited I_{sus} voltage independently, indicating that Ang II's inhibition of I_{sus} is not due to a positive shift in the voltage-dependent activation of I_{sus}, but mainly to a decrease in the maximum attainable conductance at positive potentials. In the following experiments, the Ang II-induced changes in I_{sus} were determined at +50 mV.

Concentration dependence of Ang II inhibition of I_{sus}

We further tested the concentration dependence of the Ang II inhibition of I_{sus} (at +50 mV). As shown in Fig. 4, 30 nM~3 μM Ang II inhibited I_{sus} concentration dependently. Ang II at the lowest concentration tested (10 nM) did not affect I_{sus} so that 30 nM was considered the threshold for significant suppression; the IC_{50}, Hill coefficient and B_{max} calculated with Eq. 1 were 240 nM, 1.0 and 19.4%, respectively. The percentage inhibition by Ang II at 30, 100, 300, 1,000 and 3,000 nM was 2.9±0.5, 5.6±0.6, 10.0±2.9, 17.1±2.3 and 17.3±2.5%, respectively. We used 1 μM Ang II in the following experiments to obtain nearly the maximum effect on I_{sus}.

Ang II inhibits K^+ current components of I_{sus}

Although the sustained outward currents of rat ventricular myocytes recorded with the method as used in this study are mainly K^+ channel currents, they also include other background currents (I_{bg}) [37], e.g. electrogenic exchanger currents, non-specific cation channel currents, anion channel currents and leak currents due to the relatively low seal resistance. Thus, the block of I_{sus} observed in this study may reflect the block of I_{bg} rather than K^+ currents. To determine whether the Ang II inhibition of I_{sus} is due to the inhibition of K^+ current components, therefore, we examined the effects of Ang II on outward currents after replacing external and internal K^+ by Cs^+ or Na^+ (Fig. 5). The outward currents recorded in K^+-free solutions were much smaller than those in normal (K^+-rich) solutions. Under K^+-free conditions, 1 μM Ang II did not reduce the outward currents recorded during ramp pulses or the sustained component evoked by step pulses: the sustained outward currents measured at the end of step pulses in the absence and presence of 1 μM Ang II were nearly identical (3.0±0.4 and 3.0±0.3 pA pF^{-1}, respectively, n=5). In contrast, 1 μM Ang II significantly reduced I_{sus} from 11.3 ±1.0 to 9.4±0.8 pA pF^{-1} (n=7) under normal (K^+-rich) conditions. These results suggest that the observed Ang II-mediated inhibition of I_{sus} is due to inhibition of the K^+ current component.

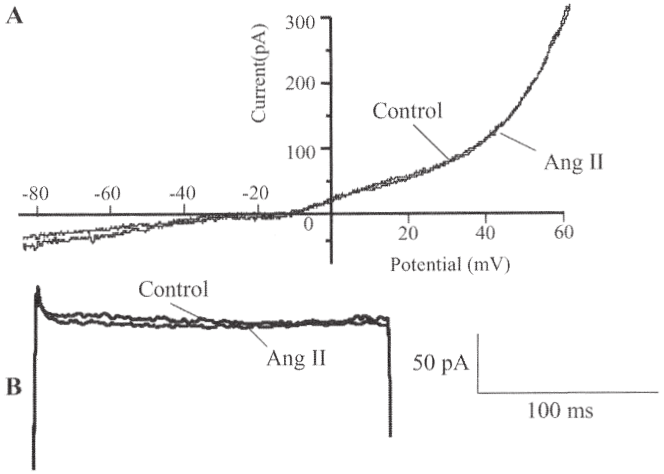

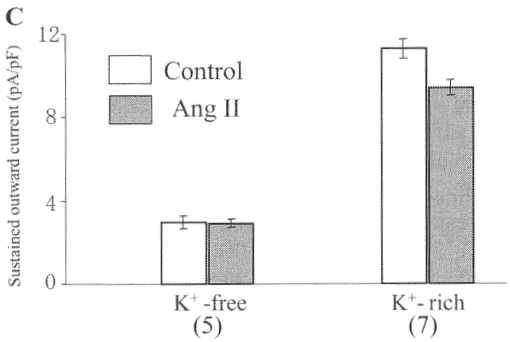

Fig. 5A–C Effects of Ang II on I_{sus} under K^+-free conditions. **A**, **B** The effects of 1 μM Ang II on outward currents recorded during ramp pulses (**A**) or step pulses to +50 mV (**B**) were tested with external and internal K^+ being replaced by Cs^+ or Na^+. The *horizontal line* in **B** indicates zero current. **C** Summary of the amplitude of the sustained outward components (at +50 mV) measured before and during applications of 1 μM Ang II with the normal Tyrode (K^+-rich) or K^+-free solution. Means±SEM; *n* in *parentheses*

Ang II inhibits I_{sus} via AT_1 receptors

Figure 6 shows the effects of Ang II receptor blockers on the Ang II inhibition of I_{sus}. Pretreatment with the AT_1 receptor blocker valsartan (Val, 1 μM) prevented the Ang II-induced block of I_{sus}, whereas pretreatment with the AT_2 receptor blocker PD123,319 (PD, 1 μM) did not. As summarized in Fig. 7, the percentage inhibition of I_{sus} by 1 μM Ang II was 17.1±2.3 (n=7) with no blocker, −0.8 ±1.8 (n=5) in the presence of 1 μM Val and 13.9±1.2 (n=5) in the presence of 1 μM PD. These results indicate that Ang II inhibits I_{sus} via the AT_1 receptor. Val and PD themselves had no significant effects on I_{sus}.

Subcellular mechanisms of I_{sus} modulation by Ang II

Ion channel functions are modulated via phosphorylation of the channel protein [27]. In the present study, therefore, we focused on the roles of the protein kinases in the modulation of I_{sus} by Ang II. To determine whether PKA and PKC are involved in the Ang II inhibition of I_{sus}, we examined the antagonizing effects of PKA or PKC inhibitors on the Ang II inhibition of I_{sus} (Fig. 8). Ang II did not decrease I_{sus} in the presence of the PKC inhibitors PKC19–36 (20 μM) or calphostin C (200 nM): the percentage changes in I_{sus} were +4.6±1.8 (n=5) and +1.6±1.4 (n=5), respectively. In contrast, Ang II strongly decreased I_{sus} in the presence of a PKA inhibitor, PKA6–22 (100 μM): the percentage change in I_{sus} was −33.7±5.1 (n=5), which was significantly greater than the −17.1±2.3 (n=7) in the absence of the inhibitor. The protein kinase inhibitors themselves appeared not to exert a significant effect on I_{sus}, because the amplitude of I_{sus} did not significantly change during pretreatments with the inhibitors (before exposure to Ang II).

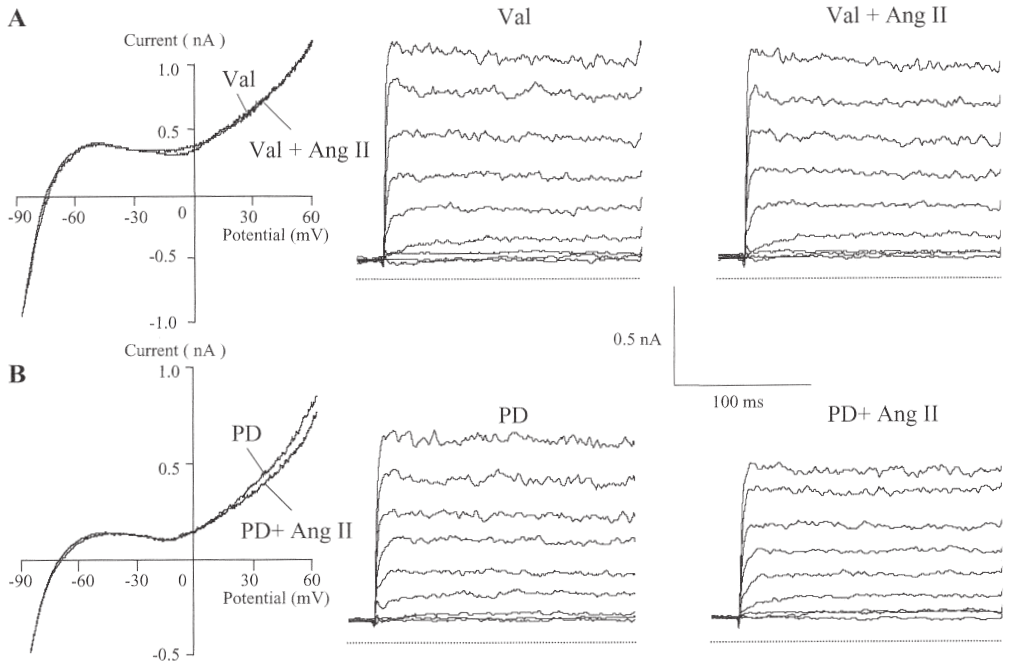

Fig. 6A, B Effects of Ang II receptor blockers on the Ang II inhibition of I_{sus}. The AT_1 receptor blocker valsartan (*Val*, 1 μM, **A**) or the AT_2 receptor blocker PD123,319 (*PD*, 1 μM, **B**) was perfused for 10 min before application of 1 μM Ang II. Pulse protocols for current recordings as in Fig. 1. The *horizontal lines* indicate zero current

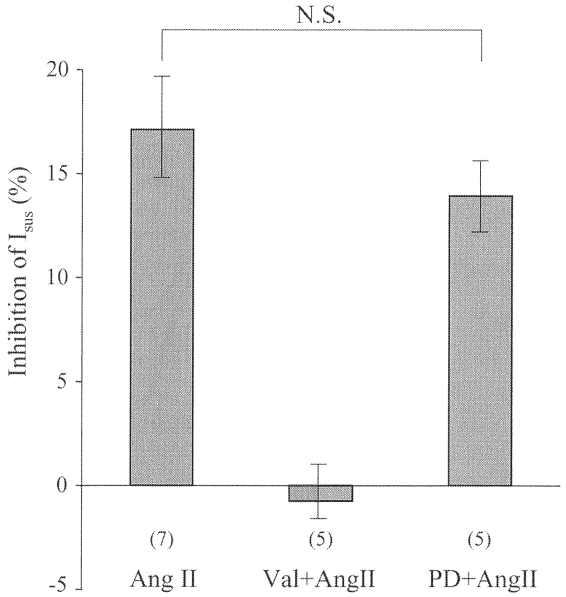

Fig. 7 Summary of Ang II-mediated inhibition of I_{sus} in the absence and presence of the AT_1 receptor blockers valsartan and the AT_2 blocker PD123,319. Means±SEM; *n* in *parentheses*

Effects of Ang II on APD

To determine whether Ang II prolongs APD in the rat ventricle, we also examined the effects of 1 μM Ang II on APD in rat ventricular myocytes. Application of 1 μM Ang II did not significantly change APD (Fig. 9, left). This may have been due to the unique action potential waveform, i.e. the exceptionally short APD (lack of the plateau phase during which I_{sus} could be activated), in rat ventricular myocytes probably due to the high density of I_{to} [43, 35]. Suppression of I_{sus} by ≈17% may not influence such a short APD. Therefore, we used the Ca^{2+} channel agonist BAY K8644 to prolong the control APD and create a plateau phase; 1 μM BAY K8644 prolonged the control APD_{90} by ≈250%. In the presence of BAY K8644, 1 μM Ang II reversibly prolonged APD_{90} by ≈20% (Fig. 9, right). Pretreatment with the AT_1 receptor blocker (Val) or PKC inhibitors abolished this effect of Ang II on APD (data not shown).

Discussion

In the present study, we investigated the effects of Ang II on I_{sus} in isolated rat ventricular myocytes using the whole-cell patch-clamp technique. The results clearly show that Ang II inhibits I_{sus} via the AT_1 receptor and activation of PKC. In the following, we will discuss the pathophysiological significance of the Ang II inhibition of I_{sus}, as well as the limitations and perspectives of our study.

Isolation of I_{sus} in rat ventricular myocytes

There are two distinct, depolarization-activated K^+ currents, I_{to} and the delayed-rectifier K^+ current, in rat ventricular myocytes [3]. The delayed-rectifier K^+ current may be divided into two components, I_k and I_{sus} [37]. To isolate I_{sus}, we followed the procedures of Casis et al. [6], as mentioned in Materials and methods. Because I_{to} and I_k are almost completely inactivated at a holding potential of −20 mV, the outward currents measured in this study reflect only the I_{sus} component. Himmel et al. [23] investigated the effects of some pharmacological agents on I_{sus}: 4-AP at 0.1~1 mM only slightly reduced I_{sus}; TEA at 1~10 mM reduced I_{sus} concentration dependently with 10 mM TEA inhibiting I_{sus} by 30%. The pharmacological responses of the sustained outward currents recorded in this study were very similar (data not shown). Therefore, we believe that the sustained outward current measured in our experiments is identical to the I_{sus} in the previous reports. As already mentioned, I_{sus} recorded in this study is a combination of various currents including K^+ currents

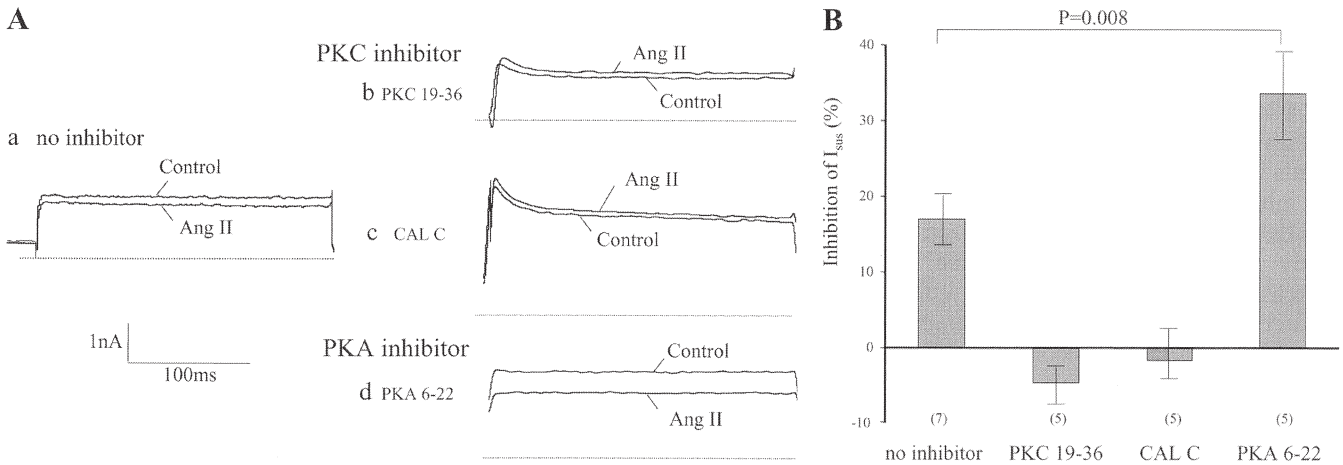

Fig. 8A, B Effects of protein kinase (PK) inhibitors on Ang II-mediated inhibition of I_{sus}. **A** Representative currents recorded with the pipette solution containing no inhibitor (*a*), 20 μM PKC19–36 (*b*), 200 nM calphostin C (*CAL C*, *c*), or 100 μM PKA6–22 (*d*). The currents were elicited by the test pulses of +50 mV just before and at 5 min after application of 1 μM Ang II. The *horizontal lines* indicate zero current. **B** Summary of experiments as in **A**. Means±SEM; *n* in the *parentheses*

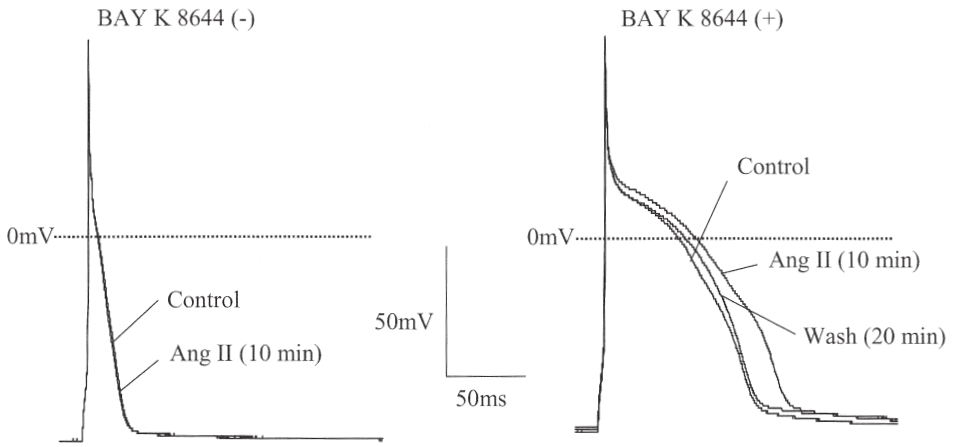

Fig. 9 Effects of Ang II on APD in the absence or presence of BAY K8644. *Left*: lack of effect of a 10-min exposure to 1 μM Ang II on action potential duration to 90% repolarization (APD_{90}). *Right*: prolongation of APD_{90} by 1 μM Ang II after 20 min pretreatment with the Ca^{2+} channel agonist BAY K8644 (1 μM) and partial reversal after washout of Ang II

and I_{bg}. Thus, further characterization of I_{sus} using specific blockers for each current component would be required for identification of the ion channels responsible for the I_{sus}.

Mechanisms of Ang II modulation of I_{sus} (involvement of protein kinases)

This study showed that Ang II modulates I_{sus} via the AT_1 receptor. The AT_1 receptor fulfils its major physiological functions through the $G_{q/11}$ protein that activates phospholipase C-β, leading to phosphoinositide hydrolysis, stimulation of IP_3/calcium signalling and activation of PKC [17]. The PKC activator, 1,2-dioctanoyl-rac-glycerol, attenuates the outward current I_{ss} (consisting of I_{sus} and partially inactivated I_k) in rat ventricular myocytes [38]. Our data demonstrating antagonism between PKC inhibitors and Ang II-mediated inhibition of I_{sus} are compatible with these reports, suggesting the involvement of PKC activation in the I_{sus} block by Ang II (see Fig. 8). On the other hand, Ang II receptors in the rat myocardial sarcolemma are reportedly coupled negatively to adenylate cyclase via G_i protein [1]. Because activation of PKA is known to inhibit I_{sus} [37], Ang II may enhance I_{sus} by inhibiting PKA. In our study, Ang II slightly (but not significantly) enhanced I_{sus} in the presence of the PKC inhibitors and strongly decreased I_{sus} in the presence of the PKA inhibitor (see Fig. 8). These results suggest that Ang II may enhance I_{sus} by inhibiting PKA. Further experiments will be required to clarify how Ang II modulates I_{sus} via inhibition of PKA.

The inhibitory effect of Ang II on I_{sus} observed in this study was relatively small. Since the Ang II-induced increase of L-type Ca^{2+} channel current ($I_{Ca,L}$) is much greater in perforated-patch recordings than in the conventional ruptured-patch recording [25] the relatively small effect of Ang II on I_{sus} might have been due to cell dialysis. We therefore explored the Ang II effect on I_{sus} in amphotericin B-perforated patches. In contrast to [25], however, Ang II-mediated inhibition of I_{sus} was not greater in perforated-patch recordings (data not shown). This inconsistency may be due, at least in part, to the difference in the subcellular mechanisms of channel modulation: PKC does not contribute to the Ang II-induced activation of $I_{Ca,L}$ [25], whereas Ang II inhibits I_{sus} by activating PKC.

In this study, we investigated only the "acute" effect of Ang II on I_{sus}. Ang II reportedly causes "chronic" suppression of the steady-state outward current I_{ss} (comprising I_{sus} and partially inactivated I_k), as well as I_{to}, in rat ventricular myocytes under pathological conditions (e.g. diabetes, hypothyroidism) by activating PKC and attenuating the synthesis of the K^+ channel proteins, which may be one of the mechanisms of cardiac arrhythmias [39, 40]. Thus, the acute and chronic actions of Ang II possibly cause a marked decrease in I_{sus} and lead to arrhythmias by preventing repolarization under pathological conditions.

Effects of Ang II and I_{sus} inhibition on APD

Whilst it is likely that the I_{sus} suppression by Ang II contributes to prolongation of APD in ventricular myocytes, this remains to be clarified. Studies have suggested that the decrease in I_{sus} or I_{ss} is, at least in part, responsible for the prolongation of APD in the rat ventricle: e.g. endothelin-1 may prolong APD via inhibition of I_{sus} [26]. In addition, APD prolongation in the diabetic [7] or cirrhotic rat [45] is concomitant with decreases in I_{sus} and I_{ss}, respectively. Nevertheless, there is no evidence that Ang II prolongs APD in rat ventricular myocytes. Indeed, Ang II at 1 nM shortens APD in muscle trabeculae of rat right ventricles [14] and 1 μM Ang II has no effect on ventricular or atrial action potentials in the rat [10]. In our study, however, 1 μM Ang II significantly prolonged APD_{90} of rat ventricular myocytes after APD had been lengthened by BAY K8644, while not changing APD in the absence of BAY K8644 (Fig. 9). This finding may reflect Ang II-mediated prolongation of APD by the suppression of I_{sus} when the control action potential exhibits a relatively long APD with a plateau phase (phase 2) during which I_{sus} can be activated, as in human myocytes. A 15% inhibition of the sustained outward current significantly lengthens APD in human atrial myocytes [34]. Because the APD (phase 2) of human

cardiac myocytes is longer in the ventricle than in the atrium [9], a small degree of inhibition of sustained outward currents may significantly lengthen APD in human ventricular myocytes in which the contribution of sustained currents to repolarization could be relatively large. Nevertheless, there are no data on the effect of Ang II on the human ventricular action potential and future experiments should address the possibility of human ventricular myocytes with longer APD exhibiting high sensitivity to the action of Ang II.

It should be noted that Ang II-mediated modulation of other ionic currents must be taken into account when the effects of Ang II on APD are considered: in human myocytes, inhibition of I_{Ks} by Ang II (e.g. [11, 46]) may enhance APD (phase 2) prolongation in combination with I_{sus} suppression; whilst concomitant inhibition of inward currents such as $I_{Ca,L}$ (e.g. [18]) may offset the lengthening effect of I_{sus} suppression on APD. Further experiments examining Ang II modulation of each current component and simulation studies using mathematical models will be required to clarify how Ang II modulates APD in human ventricular myocytes and whether inhibition of the sustained outward currents is involved in the arrhythmogenicity of Ang II in the human heart.

Relevant concentration of Ang II

The Ang II concentrations of 30 nM~3 μM used in the present study and the IC_{50} for blockade of I_{sus} of 240 nM are much higher than the normal plasma concentrations (≈100 pM in rats [33]). At plasma concentrations much lower than 30 nM, therefore, Ang II would not affect I_{sus} in the rat ventricle. However, the Ang II concentration may be much higher in the tissue than in the plasma. The circulating renin-angiotensin system (RAS) has been thought to be the primary endocrine system designed for the general mediation of the effects of renin on the angiotensin production in plasma. Recent evidence, however, suggests that Ang II is mainly produced in peripheral tissues [5]. All the components of RAS have been detected in the heart [29], indicating that the heart is not only a target but also a site of endocrine or paracrine Ang II formation. Direct measurements of Ang II levels in the dog heart using the microdialysis technique have shown that the Ang II concentration under control conditions is >100-fold higher in the interstitial fluid space of the ventricular muscle (6,053±647 pM) than in aortic (21 ±38 pM) or coronary sinus (15±41 pM) plasma (all n=6) [13]. Moreover, in clinical studies measuring the aorta-coronary sinus concentration gradients of Ang II, cardiac Ang II generation increased with progression of heart failure [32]. Under pathological conditions in which Ang II may cause arrhythmias, therefore, the Ang II concentration in ventricular tissues may well exceed the 30 nM at which Ang II inhibits I_{sus} significantly. Further investigations will be required to determine how the Ang II concentration increases in human cardiac tissues under pathological conditions.

Limitations and perspectives of our study

We have shown that the I_{sus} suppression observed in this study is not due to a positive shift in the activation curve but due to the decrease in the maximum conductance. However, we could not clarify the kinetic mechanisms underlying the decrease in the maximum conductance of I_{sus}, induced probably via the phosphorylation of the channel protein by PKC. Single-channel recordings as well as molecular identification of I_{sus}, although impossible at present, will be needed for further clarification of the kinetic mechanisms of the I_{sus} inhibition by Ang II.

One of our goals is to determine whether Ang II leads to cardiac arrhythmias by modulating I_{sus} or other K^+ currents in human ventricular or atrial myocytes. In human atrial myocytes, the ultrarapid delayed-rectifier K^+ current (I_{Kur}; referred to as I_{sus} in [34]) which is kinetically similar to I_{sus} in rat ventricular myocytes but much more sensitive to 4-AP has been recorded [16]. However, there is little information on the sustained component of outward K^+ currents in human ventricular myocytes, although small, sustained outward currents similar to I_{Kur} but insensitive to 4-AP, like I_{sus} in the rat ventricle, have been recorded [28]. Thus, we can not conclude that the effects of Ang II on sustained outward currents in human myocytes are essentially the same as those on I_{sus} in the rat ventricle. Molecular identification and biophysical or pharmacological characterizations of the sustained outward currents in the human ventricle, as well as I_{sus} in the rat ventricle, remain to be performed.

Acknowledgements This work was supported in part by Kanazawa Medical University Grant for promoted Research S2001-14 (to Y. Kurata), and Kanazawa Medical University Grant for Collaborative Research C2003-1 (to Y. Kurata and T. Shibamoto).

References

1. Anada-Strivastava MB (1989) Angiotensin II receptors negatively coupled to adenylate cyclase in rat myocardial sarcolemma. Biochem Pharmacol 38:489–496
2. Anvari A, Türel Z, Schmidt A, Yilmaz N, Mayer G, Huber K, Schuster E, Gottsauner-Wolf M (1999) Angiotensin-converting enzyme and angiotensin II receptor 1 polymorphism in coronary disease and malignant ventricular arrhythmias. Cardiovasc Res 43:879–883
3. Apkon M, Nerbonne JM (1991) Characterization of two distinct depolarization-activated K^+ currents in isolated adult rat ventricular myocytes. J Gen Physiol 97:973–1011
4. Baker KM, Chernin MI, Wixon SK, Aceto JF (1990) Renin-angiotensin system involvement in pressure-overload cardiac hypertrophy in rats. Am J Physiol 259:H324–H332
5. Campbell DJ (1985) The site of angiotensin production. J Hypertens 3:199–207
6. Casis O, Iriarte M, Gallego M, Sánchez-Chapula J (1998) Differences in regional distribution of K^+ current densities in rat ventricle. Life Sci 63:391–400
7. Casis O, Gallego M, Iriarte M, Sánchez-Chapula JA (2000) Effects of cardiomyopathy on regional electrophysiologic characteristics of rat ventricular. Diabetologia 43:101–109

8. Chobanian AV, Haudenschild CC, Nickerson C, Drago R (1990) Antiatherogenic effect of captopril in the Watanabe heritable hyperlipidemic rabbit. Hypertension 15:327–331
9. Cohen NM, Lederer WJ (1993) Calcium current in single human cardiac myocytes. J Cardiovasc Electrophysiol 4:422–437
10. Cox MH, O S-J, Gasparo M de, Mukherjee R, Hewett KW, Spinale FG (1997) Myocardial electrophysiological properties in the presence of an AT_1 angiotensin II receptor antagonist. Basic Res Cardiol 92:129–138
11. Daleau P, Turgeon J (1994) Angiotensin II modulates the delayed rectifier potassium current of guinea pig ventricular myocytes. Pflugers Arch 427:553–555
12. Daugherty A, Manning MW, Cassis LA (2000) Angiotensin II promotes atherosclerotic lesions and aneurysms in apolipoprotein E-deficient mice. J Clin Invest 105:1605–1612
13. Dell'Italia LJ, Meng QC, Balcells E, Wei CC, Palmer R, Hageman GR, Durand J, Hankes GH, Oparil S (1997) Compartmentalization of Angiotensin II generation in the Dog heart. J Clin Invest 100:253–258
14. De Mello WC, Crespo MJ (1995) Cardiac refractoriness in rats is reduced by angiotensin II. J Cardiovasc Pharmacol 25:51–56
15. Dinh DT, Frauman AG, Johnston CI, Fabiani ME (2001) Angiotensin receptors: distribution, signaling and function. Clin Sci 100:481–492
16. Escande D, Coulombe A, Faivre JF, Deroubaix E, Coraboeuf E (1987) Two types of transient outward currents in adult human atrial cells. Am J Physiol 252:H142–H148
17. Gasparo M de, Catt KJ, Inagami T, Wright JW, Unger TH (2000) International Union of Pharmacology. XXIII. The angiotensin II receptors. Pharmacol Rev 52:415–472
18. Habuchi Y, Lu L-L, Morikawa J, Yoshimura M (1995) Angiotensin II inhibition of L-type Ca^{2+} current in sinoatrial node cells of rabbits. Am J Physiol 268:H1053–H1060
19. Hamill OP, Marty A, Neher E, Sakmann B, Sigworth FJ (1981) Improved patch-clamp techniques for high-resolution current recording from cells and cell-free membrane patches. Pflugers Arch 391:85–100
20. Harada K, Komuro I, Hayashi D, Sugaya T, Murakami K, Yazaki Yoshio (1998) Angiotensin II type Ia receptor is involved in the occurrence of reperfusion arrhythmias. Circulation 97:315–317
21. Hausdorff WP, Sekura RD, Aguilera G, Catt KJ (1987) Control of aldosterone production by angiotensin II is mediated by two guanine nucleotide regulatory proteins. Endocrinology 120:1668–1678
22. Hein L, Stevens ME, Barsii GS, Pratt RE, Kobilka BK (1997) Overexpression of angiotensin AT_1 receptor transgene in the mouse myocardium produces a lethal phenotype associated with myocyte hyperplasia and heart block. Proc Nat Acad Sci USA 94:6391–6396
23. Himmel HM, Wettwer E, Li Q, Ravens U (1999) Four different components contribute to outward current in rat ventricular myocytes. Am J Physiol 277:H107–H118
24. Hiura N, Wakatuki T, Yamamoto T, Nishikado A, Oki T, Ito S (2001) Effects of angiotensin II type I receptor antagonist (candesartan) in preventing fatal ventricular arrhythmias in dogs during acute myocardial ischemia and reperfusion. J Cardiovasc Pharmacol 38:729–736
25. Ichiyanagi O, Ishii K, Endoh M (2002) Angiotensin II increases L-type Ca^{2+} current in gramicidin D-perforated adult rabbit ventricular myocytes: comparison with conventional patch-clamp method. Pflugers Arch 444: 107–116
26. James AF, Ramsey JE, Reynolds AM, Hendry BM, Shattock MJ (2001) Effects of Endothelin-1 on K^+ currents from rat ventricular myocytes. Biochem Biophys Res Commun 284:1048–1055
27. Levitan IB (1985) Phosphorylation of Ion Channels. J Membr Biol 87:177–190
28. Li GR, Feng J, Yue L, Carrier M, Nattel S (1996) Evidence for two components of delayed rectifier K^+ current in human ventricular myocytes. Circ Res 78:689–696
29. Lindpaintner K, Ganten D (1991) The cardiac renin-angiotensin system: an appraisal of present experimental and clinical evidence. Circ Res 68:905–921
30. Maruyama R, Hatta E, Levi R (1999) Norepinephrine release and ventricular fibrillation in myocardia ischemia/reperfusion: roles of angiotensin and bradykinin. J Cardiovasc Pharmacol 34:913–915
31. Mazzolai L, Pedrazzini T, Nicoud F, Gabbiani G, Brunner HR, Nussberger J (2000) Increased cardiac angiotensin II levels induce right and left ventricular hypertrophy in normotensive mice. Hypertension 35:985–991
32. Neri Serneri GG, Boddi M, Cecioni I, Vanni S, Coppo M, Papa ML, Bandinelli B, Bertolozzi I, Polidori G, Toscano T, Maccherini M, Modesti PA (2001) Cardiac angiotensin II formation in the clinical course of heart failure and its relationship with left ventricular function. Circ Res 88:961–968
33. Nishiyama A, Seth DM, Navar G (2001) Renal interstitial fluid concentrations of Angiotensin I and II in anesthetized rats. Hypertension 39:129–134
34. Nygren A, Fiset C, Firek L, Clark JW, Lindblad DS, Clark RB, Giles WR (1998) Mathematical model of an adult human atrial cell. The role of K^+ currents in repolarization Circ Res 82:63–81
35. Pandit SV, Clark RB, Giles WR, Demir SS (2001) A Mathematical model of action potential heterogeneity in adult rat left ventricular myocytes. Biophys J 81:3029–3051
36. Quinn SJ, Williams GH (1988) Regulation of Aldosterone secretion. Annu Rev Physiol 50:409–426
37. Scamps F (1996) Characterization of a β-adrenergically inhibited K^+ current in rat cardiac ventricular cells. J Physiol (Lond) 491:81–97
38. Shimoni Y (1999) Protein kinase C regulation of K^+ currents in rat ventricular myocytes and its modification by hormonal status. J Physiol (Lond) 520:439–449
39. Shimoni Y, Liu XF (2003) Role of PKC in autocrine regulation of rat ventricular K^+ currents by angiotensin and endothelin. Am J Physiol 284: H1168–H1181
40. Shimoni Y, Liu XF (2003) Sex differences in the modulation of K^+ currents in diabetic rat cardiac myocytes. J Physiol (Lond) 550:401–412
41. Snyders DJ (1999) Structure and function of cardiac potassium channels. Cardiovasc Res 42:377–390
42. Tristani-Firouzi M, Chen J, Mitcheson JS, Sanguinetti MC (2001) Molecular biology of K^+ channels and their role in cardiac arrhythmias. Am J Med 110:50–59
43. Varro A, Lathrop DA, Hester SB, Nanashi PP, Papp JGY (1993) Ionic currents and action potentials in rabbit, rat, and guinea pig ventricular myocytes. Basic Res Cardiol 88:93–102
44. Walsh KB, Kass RS (1988) Regulation of a heart potassium channel by protein kinase A and C. Science 242:67–69
45. Ward CA, Ma Z, Lee SS, Giles WR (1997) Potassium currents in atrial and ventricular myocytes from a rat model of cirrhosis. Am J Physiol 273:G537–G544
46. Yang XJ, Jiang WP (1998) Angiotensin II receptor regulates ionic currents in guinea pig ventricular myocytes. J Cardiovasc Pharmacol Ther 3:1–10

ELSEVIER

Prostaglandins & other Lipid Mediators 73 (2004) 73–85

PROSTAGLANDINS
& other
LIPID MEDIATORS

Effects of platelet-activating factor and thromboxane A_2 on isolated perfused guinea pig liver

Zonghai Ruan [a,b], Toshishige Shibamoto [a,*], Tomohiro Shimo [c], Tomonobu Koizumi [b], Hideaki Tsuchida [c], Yasutaka Kurata [a], Toshitsugu Ogura [a], Keishi Kubo [b]

[a] *Department of Physiology, Division 2, Kanazawa Medical University, Uchinada 920-0293, Japan*
[b] *First Department of Medicine, Shinshu University School of Medicine, Matsumoto 390-8621, Japan*
[c] *Department of Anesthesiology, Kanazawa Medical University, Uchinada 920-0293, Japan*

Received 10 October 2003; accepted 25 November 2003

Abstract

Lipid mediators, thromboxane A_2 (TxA_2) and platelet-activating factor (PAF), are potent vasoconstrictors, and have been implicated as mediators of liver diseases, such as ischemic-reperfusion injury. We determined the effects of a TxA_2 analogue (U-46619) and PAF on the vascular resistance distribution and liver weight (wt) in isolated guinea pig livers perfused with blood via the portal vein. The sinusoidal pressure was measured by the double occlusion pressure (P_{do}), and was used to determine the pre- (R_{pre}) and post-sinusoidal (R_{post}) resistances. U-46619 and PAF concentration-dependently increased the hepatic total vascular resistance (R_t). The minimum concentration at which significant vasoconstriction occurs was 0.001 μM for PAF and 0.1 μM for U-46619. Moreover, the concentration of U-46619 required to increase R_t to the same magnitude is 100 times higher than PAF. Thus, the responsiveness to PAF was greater than that to U-46619. Both agents increased predominantly R_{pre} over R_{post}. U-46619 caused a sustained liver weight loss. In contrast, PAF also caused liver weight loss at lower concentrations, but it produced liver weight gain at higher concentrations (2.5 ± 0.3 per 10 g liver weight at 1 μM PAF), which was caused by substantial post-sinusoidal constriction and increased P_{do}. In conclusion, both TxA_2 and PAF contract predominantly the pre-sinusoidal veins. TxA_2 causes liver weight loss, while PAF at high

Abbreviations: IVC, inferior vena cava; PAF, platelet-activating factor; R_{pre}, pre-sinusoidal resistance; R_{post}, post-sinusoidal resistance; R_t, total portal-hepatic venous resistance; P_{pv}, portal venous pressure; P_{hv}, hepatic venous pressure; P_{do}, double occlusion pressure; Q, portal blood flow rate; wt, liver weight; LT, leukotriene; TxA_2, thromboxane A_2

* Corresponding author. Tel.: +81-76-218-8104; fax: +81-76-286-8010.
E-mail address: shibamo@kanazawa-med.ac.jp (T. Shibamoto).

1098-8823/$ – see front matter
doi:10.1016/j.prostaglandins.2003.11.002

concentrations increases liver weight due to substantial post-sinusoidal constriction in isolated guinea pig livers.

Keywords: PAF; The double occlusion pressure; Hepatic circulation; U-46619; Sinusoidal pressure; Microcirculation

1. Introduction

Both platelet-activating factor (PAF) and thromboxane A_2 (TxA_2) are lipid mediators with potent vasoactive actions, and are released by a variety of cells, including platelets, neutrophils, macrophages (e.g. Kupffer cells), monocytes, lymphocytes, endothelial, and smooth muscle cells, in response to various stimuli [1,2]. Either substance is implicated as a mediator of various types of liver diseases, such as endotoxin liver injury [3–5], ischemia–reperfusion liver injury [6–9], and hepatic resection [8–10]. The microcirculation of the hepatic sinusoid plays a crucial role in the integrity of liver function [11]. PAF and TxA_2 may influence the sinusoidal circulation, as a result of its vasoconstrictive action. Indeed, an infusion of the TxA_2 analogue into the isolated perfused rat liver increases portal vein pressure, indicative of constriction of the hepatic vasculature [12,13]. PAF also causes an increase in the portal vein pressure in in vivo animals [14,15] and isolated perfused livers [16,17]. More recently, we have reported by measuring the sinusoidal pressure using the hepatic vascular occlusion methods in isolated blood-perfused canine livers that the TxA_2 analogue predominantly contracts the post-sinusoidal veins [18], while PAF contracts similarly both the pre- and post-sinusoidal veins [19]. However, there might be species differences in the primary site of hepatic vasoconstriction, and the effects of these lipid mediators on the hepatic vessels of guinea pigs are not known. Therefore, we examined using the hepatic vascular occlusion methods the effects of PAF and a TxA_2 mimetic of U-46619, on hepatic vascular resistance distribution and liver weight (wt) in isolated perfused guinea pig livers.

2. Materials and methods

Twenty-five male Hartley guinea pigs weighing 351 ± 31 (S.D.) g were used in this study. The experiments conducted in the present study were approved by the Animal Research Committee of Kanazawa Medical University.

2.1. Isolated liver preparation

The animals were anesthetized with pentobarbital sodium (35 mg kg^{-1}, i.p.) and mechanically ventilated with room air. The methods for the isolated perfused guinea pig liver preparation were previously described [20]. In brief, a polyethylene tube was placed in the right carotid artery. After laparotomy, the cystic duct and the hepatic artery were ligated and the bile duct was cannulated with the polyethylene tube (1.0 mm i.d., 1.3 mm o.d.).

At 5 min after intra-arterial heparinization (500 U kg^{-1}), 8–9 ml of blood was withdrawn through the carotid arterial catheter. The intra-abdominal inferior vena cava (IVC) above the renal veins was ligated, and the portal vein was cannulated with a stainless cannula (2.1 mm i.d., 3.0 mm o.d.) for portal perfusion. After thoracotomy, the supradiaphragmatic IVC was cannulated with the same size stainless cannula, then portal perfusion was begun with the heparinized autologous blood that was diluted with 5% bovine albumin (Sigma) in Krebs solution (118 mM NaCl, 5.9 mM KCl, 1.2 mM $MgSO_4$, 2.5 mM $CaCl_2$, 1.2 mM NaH_2PO_4, 25.5 mM $NaHCO_3$, and 5.6 mM glucose) at H_{ct} of 8%. The liver was rapidly excised, suspended from an isometric transducer (TB-652T, Nihon-Kohden, Japan) and weighed continuously throughout the experimental period.

The liver was perfused recirculatingly at a constant flow rate via the portal vein with blood that was pumped using a Masterflex pump from the venous reservoir through a heat exchanger (37 °C). The recirculating blood volume was 40 ml. The perfused blood in the reservoir was oxygenated by bubbling with 95% O_2 and 5% CO_2. The portal venous (P_{pv}) and the hepatic venous (P_{hv}) pressures were measured using pressure transducers (TP-400T, Nihon-Kohden) attached by sidearm to the appropriate cannulas with the reference points at the hepatic hilus. To occlude inflow and outflow perfusion lines simultaneously for measurement of the double occlusion pressure (P_{do}), two solenoid valves were placed in a position that each sidearm cannula was between the corresponding solenoid valve and the liver. Portal blood flow rate (Q) was measured with an electromagnetic flow meter (MFV 1200, Nihon-Kohden), and the flow probe was positioned in the inflow line. Bile was collected drop by drop in a small tube suspended from the force transducer (SB-1T, Nihon-Kohden). One bile drop yielded 0.027 g and the time between drops was measured for determination of the bile flow rate [21]. The hepatic vascular pressures, blood flow rate, liver weight, and bile weight were monitored continuously and displayed through a thermal physiograph (RMP-6008, Nihon-Kohden). Outputs were also digitized by the analog–digital converter at a sampling rate of 100 Hz. These digitized values were displayed and recorded using a personal computer for later determination of P_{do}.

2.2. Experimental protocol

Hepatic hemodynamic parameters were observed for at least 20 min after the start of perfusion until an isogravimetric state (no weight gain or loss) was obtained by adjusting the flow rate and the height of the reservoir at a P_{pv} of 7.6 ± 1.1, a P_{hv} of 0–1 cmH_2O, and at a Q of 42.5 ± 6.0 ml min^{-1} per 10 g wt. After the baseline measurements, the perfused livers were divided into the following two groups of the PAF and U-46619 groups. A stock solution of PAF (Sigma) and U-46619 were made by dissolving 1 mg PAF or 100 μg U-46619, respectively, in 1 ml 99.5% ethanol, and stored at −20 °C. To determine the concentration dependence, PAF or U-46619 was administered as a bolus into the reservoir to gain the final concentration of 0.001–1 μM. The effect of U-46619 was further examined at a high concentration of 3 μM. At least 10 min was allowed for stabilization of each variable between doses.

The hepatic sinusoidal pressure was measured by the double occlusion method [22,23]. Both the inflow and outflow lines were simultaneously and instantaneously occluded for

10 s using the solenoid valves, after which P_{pv} and P_{hv} rapidly equilibrated to a similar or identical pressure, which was P_{do}. Actually, P_{do} values were obtained from the digitized data of P_{pv} and P_{hv} using an original program (LIVER software, Biomedical Science, Kanazawa, Japan). In each experimental group, P_{do} was measured at baseline and 2, 4, 6, and 10 min after injection of PAF or U-46619, and then at a 10-min interval up to 60 min.

The total portal-hepatic venous (R_t), pre-sinusoidal (R_{pre}), and post-sinusoidal (R_{post}) resistances were calculated as follows:

$$R_t = \frac{(P_{pv} - P_{hv})}{Q} \quad (1)$$

$$R_{pre} = \frac{(P_{pv} - P_{do})}{Q} \quad (2)$$

$$R_{post} = \frac{(P_{do} - P_{hv})}{Q} \quad (3)$$

2.3. Statistics

All results are expressed as the means ± S.D. ANOVA followed by Bonferroni's test was used to test for significant differences. Differences were considered as statistically significant at P values less than 0.05.

3. Results

3.1. Effect of PAF on hepatic hemodynamic variables, liver weight, and bile flow

Fig. 1 shows a representative example of variables after an injection of PAF. Soon after an injection of PAF at 0.1 μM, vasoconstriction occurred, as evidenced by an increase in P_{pv}. P_{pv} increased from the baseline of 7.7 ± 0.8 cmH_2O to the peak of 34.0 ± 7.8 cmH_2O within 2–4 min after PAF injection. P_{hv} and blood flow did not change because of the constant flow rate perfusion. The double occlusion maneuver performed at 4 min after PAF revealed that P_{do} increased from the baseline value of 3.4 ± 0.2 cmH_2O to 8.2 ± 1.1 cmH_2O. At this maximal vasoconstriction, the pressure gradient of P_{do}-to-P_{hv} was significantly increased from the baseline of 3.0 ± 0.2 cmH_2O to 7.9 ± 1.0 cmH_2O, indicating an increase in R_{post}. However, the increase in the P_{pv}-to-P_{do} gradient from 4.4 ± 1.0 cmH_2O to 25.8 ± 6.8 cmH_2O was much greater than that in the P_{do}-to-P_{hv} gradient, indicating a greater increase in R_{pre} than R_{post}. Concomitant with hepatic vasoconstriction, the liver weight showed a biphasic response of the initial decrease followed by a gradual increase, reaching the peak of 2.1 ± 0.9 per 10 g wt at 20 min. Bile flow decreased to 51 ± 16% of the baseline at 10 min, followed by a gradual recovery to 89 ± 13% at the end of the experimental period.

Table 1 shows the basal hemodynamic variables. Fig. 2 shows the peak levels in R_{pre}, R_{post}, R_t, R_{post}/R_t ratio, wt change, and bile flow after injections of PAF (closed column). At concentrations higher than 0.001 μM, apparent venoconstriction was observed. R_t and R_{pre} showed concentration-dependent increases with peak levels of 5.1-fold the baseline

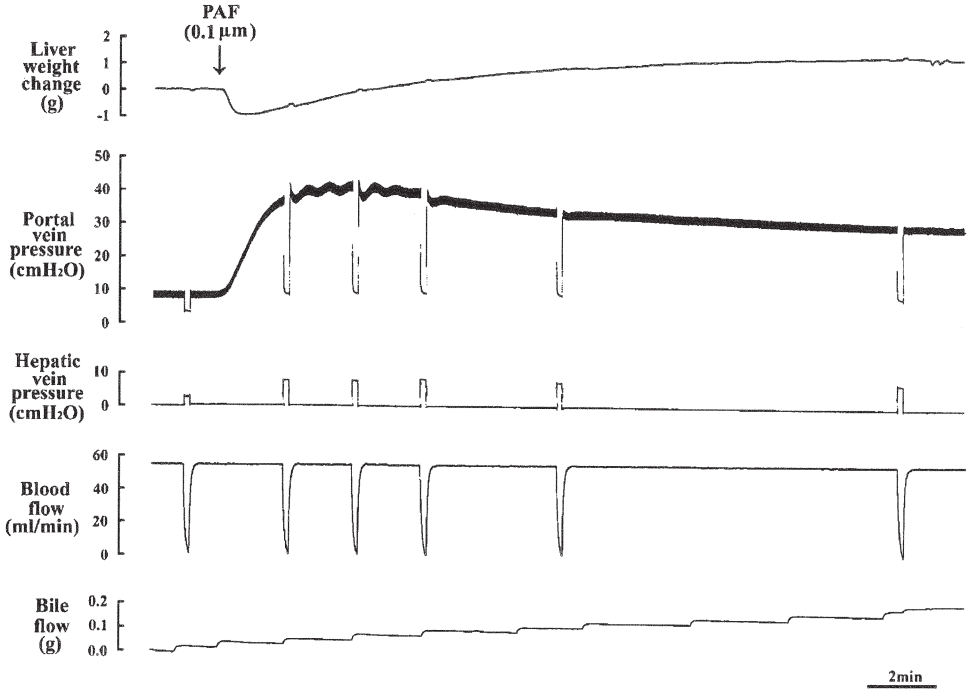

Fig. 1. A representative recording of the response to PAF at 0.1 μM of a guinea pig liver.

($0.21 \pm 0.03\,cmH_2O\,ml^{-1}\,min^{-1}$ per 10 g wt versus $1.06 \pm 0.32\,cmH_2O\,ml^{-1}\,min^{-1}$ per 10 g wt; baseline versus peak) and 6.9-fold the baseline ($0.13 \pm 0.01\,cmH_2O\,ml^{-1}\,min^{-1}$ per 10 g wt versus $0.88 \pm 0.28\,cmH_2O\,ml^{-1}\,min^{-1}$ per 10 g wt; baseline versus peak), respectively, at the maximum concentration of 1 μM PAF. In contrast, R_{post} also increased but reached maximum levels at the submaximum concentration of 0.1 μM PAF. Actu-

Table 1
Basal hemodynamic variables of isolated perfused guinea pig livers in the PAF and U-46619 groups

	PAF	U-46619
Number of animals	21	20
Portal pressure (cmH_2O)	7.9 ± 1.1	7.4 ± 1.0
Hepatic venous pressure (cmH_2O)	0.46 ± 0.28	0.32 ± 0.26
Double occlusion pressure (cmH_2O)	3.4 ± 0.5	3.2 ± 0.5
Blood flow rate ($ml^{-1}\,min^{-1}$ per 10 g)	45 ± 5	40 ± 6
Total vascular resistance ($cmH_2O\,ml^{-1}\,min^{-1}$ per 10 g)	0.17 ± 0.03	018 ± 0.04
Pre-sinusoidal resistance ($cmH_2O\,ml^{-1}\,min^{-1}$ per 10 g)	0.10 ± 0.02	0.11 ± 0.03
Post-sinusoidal resistance ($cmH_2O\,ml^{-1}\,min^{-1}$ per 10 g)	0.07 ± 0.01	0.08 ± 0.02
R_{post}/R_t ratio	0.42 ± 0.05	0.42 ± 0.06

Values are given as means ± S.D.

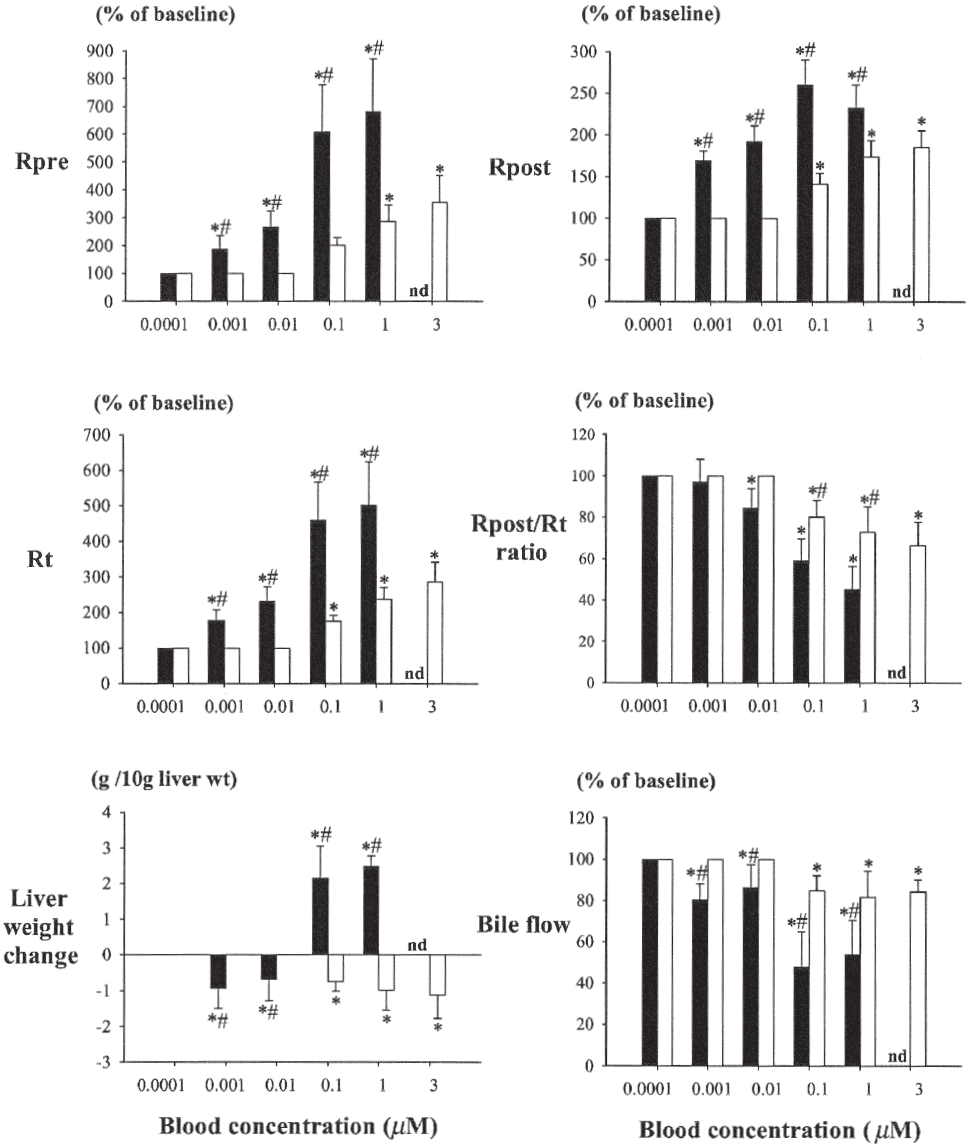

Fig. 2. The peak changes in the total (R_t), pre- (R_{pre}), and post-sinusoidal (R_{post}) resistances, the R_{post}/R_t ratio, bile flow and liver weight change at 0.001–3 μM of PAF (closed column) and U-46619 (open column) as expressed by percentage of the baseline in guinea pig livers. Values are given as means ± S.D., $n = 5$–7. * $P < 0.05$ vs. the baseline. # $P < 0.05$ vs. PAF. The "nd" indicates that effects of 3 μM PAF was not examined.

ally the peak R_{post} at 0.1 μM PAF was not significantly different from that at 1 μM PAF, which was 2.3-fold the baseline ($0.08 \pm 0.02\ cmH_2O\ ml^{-1}\ min^{-1}$ per 10 g wt versus $0.19 \pm 0.04\ cmH_2O\ ml^{-1}\ min^{-1}$ per 10 g wt; baseline versus peak). Thus, the R_{post}/R_t ratio decreased concentration-dependently as shown in Fig. 2. R_{pre} and R_{post} recovered to the

baseline level at 50 min in the 0.001 and 0.01 μM PAF groups, but did not return to the baseline levels in 0.1 and 1 μM PAF groups.

Liver weight decreased and gradually returned to the baseline after PAF at concentrations of 0.001–0.01 μM. At PAF concentrations higher than 0.1 μM, the liver weight showed a biphasic change characterized by an initial decrease followed by increase, as shown in Fig. 1. In response to 1 μM PAF, liver weight increased to the peak of 2.5 ± 0.3 per 10 g wt at 30 min. There are no significant differences in peak liver weight levels between the 0.1 and 1 μM PAF groups.

3.2. *Effects of U-46619 on hepatic hemodynamic variables, liver weight, and bile flow*

Fig. 3 shows a representative example of variables after an injection of U-46619. P_{pv} increased from the baseline of 7.5±1.2 cmH_2O to the peak of 20.1 ± 2.4 cmH_2O within 2–4 min after an injection of U-46619 at the maximal concentration of 3 μM. However, the liver weight decreased, reaching the nadir of −1.1 ± 0.6 per 10 g wt at 2–4 min, followed by a gradual return to the baseline level within 30 min. P_{do} increased from the baseline of 3.2 ± 0.6 cmH_2O to 5.5 ± 0.9 cmH_2O at 2 min, which was small as compared with the response to PAF. At the maximal vasoconstriction, the increase in P_{pv}-to-P_{do} gradient from 4.3±1.1 cmH_2O to 14.6±1.8 cmH_2O was much greater than that in the P_{do}-to-P_{hv} gradient from the baseline of 2.7 ± 0.6 cmH_2O to 5.0 ± 0.9 cmH_2O, indicating a greater increase in R_{pre} than R_{post} in response to U-46619. Bile flow also decreased to 90.8 ± 10.5% of the baseline at 2 min, followed by a gradual recovery to 98.4 ± 6.2% at 6 min.

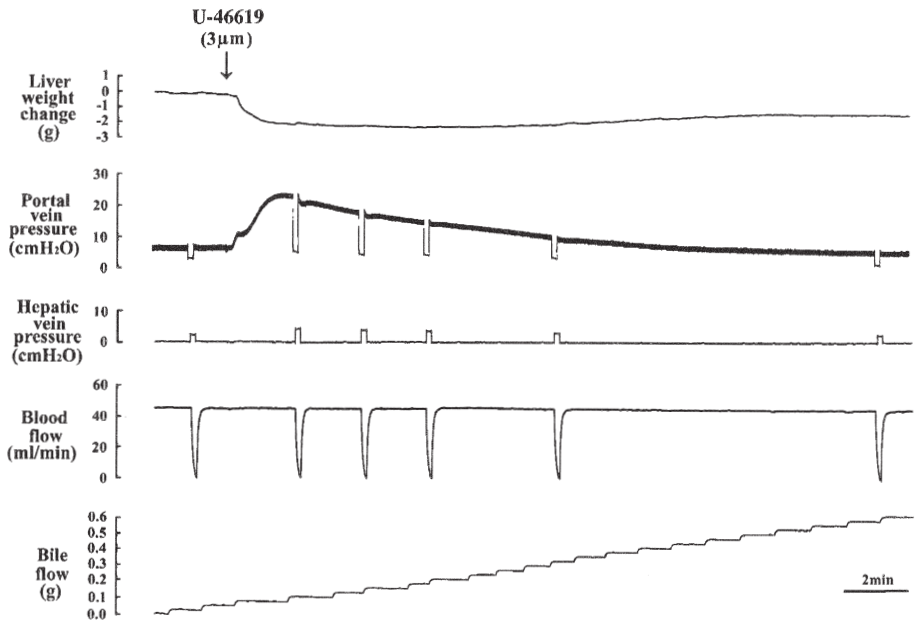

Fig. 3. Representative recordings of the responses to U-46619 at 3 μM of a guinea pig liver.

Fig. 2 shows the peak levels in R_{pre}, R_{post}, R_t, R_{post}-to-R_t ratio, wt change, and bile flow after injections of U-46619 (open column). At concentration ranging 0.1–3 μM, U-46619 causes concentration-dependent increases in R_t and R_{pre}. In contrast, U-46619 increased R_{post}, but there are no significant differences in peak R_{post} at 0.1–3 μM U-46619. Similar to PAF, the increase in R_{pre} was greater than that in R_{post} after U-46619; R_{pre} increased to 3.4 times the baseline, while R_{post} increased to only 1.8 times the baseline in response to 3 μM U-46619. This predominant pre-sinusoidal constriction over post-sinusoidal constriction was reflected by a progressive decrease in R_{post}/R_t ratio, as shown in Fig. 2. Fig. 2 also shows that the concentration required to increase R_t to the same magnitude is 100 times higher in U-46619 than in PAF. At the comparable R_t levels between PAF and U-46619, the corresponding R_{post} in U-46619 groups was smaller than that in PAF groups, indicating that U-46619 more preferentially contracts the pre-sinusoids than PAF. R_t, R_{pre}, and R_{post} recovered almost to the baseline levels within 30 min after U-46619.

Liver weight showed a significant decrease from the baseline, but no significant differences among individual concentrations of U-46619 groups. Bile flow decreased slightly in response to U-46619.

4. Discussion

The present study has shown that both PAF and U-46619 contract predominantly the pre-sinusoidal veins over the post-sinusoidal veins in isolated perfused guinea pig livers. U-46619 causes liver weight loss, while PAF at high concentrations increases liver weight due to substantial post-sinusoidal constriction.

We have recently reported using the same isolated guinea pig liver preparation that hepatic anaphylaxis induced by ovalbumin antigens causes marked venoconstriction and liver weight gain, which could account for the portal hypertension and hepatic congestion associated with anaphylactic shock [20]. Anaphylactic reaction is accompanied by an increased release of vasoactive substances, such as histamine [24,25], PAF [24], and TxA_2 [24,26]. The hepatic responses to high concentrations of PAF in the present study, characterized by substantial post-sinusoidal constriction and liver weight gain, may be compatible with the previous finding of hepatic vascular anaphylaxis in guinea pigs [20]. In contrast, either histamine or TxA_2 does not seem to be main mediators responsible for the guinea pig hepatic anaphylaxis, because the post-sinusoidal response to histamine was short-lasting [27], and that to TxA_2 was weak with resultant liver weight loss, but not weight gain, as shown in the present study.

PAF may contribute to various types of liver injury, at least in part, through post-sinusoidal constriction in dogs [8,19] and guinea pigs. PAF-induced hepatic venoconstriction may cause outflow block of the sinusoids and increase the sinusoidal pressure, resulting in increased transvascular fluid exudation into the interstitium and water accumulation, which in turn could compress mechanically the sinusoids. These latter two mechanisms may induce poor perfusion and decreased oxygen delivery to hepatocytes and eventually hypoxia in the sinusoids and therefore may account for the roles of PAF in the liver injury. In contrast to PAF, TxA_2 itself do not seem to have edematogenic actions in guinea pig because of its weak post-sinusoidal contractility. However, in dogs, TxA_2 could in-

duce hepatic congestion and hence contribute to liver injury due to vigorous contraction of the post-sinusoids [9,18]. Thus, it is important to take account of the species differences when the roles of these lipid mediators are evaluated in the pathogenesis of the liver injury.

Hepatic vascular responsiveness to various vasoactive substances differs depending on the vascular segments and the animal species. Histamine causes marked constriction of the hepatic vein in dogs [28,29] and guinea pigs [27], while it does not constrict hepatic vessels of cats [30] and rats [27]. In contrast, norepinephrine contracts preferentially the pre-sinusoidal vessels similarly in dog [31,32], rat [31,32], rabbit [23,31,33], and guinea pig [27]. Although PAF and TxA_2 increased the portal venous pressure in rat livers [12,13,19], there are only a limited number of investigations that determined the changes in the hepatic longitudinal vascular resistance distribution in response to PAF or TxA_2. We previously reported using canine isolated blood-perfused livers that TxA_2 constricts predominantly the hepatic vein [18], while PAF constricts both portal veins and hepatic veins similarly [19]. We herein demonstrated that both PAF and TxA_2 contract predominantly pre-sinusoidal veins over post-sinusoidal veins in isolated perfused guinea pig livers, although the post-sinusoidal venoconstrictive action of TxA_2 was weaker than that of PAF.

The mechanism whereby PAF or U-46619 constricts predominantly the pre-sinusoids over the post-sinusoids in guinea pig is not known. One possibility may be related to platelet and neutrophil aggregation because either PAF or TxA_2 can activate these cells resulting in intravascular aggregation [1,2,34]. The aggregation of neutrophils and platelets may obliterate the sinusoids, which could represent an increase in the pre-sinusoidal resistance. However, this assumption seems unlikely because heparin that was used in the present study has been shown not only to inhibit adhesion of leukocyte in the endothelium [35] but also to cause platelet dysfunction [36]. Thus, even if platelet or leukocyte aggregation had occurred, they might have played a minor role in the vascular resistance change in the present study. The second, contraction of the hepatic pericytes, hepatic stellate cells, may account for either PAF- or U-46619-induced pre-sinusoidal venoconstriction. Hepatic stellate cells are located around the endothelial cells and their multiple cellular appendages reach out to wrap around the sinusoid [37]. Hepatic stellate cells are highly contractile in response to PAF and TxA_2 [38]. PAF and TxA_2 could contract sinusoidal hepatic stellate cells directly, resulting in increased sinusoidal resistance, which might represent increased pre-sinusoidal resistance. However, Zhang et al. [39] recently reported that sinusoidal constriction induced by hepatic stellate cells is not responsible for an increase in the portal pressure, when endothelin-1 was infused into isolated rat livers. Moreover, Ekataksin and Kaneda [40] and McCuskey et al. [41] formulated anatomical arguments against the vasomotor activity of intact stellate cells. Thus, further investigation may be required for this possibility. Finally, a more plausible explanation may be that functional PAF and TxA_2 receptors are distributed abundantly in the smooth muscle cells of the guinea pig pre-sinusoidal vein as compared with those of the post-sinusoidal vein. The finding that PAF at high concentrations increased substantially the post-sinusoidal resistance as compared with U-46619 might suggest that the post-sinusoidal smooth muscle cells contain a large number of PAF receptors but a relatively small number of TxA_2 receptors, although PAF receptors might distribute more abundantly in pre-sinusoids than in post-sinusoids. However, there is no direct evidence of the presence of nonhomogenous distribution of PAF or TxA_2 receptors in guinea pig hepatic vessels.

We believe that the hepatic vasoconstrictive response to PAF and U-46619 in the present study was due to the direct effects of these substances, because the vasoconstriction occurred immediately after injection of either PAF or U-46619 without a latent period which might have been required for activation, release or synthesis of the other vasoconstrictors. However, we cannot rule out a possibility of the modulation of an endogenous hepatic vasoconstrictor that could be released by U-46619 or PAF. In organs other than livers, some of the vasoconstrictive effects of TxA_2 seem to be mediated by the induction of leukotriene (LT) C_4 and LTD_4 [42], and endothelins [43]. PAF is also able to activate the hepatic intravascular macrophages of Kupffer cells, with resultant release of the cyclooxygenase metabolites [44]. Actually, functionally active PAF receptors are demonstrated on the Kupffer cells [45].

In the present study, U-46619 and PAF at low concentrations cause liver weight loss. However, liver weight increased in response to PAF at concentrations higher than 0.1 μM. The decrease in liver weight after U-46619 and PAF at low concentrations may be produced by pre-sinusoidal constriction which may have prevented the entrance of blood into the liver capillaries, resulting in weight loss. The liver weight gain after PAF at high concentrations may be caused by substantial post-sinusoidal constriction and an increase in P_{do}, both of which would lead to hepatic congestion, and enhanced extravascular fluid filtration and interstitial water accumulation.

P_{do}, which is the determinant of transvascular fluid movement and hepatic congestion, was increased concomitant with the weight gain at high concentrations of PAF, while the liver whose P_{do} was not so much increased showed a liver weight loss due to pre-sinusoidal constriction. This finding suggests that the magnitude of increased P_{do} represents the liver weight change. Fig. 4 shows the relationship between the peak P_{do} and liver weight change in the PAF and U-46619 groups. There was a significant correlation between the P_{do} and wt (wt = 0.81, P_{do} = 4.98, r = 0.882, P < 0.0001). This finding indicated that the wt change was strongly associated with the P_{do} increase. The isolated perfused liver with

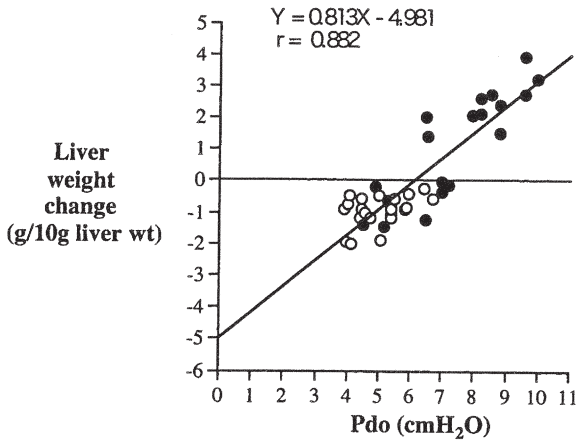

Fig. 4. Relationship between peak P_{do} values and liver weight (wt) changes after injections of U-46619 (open circle, n = 20) and PAF (closed circle, n = 22). Equations of linear lines are given in the text.

pre-sinusoidal venoconstriction does not show liver weight gain until post-sinusoidal vessels contract enough to elevate P_{do} higher than approximately 8 cmH_2O.

In conclusion, PAF as well as a TxA_2 analogue, U-46619, contract predominantly the pre-sinusoidal veins over the post-sinusoidal veins. The post-sinusoidal venoconstrictive action of TxA_2 was weaker than that of PAF. TxA_2 causes liver weight loss, while PAF at high concentrations increases liver weight due to substantial post-sinusoidal constriction and increased P_{do} in isolated guinea pig livers.

Acknowledgements

This work was supported by a grant for Collaborative Research from Kanazawa Medical University (C2003-1) and a grant-in-aid for Scientific Research from the Ministry of Education, Culture, Sports, Sciences and Technology of Japan (No. 15591665).

References

[1] Braquet P, Touqui L, Shen TY, Vargaftig BB. Perspective in platelet-activating factor research. Pharmacol Rev 1987;39:97–145.
[2] Samuelsson B, Goldyne M, Granstrom E, Hamberg M, Hammarstrom S, Malmsten C. Prostaglandins and thromboxanes. Ann Rev Biochem 1978;47:997–1029.
[3] Kitagawa S, Kubota Y, Yamaguchi T, Fujimura K, Binnaka T, Tani K, et al. Role of endogenous platelet-activating factor (PAF) in endotoxin-induced portal hypertension in rats. J Gastroenterol Hepatol 1992;7:481–5.
[4] Guarner F, Wallace JL, MacNaughton WK, Ibbotson GC, Arroyo V, Rodes J. Endotoxin-induced ascites formation in the rat: partial mediation by platelet-activating factor. Hepatology 1989;10:788–94.
[5] Ishiguro S, Arii S, Monden K, Adachi Y, Funaki N, Higashitsuji H, et al. Identification of the thromboxane A_2 receptor in hepatic sinusoidal endothelial cells and its role in endotoxin-induced liver injury in rats. Hepatology 1994;20:1281–6.
[6] Ontell SJ, Makowka L, Trager J, Mazzaferro V, Ove P, Starzl TE. Pharmacologic modulation of experimental postischemic hepatic function. Ann Surg 1989;209:200–10.
[7] Ishiguro S, Arii S, Monden K, Fujita S, Nakamura T, Niwano M, et al. Involvement of thromboxane A_2-thromboxane A_2 receptor system of the hepatic sinusoid in pathogenesis of cold preservation/reperfusion injury in the rat liver graft. Transplantation 1995;59:957–61.
[8] Iwazaki S, Takeyoshi I, Ohawada S, Sunose Y, Tsutsumi H, Kawashima Y, et al. FR128998 ameliorates liver injury in extended liver resection with ischemia in dogs. Hepatogastroenterology 2001;48:197–202.
[9] Takeyoshi I, Sunose Y, Iwazaki S, Tsutsumi H, Aiba M, Kasahara M, et al. The effect of a selective cycloxygenase-2 inhibitor in extended liver resection with ischemia in dogs. J Surg Res 2001;100:25–31.
[10] Shimada M, Matsumata T, Taketomi A, Shirabe K, Yamamoto K, Sugimachi K. The role of prostaglandins in hepatic resection. Prostaglandins Leukot Essent Fatty Acids 1994;50:65–8.
[11] Chun K, Zhang J, Biewer J, Ferguson D, Clemens MG. Microcirculatory failure determines lethal hepatocyte injury in ischemic/reperfusion rat livers. Shock 1994;1:3–9.
[12] Fisher RA, Robertson SM, Olson MS. Stimulation of glycogenolysis and vasoconstriction in the perfused rat liver by the thromboxane A_2 analogue U-46619. J Biol Chem 1987;262:4631–8.
[13] Haussinger D, Stehle T, Gerok W. Effects of leukotrienes and the thromboxane A_2 analogue U-46619 in isolated perfused rat liver. Metabolic, hemodynamic and ion-flux responses. Biol Chem Hoppe Seyler 1988;369:97–107.
[14] Bessin P, Bonnet J, Apffel D, Soulard C, Desgroux L, Pelas I, et al. Acute circulatory collapse caused by platelet-activating factor (PAF-acether) in dogs. Eur J Pharmacol 1983;86:403–13.

[15] Hines KL, Braillon A, Fisher RA. PAF increases hepatic vascular resistance and glycogenolysis in vivo. Am J Physiol 1991;260:G471–80.
[16] Lapointe DS, Olson MS. Alteration of hepatic tissue spaces by platelet-activating factor and phenylephrine. Hepatology 1989;9:278–84.
[17] Buxton DB, Fisher RA, Hanahan DJ, Olson MS. Platelet-activating factor mediated vasoconstriction and glycogenolysis in the perfused rat liver. J Biol Chem 1986;261:644–9.
[18] Urayama H, Shibamoto T, Wang HG, Koyama S. Thromboxane A_2 analogue contracts predominantly the hepatic veins in isolated canine livers. Prostaglandins 1996;52:483–95.
[19] Wang HG, Shibamoto T, Koyama S. Effect of platelet-activating factor on hepatic capillary pressure in isolated dog liver. Prostaglandins Leukot Essent Fatty Acids 1997;57:293–8.
[20] Ruan Z, Shibamoto T, Shimo T, Tsuchida H, Koizumi T, Nishio M. Nitric oxide, but not carbon monoxide, attenuates anaphylaxis-induced postsinusoidal contraction and congestion in guinea pig liver. Am J Physiol Regul Integr Comp Physiol 2004;286:R94–100.
[21] Ling YQ, Shibamoto T, Honda T, Kamikado C, Hironaka E, Hongo M, et al. Increased sinusoidal pressure is associated with early liver weight gain in ischemia–reperfusion injury in isolated perfused rat liver. J Surg Res 2000;88:70–7.
[22] Yamaguchi Y, Shibamoto T, Hayashi T, Saeki Y, Tanaka S. Hepatic vascular response to anaphylaxis in isolated canine liver. Am J Physiol 1994;267:R268–74.
[23] Shibamoto T, Wang HG, Miyahara T, Tanaka S, Haniu H, Koyama S. Presinusoidal vessels predominantly contract in response to norepinephrine, histamine, and KCl in rabbit liver. J Appl Physiol 1999;87:1404–12.
[24] Kemp SF, Lockey RF. Anaphylaxis: a review of causes and mechanisms. J Allergy Clin Immunol 2002;110:341–8.
[25] Ojers G, Holmes CA, Dragsted CA. The relation of the liver histamine to anaphylactic shock in dogs. J Pharmacol Exp Ther 1941;72:33.
[26] Hamberg M, Svensson J, Hedqvist P, Strandberg K, Samuelsson B. Involvement of endoperoxides and thromboxanes in anaphylactic reactions. Adv Prostaglandin Thromboxane Res 1976;1:495–501.
[27] Shibamoto T, Narushima M, Ling YQ, Shimo T, Tsuchida H, Kurata Y, et al. Different hepatic vascular response to norepinephrine and histamine between guinea pig and rat. Acta Physiol Scand 2004 (in press).
[28] Mahfouz M, Aida G. Pharmacodynamic of intrahepatic circulation in shock. Surgery 1967;61:755–62.
[29] Lautt WW, Legare DJ. Effect of histamine, norepinephrine, and nerves on vascular pressures in dog liver. Am J Physiol 1987;252:G472–8.
[30] Greenway CV, Lautt WW. Effects of infusions of catecholamines, angiotensin, vasopressin and histamine on hepatic blood volume in the anaesthetized cat. Br J Pharmacol 1972;44:177–84.
[31] Bohlen HG, Maass-Moreno R, Rothe CF. Hepatic venular pressures of rats, dogs, and rabbits. Am J Physiol 1991;261:G539–47.
[32] Shibamoto T, Wang HG, Tanaka S, Koyama S. Hepatic capillary pressure is estimated using triple vascular occlusion method in isolated canine liver. Am J Physiol 1996;271:R1130–41.
[33] Rothe CF, Maass-Moreno R. Hepatic venular resistance responses to norepinephrine, isoproterenol, adenosine, histamine, and ACh in rabbits. Am J Physiol Heart Circ Physiol 1998;274:H777–85.
[34] Oates JA, Fitzgerald GA, Branch RA, Jackson EK, Knapp HR, Roberts II LJ. Clinical implications of prostaglandin and thromboxane A_2 formation (1). New Engl J Med 1988;319:689–98.
[35] Bazzoni G, Beltran NA, Mascellani G, Bianchini P, Dejana E, Del Maschio A. Effect of heparin, dermatan sulfate, and related oligo-derivatives on human polymorphonuclear leukocyte functions. J Lab Clin Med 1993;121:268–75.
[36] Khuri SF, Valeri CR, Loscalzo J, Weinstein MJ, Birjiniuk V, Healey NA, et al. Heparin causes platelet dysfunction and induces fibrinolysis before cardiopulmonary bypass. Ann Thorac Surg 1995;60:1008–14.
[37] Wake K. Perisinusoidal stellate cells (fat-storing cells, interstitial cells, lipocytes), their related structure in and around the liver sinusoids, and Vitamin A-storing cells in extrahepatic organs. Int Rev Cytol 1980;66:303–53.
[38] Rockey DC. Hepatic blood flow regulation by stellate cells in normal and injured liver. Semin Liver Dis 2001;21:337–49.
[39] Zhang JX, Bauer M, Clemens MG. Vessel- and target cell-specific actions of endothelin-1 and endothelin-3 in rat liver. Am J Physiol 1995;269:G269–77.
[40] Ekataksin W, Kaneda K. Liver microvascular architecture: an insight into the pathophysiology of portal hypertension. Semin Liver Dis 1999;19:359–82.

[41] McCuskey R, Ito Y, McCuskey M, Ekataksin W, Wake K. Morphological mechanisms for regulating blood flow through hepatic sinusoids: 1998 update and overview. In: Wisse E, Knock D, De Zanger R, editors. Cell of the hepatic sinusoid. Rijswijk: Kupffer Cell Foundation; 1999. p. 129–34.
[42] Soifer SJ, Schreiber MD, Heymann MA. Leukotriene antagonists attenuate thromboxane-inducible pulmonary hypertension. Pediatr Res 1989;26:83–7.
[43] Yamamoto T, Hosoki K, Karasawa T. Possible involvement of endothelin in thromboxane A_2 receptor agonist (U-46619)-induced angina in the rat. Eur J Pharmacol 1993;250:189–91.
[44] Altin JG, Dieter P, Bygrave FL. Evidence that Ca^{2+} fluxes and respiratory, glycogenolytic and vasoconstrictive effects induced by the action of platelet-activating factor and L-α-lysophosphatidylcholine in the perfused rat liver are mediated by products of the cyclo-oxygenase pathway. Biochem J 1987;245:145–50.
[45] Chao W, Liu H, DeBuysere M, Hanahan DJ, Olson MS. Identification of receptors for platelet-activating factor in rat Kupffer cells. J Biol Chem 1989;264:13591–8.

J Pharmacol Sci **95**, 420 – 425 (2004)

Journal of Pharmacological Sciences

Full Paper

Uridine 5'-Triphosphate Stimulates Alveolar Fluid Clearance in the Isolated Rat Lungs

Tsutomu Sakuma[1,*], Xiu Gu[1], Makoto Sugita[1], Motoyasu Sagawa[1], Maki Sakuda[2], and Hirohisa Toga[2]

Departments of [1]Thoracic Surgery and [2]Respiratory Medicine, Kanazawa Medical University, 1-1 Daigaku, Uchinada, Ishikawa 920-0293, Japan

Received March 23, 2004; Accepted June 15, 2004

Abstract. Uridine 5'-triphosphate (UTP) increases chloride secretion followed by fluid movement into the proximal airspaces. However, little is known about whether UTP affects fluid movement in the distal airspaces. We studied the effect of UTP on basal and stimulated alveolar fluid clearance in the isolated rat lungs. Isosmotic 5% albumin solution was instilled into the alveolar spaces of isolated rat lungs, which were then inflated with 100% oxygen at an airway pressure of 7 cmH_2O. Alveolar fluid clearance was measured by the progressive increase in albumin concentrations over 1 h. Although UTP ($10^{-9} - 10^{-6}$ M) did not increase alveolar fluid clearance, UTP ($10^{-5} - 10^{-3}$ M) and isoproterenol (10^{-5} M), a β-adrenergic agonist, increased alveolar fluid clearance by 40% and 120% of the basal values, respectively. A combined treatment of UTP (10^{-4} M, 10^{-3} M) and isoproterenol increased alveolar fluid clearance by 280% of the basal value. The effects of UTP in the presence and absence of isoproterenol were abolished by blockers of a P2 purinoceptor and chloride channels. These results indicate that UTP stimulates alveolar fluid clearance in the distal airspaces of rat lungs.

Keywords: β-adrenergic agonist, purinoceptor, chloride channel, alveolar epithelium

Introduction

The mechanisms responsible for alveolar fluid clearance have been studied over the past two decades (1). The initial step in alveolar fluid clearance is to move alveolar sodium ions through apical sodium channels and basolateral Na^+-K^+ ATPase on the alveolar epithelia (2, 3). Osmotic gradients created by these transported ions drive alveolar fluid from the alveolar spaces (4) and may result in the resolution of alveolar edema (5).

β-Adrenergic agonists stimulate alveolar fluid clearance in the normal and pathological lungs (1). The prevailing idea was that activation of adrenergic-receptors increases the open probability of sodium channels, leading to an increase in apical membrane sodium permeability and an increase in sodium and fluid uptake from the alveolar space (6). Recent studies indicated that the effect of β-adrenergic agonists was primarily mediated by chloride ion transport (7). A series of complementary approaches using wild-type and cystic fibrosis ΔF508 mice, as well as in the isolated human lungs, defined the role of Cl^- transport in fluid clearance in the distal airspaces of intact mouse and human lungs (8). However, little is known about the identity and role of chloride channels in alveolar fluid clearance (9).

Extracellular uridine 5'-triphosphate (UTP) is an agonist of the $P2Y_2$ receptor that is found in type II alveolar epithelial cells (10 – 12). UTP has several effects on the proximal airway epithelia. For example, UTP was effective in vivo chloride secretagogues in the nasal epithelia of patients with cystic fibrosis (CF) (13). UTP inhibited sodium transport in non-CF and CF airways in human upper airway epithelial cells (14). Luminal UTP stimulates Cl^- secretion by a Ca^{2+}-independent mechanism and inhibits Na^+ absorption by a Ca^{2+}-dependent mechanism in intact distal bronchi isolated from porcine lungs (15). Therefore it was expected that UTP might increase chloride secretion in combination with the decrease in sodium absorption and then resulted in the accumulation of fluid in the airways (13). If UTP has these effects in the distal

*Corresponding author. FAX: +81-76-286-1207
E-mail: sakuma-t@kanazawa-med.ac.jp

airspaces, UTP would inhibit alveolar fluid clearance and deteriorate the resolution of alveolar edema.

Therefore, our first objective was to determine if UTP has effect on basal alveolar fluid clearance in the isolated rat lungs. Our second objective was to determine if UTP has effect on isoproterenol, a β-adrenergic agonist, to stimulate alveolar fluid clearance in the isolated rat lungs. Our third objective was to determine the mechanisms responsible for the effects of UTP on basal alveolar fluid clearance and isoproterenol to stimulate alveolar fluid clearance.

Materials and Methods

Materials

UTP was obtained from Kirin Co., Ltd. (Tokyo). Glibenclamide (a blocker of cystic fibrosis transmembrane conductance regulator CFTR), isoproterenol (a β-adrenergic agonist), 5-nitro-2-(3-phenylpropylamino) benzoate (NPPB, a non-selective chloride channel antagonist), propranolol (a β-adrenergic antagonist), and suramin (a non-selective P2 purinergic antagonist) were obtained from Sigma (St. Louis, MO, USA).

Experimental protocol

All rats received humane care and this study was approved by the Committee for Animal Experiments at Kanazawa Medical University. Alveolar fluid clearance was measured in the isolated rat lungs in the absence of pulmonary perfusion or ventilation (16, 17). Briefly, male Sprague-Dawley rats (200 – 250 g; Japan SLC, Inc., Hamamatsu) were anesthetized with intraperitoneal pentobarbital sodium (50 mg/kg). An endotracheal tube was inserted through a tracheostomy. The rats were exsanguinated via the abdominal aorta and the trachea, bilateral lungs, and heart were excised en bloc through a median sternotomy. Warmed isotonic saline solution (7 ml/kg, 37°C) containing 5% bovine albumin was instilled into both lungs, followed by 4 ml oxygen to deliver all the instilled fluid into the alveolar spaces. The lungs were placed in a humid incubator at 37°C and inflated with 100% oxygen at an airway pressure of 7 cmH_2O. Alveolar fluid was aspirated 1 h after instillation.

Effect of UTP on basal alveolar fluid clearance: To determine if UTP changed basal alveolar fluid clearance, albumin solution containing UTP (10^{-9} M, n = 4; 10^{-8} M, n = 4; 10^{-7} M, n = 4; 10^{-6} M, n = 4; 10^{-5} M, n = 6; 10^{-4} M, n = 6; 10^{-3} M, n = 6) was instilled into the alveolar spaces of isolated rat lungs. Since UTP increased basal alveolar fluid clearance, we examined if the effect of UTP on basal alveolar fluid clearance was mediated via a P2 purinoceptor or chloride channels. Suramin (10^{-3} M, n = 4), NPPB (10^{-4} M, n = 4), or glibenclamide (10^{-3} M, n = 4) was added to albumin solution in the presence of UTP (10^{-4} M) and instilled into the distal airspaces of rat lungs. As a control, albumin solution was instilled into the alveolar spaces of isolated rat lungs (n = 16). In addition, we examined if basal alveolar fluid clearance was mediated via a $P2Y_2$ purinoceptor or chloride channels. Suramin (10^{-3} M, n = 4), NPPB (10^{-4} M, n = 4), or glibenclamide (10^{-3} M, n = 4) was added to albumin solution and instilled into the alveolar spaces of rat lungs. Samples of alveolar fluid were collected 1 h after instillation.

Effect of UTP on alveolar fluid clearance in the presence of isoproterenol: We previously reported that 10^{-5} isoproterenol increased alveolar fluid clearance in the isolated rat lungs and ICI-118,551, a selective β_2-adrenergic antagonist, inhibited the effect of isoproterenol to stimulate alveolar fluid clearance (18). Therefore, we determined if UTP changed the effect of isoproterenol to stimulate alveolar fluid clearance. Albumin solution containing isoproterenol (10^{-5} M) and UTP (10^{-7} M, n = 4; 10^{-6} M, n = 4; 10^{-5} M, n = 6; 10^{-4} M, n = 6; 10^{-3} M, n = 12) was instilled into the alveolar spaces of isolated rat lungs. As a control, albumin solution containing isoproterenol (10^{-5} M, n = 12) was instilled into the alveolar spaces of isolated rat lungs. Samples of alveolar fluid were collected 1 h after instillation.

Effect of suramin, NPPB, glibenclamide, and propranolol on alveolar fluid clearance in the presence of isoproterenol: We examined if the effect of isoproterenol on alveolar fluid clearance was mediated through a $P2Y_2$ purinoceptor and chloride channels. Suramin (10^{-3} M, n = 4), NPPB (10^{-4} M, n = 4), or glibenclamide (10^{-3} M, n = 4) was added to albumin solution in the presence of isoproterenol (10^{-5} M) and instilled into the distal airspaces of rat lungs. In addition, to examine if the effect of isoproterenol was mediated through β-adrenoceptors, propranolol (10^{-4} M) was added to albumin solution in the presence of isoproterenol (10^{-5} M) and instilled into the distal airspaces of rat lungs (n = 4). Samples of alveolar fluid were collected 1 h after instillation.

Mechanisms responsible for the effect of UTP to enhance alveolar fluid clearance in the presence of isoproterenol: Since UTP enhanced the effect of UTP to simulate alveolar fluid clearance, we examined if the effect of UTP on isoproterenol to stimulate alveolar fluid clearance was mediated via a $P2Y_2$ purinoceptor, a non-selective chloride channel, or CFTR. Suramin (10^{-3} M, n = 4), NPPB (10^{-4} M, n = 4), or glibenclamide (10^{-3} M, n = 4) was added to albumin solution in the presence of UTP (10^{-4} M) and isoproterenol (10^{-5} M),

and instilled into the distal airspaces of rat lungs. Samples of alveolar fluid were collected 1 h after instillation.

Measurements

Alveolar fluid clearance: The protein concentrations in the instilled and aspirated solutions were measured by the pyrogallol red protein dye-binding method (SRL, Inc., Tokyo). Alveolar fluid clearance was estimated by the progressive increase in the concentration of albumin (16, 17). Alveolar fluid clearance (AFC) was calculated as follows:

$$AFC = [(Vi - Vf) / Vi] \times 100$$

where V is the volume of the instilled albumin solution (i) and the final alveolar fluid (f).

$$Vf = (Vi \times Pi) / Pf$$

where P is the concentration of protein in the instilled albumin solution (i) and the final alveolar fluid (f). The term alveolar does not imply that all reabsorption occurs across the alveolar epithelial cells because the distal bronchial epithelia can also transport sodium.

Osmolality: Osmolality in albumin solution was measured by a freezing point depression method using an osmometer (Fiske One-Ten Osmometer; Fiske Associates, Norwood, MA, USA).

Statistics

Data are summarized as the mean and standard deviation. The data were analyzed by a one-way analysis of variance (ANOVA) with the Student-Newman-Keuls post hoc test when multiple comparisons were needed. Differences with a P value of <0.05 were regarded as significant.

Results

An addition of 10^{-3} M UTP to albumin solution did not change osmolality levels (296 ± 4 mOsm/kgH_2O in the solution containing 10^{-3} M UTP and 295 ± 2 mOsm /kgH_2O in the control solution).

Basal alveolar fluid clearance was $6.9 \pm 2.2\%$ of the instilled volume in the isolated rat lungs. UTP (10^{-5} – 10^{-3} M) increased alveolar fluid clearance to approximately 1.4-fold the basal value, although UTP (10^{-9} – 10^{-6} M) did not (Fig. 1). Suramin, NPPB, and glibenclamide did not change basal alveolar fluid clearance (Fig. 2). However, these agents abolished the effect of UTP to stimulate basal alveolar fluid clearance.

Isoproterenol (10^{-5} M) increased alveolar fluid clearance to 2.2-fold the basal value (Fig. 3). An additional treatment of UTP ranging from 10^{-5} to 10^{-3} M increased alveolar fluid clearance in a dose-dependent fashion. A combined treatment of UTP (10^{-4} M, 10^{-3} M) and

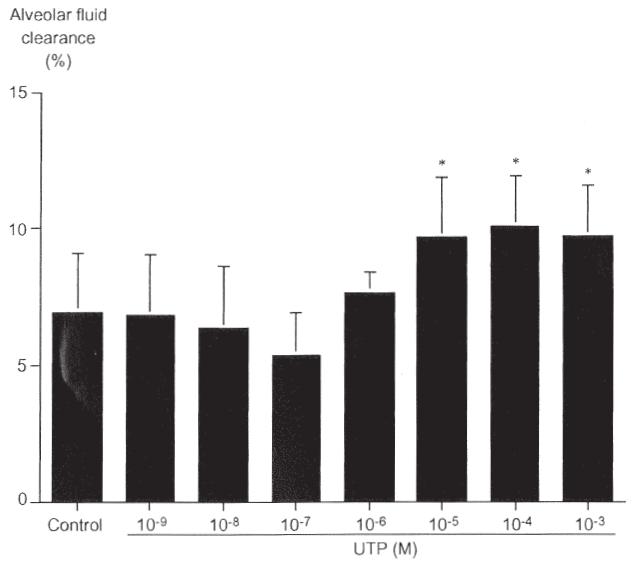

Fig. 1. Dose-dependent effect of UTP on basal alveolar fluid clearance. *P<0.05 *vs* control value.

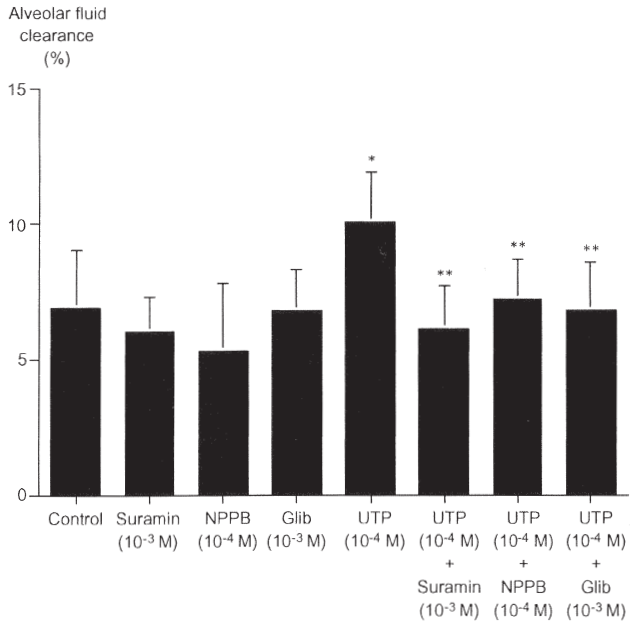

Fig. 2. Mechanisms responsible for the effect of UTP to stimulate basal alveolar fluid clearance. *P<0.05 *vs* control value. **P<0.05 *vs* value in the presence of UTP. Glib: glibenclamide.

isoproterenol increased alveolar fluid clearance to 3.8-fold basal value.

Suramin, NPPB, and glibenclamide had no effect on isoproterenol to stimulate alveolar fluid clearance (Fig. 4). Propranolol abolished the effect of isoproterenol to stimulate alveolar fluid clearance.

Suramin, NPPB, and glibenclamide inhibited the

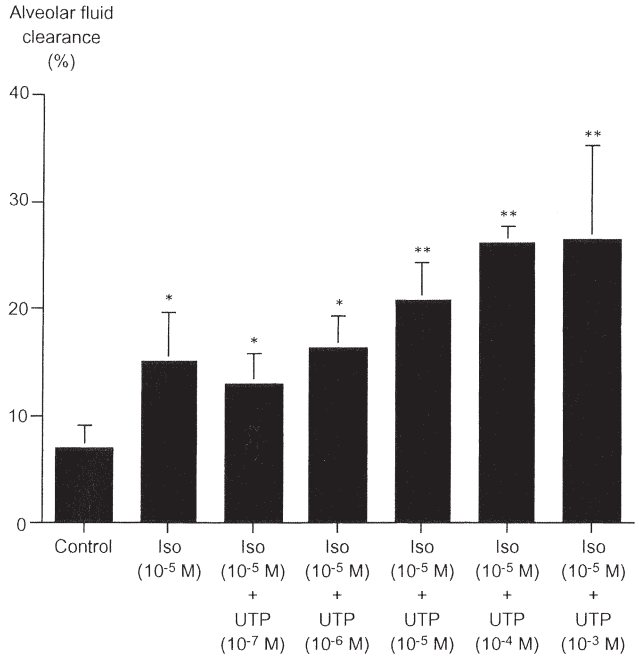

Fig. 3. Dose-dependent effect of UTP on isoproterenol to stimulate alveolar fluid clearance. *P<0.05 *vs* control value. **P<0.05 *vs* value in the presence of isoproterenol. Iso: isoproterenol.

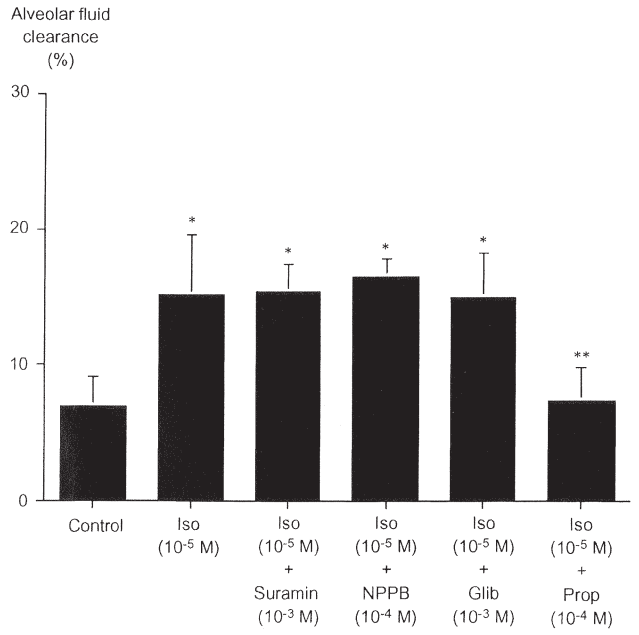

Fig. 4. Effect of suramin, NPPB, glibenclamide, and propranolol on isoproterenol to stimulate alveolar fluid clearance. *P<0.05 *vs* control value. **P<0.05 *vs* value in the presence of isoproterenol. Iso: isoproterenol, Glib: glibenclamide, Prop: propranolol.

effect of UTP to stimulate alveolar fluid clearance in the presence of isoproterenol (Fig. 5).

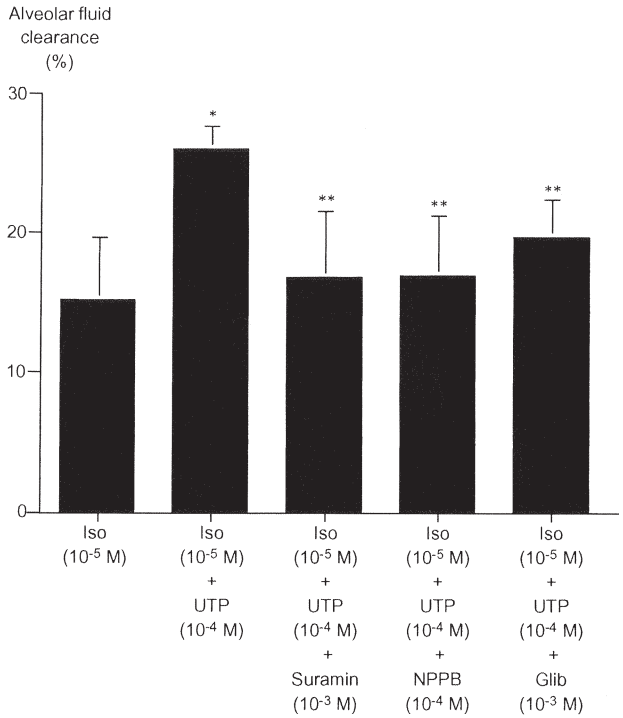

Fig. 5. Mechanisms responsible for the effect of UTP to stimulate alveolar fluid clearance. *P<0.05 *vs* value in the presence of isoproterenol. **P<0.05 *vs* value in the presence of isoproterenol and UTP. Iso: isoproterenol, Glib: glibenclamide.

Discussion

UTP increased basal alveolar fluid clearance and also enhanced the effect of isoproterenol to stimulate alveolar fluid clearance in rat lungs. To determine the mechanisms responsible for these findings, we tested three hypotheses. First, we tested whether the effect of UTP was mediated via a P2 purinoceptor. Suramin, a non-selective P2 purinoceptor antagonist, was administered in combination with UTP and/or isoproterenol. Although suramin had no effect on isoproterenol to stimulate alveolar fluid clearance, suramin abolished the effect of UTP in the presence and absence of isoproterenol. Therefore, the effect of UTP was mediated via a P2 purinoceptor. Second, we tested if the effect of UTP to stimulate alveolar fluid clearance was mediated via chloride channels. The results revealed that NPPB did not inhibit either basal alveolar fluid clearance or the effect of isoproterenol on alveolar fluid clearance, but inhibited the effect of UTP to stimulate basal alveolar fluid clearance. In addition, NPPB abolished the effect of UTP on isoproterenol to stimulate alveolar fluid clearance. NPPB is a potent inhibitor of chloride channels, but a non-selective inhibitor (7). Therefore, we tested the effect of glibenclamide that is a more

specific inhibitor of chloride ion transport via CFTR (8). Glibenclamide had the similar effects as NPPB. Therefore, it is likely that the effect of UTP was mediated via a glibenclamide-sensitive chloride channel.

Previously it was reported that there was a cumulative effect of keratinocyte growth factor and β-adrenergic agonist on alveolar fluid clearance (19). In contrast, when alveolar fluid clearance was increased by catecholamine-independent mechanisms, an additive effect with β-adrenergic therapy was not achieved (20). In the present study, there was a cumulative effect of UTP and isoproterenol in alveolar fluid clearance. NPPB abolished the effect of UTP on isoproterenol to stimulate alveolar fluid clearance. In addition, glibenclamide, a selective blocker of CFTR abolished the effect of UTP on isoproterenol to stimulate alveolar fluid clearance. Therefore, it is likely that chloride channels play a role in the cumulative effect of UTP in the presence of isoproterenol.

The effect of UTP on alveolar epithelial cells may be different from that on bronchial epithelial cells. In bronchial airways, the increase of intracellular Ca^{2+} stimulate chloride secretion into the luminal side in the bronchus (21). Epinephrine, a β-adrenergic agonist, increased bronchial cell membrane permeability to chloride and probably stimulated a specific chloride pump (22). β-Agonists stimulate chloride ion secretion in canine airway epithelial cells, suggesting that β-agonists increase water secretion into the airways (23). In contrast, in distal airways, chloride movement via CFTR plays an important role in isoproterenol- and terbutaline-stimulated alveolar fluid clearance (8). An adrenergic stimulation of transepithelial sodium absorption across the alveolar epithelium occurs indirectly by activation of apical chloride channels, resulting in hyperpolarization and an increased driving force for sodium uptake through amiloride-sensitive sodium channels (6). These reports support our results.

The results in this study are inconsistent with the previous findings from other laboratories First, glibenclamide did not inhibit the effect of isoproterenol in this study. However, glibenclamide inhibited the effect of isoproterenol and terbutaline in mice and human lungs, respectively (8). Since the rate of alveolar fluid clearance in rat was lower than that in mouse, it is possible that the low rate of alveolar fluid clearance has contributed to the absence of the effect of glibenclamide on alveolar fluid clearance in the presence of isoproterenol. In the human lung study, the lungs were exposed to severe hypothermia and thereafter rewarmed before the measurements (8). Therefore, the difference in experimental preparation might have induced the discrepancy between the effects of glibenclamide in the rat and human lungs. Second, Davis et al. reported that UTP decreased alveolar fluid clearance in mice (24). Although it is unclear how the difference was induced, their results seem to be consistent with the effect of UTP on the proximal airways. Further studies are needed to clarify whether there is a species difference in the effect of UTP on alveolar fluid clearance and in the effect of glibenclamide on alveolar fluid clearance in the presence of β-adrenergic agonist. Especially, the effect of UTP on alveolar fluid clearance should be examined in the human lungs.

Was the effect of UTP taking place in the proximal airways? First, the instilled albumin solution was delivered into the distal airways by the following injection of 4 ml of oxygen. Second, Evans blue dye bound with albumin revealed that the instilled solution was delivered into the distal airspaces in the rat lungs (16). In addition, protein concentration in liquid aspirated with a catheter wedged from the distal air spaces is a good reflection of alveolar fluid protein concentration (25). Third, if the instilled solution remained in the proximal airways, UTP should decrease alveolar fluid clearance, because luminal UTP stimulated Cl^- secretion and inhibits Na^+ absorption from porcine lungs (15). However, the results were the opposite. Therefore, it is unlikely that the effect of UTP took place in the proximal airways.

In summary, UTP increased basic alveolar fluid clearance and enhanced the effect of isoproterenol to stimulate alveolar fluid clearance in isolated rat lungs. The effect of UTP was inhibited with a blocker of P2 purinoceptor and by blockers of chloride channels. These results indicate that UTP increases net alveolar fluid clearance in the distal air spaces.

Acknowledgments

This study was supported by Grants for Project Research from High-Technology Center of Kanazawa Medical University (H2003-7, H2004-7), Grants for Collaborate Research of Kanazawa Medical University (C2003-1, C2004-1), and a Grant-in-Aid for Scientific Research from the MEXT, Japan (14571287).

References

1 Matthay MA, Folkesson HG, Clerici C. Lung epithelial fluid transport and the resolution of pulmonary edema. Physiol Rev. 2002;82:569–600.
2 Saumon G, Basset G. Electrolyte and fluid transport across the mature alveolar epithelium. J Appl Physiol. 1993;74:1–15.
3 Matalon S, Benos DJ, Jackson RM. Biophysical and molecular properties of amiloride-inhibitable Na^+ channels in alveolar epithelial cells. Am J Physiol. 1996;271:L1–L22.

4 Matthay MA, Folkesson HG, Verkman AS. Salt and water transport across alveolar and distal airway epithelia in the adult lung. Am J Physiol. 1996;270:L487–L503.
5 Frank JA, Wang Y, Osorio O, Matthay MA. Beta-adrenergic agonist therapy accelerates the resolution of hydrostatic pulmonary edema in sheep and rats. J Appl Physiol. 2000;89:1255–1265.
6 O'Grady SM, Jiang X, Ingbar DH. Cl-channel activation is necessary for stimulation of Na transport in adult alveolar epithelial cells. Am J Physiol Lung Cell Mol Physiol. 2000; 278:L239–L244.
7 Jiang X, Ingbar DH, O'Grady SM. Adrenergic stimulation of Na^+ transport across alveolar epithelial cells involves activation of apical Cl^- channels. Am J Physiol. 1998;275:C1610–C1620.
8 Fang X, Fukuda N, Barbry P, Sartori C, Verkman AS, Matthay MA. Novel role for CFTR in fluid absorption from the distal airspaces of the lung. J Gen Physiol. 2002;119:199–207.
9 O'Grady SM, Lee SY. Chloride and potassium channel function in alveolar epithelial cells. Am J Physiol Lung Cell Mol Physiol. 2003;284:L689–L700.
10 Rice WR, Singleton FM. P2Y-purinoceptor regulation of surfactant secretion from rat isolated alveolar type II cells is associated with mobilization of intracellular calcium. Br J Pharmacol. 1987;91:833–838.
11 Isohama Y, Rooney SA. Glucocorticoid enhances the response of type II cells from newborn rats to surfactant secretagogues. Biochim Biophys Acta. 2001;1531:241–250.
12 Gobran LI, Rooney SA. Surfactant secretagogue activation of protein kinase C isoforms in cultured rat type II cells. Am J Physiol. 1999;277:L251–L256.
13 Knowles MR, Olivier KN, Hohneker KW, Robinson J, Bennett WD, Boucher RC. Pharmacologic treatment of abnormal ion transport in the airway epithelium in cystic fibrosis. Chest. 1995;107:71S–76S.
14 Mall M, Wissner A, Gonska T, Calenborn D, Kuehr J, Brandis M, et al. Inhibition of amiloride-sensitive epithelial Na^+ absorption by extracellular nucleotides in human normal and cystic fibrosis airways. Am J Respir Cell Mol Biol. 2000;23:755–761.
15 Inglis SK, Collett A, McAlroy HL, Wilson SM, Olver RE. Effect of luminal nucleotides on Cl^- secretion and Na^+ absorption in distal bronchi. Pflugers Arch. 1999;438:621–627.
16 Sakuma T, Folkesson HG, Suzuki S, Okaniwa G, Fujimura S, Matthay MA. Beta-adrenergic agonist stimulated alveolar fluid clearance in ex vivo human and rat lungs. Am J Respir Crit Care Med. 1997;155:506–512.
17 Sakuma T, Hida M, Nambu Y, Osanai K, Toga H, Takanashi K, et al. Beta1-adrenergic agonist is a potent stimulator of alveolar fluid clearance in hyperoxic rat lungs. Jpn J Pharmacol. 2001;85:161–166.
18 Sakuma T, Tuchihara C, Ishigaki M, Osanai K, Nambu Y, Toga H, et al. Beta1-adrenoceptor stimulation by high-dose terbutaline downregulates terbutaline-stimulated alveolar fluid clearance in ex vivo rat lung. Exp Lung Res. 2001;27:453–468.
19 Wang Y, Folkesson HG, Jayr C, Ware LB, Matthay MA. Alveolar epithelial fluid transport can be simultaneously upregulated by both KGF and beta-agonist therapy. J Appl Physiol. 1999;87:1852–1860.
20 Folkesson HG, Matthay MA, Westrom BR, Kim KJ, Karlsson BW, Hastings RH. Alveolar epithelial clearance of protein. J Appl Physiol. 1996;80:1431–1445.
21 Bonnans C, Mainprice B, Chanez P, Bousquet J, Urbach V. Lipoxin A4 stimulates a cytosolic Ca^{2+} increase in human bronchial epithelium. J Biol Chem. 2003;278:10879–10884.
22 Al-Bazzaz FJ, Cheng E. Effect of catecholamines on ion transport in dog tracheal epithelium. J Appl Physiol. 1979;47: 397–403.
23 McCann JD, Welsh MJ. Regulation of Cl^- and K^+ channels in airway epithelium. Annu Rev Physiol. 1990;52:115–135.
24 Davis IC, Sullender WM, Hickman-Davis JM, Lindsey JR, Matalon S. Nucleotide-mediated inhibition of alveolar fluid clearance in BALB/c mice after respiratory syncytial virus infection. Am J Physiol Lung Cell Mol Physiol. 2004;286:L112–L120.
25 Berthiaume Y, Broaddus VC, Gropper MA, Tanita T, Matthay MA. Alveolar liquid and protein clearance from normal dog lungs. J Appl Physiol. 1988;65:585–593.

金医大誌（J. Kanazawa Med. Univ.）29：91－96, 2004

Effects of α_1-, β_1-, β_2-, β_3-Adrenergic Agonists on Alveolar Fluid Clearance in Isolated Rat Lungs

Xiu Gu [1], Makoto Sugita [1], Motoyasu Sagawa [1], Maki Sakuda [2], Kazuhiro Osanai [2], Hirohisa Toga [2] and Tsutomu Sakuma [1]

Abstract: **Objective** The objective of this study was to determine if α_1-, β_1-, β_2- and, β_3-adrenergic agonists stimulated alveolar fluid clearance in the isolated rat lungs and to determine the mechanism responsible for their effects. **Methods** Isotonic 5% albumin solutions containing different pharmacological agents were instilled into the distal airways in the isolated rat lungs. The lungs were inflated with 100% oxygen at 7cm H_2O and placed in a humid incubator at 37℃. Alveolar fluid clearance was estimated by the progressive increase in the albumin concentration over 1 hour after instillation. **Results** Basal alveolar fluid clearance was 6.9 ± 2.2%/h of instilled volume. Phenylephrine (an α_1-adrenergic agonist) increased alveolar fluid clearance by 109%. Prazosin (a selective α_1-adrenergic antagonist) and ICI-118551 (a β_2-adrenergic antagonist) significantly inhibited the increase in alveolar fluid clearance caused by phenylephrine, whereas yohimbine (an α_2-adrenergic antagonist) did not. Denopamine (a β_1-adrenergic agonist), terbutaline (a β_2-adrenergic agonist), and BRL-37344 (a β_3-adrenergic agonist) increased alveolar fluid clearance. Atenolol (a β_1-adrenergic antagonist) abolished the effect of denopamine, but did not inhibit the effects of terbutaline and BRL-37344. ICI-118551 abolished the effect of terbutaline and BRL-37344, and also inhibited the effects of denopamine in part. SR-59230A (a β_3-adrenergic antagonist) inhibited the effects of BRL-37344 and terbutaline in part, but did not change the effect of denopamine. **Conclusions** These results indicate that phenylephrine, denopamine, terbutaline and BRL-37344 are potent stimulators of alveolar fluid clearance in the rat lungs. The increase in alveolar fluid clearance caused by phenylephrine can be mediated via α_1-adrenoceptors. The effects of denopamine and terbutaline are mediated via β_1- and β_2-adrenoceptors, respectively. The effects of BRL-37344 may be mediated via β_2-adrenoceptors.

Key words : alveolar epithelium, adrenoceptor, pulmonary edema, acute lung injury

Introduction

Alveolar fluid clearance, an important function of the alveolar epithelium, plays an important role in recovery from pulmonary edema. The basic mechanisms that drive the removal of edema fluid from the distal airspaces of the lung have been established over the past two decades(1). There is a close relationship between the alveolar fluid clearance capacity and resolution of pulmonary edema(2). An impairment of alveolar fluid clearance may predispose a patient to a critical condition due to pulmonary edema(3). Experimental studies have shown that intact alveolar epithelial fluid transport function is critical for resolution of pulmonary edema and acute lung injury(3-5). In addition, the increase in alveolar fluid clearance can accelerate the resolution of pulmonary edema fluid(6-11). Therefore, the study to elucidate the mechanisms responsible for alveolar fluid clearance has clinical importance in the treatment of pulmonary edema. We previously reported that β_1- and β_2-adrenergic agonists increased alveolar fluid clearance(12,13). However, it is uncertain if an α_1- or a β_3-adrenergic

[1] *Division of Thoracic Surgery, Kanazawa Medical University*
[2] *Division of Respiratory Medicine, Kanazawa Medical University*
Correspondent to: Tsutomu Sakuma, Division of Thoracic Surgery, Kanazawa Medical University, Ishikawa 920-0293, Japan
Accepted: September 6, 2004

agonist increases alveolar fluid clearance. In addition, there is no study in which all α_1-, β_1-, β_2-and β_3-adrenergic agonists were used under the same experimental preparation. Therefore, the objectives of this study were to determine if α_1-, β_1-, β_2-and β_3-adrenergic agonists stimulated alveolar fluid clearance in the isolated rat lungs and to determine the mechanism responsible for the effects of adrenergic agonists.

Materials and Methods

Materials

Denopamine (a β_1-adrenergic agonist) was obtained from Tanabe Pharmaceutical Co., Ltd. (Tokyo, Japan). Phenylephrine (an α_1-adrenergic agonist), prazosin (an α_1-adrenergic antagonist), yohimbine (an α_2-adrenergic antagonist), terbutaline (a β_2-adrenergic agonist), BRL-37344 (a β_3-adrenergic agonist), atenolol (a β_1-adrenergic antagonist), ICI-118551 (a β_2-adrenergic antagonist), and SR-59230A (a β_3-adrenergic antagonist) were obtained from Sigma (St Louis, MO, USA).

Experimental Protocol

All rats received humane care and this study was approved by the Committee for Animal Experiments at Kanazawa Medical University. Alveolar fluid clearance was measured in the isolated rat lungs in the absence of pulmonary perfusion or ventilation. Briefly, male Sprague-Dawley rats (285 ± 25g, n=171, Japan SLC, Inc., Hamamatsu, Japan) were anesthetized with intraperitioneal pentobarbital sodium (50mg/kg). An endotracheal tube was inserted through a tracheostomy. The rats were exsanguinated via the abdominal aorta. The trachea, lungs and heart were isolated *en bloc* to measure alveolar fluid clearance. Isotonic saline solution (2ml, 37℃) containing 5% bovine albumin was instilled into the both lungs, followed by 4ml oxygen to deliver all the instilled solution into the alveolar spaces. The lungs were placed in a humid incubator at 37℃ and inflated with 100% oxygen at an airway pressure of 7cm H_2O. Alveolar fluid was aspirated after 1 hour of incubation.

Effects of α- and β-adrenergic antagonists on basal alveolar fluid clearance

The effects of α- and β-adrenergic antagonists on basal alveolar fluid clearance were determined. Isotonic 5% albumin solutions containing prazosin (10^{-4}M, n=4), yohimbine (10^{-4}M, n=4), atenolol (10^{-4}M, n=4), ICI-118551 (10^{-4}M, n=4), or SR-59230A (10^{-4}M, n=4) were instilled into the rat lungs.

Effects of phenylephrine on alveolar fluid clearance

First, dose-dependent effects of phenylephrine on alveolar fluid clearance were determined. Isotonic 5% albumin solutions containing phenylephrine (10^{-5}M, n=4; 10^{-6}M, n=4; 10^{-7}M, n=4; 10^{-8}M, n=4; 10^{-9}M, n=4) were instilled into the rat lungs. As control, isotonic 5% albumin solutions in the absence of phenylephrine were instilled into the rat lungs (n=6). Second, to determine the mechanism responsible for the increase in alveolar fluid clearance in the presence of phenylephrine, yohimbine (10^{-4}M, n=4), prazosin (10^{-4}M, n=6), or ICI-118551 (10^{-4}M, n=6) was added to the albumin solutions containing 10^{-5}M phenylephrine and instilled into the isolated rat lungs.

Effects of denopamine on alveolar fluid clearance

We determined if denopamine increased alveolar fluid clearance in the rat lungs. Isotonic 5% albumin solutions containing denopamine (10^{-5}M) were instilled into the rat lungs (n=4). To determine if the effect of denopamine was mediated via β_1-, β_2-, or β_3-adrenoceptors, atenolol (10^{-4}M, n=4), ICI-118551 (10^{-4}M, n=7), or SR-59230A (10^{-4}M, n=4) was added to isotonic 5% albumin solution containing denopamine (10^{-5}M) and instilled into the rat lungs.

Effects of terbutaline on alveolar fluid clearance

We determined if terbutaline increased alveolar fluid clearance in the rat lungs. Isotonic 5% albumin solutions containing terbutaline (10^{-5}M) were instilled into the rat lungs (n=4). To determine if the effect of terbutaline was mediated via α_1-, β_1-, β_2-, or β_3-adrenoceptors, prazosin (10^{-4}M, n=4), atenolol (10^{-4}M, n=8), ICI-118551 (10^{-4}M, n=4), or SR-59230A (10^{-4}M, n=4) was added to isotonic 5% albumin solution containing terbutaline (10^{-5}M) and instilled into the rat lungs.

Effects of a combined treatment of denopamine and terbutaline on alveolar fluid clearance

To determine if both β_1-and β_2-adrenoceptors were simultaneously stimulated by a combined treatment of β_1-and β_2-adrenergic agonists, isotonic 5% albumin solutions containing denopamine (10^{-5}M) and terbutaline (10^{-5}M) were instilled into the rat lungs (n=4). We determined if selective β-adrenergic antagonists inhibited the effect of a combined treatment of denopamine and terbutaline on alveolar fluid clearance. Atenolol (10^{-4}M, n=4), ICI-118551 (10^{-4}M, n=4), SR-59230A (10^{-4}M, n=4), or atenolol (10^{-4}M) in combination with ICI-118551 (10^{-4}M, n=4) was added to isotonic 5% albumin solution containing denopamine (10^{-5}M) and terbutaline (10^{-5}M) and instilled into the rat lungs.

Effects of BRL-37344 on alveolar fluid clearance

We determined if BRL-37344 increased alveolar fluid clearance in the rat lungs. First, dose-response effects of BRL-37344 on alveolar fluid clearance were determined. Isotonic 5% albumin solutions containing BRL-37344 (10^{-4}M, n=4; 10^{-5}M, n=4; 10^{-6}M, n=4; 10^{-7}M, n=4; 10^{-8}M, n=4; 10^{-9}M, n=4) were instilled into the rat lungs. Second, to determine if the

effect of BRL-37344 was mediated via β_1-, β_2-, or β_3-adrenoceptors, atenolol (10^{-4}M, n=4), ICI-118551 (10^{-4} M, n=6), or SR-59230A (10^{-4}M, n=8) was added to isotonic 5% albumin solution containing BRL-37344 (10^{-5}M) and instilled into the rat lungs. In addition, we determined if a combined treatment of ICI-118551 and SR-59230A abolished the effect of BRL-37344 to stimulate alveolar fluid clearance. Both ICI-118551 (10^{-4}M) and SR-59230A (10^{-4}M) were added to isotonic 5% albumin solution containing BRL-37344 (10^{-5}M) and instilled into the rat lungs (n=4).

Alveolar fluid clearance

Albumin concentration was measured with the pyrogallol red protein dye-binding method (SRL Inc., Tokyo, Japan), and the alveolar fluid clearance (AFC) was calculated by the change of albumin concentration (13).

AFC=[(Vi-Vf)/Vi]$\times$ 100, Vf=Vi $\times$ Pi/Pf.

V means the volume of the instilled albumin solution (i) and the final alveolar fluid (f). P means the concentration of protein in the instilled albumin solution (i) and the final alveolar fluid (f).

The term alveolar does not imply that all reabsorption occurs across the alveolar epithelial cells because the distal bronchial epithelia can also transport sodium.

Statistics

Data are summarized as the mean and standard deviation. The data were analyzed by a one-way analysis of variance (ANOVA) with the Student-Newman-Keuls post-hoc test. Differences with a p value of<0.05 were regarded as significant.

Results

Basal alveolar fluid clearance was 6.9 $\pm$ 2.2% of instilled volume (Figure 1). Prazosin, atenolol, ICI-118551, and SR-59230A did not change basal alveolar fluid clearance. However, yohimbine increased basal alveolar clearance.

Although 10^{-9}M phenylephrine did not increase alveolar fluid clearance, 10^{-8}M~10^{-5}M phenylephrine did (Figure 2).

Prazosin and ICI-118551 significantly inhibited the increase in alveolar fluid clearance caused by phenylephrine (Figure 3). However, yohimbine did not change alveolar fluid clearance in the presence of phenylephrine.

Denopamine increased alveolar fluid clearance (Figure 4). Atenolol abolished the effect of denopamine to stimulate alveolar fluid clearance. ICI-118551 inhibited the effect of denopamine to stimulate alveolar fluid clearance in part. SR-59230A did not change the effect of denopamine.

Terbutaline increased alveolar fluid clearance (Figure 5). ICI-118551 abolished the effect of

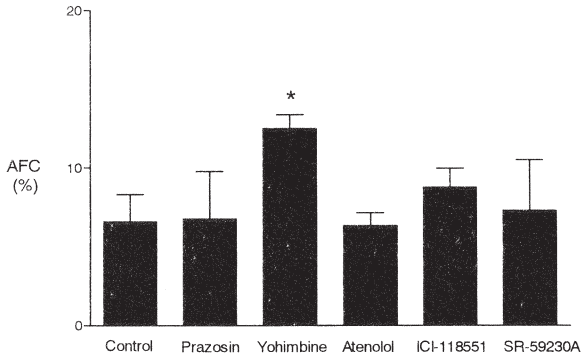

Figure 1. Effects of α- and β-adrenregic antagonists on basal alveolar fluid clearance. *p<0.001 vs control. AFC: alveolar fluid clearance.

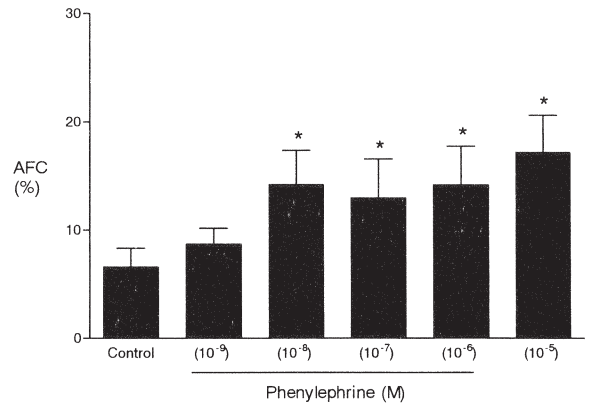

Figure 2. Effects of phenylephrine on alveolar fluid clearance. *p<0.001 vs control. AFC: alveolar fluid clearance.

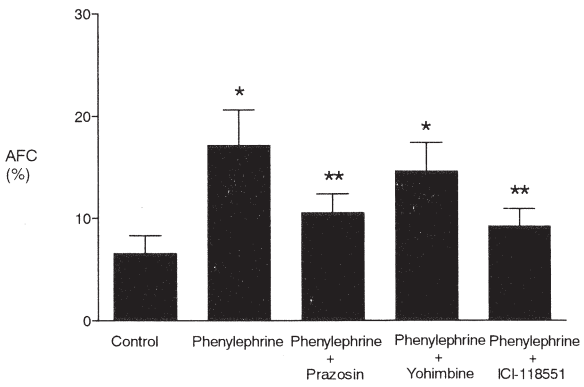

Figure 3. Effects of α- and β_2-antagonists on phenylephrine to simulate alveolar fluid clearance. *p<0.001 vs control. **p<0.001 vs phenylephrine. AFC: alveolar fluid clearance.

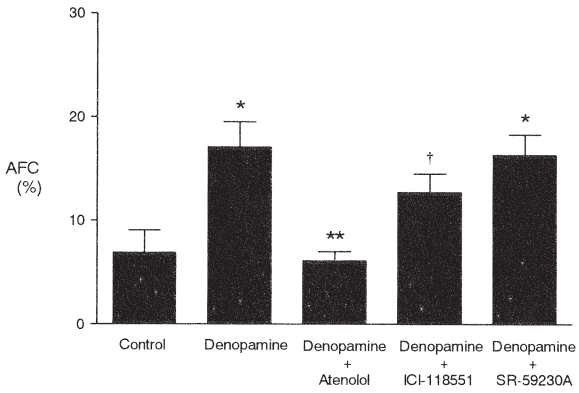

Figure 4. Effects of denopamine on alveolar fluid clearance. *$p<0.001$ vs control. **$p<0.001$ vs denopamine. †$p<0.001$ vs control and denopamine. AFC: alveolar fluid clearance.

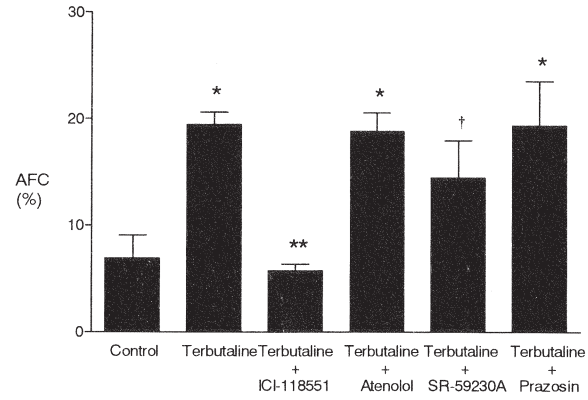

Figure 5. Effects of terbutaline on alveolar fluid clearance. *$p<0.001$ vs control. **$p<0.001$ vs terbutaline. †$p<0.001$ vs control and $p<0.01$ vs terbutaline. AFC: alveolar fluid clearance.

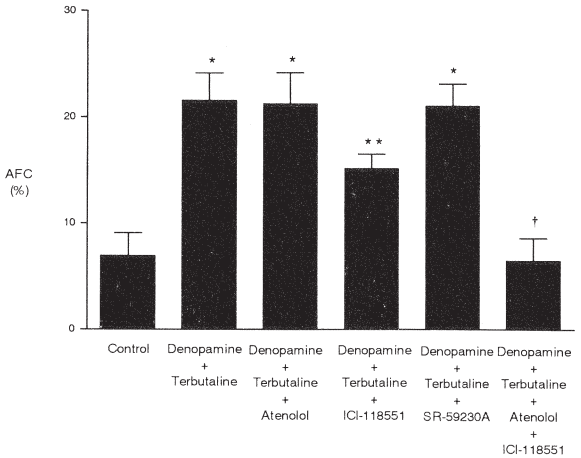

Figure 6. Effects of a combined treatment of denopamine and terbutaline on alveolar fluid clearance. *$p<0.001$ vs control. **$p<0.001$ vs control and $p<0.01$ vs denopamine+terbutaline. †$p<0.001$ vs denopamine+terbutaline and denopamine+terbutaline+ICI-118551. AFC: alveolar fluid clearance.

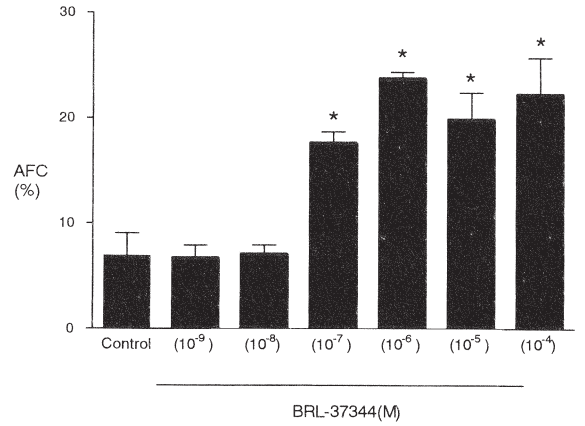

Figure 7. Dose-dependent effects of BRL-37344 on alveolar fluid clearance. *$p<0.001$ vs control. AFC: alveolar fluid clearance.

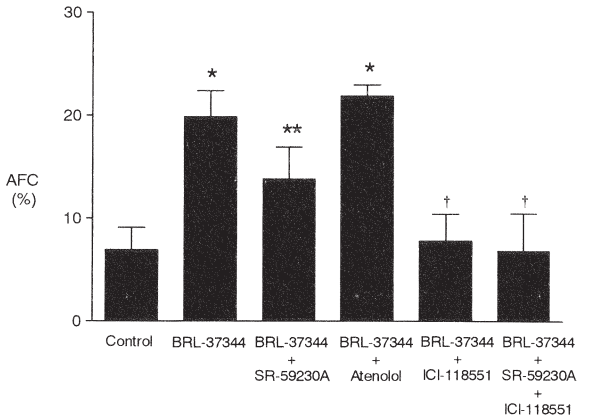

Figure 8. Effects of β-adrenergic antagonists on BRL-37344 to stimulate alveolar fluid clearance. *$p<0.001$ vs control. **$p<0.001$ vs control and BRL-37344. †$p<0.001$ vs BRL-37344 and BRL-37344+SR-59230A. AFC: alveolar fluid clearance.

terbutaline to stimulate alveolar fluid clearance. Atenolol and prazosin did not change the effect of terbutaline. However, SR-59230A inhibited the effect of terbutaline in part.

A combined treatment of denopamine and terbutaline increased alveolar fluid clearance (Figure 6). Atenolol and SR-59230A did not change the effect of the combined treatment of denopamine and terbutaline. However, ICI-118551 inhibited the effect of the combined treatment of denopamine and terbutaline in part. A combined treatment of atenolol and ICI-118551 completely inhibited the effect of a combined treatment of denopamine and terbutaline.

BRL-37344 increased alveolar fluid clearance in a dose-dependent manner (Figure 7). Although ~10^{-8}M BRL-37344 did not increase alveolar fluid clearance, 10^{-7}~M BRL-37344 did and 10^{-6}M exerted the maximum effects. SR-59230A inhibited the effects of BRL-37344 to stimulate alveolar fluid clearance in part (Figure 8). Atenolol did not change the effect of BRL-37344. However, ICI-118551 abolished the effects of BRL-37344 to stimulate alveolar fluid clearance. A combined treatment of ICI-118551 and SR-59230A also abolished the effect of BRL-37344.

Discussion

The major finding of this study is that α- and β-adrenergic agonists are potent stimulators of alveolar fluid clearance in the isolated rat lungs.

The first objective in this study was to determine if an α_1-adrenergic agonist, phenylephrine, increased alveolar fluid clearance. We found that phenylephrine increased alveolar fluid clearance. The effect was inhibited by α_1-and β_2-adrenergic antagonists. Recently, it was reported that norepinephrine, a dominant α-adrenergic agonist, increased alveolar fluid clearance(14). Since α_1-and α_2-adrenoceptors are present on alveolar type II epithelial cells(15), and an α_1-blocker, prazosin, inhibited the effect of phenylephrine, the effect of phenylephrine may be mediated via α_1-adrenoceptor.

Interestingly the effect of phenylephrine was inhibited by ICI-118551, a β_2-adrenergic antagonist. Since prazosin did not inhibit the effect of terbutaline, it is unlikely that prazosin played a role as a β_2-adrenergic antagonist. Therefore, it is likely that ICI-118551 had an effect as an α_1-adrenergic antagonist. The result is consistent with the results in the perfused rat lungs(14).

The second objective was to determine the effect of three β-adrenergic agonists on alveolar fluid clearance. We found that all β-agonists were potent stimulators of alveolar fluid clearance in the isolated rat lungs.

Atenolol, a β_1-aderenergic antagonist, abolished the effect of denopamine, but did not inhibit the effect of terbutaline. ICI-118551 abolished the effect of terbutaline, and also inhibited the effect of denopamine in part. In addition, ICI-118551 inhibited the effect of a combined treatment of denopamine and terbutaline in part, and a combined treatment of atenolol and ICI-118551 abolished the effect of a combined treatment of denopamine and terbutaline on alveolar fluid clearance. Therefore, it is likely that atenolol played a role as a selective β_1-adrenergic antagonist, and ICI-118551 played a role as a predominant β_2-adrenergic antagonist and a role as a β_1-adrenergic antagonist in part. Terbutaline mainly stimulated β_2-adrenoceptors and also stimulated β_1-adrenoceptors in part. The effects of denopamine and terbutaline are consistent with the results from our laboratory and other laboratories(12,16-19).

BRL-37344 increased alveolar fluid clearance. SR-59230A did not abolish the effect of BRL-37344, but inhibited the effect in part. Then, we examined the effect of ICI-118551 on BRL-37344 to stimulate alveolar fluid clearance, and found that ICI-118551 abolished the effect of BRL-37344. In addition, a combined treatment of ICI-118551 and SR-59230A had the inhibitory effect similar to ICI-118551 alone. Therefore, we determined if SR-59230A had effects as a β_1- or β_2-adrenergic antagonist on alveolar fluid clearance and found that SR-59230A had the inhibitory effect as a β_2-adrenergic antagonist in part. There may be three explanations accounting for the results of BRL-37344. First, the effect of BRL-37344 on alveolar fluid clearance was mediated via β_2-adrenoceptors. The inhibitory effect of ICI-118551 supports the effect mediated via β_2-adrenoceptors. Second, the effect of BRL-37344 on alveolar fluid clearance was mediated via β_3-adrenoceptors, not via β_2-adrenoceptors. If ICI-118551 had the effect as a β_3-adrenergic antagonist, this hypothesis was accounted by the results. However, it is still uncertain. Third, the effect of BRL-37344 on alveolar fluid clearance was mediated via β_2- and β_3-adrenoceptors. Since SR-59230A did not abolish the effect of BRL-37344, this hypothesis remains to be elucidated. Further studies are needed to determine the mechanisms responsible for the effect of BRL-37344 on alveolar fluid clearance.

Yohimbine, an α_2-adrenergic antagonist, increased basal alveolar fluid clearance. The increase in alveolar fluid clearance in the presence of yohimbine is consistent with the movement of sodium from the alveolar spaces(14). However, the mechanism for the increase is uncertain.

In summary, phenylephrine, denopamine, terbutaline and BRL-37344 are potent stimulators of alveolar fluid clearance in the rat lungs. The effect of phenylephrine is mediated via α_1-adrenoceptors. The effects of denopamine and terbutaline are mediated via β_1- and β_2-adrenoceptors, respectively. The effect of BRL-37344 may be mediated via β_2-adrenoceptors.

This study was supported by Grant for Project Research from High-Technology Center of Kanazawa Medical University (H2003-7, H2004-7), Grant for Collaborative Research from Kanazawa Medical University (C2003-1, C2004-1), and Grant-In-Aid for Scientific Research from the MEXT of Japan (14571287).

Refernces

1. Crandall ED, Heming TA, Palombo RL et al: Effects of terbutaline on sodium transport in isolated perfused rat lung. J Appl Physiol 1986; **60:** 289-94.
2. Mattay MA, Folkesson HG, Clerici C: Lung epithelial fluid transport and the resolution of pulmonary edema. Physiol Rev 2002; **82:** 569-600.
3. Ware LB, Matthay MA: Alveolar fluid clearance is impaired in the majority of patients with acute lung injury and the acute respiratory distress syndrome. Am J Respir Crit Care Med 2001; **163:** 1376-83.
4. Sartori C, Matthay MA: Alveolar epithelial fluid transport in acute lung injury: new insights. Eur Respir J 2002; **20:** 1299-313.
5. Berthiaume Y, Folkesson HG, Matthay MA: Lung edema clearance: 20 years of progress: invited review: alveolar edema fluid clearance in the injured lung. J Appl Physiol 2002; **93:** 2207-13.
6. Frank JA, Wang Y, Osorio O et al: Beta-adrenergic agonist therapy accelerates the resolution of hydrostatic pulmonary edema in sleep and rats. J Appl Physiol 2000; **89:** 1255-65.
7. Morgan EE, Hodnichak CM, Stader SM et al: Prolonged isoproterenol infusion impairs the ability of β_2-agonists to increase alveolar liquid clearance. Am J Physiol Lung Cell Mol Physiol 2002; **282:** L666-74.
8. Berthiaume Y, Broaddus VC, Gropper MA et al: Alveolar liquid and protein clearance from normal dog lungs. J Appl Physiol 1988; **65:** 585-93.
9. Grimme JD, Lane SM, Maron MB: Alveolar liquid clearance in multiple nonperfused canine lung lobes. J Appl Physiol 1997; **82:** 348-53.
10. Berthiaume Y, Staub NC, Matthay MA: Beta-adrenergic agonists increase lung liquid clearance in anesthetized sheep. J Clin Invest 1987; **79:** 335-43.
11. Campbell AR, Folkesson HG, Berthiaume Y et al: Alveolar epithelial fluid clearance persists in the presence of moderate left atrial hypertension in sheep. J Appl Physiol 1999; **86:** 139-51.
12. Sakuma T, Tuchihara C, Ishigaki M et al: Denopamine, a β_1-adrenergic agonist, increases alveolar fluid clearance in ex vivo rat and guinea pig lungs. J Appl Physiol 2001; **90:** 10-6.
13. Sakuma T, Folkesson HG, Suzuki S et al: Beta-adrenergic agonist stimulated alveolar fluid clearance in ex vivo human and rat lungs. Am J Respir Crit Care Med 1997; **155:** 506-12.
14. Azzam ZS, Adir Y, Crespo A et al: Norepinephrine increases alveolar fluid reabsorption and Na, K-ATPase activity. Am J Respir Crit Care Med. 2004 Jul 15 [Epub ahead of print].
15. Keeney SE, Oelberg DG: Alpha 1-adrenergic and muscarinic receptors in adult and neonatal rat type II pneumocytes. Lung 1993; **171:** 355-66.
16. Lasnier JM, Wangensteen OD, Schmitz LS et al: Terbutaline stimulates alveolar fluid resorption in hyperoxic lung injury. J Appl Physiol 1996; **81:** 1723-9.
17. Icard P, Saumon G: Alveolar sodium and fluid transport in mice. Am J Physiol 1999; **277:** L1232-8.
18. Lane SM, Maender KC, Awender NE et al: Adrenal epinephrine increases alveolar liquid clearance in a canine model of neurogenic pulmonary edema. Am J Respir Crit Care Med 1998; **158:** 760-8.
19. Sakuma T, Tuchihara C, Ishigaki M et al: Beta1-adrenoceptor stimulation by high-dose terbutaline downregulates terbutaline-stimulated alveolar fluid clearance in ex vivo rat lung. Exp Lung Res 2001; **27:**453-68.

Clinical and Experimental Pharmacology and Physiology (2005) **32**, 288–293

ANAPHYLACTIC HEPATIC VENOCONSTRICTION IS ATTENUATED BY NITRIC OXIDE RELEASED VIA SHEAR STRESS-DEPENDENT AND -INDEPENDENT MECHANISMS IN GUINEA PIG

Toshishige Shibamoto,* Zonghai Ruan,* Sen Cui,* Yasutaka Kurata,* Tomonobu Koizumi† and Keishi Kubo†

**Department of Physiology, Kanazawa Medical University, Uchinada and †First Department of Medicine, Shinshu University School of Medicine, Matsumoto, Japan*

SUMMARY

1. The role of shear stress in nitric oxide (NO)-mediated attenuation of anaphylactic venoconstriction was studied using an isolated ovalbumin-sensitized guinea pig liver.

2. Guinea pigs were actively sensitized by a subcutaneous injection of 1 mg ovalbumin. Two weeks after sensitization, the livers were perfused with diluted blood under constant flow or constant perfusion pressure. The constant flow could result in increased shear stress during constriction, while the constant perfusion pressure could prevent changes in shear stress. Using the double occlusion technique to estimate the hepatic sinusoidal pressure, pre- and postsinusoidal constriction was evaluated. Hepatic anaphylaxis was induced by an injection of ovalbumin (4 μg) into the perfusate, the volume of which was 40 mL.

3. Under either constant flow or pressure, anaphylaxis caused venoconstriction of predominantly presinusoids over postsinusoids, although anaphylactic venoconstriction under constant pressure was significantly greater than that under constant flow. When shear stress was held constant by maintaining constant perfusion pressure, a NO synthase inhibitor, N^{ω}-nitro-L-arginine methyl ester (L-NAME, 100 μmol/L), potentiated similarly both pre- and postsinusoidal constriction induced by anaphylaxis. This suggests that hepatic anaphylaxis shear stress-independently generates NO, resulting in dilatation of both pre- and postsinusoidal vessels in a similar magnitude. In contrast, when shear stress was allowed to rise under constant flow, anaphylactic presinusoidal constriction was preferentially potentiated by L-NAME.

4. Hepatic anaphylaxis can increase NO production in a shear stress-independent manner and dilates similarly both pre- and postsinusoids, while NO produced in a shear stress-dependent manner attenuates predominantly venoconstriction of the presinusoids where shear stress is preferentially increased.

Correspondence: Dr Toshishige Shibamoto, Department of Physiology, Kanazawa Medical University, Uchinada 920-0293, Japan.
Email: shibamo@kanazawa-med.ac.jp

Received 9 October 2004; revision 26 November 2005; accepted 16 January 2005.

Key words: anaphylaxis, double occlusion pressure, hepatic circulation, nitric oxide, shear stress.

INTRODUCTION

Nitric oxide (NO) is produced by the activation of the NO synthase 3 present in endothelial cells either by hormonal or physical stimuli such as shear stress and then regulates the vascular system.[1,2] The modulation of peripheral resistance by NO has been shown to be a result of relaxation of the vascular smooth muscle. We have recently shown that hepatic anaphylactic venoconstriction is characterized by predominant presinusoidal constriction over postsinusoidal constriction and that NO attenuates preferentially constriction of these constricted extensively presinusoidal vessels, where increased shear stress could have augmented markedly contracted presinusoidal vessels in isolated guinea pig liver perfused at a constant flow.[3] We assume that increased shear stress at the presinusoids with strong constriction may account for the vulnerability of the presinusoids to NO; anaphylaxis causes NO release from endothelium of the same presinusoidal vessel, leading to relaxation of the adjacent presinusoidal vascular smooth muscle cells in a paracrine manner. However, it is expected that anaphylactic reaction per se can release NO from endothelial cells via the shear stress-independent mechanism through humoral substances; most mediators of anaphylaxis, such as histamine,[4,5] leukotrienes,[6] thromboxane (Tx) A_2[5] and platelet-activating factor (PAF),[7] stimulate NO release from the vascular endothelium.

However, it is not known whether NO could be substantially released via a shear stress-independent mechanism in the liver vasculature exposed to anaphylaxis and could modulate anaphylactic hepatic venoconstriction. If so, it remains unknown which segment of the hepatic vessels is affected by NO released shear stress-independently.

Macedo and Lautt recently showed that if vasoconstriction is induced in a situation where blood flow is allowed to decline and perfusion pressure is not elevated, shear stress does not increase.[8] In contrast, if flow is held steady, shear stress increases at the site of the constriction and leads to NO release.[8] Thus, to achieve the above-mentioned objectives, hepatic anaphylaxis was examined with isolated guinea pig livers, that were perfused under constant flow or constant pressure to obtain situations with or without shear

stress, respectively, in the presence of a NO synthase inhibitor, N^{ω}-nitro-L-arginine methyl ester (L-NAME) or D-NAME, an inactive enantiomer of L-NAME. The hepatic vasoconstrictive site was determined by measuring the sinusoidal pressure using the vascular occlusion methods.[9,10]

METHODS

Twenty-four male Hartley guinea pigs weighing 346 ± 17 g (SD) were used in the current study. The present experiments were approved by the Animal Research Committee of Kanazawa Medical University. Guinea pigs were actively sensitized by a subcutaneous injection of an emulsion made by mixing equal volumes of complete Freund's adjuvant (0.5 mL) with 1 mg ovalbumin (grade V; Sigma, St. Louis, MO, USA) dissolved in physiological saline (0.5 mL). Two weeks after sensitization, the perfusion experiment was performed.

Isolated liver preparation

The animals were anaesthetized with pentobarbital sodium (35 mg/kg, i.p.) and mechanically ventilated with room air. The basic methods for isolated perfused liver was described elsewhere.[3,9,10] In brief, a polyethylene tube was placed in the right carotid artery. After laparotomy, the cystic duct and the hepatic artery were ligated and the bile duct was cannulated with a small polyethylene tube. At 5 min after intra-arterial heparinization (500 U/kg), 8–9 mL of blood was withdrawn through the carotid arterial catheter. The intra-abdominal inferior vena cava (IVC) above the renal veins was ligated and the portal vein was cannulated with a stainless cannula (2.1 mm internal diameter, 3.0 mm outer diameter) for portal perfusion. After thoracotomy, for the outflow line, the supradiaphragmatic IVC was cannulated with the same size stainless cannula, then portal perfusion was begun with the heparinized autologous blood that was diluted with 5% bovine albumin (Sigma) in Krebs' solution ((in mmol) NaCl 118; KCl 5.9; $MgSO_4$ 1.2; $CaCl_2$ 2.5; NaH_2PO_4 1.2; $NaHCO_3$ 25.5; glucose 5.6) at haematocrit of 8%. The liver was rapidly excised, suspended from an isometric transducer (TB-652T, Nihon-Kohden, Tokyo, Japan) and weighed continuously throughout the experimental period.

The liver was perfused recirculatingly at a constant flow rate or a constant pressure via the portal vein. For the constant flow perfusion, the circulating blood was pumped using a variable speed pump (Master-flex; Cole Parmer, Chicago, IL, USA) from the outflow reservoir through a heat exchanger (37°C) and a windkessel chamber to trap air bubbles as well as to buffer pressure fluctuations generated by the pump.[3] The flow rate and the height of the outflow reservoir could be adjusted at any desired levels of portal venous pressure (Ppv) and hepatic venous pressure (Phv). For the constant pressure perfusion, the blood was pumped from the outflow reservoir through a heat exchanger (37°C) into the inflow reservoir, from which the blood flows gravimetrically into the portal cannula. An overflow tube was connected to the inflow and outflow reservoirs to maintain a constant portal perfusion pressure. The height of each reservoir could be adjusted independently to maintain Ppv and Phv at any desired level.[10]

In livers perfused either under constant flow or under constant pressure, the recirculating blood volume was 40 mL. The perfused blood in the outflow reservoir was oxygenated by bubbling with 95% O_2 and 5% CO_2. Portal venous pressure and Phv were measured using pressure transducers (TP-400T, Nihon-Kohden) attached by a sidearm to the appropriate cannulas with the reference points at the hepatic hilus. To occlude inflow and outflow perfusion lines simultaneously for measurement of the double occlusion pressure (Pdo), two solenoid valves were placed in a position that each sidearm cannula was between the corresponding solenoid valve and the liver. Portal blood flow rate (Q) was measured with an electromagnetic flow meter (MFV 1200, Nihon-Kohden) and the flow probe was positioned in the inflow line. Bile was collected drop by drop in a small tube suspended from the force transducer (SB-1T, Nihon-Kohden). One bile drop yielded 0.027 g and the time between drops was measured for determination of the bile flow rate.[3] The hepatic vascular pressures, blood flow rate, liver weight and bile weight were monitored continuously and displayed through a thermal physiograph (RMP-6008, Nihon-Kohden). Outputs were also digitized by the analogue-digital converter at a sampling rate of 100 Hz. These digitized values were displayed and recorded using a personal computer for later determination of Pdo.

Experimental protocols

Hepatic haemodynamic parameters were observed for at least 20 min after the start of perfusion until an isogravimetric state (no weight gain or loss) was obtained. Then, the livers perfused either under constant flow or under constant pressure were further divided into the following two groups of the D-NAME and L-NAME groups, in which L-NAME (100 μmol/L: Sigma) and D-NAME (100 μmol/L: Sigma) was administered into the reservoir, respectively. Thus, any livers studied were pretreated with either L-NAME or D-NAME. Ovalbumin 4 μg was injected into the reservoir at 10 min after injection of L-NAME or D-NAME. This dose of 4 μg ovalbumin was smaller than that of our previous study (0.1 mg ovalbumin).[3] The reason for adopting this smaller dose was that ovalbumin more than 4 μg caused strong anaphylactic venoconstriction, resulting in cessation of perfusion flow under constant pressure.

The hepatic sinusoidal pressure was measured by the double occlusion method.[9,10] Both the inflow and outflow lines were simultaneously and instantaneously occluded for 10 s using the solenoid valves, after which Ppv and Phv rapidly equilibrated to a similar or identical pressure, which was Pdo. Actually, Pdo values were obtained from the digitized data of Ppv and Phv using an original program (LIVER software, Biomedical Science, Kanazawa, Japan). In each group, Pdo was measured at the baseline, just prior to an injection of antigen and 4 and 6 min after antigen and then at a 10 min interval for 60 min. However, all comparisons were made during the peak of the constrictor response.

The total portal-hepatic venous resistance (Rt), presinusoidal resistance (Rpre) and postsinusoidal resistance (Rpost) were calculated as follows:

$$Rt = (Ppv - Phv)/Q \quad [1]$$

$$Rpre = (Ppv - Pdo)/Q \quad [2]$$

$$Rpost = (Pdo - Phv)/Q \quad [3]$$

Statistics

All results are expressed as the means ± SD. Analysis of variance followed by Bonferroni's test was used to test for significant differences. Differences were considered as statistically significant at *P*-values less than 0.05.

RESULTS

The effect of L-NAME on basal hepatic circulation

After injection of L-NAME into the blood of constant flow-perfused liver, Ppv increased significantly from 7.4 ± 0.2 to 8.3 ± 0.5 cm H_2O. In constant pressure-perfused livers, L-NAME injection caused a decrease in blood flow from 45 ± 6 to 39 ± 7 mL/min per 10 g liver. However, D-NAME injection did not cause any changes in haemodynamic variables in either constant flow- or constant pressure-perfused liver. These findings indicate that endogenous NO dilates the hepatic vessels in basal states of isolated guinea pig livers perfused at a constant flow or constant pressure and that L-NAME (100 μmol/L) inhibits NO synthase in the present isolated blood-perfused guinea pig livers.

Constant flow perfusion study

Figure 1a shows a representative example of the response to an injection of 4 μg ovalbumin of a D-NAME-pretreated liver perfused at a constant flow. Within 1 min after an injection of

ovalbumin, venoconstriction occurred as evidenced by an increase in Ppv. Portal venous pressure reached peak levels of 14.8 ± 1.7 cm H_2O from the baseline of 7.3 ± 0.4 cm H_2O, as shown in Table 1. The Ppv-to-Phv gradient, the determinant of Rt, increased 2.1 times the baseline, indicating that Rt increased by the same degree, as shown in Fig. 2. The double occlusion manoeuvre performed at 4 min after antigen administration revealed the sinusoidal pressure of Pdo higher than that of the baseline. The Pdo-to-Phv gradient increased from the baseline of 2.9 ± 0.3 to 4.4 ± 0.6 cm H_2O, indicating an increase in Rpost. However, the increase in the Ppv-to-Pdo gradient (3.9 ± 0.4 vs 9.8 ± 1.3, baseline vs peak) was greater than that in the Pdo-to-Phv gradient, indicating a greater increase in Rpre than Rpost. The liver weight did not show any significant changes after antigen. Concomitant with venoconstriction, bile flow slightly decreased to 74% of the baseline.

The L-NAME pretreatment augmented the antigen-induced increase in Ppv by 7.2 cm H_2O, as compared with the D-NAME group (Table 1). Thus, the peak Rt levels in the L-NAME group was greater by 1.7-fold than that in the D-NAME group. However, L-NAME did not affect postantigen Pdo, as compared with the D-NAME groups. This indicates that L-NAME augmented peak Rpre (0.36 ± 0.12 vs 0.21 ± 0.04 cmH_2O/mL/min per 10 g liver weight; L-NAME vs D-NAME group), but not Rpost (0.09 ± 0.02 vs 0.09 ± 0.02 cmH_2O/mL/min per 10 g liver; L-NAME vs D-NAME group). This is reflected by significant greater values of postantigen Rpre/Rt ratio in the L-NAME group than the D-NAME group, as shown in Fig. 2.

Constant pressure perfusion study

Figure 1b shows a representative example of the response to 4 μg ovalbumin of the D-NAME-pretreated liver perfused under constant pressure. Under constant pressure perfusion, venoconstriction was detected by a decrease in portal blood flow. Actually, the blood flow decreased from the baseline of 47 ± 6 to the nadir, 18 ± 4 mL/min per 10 g liver weight at 4 min after antigen injection. Although the height of the inflow reservoir was held constant, Ppv increased only slightly in response to antigen. The Phv was decreased as a result of a decrease in blood flow. Thus, the anaphylactic venoconstriction caused an increase in Rt by 3.5-fold at the baseline level after antigen administration, as shown in Fig. 3. The Pdo at 4 min was slightly decreased from the baseline value. Accordingly, the increase in Ppv-to-Pdo gradient was greater than that in the Pdo-to-Phv gradient, indicating a greater increase in Rpre than Rpost, the findings consistent with the result obtained from the constant flow-perfused livers, as described above. Concomitants with a decrease in blood flow, the liver weight decreased by 1.9 ± 0.8 g/10 g. The bile flow was also decreased to 62% of baseline after antigen administration.

Under constant pressure perfusion, L-NAME also augmented anaphylactic venoconstriction, as evidenced by a greater decrease in blood flow in the L-NAME group than that in the D-NAME group (Table 1). The peak Rt levels in the L-NAME group were greater by 1.9-fold than that in the D-NAME, as shown in Fig. 3. However, there are no significant differences in peak levels of Ppv, Pdo, or Phv after antigen between the L-NAME and D-NAME groups.

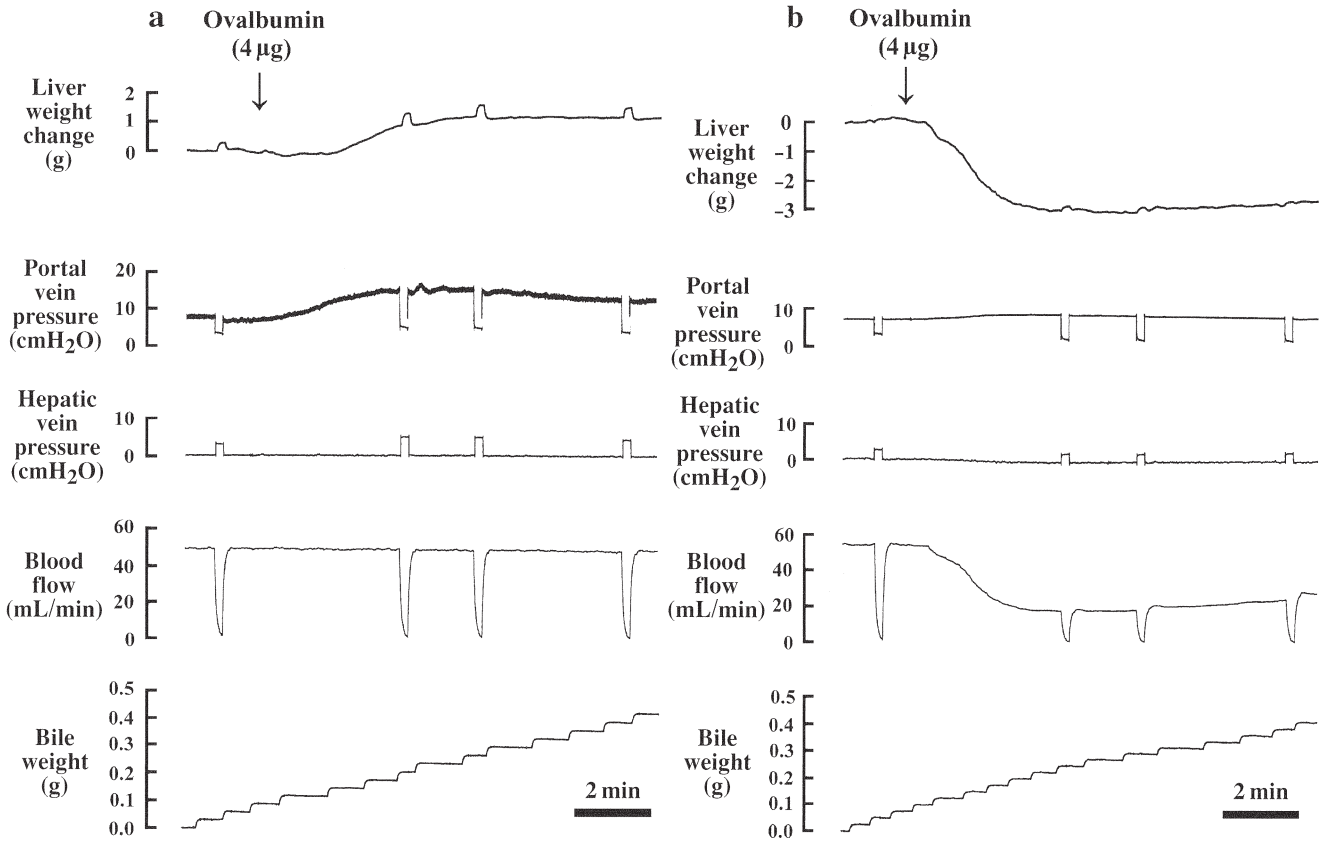

Fig. 1 Representative recordings of the response to the antigen, ovalbumin 4 μg under a constant flow perfusion (a) and a constant pressure perfusion (b).

Table 1 Baseline and peak values of haemodynamic variables after an injection of antigen in isolated guinea pig livers

Groups		Constant flow				Constant pressure			
		D-NAME ($n = 6$)		L-NAME ($n = 6$)		D-NAME ($n = 6$)		L-NAME ($n = 6$)	
Number of animals		Baseline	Peak	Baseline	Peak	Baseline	Peak	Baseline	Peak
Ppv	(cmH_2O)	7.3 ± 0.4	14.8 ± 1.7*	8.3 ± 0.5	22.0 ± 6.2*#	7.6 ± 0.1	8.9 ± 0.2*	8.2 ± 0.4	9.5 ± 0.4*
Phv	(cmH_2O)	0.5 ± 0.2	0.5 ± 0.2	0.4 ± 0.2	0.4 ± 0.2	0.3 ± 0.2	–0.4 ± 0.3*	0.4 ± 0.2	–0.5 ± 0.2*
Pdo	(cmH_2O)	3.4 ± 0.2	4.9 ± 0.6*	3.5 ± 0.2	5.0 ± 0.8*	3.2 ± 0.2	2.4 ± 0.1*	3.4 ± 0.3	2.3 ± 0.5*
Blood flow	(ml/min/10 g)	49 ± 5	49 ± 5	47 ± 6	47 ± 6	47 ± 6	18 ± 4*	39 ± 7	11 ± 3*#
Bile flow	(g/min)	0.038 ± 0.011	0.028 ± 0.010*	0.037 ± 0.008	0.021 ± 0.008*	0.034 ± 0.006	0.021 ± 0.005*	0.027 ± 0.006	0.013 ± 0.003*#

Values are means ± SD. Ppv, portal vein pressure; Phv, hepatic venous pressure; Pdo, double occlusion pressure. *$P < 0.05$ versus baseline. #$P < 0.05$ versus the corresponding D-NAME group.

Accordingly, the peak levels in both Rpre and Rpost were significantly and similarly greater in the L-NAME than that in the D-NAME group (1.9- and 1.8-fold). This is reflected by no significant differences in postantigen Rpre/Rt ratio between these two groups. This indicates that L-NAME augmented similarly in magnitude the antigen-induced increase in Rpre and Rpost.

DISCUSSION

The present study shows that NO synthesis inhibition augmented anaphylactic venoconstriction in isolated guinea pig livers perfused either under constant pressure or constant flow. These findings indicate that hepatic anaphylaxis can release NO not only via the shear stress-dependent mechanism (under constant flow perfusion) but also via the shear stress-independent mechanism (under constant pressure perfusion). Furthermore, NO released in the shear stress-independent manner dilates both pre- and postsinusoidal vessels similarly. In contrast, NO released in the shear stress-dependent manner attenuates predominantly venoconstriction of the presinusoids where shear stress is preferentially increased.

Hepatic venoconstriction that occurs under constant pressure perfusion does not necessarily accompany NO release. Actually, in the *in vivo* cat experiment, L-NAME, an inhibitor of NO synthesis, did not augment noradrenaline-induced hepatic venoconstriction under constant pressure, but it did under constant flow.[11] The same findings were also observed in perfused rat livers.[12] Thus, the finding of the present study that L-NAME potentiates anaphylactic

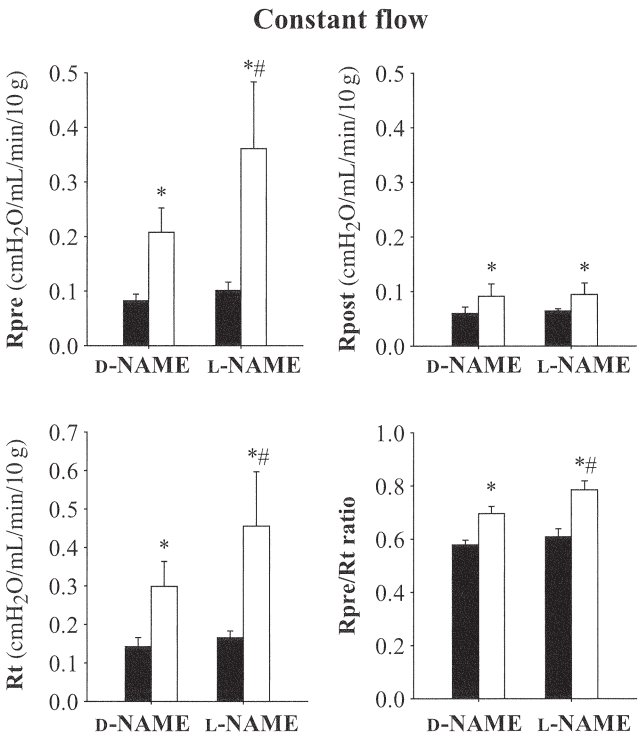

Fig. 2 The baseline (closed columns) and peak levels (open columns) of the pre (Rpre) and postsinusoidal (Rpost) resistances, the total hepatic vascular resistance (Rt) and the Rpre-to-Rt ratio under constant flow perfusion after an injection of the antigen in the D-NAME and L-NAME groups. Values are given as mean ± SD. $n = 7$. *$P < 0.05$ versus the baseline. #$P < 0.05$ versus the D-NAME group.

hepatic venoconstriction under constant pressure perfusion is interesting and contrasts with the more physiological venoconstriction induced by noradrenaline, a mediator released tonically from the sympathetic nerve endings.

The methodological basis of the present study to explore the roles of shear stress in the perfused livers was derived from the assumption proposed by Macedo and Lautt.[8] In isolated perfused vessels, the relationship between the wall shear stress (τ) and blood flow (Q), internal radius (r) and blood viscosity (η) is given as follows: $\tau = (m + 2)\ \eta Q/(\pi r^3)$.[13]

The value of m depends on the flow condition; with laminar flow, $m = 2$ and with turbulent flow $m > 2$. The value of m in our preparation was assumed to remain constant during the experiments. Under constant flow when Q remains constant, anaphylactic venoconstriction causes a decrease in r, thereby an increase in shear stress. If turbulence did increase at the constricted site, shear stress would further increase. When anaphylactic vasoconstriction was induced under constant pressure perfusion, flow was reduced such that the ratio of flow to the radius of the vessels was maintained constant, as defined by this cubic relationship. Therefore, the wall shear stress should be maintained constant throughout this experiment, if perfusion pressure is held constant.[8]

The mechanism why NO was released during hepatic anaphylaxis in a shear stress-independent fashion, i.e. under constant pressure perfusion, may be ascribed to humoral substances released by anaphylactic reaction per se. We assume that the chemical mediators such as PAF, TxA_2, histamine, leukotriene and serotonin might act on the corresponding receptor of the endothelium, resulting in the subsequent activation of endothlial nitric oxide synthase and production of NO. Actually it is reported that most mediators of anaphylaxis, such as histamine,[4,5] leukotrienes,[6] TxA_2[5] and PAF,[7] all stimulate NO release from the vascular endothelium.

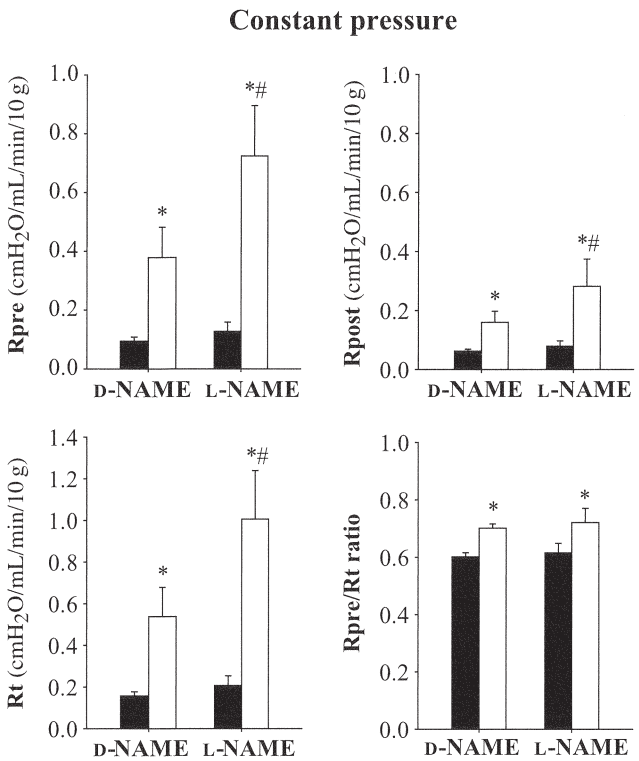

Fig. 3 The baseline (closed columns) and peak levels (open columns) of the pre (Rpre) and postsinusoidal (Rpost) resistances, the total hepatic vascular resistance (Rt) and the Rpre-to-Rt ratio under constant pressure perfusion after an injection of the antigen in the D-NAME and L-NAME groups. Values are given as mean ± SD. $n = 7$. $^*P < 0.05$ versus the baseline. $^\#P < 0.05$ versus the D-NAME group.

One of the most interesting findings of the present study is that the amplitude of the L-NAME-induced potentiation of anaphylactic venoconstriction is similar for presinusoids and postsinusoids. This may suggest that NO was generated from both pre- and postsinusoids. The exact mechanism for this NO release at pre- and postsinusoids is not known. Hepatic interstitial mast cells might release the above-mentioned mediators, which then diffuse along all of the hepatic vessels and bind endothelial receptors, causing endothelial release of NO, which then relaxes the adjacent smooth muscle cells, with resultant relaxation of pre- and postsinusoidal vessels. However, the morphological study revealed that livers from normal guinea pigs contained substantial numbers of alcian blue positive mast cells distributed mainly in the connective tissue of portal tracts.[14] However, although local and systemic anaphylaxis has been presumed to be caused predominantly, if not exclusively, through the activation of mast cells, other cell types, such as macrophages and lymphocytes, also release certain inflammatory mediators upon stimulation with specific antigens.[15–17] In the livers, there are a large number of intravascular resident macrophages, called Kupffer cells. The mediators released intravascularly from these Kupffer cells might have diffused and reacted with endothelium of the pre- and post sinusoids. Further studies are required in this respect.

Under constant flow perfusion, the anaphylactic venoconstriction of the presinusoids was exclusively augmented by a NO synthase inhibitor of L-NAME. This result is consistent with our previous results[3] in that L-NAME pretreatment augmented the anaphylaxis-induced increase in Rpre by 120%, while it did increase in Rpost only by 20% in constant flow perfused guinea pig livers challenged with the higher dose of antigen (0.1 mg). These findings suggest that NO might be released during anaphylaxis selectively in presinusoidal vessels of constant flow perfused livers. The mechanism for this selective vulnerability of presinusoids to NO may be considered as follows; as shown in the constant flow D-NAME group, anaphylaxis constricted predominantly presinusoidal vessels, where elevated shear stress increased NO release from the same presinusoidal endothelium, leading to relaxation of the adjacent presinusoidal vascular smooth muscle cells in a paracrine manner.

N^ω-Nitro-L-arginine methyl ester augmented anaphylactic venoconstriction in guinea pig livers perfused either at the constant flow (shear stress elevated) or at the constant pressure (shear stress not elevated). Nitric oxide released in a shear stress-independent manner attenuates hepatic venoconstriction of both pre- and postsinusoids similarly, while NO produced in a shear stress-dependent manner attenuates predominantly venoconstriction of the presinusoids where shear stress is preferentially increased.

ACKNOWLEDGEMENTS

The present study was supported by a Grant for Collaborative Research from Kanazawa Medical University (C2003-1) and a Grant-in-Aid for Scientific Research from the Ministry of

Education, Culture, Sports, Sciences and Technology of Japan (No. 15591665).

REFERENCES

1. Moncada S, Higgs A. The L-arginine-nitric oxide pathway. *N. Engl. J. Med.* 1993; **329**: 2002–12.
2. Rees DD, Palmer RMJ, Moncada S. Role of endothelium-derived nitric oxide in regulation of blood pressure. *Proc. Natl. Acad. Sci. USA* 1989; **86**: 3375–8.
3. Ruan Z, Shibamoto T, Shimo T, Tsuchida H, Koizumi T, Nishio M. NO, but not CO, attenuates anaphylaxis-induced postsinusoidal contraction and congestion in guinea pig liver. *Am. J. Physiol. Regul. Integr. Comp. Physiol.* 2004; **286**: R94–100.
4. Lamparter B, Gross SS, Levi R. Nitric oxide and the cardiovascular actions of histamine. *Agents Actions* 1992; (Special conference issue): C187–90.
5. Lantoine F, Iouzalen L, Devynck MA, Millanvoye-Van Brussel E, David-Dufilho M. Nitric oxide production in human endothelial cells stimulated by histamine requires Ca^{2+} influx. *Biochem. J.* 1998; **330**: 695–9.
6. Sakuma I, Gross S, Levi R. Peptidoleukotrienes induce an endothelium-dependent relaxation of guinea pig main pulmonary artery and thoracic aorta. *Prostaglandins* 1987; **34**: 685–96.
7. Kamata K, Mori T, Shigenobu K, Kasuya Y. Endothelium-dependent vasodilator effects of platelet activating factor on rat resistance vessels. *Br. J. Pharmacol.* 1989; **98**: 1360–4.
8. Macedo MP, Lautt WW. Shear-induced modulation by nitric oxide of sympathetic nerves in mesenteric artery. *Can. J. Physiol. Pharmacol.* 1996; **74**: 692–700.
9. Shibamoto T, Wang HG, Miyahara T, Tanaka S, Haniu H, Koyama S. Presinusoidal vessels predominantly contract in response to norepinephrine, histamine, and KCl in rabbit liver. *J. Appl. Physiol.* 1999; **87**: 1404–12.
10. Yamaguchi Y, Shibamoto T, Hayashi T, Saeki Y, Tanaka S. Hepatic vascular response to anaphylaxis in isolated canine liver. *Am. J. Physiol. Regul. Integr. Comp. Physiol.* 1994; **267**: R268–74.
11. Macedo MP, Lautt WW. Shear-induced modulation of vasoconstriction in the hepatic artery and vein by nitric oxide. *Am. J. Physiol. Gastrointest. Liver Physiol.* 1998; **274**: G253–60.
12. Pastor CM, Hadengue A. Shear stress modulates the vascular tone in perfused livers isolated from normal rats. *Hepatology* 2000; **32**: 786–91.
13. Kamiya A, Togawa T. Adaptative regulation of wall shear stress to flow change in the canine carotid artery. *Am. J. Physiol. Heart Circ. Physiol.* 1980; **239**: H14–21.
14. Hagmann W, Hacker HJ, Buchholz U. Resident mast cells are the main initiators of anaphylactic leukotriene production in the liver. *Hepatology* 1992; **16**: 1477–84.
15. Conrad DH, Campbell KA, Bartleft WC, Squire CM, Dierks SE. Structure and function of the low affinity IgE receptor. *Adv. Exp. Med. Biol.* 1994; **347**: 17–30.
16. Dessaint JP, Capron A. IgE and inflammatory cells: The cellular networks in allergy. *Int. Arch. Allergy Appl. Immunol.* 1989; **90** (Suppl. 1): 28–31.
17. Kikutani H, Yokota A, Uchibayashi N *et al*. Structure and function of Fc epsilon receptor II (Fc epsilon RII/CD23): A point of contact between the effector phase of allergy and B cell differentiation. *Ciba Found. Symp.* 1989; **147**: 23–31.

Basic Science Investigations

Respiration

Respiration 2005;72:189–196
DOI: 10.1159/000084051

Received: March 31, 2004
Accepted after revision: September 9, 2004

Catecholamine Clearance from Alveolar Spaces of Rat and Human Lungs

Tsutomu Sakuma[a] Xiu Gu[a] Makoto Sugita[a] Motoyasu Sagawa[a]
Maki Sakuda[b] Hirohisa Toga[b]

[a]Thoracic Surgery, [b]Pulmonary Medicine, Kanazawa Medical University, Uchinada, Ishikawa, Japan

Key Words
Norepinephrine · Epinephrine · Amiloride · Benzamil · Alveolar epithelium

Abstract
Background: Although aerosolized β-adrenergic agonists have been used as a therapy for the resolution of pulmonary edema, the mechanisms of catecholamine clearance from the alveolar spaces of the lung are not well known. ***Objective:*** To determine whether catecholamine clearance from the alveolar spaces is correlated with the fluid transport capacity of the lung. ***Methods:*** Albumin solution containing epinephrine (10^{-7} *M*) or norepinephrine (10^{-7} *M*) was instilled into the alveolar spaces of isolated rat and human lungs. Alveolar fluid clearance rate was estimated by the progressive increase in the albumin concentration over 1 h. Catecholamine clearance rate was estimated by the changes in catecholamine concentration and alveolar fluid volume over 1 h. ***Results:*** The norepinephrine clearance rate was faster than the epinephrine clearance rate in the rat and human lungs. In the rat lungs, amiloride (a sodium channel blocker) caused a greater decrease in alveolar fluid clearance and epinephrine clearance rate than propranolol (a nonselective β-adrenergic antagonist). Although propranolol and phentolamine (an α-adrenergic antagonist), and 5-(N-ethyl-N-isoprophyl)amiloride (a Na^+/H^+ antiport blocker) changed neither the alveolar fluid clearance nor the norepinephrine clearance rate, amiloride and benzamil (a sodium channel blocker) decreased both clearance rates. As in the rat lungs, amiloride decreased alveolar fluid and norepinephrine clearance rates in the human lungs. ***Conclusion:*** These results indicate that the catecholamine clearance rate from the alveolar spaces is correlated with alveolar fluid clearance in rat and human lungs.

Introduction

The mechanism responsible for ion and fluid transport across the alveolar epithelia has been studied over two decades. The initial step in alveolar fluid clearance is the absorption of alveolar sodium ions through apical sodium channels into the alveolar epithelial cells, and then the exchange of sodium and potassium ions through basolateral Na^+-K^+ ATPase [1–3]. Amiloride is a potent blocker of sodium channels on the apical membrane of alveolar epithelial cells and has been shown to impair the rate of alveolar fluid clearance [2, 4]. In contrast, β-adrenergic

KARGER
Fax + 41 61 306 12 34
E-Mail karger@karger.ch
www.karger.com

0025–7931/05/0722–0189$22.00/0

Accessible online at:
www.karger.com/res

Tsutomu Sakuma, MD
Thoracic Surgery, Kanazawa Medical University
Uchinada
Ishikawa 920-0293 (Japan)
Tel./Fax +81 76 286 1207, E-Mail sakuma-t@kanazawa-med.ac.jp

agonists stimulate alveolar fluid clearance under normal and pathological conditions in mice [5], rats [6–9], dogs [10, 11] and sheep [12, 13]. We have reported that terbutaline and salmeterol, two selective β_2-adrenergic agonists, increase alveolar fluid clearance in isolated human lungs [14–17]. In addition, exogenous catecholamine (epinephrine or norepinephrine) increase alveolar fluid clearance in sheep [12], guinea pig [18], and rat [19]. Therefore, β-adrenergic agonists have been considered as therapeutic agents for accelerating the resolution of pulmonary edema [3, 20].

Another important function of the alveolar epithelial barrier is that it provides a large surface area for the transfer of instilled materials to the circulation [21–24]. Therefore, catecholamines have been administered into the airspaces with the goal of delivering them into the pulmonary circulation and heart in patients requiring cardiopulmonary resuscitation [25]. Since the effect of a β-adrenergic agonist therapy on alveolar fluid clearance depends on its concentration in the alveolar fluid [9, 16], rapid clearance from the alveolar space could diminish its efficacy. Indeed, amiloride concentrations of 10^{-4}–10^{-3} *M* are necessary in vivo to inhibit alveolar fluid clearance because of its rapid clearance rate from the alveolar spaces [26]. In rabbit lung preparations in which saline solution containing 10^{-3} *M* amiloride was instilled, approximately 23% of the initial amiloride was cleared from the alveolar spaces over 1 h [27]. However, little is known regarding the mechanism responsible for the clearance of β-adrenergic agonists from the distal airspaces.

Therefore, our first objective was to determine the clearance rates of catecholamines (epinephrine and norepinephrine) in isolated rat lungs. Our second objective was to determine whether α- and β-adrenergic antagonists changed the catecholamine clearance rate. Our third objective was to determine whether sodium channel blockers changed the catecholamine clearance rate. Our final objective was to determine the catecholamine clearance rate in the isolated human lungs.

Methods

Materials

Amiloride, benzamil, epinephrine, 5-(N-ethyl-N-isoprophyl)amiloride, norepinephrine, phentolamine, and propranolol were obtained from Sigma (St. Louis, Mo., USA).

Experimental Protocol

All rats received humane care and this study was approved by the Committee for Animal Experiments at Kanazawa Medical University. Alveolar fluid clearance was measured in the isolated rat lungs in the absence of pulmonary perfusion or ventilation [9, 16, 28, 29]. Briefly, male Sprague-Dawley rats (200–250 g, Japan SLC, Inc., Hamamatsu, Japan) were anesthetized with intraperitoneal pentobarbital sodium (50 mg/kg). An endotracheal tube was inserted through a tracheostomy. The rats were exsanguinated via the abdominal aorta and the trachea, bilateral lungs, and heart were excised en bloc through a median sternotomy. Warmed physiological saline solution (7 ml/kg, 37 °C) containing 5% bovine albumin was instilled into both lungs, followed by 4 ml oxygen to deliver all the instilled fluid into the alveolar spaces. The lungs were placed in a humid incubator at 37 °C and inflated with 100% oxygen at an airway pressure of 7 cm H_2O. Alveolar fluid was aspirated 1 h after instillation.

Catecholamine Clearance Rate in Isolated Rat Lungs

To determine the catecholamine clearance rate under basal conditions, albumin solution containing epinephrine (10^{-7} *M*, n = 8) or norepinephrine (10^{-7} *M*, n = 8) was instilled into the alveolar spaces of isolated rat lungs. As a control, albumin solution in the absence of any catecholamine was instilled into the alveolar spaces of isolated rat lungs (n = 8).

Effects of Propranolol and Amiloride on the Epinephrine Clearance Rate in Isolated Rat Lungs

To determine if epinephrine clearance was mediated via β-adrenergic receptors, propranolol (10^{-5} *M*), a β-adrenergic antagonist, was added to an albumin solution containing epinephrine (10^{-7} *M*) and instilled into the alveolar spaces of isolated rat lungs (n = 4). In addition, to determine whether epinephrine clearance was mediated via amiloride-sensitive sodium channels, amiloride (10^{-3} *M*) was added to albumin solution containing epinephrine (10^{-7} *M*) and instilled into the alveolar spaces of isolated rat lungs (n = 4).

Effects of Adrenergic Antagonists and Sodium Channel Blockers on the Norepinephrine Clearance Rate in Isolated Rat Lungs

Since the norepinephrine clearance rate was faster than the epinephrine clearance rate, we determined the effect of adrenergic antagonists and sodium channel blockers on the faster norepinephrine clearance rate in rat lungs. Phentolamine (10^{-5} *M*, n = 4), an α-adrenergic antagonist, or propranolol (10^{-5} *M*, n = 4) was added to albumin solution containing norepinephrine (10^{-7} *M*) and instilled into the alveolar spaces of rat lungs. In addition, amiloride (10^{-3} *M*, n = 6) or benzamil (10^{-3} *M*, n = 6), a sodium channel blocker, or 5-(N-ethyl-N-isoprophyl)amiloride (EIPA, 10^{-3} *M*, n = 4), an Na^+/H^+ antiport blocker, was added to albumin solution containing norepinephrine (10^{-7} *M*) and instilled into the alveolar spaces of isolated rat lungs.

Effects of Initial Norepinephrine Concentration on the Norepinephrine Clearance Rate in Isolated Rat Lungs

To determine whether the norepinephrine clearance rate was dependent on the instilled concentration of norepinephrine, an albumin solution containing a higher concentration of norepinephrine (10^{-5} *M*) was instilled into the alveolar spaces of isolated rat lungs (n = 5).

Catecholamine Clearance Rate in Isolated Human Lungs

This study was approved by the Human Research Committee in Kanazawa Medical University. Human lungs were obtained from patients who underwent pulmonary resections for bronchogenic car-

cinoma. Informed consent was given by each patient before the operation. There were no fibrous or emphysematous lesions as assessed by preoperative chest radiographs and computed tomograms. Nor were any macroscopic emphysematous changes found when the lungs were removed from the thorax. The pulmonary function tests before the operation were normal (vital capacity: 93 ± 8% of the predicted value, forced expiratory volume in 1 s: 82 ± 11% of forced vital capacity). The surgical procedure was described previously [14–16]. The segmental bronchus was occluded by a 10-french balloon catheter immediately after removal of the lung. We chose the occluded segment that was located furthest away from the tumor. A warmed physiological saline solution (45 ml, 37°C) containing 5% bovine albumin and catecholamine (10^{-7} *M* epinephrine; n = 4, or 10^{-7} *M* norepinephrine; n = 4) was instilled into the distal airspaces through the catheter. To determine the effect of amiloride on the norepinephrine clearance rate, a warmed physiological saline solution containing 5% bovine albumin and norepinephrine (10^{-7} *M*) and amiloride (10^{-3} *M*) was instilled into the distal airspaces (n = 4). After instillation, the lungs were inflated with 100% oxygen at an airway pressure of 7 cm H_2O. Alveolar fluid was aspirated 1 h after instillation. Aspirated alveolar fluid (1–2 ml) was centrifuged at 3,000 rpm for 10 min, and supernatant was obtained for the measurement of the protein and catecholamine concentrations.

Metabolism of Catecholamine in the Alveolar Spaces

To determine whether exogenous norepinephrine and epinephrine were metabolized in the alveolar spaces, we measured vanillylmandelic acid (VMA), a catecholamine metabolite, in plasma, final alveolar fluid, and flushing fluid of pulmonary vasculature from rats with instillation of 5% albumin solution containing epinephrine (10^{-7} *M*, n = 4), instillation of 5% albumin solution containing norepinephrine (10^{-7} *M*, n = 4), or instillation of 5% albumin solution alone (n = 4). After anesthesia and tracheostomy, heparin sodium (3,000 units/kg) was intravenously injected and arterial blood was obtained 60 s after heparinization. Then, the rats were exsanguinated and the lungs were used for the measurement of alveolar fluid clearance for 1 h. After the measurement of alveolar fluid clearance, the pulmonary vasculature was flushed with a warmed 0.9% saline solution (10 ml) through a catheter placed in the trunk of the pulmonary artery. Samples of flushing fluid were collected from the left atrium. VMA levels were measured by high-performance liquid chromatography (SRL, Inc., Tokyo, Japan).

Measurements

Alveolar Fluid Clearance. The protein concentrations in instilled and aspirated solutions were measured by a spectrophotometer at a wavelength of 280 nm (BioSpec-1600, Shimadzu, Kyoto, Japan). Alveolar fluid clearance was estimated by measuring the progressive increase in the concentration of albumin [9, 16, 28, 29]. Alveolar fluid clearance (AFC) was calculated as follows:

$$AFC = [(V_i - V_f)/V_i] \times 100 \quad (1)$$

where V is the volume of the instilled albumin solution (i) and the final alveolar fluid (f).

$$V_f = (V_i \times P_i)/P_f \quad (2)$$

where P is the concentration of protein in the instilled albumin solution (i) and the final alveolar fluid (f).

The term 'alveolar' does not imply that all reabsorption occurs across the alveolar epithelium because the distal bronchial epithelia can also transport sodium and fluid [28].

Catecholamine Concentration. The samples of fluid were stored at –80°C until analysis. Catecholamine concentrations in the instilled and aspirated albumin solutions were determined by high-performance liquid chromatography with a trihydroxyindole reaction [19, 29]. The catecholamine clearance rate from the alveolar spaces was calculated as the quantity of absorbed catecholamine divided by the quantity of instilled catecholamine:

$$\text{Clearance rate} = (C_i \times V_i - C_f \times V_f)/(C_i \times V_i) \quad (3)$$

where C is the concentration of catecholamine in the instilled albumin solution (i) and the final alveolar fluid (f).

Statistics

Data are summarized as the mean and standard deviation. The data were analyzed by a one-way analysis of variance (ANOVA) with the Student-Newman-Keuls post hoc test when multiple comparisons were needed (Prism 4, GraphPad Software, Inc., San Diego, Calif., USA). When comparisons were made between two experimental groups, an unpaired Student's t test was used. Differences with $p < 0.05$ were regarded as significant.

Results

Epinephrine (10^{-7} *M*) increased alveolar fluid clearance by 38% in the rat lungs. However, norepinephrine (10^{-7} *M*) did not change alveolar fluid clearance (fig. 1). The norepinephrine clearance rate (89 ± 5%/h) was greater than the epinephrine clearance rate (51 ± 5%/h). In the control rat lungs, neither epinephrine nor norepinephrine was identified in the samples of alveolar fluid 1 h after instillation.

Propranolol abolished the increase in alveolar fluid clearance induced by epinephrine and decreased the epinephrine clearance rate in the rat lungs (fig. 2). Propranolol plus amiloride further decreased both alveolar fluid clearance and the epinephrine clearance rate.

Neither propranolol nor phentolamine changed alveolar fluid clearance and the norepinephrine clearance rate in the rat lungs (fig. 3). Amiloride and benzamil decreased both alveolar fluid clearance and the norepinephrine clearance rate. However, EIPA neither changed the alveolar fluid clearance nor the norepinephrine clearance rate.

A higher concentration (10^{-5} *M*) of norepinephrine increased alveolar fluid clearance (fig. 4). However, the higher concentration did not change the norepinephrine clearance rate. The quantity of norepinephrine that was removed from the alveolar spaces depended on the initial concentration of norepinephrine in the alveolar spaces.

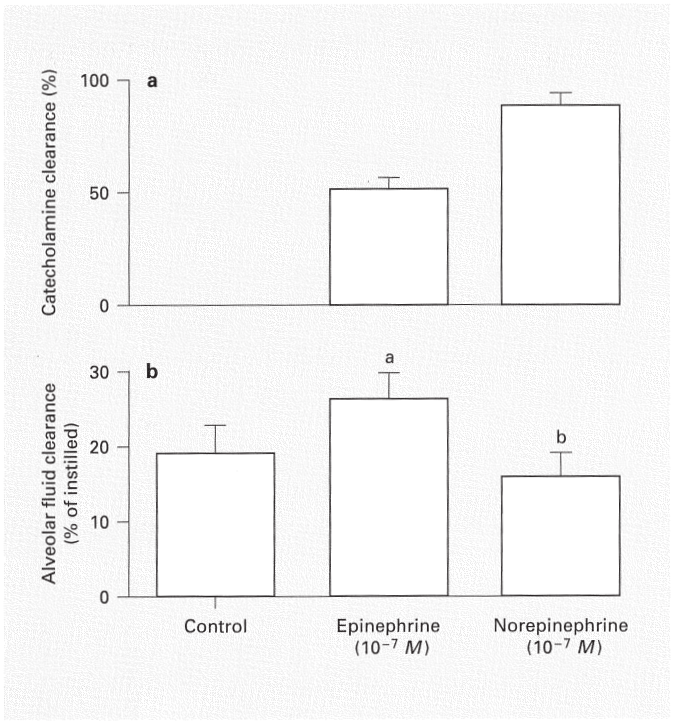

1

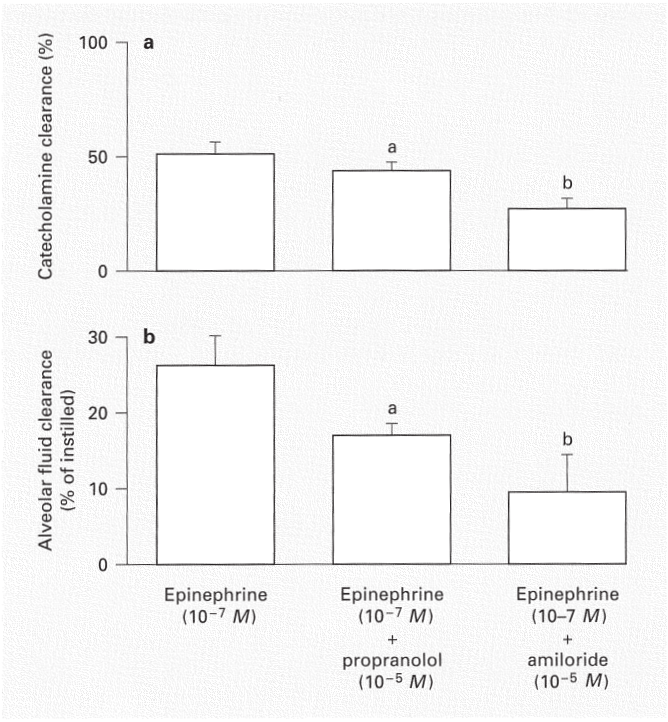

2

Fig. 1. Comparison between clearance rates of epinephrine and norepinephrine in isolated rat lungs. [a] $p < 0.05$ vs. control value; [b] $p < 0.05$ vs. corresponding values in the rat lungs treated with epinephrine. **a** Catecholamine clearance. **b** Alveolar fluid clearance.

Fig. 2. Effects of propranolol and amiloride on the epinephrine clearance rate in isolated rat lungs. [a] $p < 0.05$ vs. corresponding values in epinephrine-treated rat lungs. [b] $p < 0.05$ vs. corresponding values in rat lungs treated with epinephrine plus propranolol. **a** Catecholamine clearance. **b** Alveolar fluid clearance.

Fig. 3. Effects of adrenergic antagonists and sodium channel blockers on the norepinephrine (NE) clearance rate in isolated rat lungs. [a] $p < 0.05$ vs. corresponding values in norepinephrine-treated rat lungs. [b] $p < 0.05$ vs. corresponding values in rat lungs treated with norepinephrine plus amiloride. **a** Catecholamine clearance. **b** Alveolar fluid clearance.

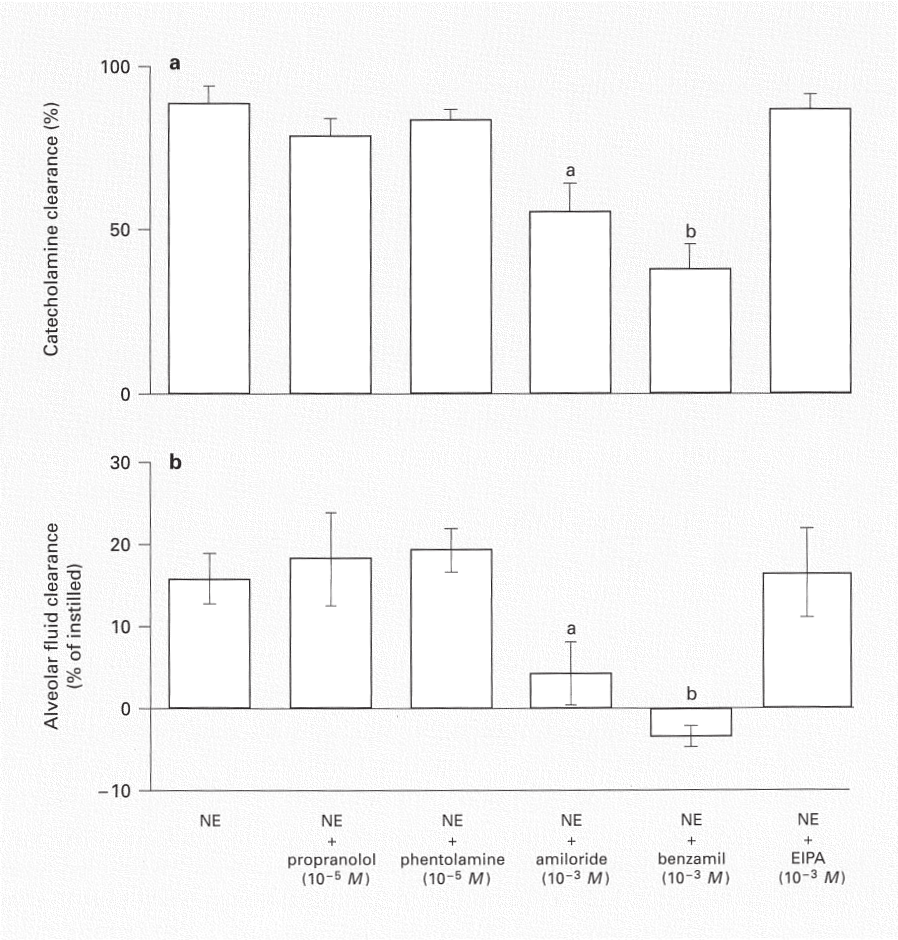

3

In the human lungs, epinephrine increased alveolar fluid clearance, whereas norepinephrine did not (fig. 5). As in rat lungs, the norepinephrine clearance rate (69 ± 14%/h) was faster than the epinephrine clearance rate (28 ± 9%/h). Amiloride decreased alveolar fluid clearance and the norepinephrine clearance rate.

The volume of flushing fluid collected from the left atrium was 9.4 ± 0.4 ml and there was no difference among the volumes from control rat lungs, epinephrine-instilled and norepinephrine-instilled rat lungs. The VMA levels in plasma were not different among the groups (10.3 ± 1.4 ng/ml in the control lungs, 10.2 ± 1.8 ng/ml in the epinephrine-instilled, and 11.0 ± 2.0 ng/ml in the norepinephrine-instilled lungs). The VMA levels in final alveolar fluid and flushing fluid were below the detection levels (<1.0 ng/ml).

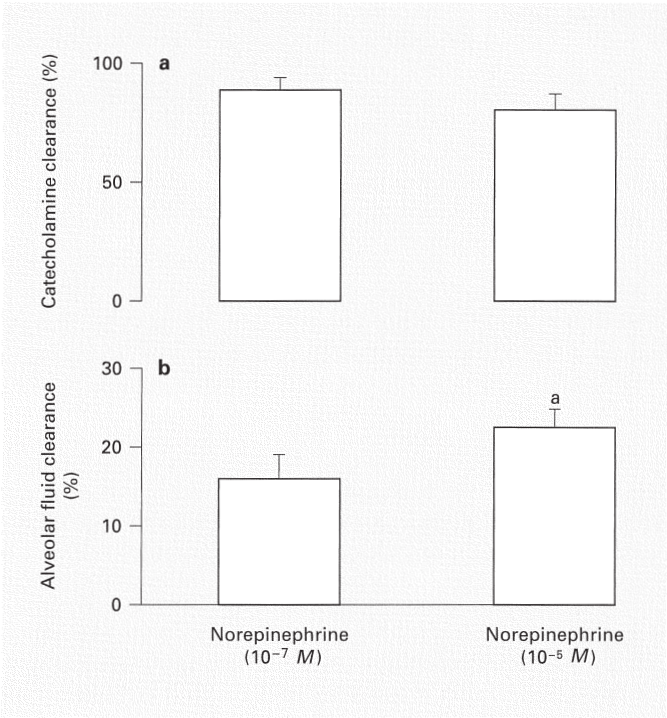

4

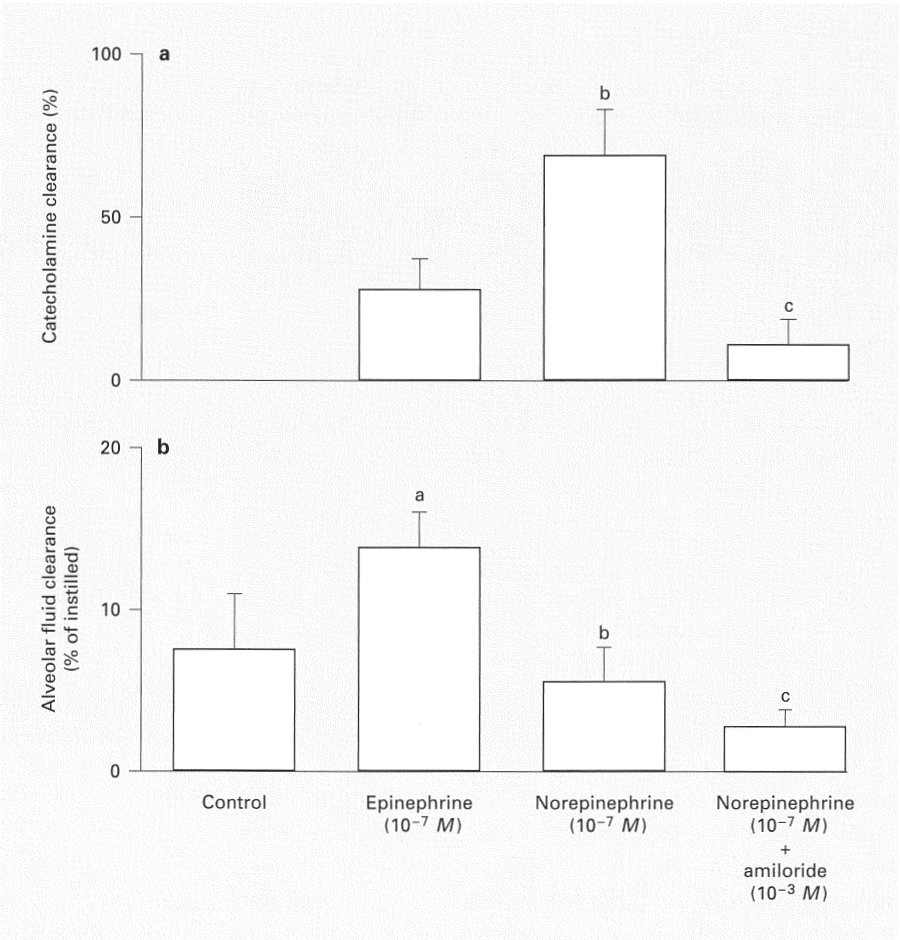

5

Fig. 4. Effects of the initial norepinephrine concentration on the norepinephrine clearance rate in isolated rat lungs. [a] $p < 0.05$ vs. corresponding value in the rat lungs treated with norepinephrine 10^{-7} *M*. **a** Catecholamine clearance. **b** Alveolar fluid clearance.

Fig. 5. Catecholamine clearance rates isolated human lungs. [a] $p < 0.05$ vs. corresponding control value. [b] $p < 0.05$ vs. corresponding values in human lungs treated with epinephrine 10^{-7} *M*. [c] $p < 0.05$ vs. corresponding values in the control lungs and in the lungs treated with norepinephrine 10^{-7} *M*. **a** Catecholamine clearance. **b** Alveolar fluid clearance.

Discussion

Several experimental preparations have been used to measure ion and fluid transport from the alveolar spaces [30]. We have developed an isolated lung preparation in which fluid clearance across the alveolar epithelial barrier was measured in the absence of perfusion and ventilation [9, 14–16, 28, 29]. Therefore, the catecholamine clearance rate from the alveolar spaces was examined in the isolated rat lungs in the absence of pulmonary perfusion and ventilation.

Clearance of catecholamines from the alveolar spaces may proceed via two major pathways: a transcellular and a paracellular pathway. Several findings in this study indicate that catecholamine clearance occurred primarily by diffusion through a paracellular pathway. First, the rate of catecholamine clearance was much higher than the rate of alveolar fluid clearance that is driven by an active sodium transport mechanism [30]. The fast catecholamine clearance in the isolated lungs was consistent with the epinephrine clearance rate in anesthetized dogs [31]. Second, α- and β-adrenergic antagonists did not impair the norepinephrine clearance rate. If catecholamine clearance was mediated through adrenergic receptors, the adrenergic antagonists should have impaired the catecholamine clearance rate as the antagonists inhibited the stimulating effect of terbutaline on alveolar fluid clearance [14]. Third, the quantity of norepinephrine that was removed from the alveolar spaces depended on the initial norepinephrine concentration in the alveolar spaces. The results are consistent with the report that the paracellular pathway has the characteristics of a dose-dependent movement [32]. These observations suggest that norepinephrine clearance is driven by diffusion through a paracellular pathway.

This study was carried out in the isolated rat lungs in the absence of perfusion and ventilation. This preparation eliminates the confounding effect of increased transvascular fluid and protein flux that may occur in injured lungs and permits independent assessment of the permeability and transport properties of the alveolar epithelium [30]. However, it has been known that stretching of alveolar epithelial cells can have a profound effect of on surfactant secretion [33], releasing growth factors [34], and the activity of extracellular signal-regulated kinase [35]. These effects may alter the ion transport capacity of alveolar epithelial cells [36]. In our previous study, alveolar fluid clearance was smaller in nonperfused and nonventilated rat lungs than in rat lungs in vivo [16]. Therefore, it is probable that catecholamine clearance might be smaller in this study than in the in vivo study. Further studies are necessary to determine the effect of ventilation or pulmonary perfusion on catecholamine clearance from the alveolar spaces.

Amiloride has been used as a potent blocker of sodium transport and net alveolar fluid clearance [2]. The effect of amiloride on alveolar fluid clearance in the rat and human lungs in this study was consistent with our prior results [14, 15]. In addition, benzamil abolished alveolar fluid clearance. These results were consistent with the results that amiloride and benzamil are potent blockers of sodium transport in cultured type II alveolar epithelial cells [37, 38].

To determine if catecholamine clearance was correlated with alveolar fluid clearance, we tested the effect of amiloride, benzamil, and EIPA on the norepinephrine clearance rate. Although amiloride and benzamil inhibited both alveolar fluid clearance and the norepinephrine clearance rate, EIPA did not inhibit either of them. Since amiloride-sensitive sodium channels play an important role in active ion and fluid transport across the alveolar epithelial cells [3, 4], it is likely that amiloride-sensitive sodium channels also play an important role in catecholamine clearance from the alveolar spaces of rat lungs. There are reports indicating that amiloride inhibits the clearance of substances through a paracellular pathway. In the perfused fluid-filled rat lungs, amiloride reduced the permeability rate of mannitol, a trace of paracellular transport from the alveolar spaces [1, 39]. In addition, amiloride inhibited both active sodium transport and mannitol permeability in the presence of these stimulatory agents [32]. Similar effects of amiloride with and without isoproterenol were reported in the study performed on cultured Clara cell epithelium from rabbit [40]. Therefore, catecholamine clearance is correlated with alveolar fluid clearance in isolated rat and human lungs.

To answer the question whether catecholamine moved into the alveolar space and affected the final catecholamine concentration in the alveolar fluid, we measured the catecholamine concentration in the final alveolar fluid of control rat lungs. Since no catecholamine was identified in the final alveolar fluid, it is unlikely that endogenous catecholamines moved into the alveolar spaces and affected the clearance rate of catecholamine.

We also investigated whether exogenous norepinephrine and epinephrine were metabolized in the alveolar spaces. VMA, a catecholamine metabolite, was measured in final alveolar fluid and flushing fluid of the pulmonary vasculature from rat lungs instilled with epinephrine and norepinephrine and found to be below the detection level

in both fluids. Therefore, it is unlikely that exogenous norepinephrine and epinephrine were metabolized in the alveolar spaces during the 1-hour experiment.

It is unclear why epinephrine and norepinephrine are cleared at different rates from the distal airspaces. Several characteristics, e.g., molecular size, radius, electric charges, may affect the absorption rates of substances [22]. The molecular sizes of epinephrine and norepinephrine are similar, but epinephrine has a methyl group and a hydroxyl group. Further studies are needed to determine the mechanisms responsible for the difference between the clearance rates of epinephrine and norepinephrine.

Summary and Conclusions

The rate of norepinephrine clearance from the alveolar spaces was faster than that of epinephrine clearance in rat and human lungs. Amiloride and benzamil decreased both alveolar fluid clearance and the norepinephrine clearance rate, whereas EIPA did not. These results indicate that the catecholamine clearance rate is correlated with alveolar fluid clearance in rat and human lungs. Since sodium channel blockers impair catecholamine clearance from the alveolar spaces, sodium channel may play a role in the mechanism responsible for catecholamine clearance from the alveolar spaces.

Acknowledgments

This study was supported by Grants for Project Research from High-Technology Center of Kanazawa Medical University (H2002–7, H2003–7), Grant for Collaborative Research from Kanazawa Medical University (C2003–1), and Grant-In-Aid for Scientific Research from the MEXT, Japan (No 14571287).

References

1 Saumon G, Basset G: Electrolyte and fluid transport across the mature alveolar epithelium. J Appl Physiol 1993;74:1–15.
2 Matalon S, Benos DJ, Jackson RM: Biophysical and molecular properties of amiloride-inhibitable Na^+ channels in alveolar epithelial cells. Am J Physiol 1996;271:L1–L22.
3 Matthay MA, Folkesson HG, Clerici C: Lung epithelial fluid transport and the resolution of pulmonary edema. Physiol Rev 2002;82:569–600.
4 Matalon S, O'Brodovich H: Sodium channels in alveolar epithelial cells: Molecular characterization, biophysical properties, and physiological significance. Annu Rev Physiol 1999;61:627–661.
5 Fang X, Fukuda N, Barbry P, Sartori C, Verkman AS, Matthay MA: Novel role for CFTR in fluid absorption from the distal airspaces of the lung. J Gen Physiol 2002;119:199–207.
6 Crandall ED, Heming TA, Palombo RL, Goodman BE: Effects of terbutaline on sodium transport in isolated perfused rat lung. J Appl Physiol 1986;60:289–294.
7 Jayr C, Garat C, Meignan M, Pittet JF, Zelter M, Matthay MA: Alveolar liquid and protein clearance in anesthetized ventilated rats. J Appl Physiol 1994;76:2636–2642.
8 Saldias F, Lecuona E, Friedman E, Barnard ML, Ridge KM, Sznajder JI: Modulation of lung liquid clearance by isoproterenol in rat lungs. Am J Physiol 1998;274:L694–L701.
9 Sakuma T, Tuchihara C, Ishigaki M, Osanai K, Nambu Y, Toga H, Takahashi K, Ohya N, Kurihara T, Matthay MA: Denopamine, a beta(1)-adrenergic agonist, increases alveolar fluid clearance in ex vivo rat and guinea pig lungs. J Appl Physiol 2001;90:10–16.
10 Berthiaume Y, Broaddus VC, Gropper MA, Tanita T, Matthay MA: Alveolar liquid and protein clearance from normal dog lungs. J Appl Physiol 1988;65:585–593.
11 Grimme JD, Lane SM, Maron MB: Alveolar liquid clearance in multiple nonperfused canine lung lobes. J Appl Physiol 1997;82:348–353.
12 Berthiaume Y, Staub NC, Matthay MA: Beta-adrenergic agonists increase lung liquid clearance in anesthetized sheep. J Clin Invest 1987;79:335–343.
13 Campbell AR, Folkesson HG, Berthiaume Y, Gutkowska J, Suzuki S, Matthay MA: Alveolar epithelial fluid clearance persists in the presence of moderate left atrial hypertension in sheep. J Appl Physiol 1999;86:139–151.
14 Sakuma T, Okaniwa G, Nakada T, Nishimura T, Fujimura S, Matthay MA: Alveolar fluid clearance in the resected human lung. Am J Respir Crit Care Med 1994;150:305–310.
15 Sakuma T, Suzuki S, Usuda K, Handa M, Okaniwa G, Nakada T, Fujimura S, Matthay MA: Preservation of alveolar epithelial fluid transport mechanisms in rewarmed human lung after severe hypothermia. J Appl Physiol 1996;80:1681–1686.
16 Sakuma T, Folkesson HG, Suzuki S, Okaniwa G, Fujimura S, Matthay MA: Beta-adrenergic agonist stimulated alveolar fluid clearance in ex vivo human and rat lungs. Am J Respir Crit Care Med 1997;155:506–512.
17 Ware LB, Fang X, Wang Y, Sakuma T, Hall TS, Matthay MA: Selected contribution: Mechanisms that may stimulate the resolution of alveolar edema in the transplanted human lung. J Appl Physiol 2002;93:1869–1874.
18 Norlin A, Finley N, Abedinpour P, Folkesson HG: Alveolar liquid clearance in the anesthetized ventilated guinea pig. Am J Physiol 1998;274:L235–L243.
19 Sakuma T, Hida M, Nambu Y, Osanai K, Toga H, Takahashi K, Ohya N, Inoue M, Watanabe Y: Effects of hypoxia on alveolar fluid transport capacity in rat lungs. J Appl Physiol 2001;91:1766–1774.
20 Crandall ED, Matthay MA: Alveolar epithelial transport. Basic science to clinical medicine. Am J Respir Crit Care Med 2001;163:1021–1029.
21 Berg MM, Kim KJ, Lubman RL, Crandall ED: Hydrophilic solute transport across rat alveolar epithelium. J Appl Physiol 1989;66:2320–2327.
22 Folkesson HG, Matthay MA, Westrom BR, Kim KJ, Karlsson BW, Hastings RH: Alveolar epithelial clearance of protein. J Appl Physiol 1996;80:1431–1445.
23 Hastings RH, Grady M, Sakuma T, Matthay MA: Clearance of different-sized proteins from the alveolar space in humans and rabbits. J Appl Physiol 1992;73:1310–1316.

24 Kim KJ, Borok Z, Crandall ED: A useful in vitro model for transport studies of alveolar epithelial barrier. Pharm Res 2001;18:253–255.
25 American Heart Association: Section 6: Pharmacological II: Agents to optimize cardiac output and blood pressure. Circulation 2000; 102(suppl I):I-129–I-135.
26 Norlin A, Lu LN, Guggino SE, Matthay MA, Folkesson HG: Contribution of amiloride-insensitive pathways to alveolar fluid clearance in adult rats. J Appl Physiol 2001;90:1489–1496.
27 Nielsen VG, Duvall MD, Baird MS, Matalon S: cAMP activation of chloride and fluid secretion across the rabbit alveolar epithelium. Am J Physiol 1998;275:L1127–L1133.
28 Sakuma T, Tsukano C, Ishigaki M, Nambu Y, Osanai K, Toga H, Takahashi K, Ohya N, Kurihara T, Nishio M, Matthay MA: Lung deflation impairs alveolar epithelial fluid transport in ischemic rabbit and rat lungs. Transplantation 2000;69:1785–1793.
29 Sakuma T, Sagawa M, Hida M, Nambu Y, Osanai K, Toga H, Takahashi K, Ohya N, Matthay MA: Time-dependent effect of pneumonectomy on alveolar epithelial fluid clearance in rat lungs. J Thorac Cardiovasc Surg 2002;124: 668–674.
30 Matthay MA, Folkesson HG, Verkman AS: Salt and water transport across alveolar and distal airway epithelia in the adult lung. Am J Physiol 1996;270:L487–L503.
31 Naganobu K, Hasebe Y, Uchiyama Y, Hagio M, Ogawa H: A comparison of distilled water and normal saline as diluents for endobronchial administration of epinephrine in the dog. Anesth Analg 2000;91:317–321.
32 Saumon G, Martet G: Effect of metabolic inhibitors on Na^+ transport in isolated perfused rat lungs. Am J Respir Cell Mol Biol 1993;9: 157–165.
33 Wirtz HR, Dobbs LG: Calcium mobilization and exocytosis after one mechanical stretch of lung epithelial cells. Science 1990;250:1266–1269.
34 Tschumperlin DJ, Dai G, Maly IV, Kikuchi T, Laiho LH, McVittie AK, Haley KJ, Lilly CM, So PT, Lauffenburger DA, Kamm RD, Drazen JM: Mechanotransduction through growth-factor shedding into the extracellular space. Nature 2004;429:83–86.
35 Correa-Meyer E, Pesce L, Guerrero C, Sznajder JI: Cyclic stretch activates ERK1/2 via G proteins and EGFR in alveolar epithelial cells. Am J Physiol Lung Cell Mol Physiol 2002;282: L883–L891.
36 Kemp PJ, Borok Z, Kim KJ, Lubman RL, Danto SI, Crandall ED: Epidermal growth factor regulation in adult rat alveolar type II cells of amiloride-sensitive cation channels. Am J Physiol 1999;277:C1058–C1065.
37 Matalon S: Mechanisms and regulation of ion transport in adult mammalian alveolar type II pneumocytes. Am J Physiol 1991;261:C727–C738.
38 Matalon S, Bridges RJ, Benos DJ: Amiloride-inhibitable Na^+ conductive pathways in alveolar type II pneumocytes. Am J Physiol 1991; 260:L90–L96.
39 Effros RM, Mason GR, Hukkanen J, Silverman P: New evidence for active sodium transport from fluid-filled rat lungs. J Appl Physiol 1989;66:906–919.
40 Van Scott MR, Davis CW, Boucher RC: Na^+ and Cl^- transport across rabbit nonciliated bronchiolar epithelial (Clara) cells. Am J Physiol 1989;256:C893–C901.

Short Communication

Japanese Journal of Physiology Vol. **55**, 143–148, 2005

Effects of Norepinephrine and Histamine on Vascular Resistance in Isolated Perfused Mouse Liver

Toshishige SHIBAMOTO, Sen CUI, Zonghai RUAN, and Yasutaka KURATA

Department of Physiology, Kanazawa Medical University, Uchinada Ishikawa, 920-0293 Japan

Abstract: Mice have frequently been used for a variety of physiological studies because of the development of genetic engineering. However, the characteristics of hepatic vessels such as the vascular resistance distribution and the reactivity to various vasoconstrictors are not known in mice. We therefore determined the basal levels of segmental vascular resistances and the effects of histamine and norepinephrine on the vascular resistance distribution of mice. The liver of male non-inbred ddY mice was excised and perfused via the portal vein with 5% bovine albumin-Krebs solution at a constant flow rate. The sinusoidal pressure was measured by the double occlusion pressure and used to determine the presinusoidal (R_{pre}) and postsinusoidal (R_{post}) resistances. The basal R_{post} comprised 53 ± 1% of the total hepatic vascular resistance. The norepinephrine and histamine increased R_{pre} in a greater magnitude than R_{post} with liver weight loss. However, the response to histamine was weaker than that to norepinephrine. Moreover, histamine-induced vasoconstriction showed tachyphylaxis. In conclusion, the presinusoidal and postsinusoidal resistances of mouse livers were similar in magnitude. The presinusoidal vessels predominantly contract in response to norepinephrine and histamine in mouse livers. [The Japanese Journal of Physiology 55: 143–148, 2005]

Key words: double occlusion pressure, isolated perfused mouse liver, sinusoidal pressure.

The passive blood mobilization to and from the liver, which influences the venous return to the heart, is critically dependent on the location and magnitude of intrahepatic vascular resistances in relation to the compliances [1]. There are species differences in the distribution of the hepatic vascular resistance. In canine livers, the presinusoidal resistance comprises approximately 50% of the total liver vascular resistance [2], but it comprises 56% and 59% in guinea pig [3] and rabbit livers [4–6], respectively, and more than 60% in rat livers [7, 8]. However, the basal hepatic vascular resistance distribution of mouse livers is not known, although mouse has been frequently used in physiological studies because of the development of genetic engineering.

Species differences are also found in the primary site of hepatic vasoconstriction. By using the vascular occlusion methods for measurement of the hepatic sinusoidal pressure [2, 9], we have recently shown that the hepatic longitudinal vascular responsiveness to vasoactive substances differs among different species, such as dogs, rabbits, rats, and guinea pigs [4–6, 9–11]. Histamine predominantly contracts the postsinusoidal veins with resultant hepatic congestion in dogs [9, 10] and guinea pigs [11], but this substance constricts presinusoidal vessels in rabbits [4]. In rat livers, histamine did not contract or dilate hepatic vessels [11]. On the other hand, norepinephrine predominantly contracts the presinusoidal veins over the postsinusoidal veins in dogs, rabbits, rats, and guinea pigs [4, 7, 9, 11]. However, the effects of these vasoconstrictors have not been determined on hepatic vascular resistance distribution in mice. Furthermore, norepinephrine is released during the critical circumstances of sympathoexcitation, such as hemorrhagic shock, but histamine could be released during liver transplantation and systemic anaphylaxis and thereby cause a disturbance of hepatic circulation [12].

Therefore we have herein established the isolated perfused mouse liver preparation, which permits the measurement of hepatic vascular pressures, including sinusoidal pressure and liver weight. We determined the basal hepatic vascular resistance distribution and the effects of histamine and norepinephrine on segmental vascular resistances in mouse livers.

Received on Feb 14, 2005; accepted on Apr 28, 2005; released online on Apr 29, 2005; DOI: 10.2170/jjphysiol.S642
Correspondence should be addressed to: Toshishige Shibamoto, Department of Physiology, Kanazawa Medical University, Uchinada Ishikawa 920-0293, Japan. Phone: +81-76-218-8104, Fax: +81-76-286-8010, E-mail: shibamo@kanazawa-med.ac.jp

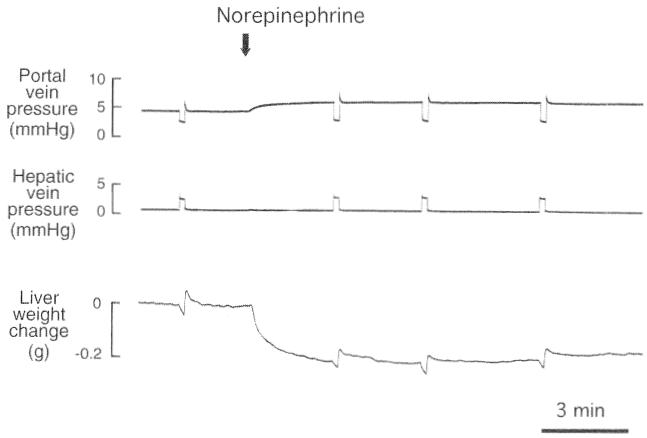

Fig. 1. A representative recording of the response to norepinephrine at 10 μM.

Methods

The study protocol was approved by the Animal Research Committee of Kanazawa Medical University in Uchinada, Japan. Thirty-two male specific-pathogen-free outbred ddY mice (43 ± 0.5 [SE] g; SLC Co., Hamamatsu, Japan), one of the most popular mouse strains in Japan, were anesthetized with pentobarbital sodium (50 mg/kg, ip) and mechanically ventilated with room air. After laparotomy, the bile duct was cut and the hepatic artery was ligated. At 5 min after an injection of heparin (500 mU/g) into the intraabdominal inferior vena cava (IVC), the IVC above the renal veins was ligated, and the portal vein was cannulated with a stainless cannula (OD 1.2 mm, ID 1.0 mm) for portal perfusion. After thoracotomy, the supradiaphragmatic IVC was cannulated through a right atrial incision with the same size stainless cannula, and portal perfusion was then begun with 5% albumin-Krebs buffer. The liver was rapidly excised, then suspended from an electric balance and weighed.

The basic method for liver perfusion was described previously [4], but each apparatus was the minimum size. The liver was perfused at a constant flow rate in a recirculating manner via the portal vein with the albumin-Krebs buffer that was pumped by a Masterflex pump from the venous reservoir through a heat exchanger (37°C). The recirculating blood volume was 30 ml. The height of the reservoir and the perfusate flow rate could be adjusted independently to maintain the portal and hepatic venous pressures at any desired level. The perfusate was oxygenated in the reservoir by continuous bubbling with 95% O_2 and 5% CO_2. We measured the portal venous (P_{pv}) and the hepatic venous (P_{hv}) pressures with pressure transducers connected to the corresponding side arm with the reference points at the hepatic hilus. To measure the double occlusion pressure (P_{do}), we placed two solenoid valves around the perfusion tubes upstream from the P_{pv} sidearm cannula and downstream from the P_{hv} sidearm cannula [4]. The perfusate flow rate (Q) was measured manually by collecting outflow perfusate for 1 min just before the baseline measurement. The same measurement was done at the end of the experiment to confirm the constancy of perfusate flow during the experimental period. The hepatic vascular pressures and liver weight (Wt) were monitored continuously and displayed through a thermal physiograph.

Hepatic hemodynamic parameters were observed for at least 20 min after the start of perfusion, during which an isogravimetric (no liver weight gain or loss) state was reached. After the baseline measurements, the perfused livers were challenged with either histamine (Sigma) or norepinephrine (Bitartrate salt, Sigma). They were injected as a bolus into the reservoir to attain the final perfusate concentration of 0.001–30 μM and 1–1,000 μM, respectively. The volume of each injected agent was adjusted to less than 0.5 ml.

The hepatic sinusoidal pressure was measured by the double occlusion method [2]. The inflow and outflow lines were simultaneously and instantaneously occluded with the solenoid valves, after which P_{pv} and P_{hv} rapidly equilibrated to a similar or identical pressure, which was P_{do}. In each experimental group, P_{do} was measured at baseline and maximal vasoconstriction.

The total portal-hepatic venous (R_t), presinusoidal (R_{pre}), and postsinusoidal (R_{post}) resistances were calculated as follows:

$$R_t = (P_{pv} - P_{hv})/Q \quad (1)$$

$$R_{pre} = (P_{pv} - P_{do})/Q \quad (2)$$

$$R_{post} = (P_{do} - P_{hv})/Q \quad (3)$$

All results are expressed as the mean ± SEM. The comparisons were made with Student's *t*-tests. A p value of less than 0.05 was considered significant.

Results

The final wet liver weight measured immediately after experiments was 1.91 ± 0.02 g. The P_{do} at the baseline states of 32 perfused mouse livers was 2.3 ± 0.1 mmHg, with P_{pv} 4.0 ± 0.1 mmHg and P_{hv} 0.5± 0.05 mmHg at Q 2.3 ± 0.05 ml/min/g liver wt. The calculated R_t was 1.55 ± 0.04 mmHg/ml/min/g liver wt. The segmental vascular resistances of R_{pre} and R_{post} were 0.74 ± 0.03 and 0.81 ± 0.02 mmHg/ml/min/g liver wt, respectively, and the R_{post}/R_t ratio was 0.53 ± 0.01. This indicates that 53% of the total portal-hepatic venous resistance of the isolated mouse livers exists in the postsinusoids.

Norepinephrine and histamine produced qualitatively the same responses: P_{pv} increased substantially, but

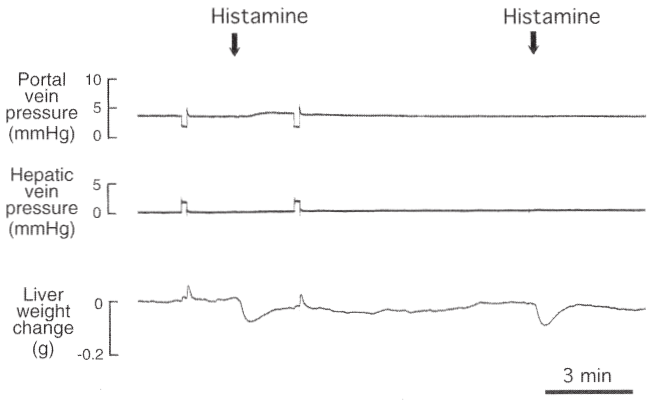

Fig. 2. Representative recordings of the responses to histamine at 1 mM. The second arrow indicates the injection of the same dose as the initial injection.

P_{do} either did not change or increased only minimally, with liver weight loss, as shown in Figs. 1 and 2. In livers treated with either norepinephrine or histamine, the P_{pv}-to-P_{do} gradient increased in a greater magnitude than the P_{do}-to-P_{hv} gradient, a finding indicating that R_{pre} was predominantly increased over R_{post}. However, the response to histamine was weaker than that to norepinephrine. Moreover, histamine-induced vasoconstriction showed tachyphylaxis (Fig. 2). Figure 3 shows the peak levels in R_{pre}, R_{post}, R_t, and Wt changes after injections of norepinephrine and histamine. R_t increased in a dose-dependent manner at 0.001–30 μM norepinephrine, reaching the maximum level of 151 ± 3% of baseline at 30 μM. This increase in R_t at 30 μM was mainly due to an increase in R_{pre} because the maximum levels of R_{pre} was 193 ± 3% of the baseline, and the corresponding levels of R_{post} was only 117 ± 3% of the baseline, as shown in Fig. 3. Histamine did not cause venoconstriction until the concentration increased to 100 μM, as shown in Fig. 3. Even at 1,000 μM histamine, R_{pre} inceased to only 145 ± 9% of the baseline, whereas R_{post} did not change significantly. Immediately after norepinephrine or histamine, the liver weight decreased and then gradually returned to the baseline. The maximal liver weight losses after injections of norepinephrine at 30 μM and histamine at 1,000 μM were approximately 0.15 and 0.03 g/g liver wt, respectively.

Discussion

There is a species difference in the distribution of segmental vascular resistances in the livers of animals, including dogs, rabbits, guinea pigs, and rats. We have recently shown by measuring the sinusoidal pressure, using the triple vascular occlusion method [9] and the double occlusion method [2], in isolated canine livers that R_{post} comprises approximately half of R_t. In contrast, R_{pre} in the other animals is greater in magnitude than R_{post}. Actually, we subsequently demonstrated that 59% of R_t exists in presinusoidal vessels in isolated rabbit livers [4, 5]. This agrees with the study of Maass-Moreno and Rothe [13], who reported that in intact rabbit livers the pressure gradient from the hepatic sinusoids averaged 59% of the total P_{pv} to the abdominal vena caval pressure gradient. Similar segmental vascular resistance distribution was found in guinea pig livers, in which R_{pre} comprises 61% of R_t [3, 11]. The rat livers show more marked predominance of R_{pre} over R_{post}; R_{pre} is 69% of R_t [11]. In the present study, for the first time we reported that the basal vascular resistance distribution of mouse livers was similar to that of canine livers because R_{pre} comprises 47% of R_t.

Species differences are also found in the hepatic vascular responsiveness to vasoactive substances. With respect to responses to histamine, this substance predominantly contracts the postsinusoidal vessels in dogs [9, 10, 14, 15] and guinea pigs [11]. On the other hand, in rabbit livers, histamine selectively increases R_{pre} in isolated-perfused liver [4], and this vasoactive amine also significantly increases R_{post} in in vivo preparations [19]. In contrast, histamine did not contract the hepatic vessels in rat livers [11, 16–18]. In the present study we showed that histamine selectively contracts the presinusoidal vessels of mouse livers, a finding similar to the results of studies on rabbit livers. The difference in the vasoconstrictive site for histamine might be ascribed, at least in part, to the different distribution of functionally active receptors between the presinusoidal vessels and the hepatic veins. The absence of vasoconstrictive responses to histamine in rat livers may be due to a lack of functional histamine receptors in rat hepatic vascular smooth muscles.

In the present study, the concentration of histamine required to produce significant hepatic vasoconstriction was 100 μM. The responsiveness of mouse hepatic vessels to histamine seems to be much weaker than to norepinephrine because the lower concentration of 0.1 μM norepinephrine can induce significant hepatic vasoconstriction, as shown in Fig. 3. Furthermore, 1,000 μM histamine increased R_t only to 1.2-fold baseline, whereas the 100 times lower concentration of 10 μM norepinephrine increased R_t to 1.4-fold baseline. A similar result was observed in isolated rabbit liver [4].

In contrast to histamine, norepinephrine predominantly contracts presinusoidal vessels over postsinusoidal vessels in dogs [7, 9], rabbits [4, 19], guinea pigs [11], and rats [11]. Actually, Rothe and colleagues, using the micropipette servonull pressure measurement technique, have recently demonstrated that the increase in the presinusoidal resistance is greater than in the postsinusoidal resistance in dogs [7], rats [7], and rabbits [19] during norepinephrine infusion. We added

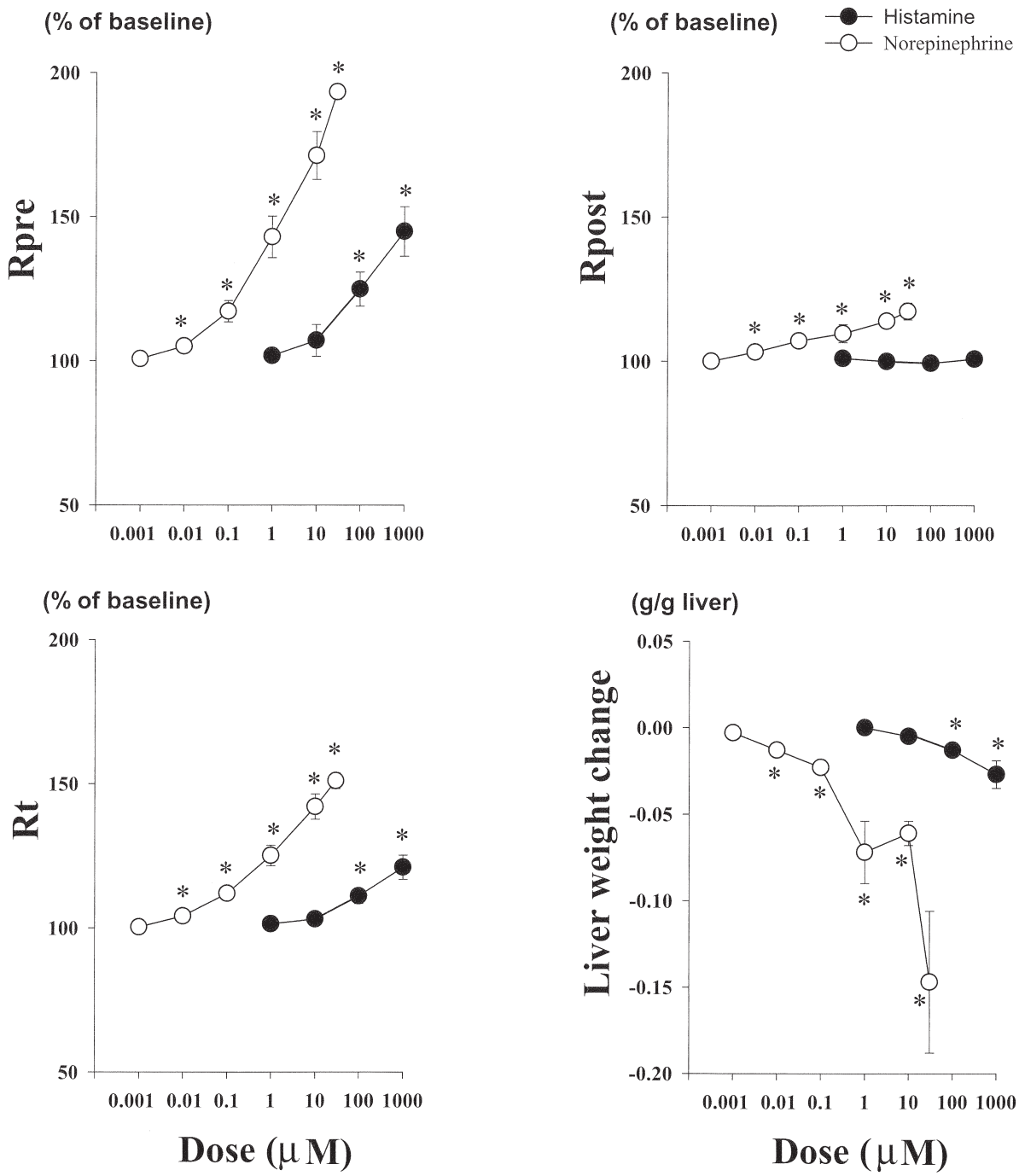

Fig. 3. The peak changes in the presinusoidal (R_{pre}) and postsinusoidal (R_{post}) resistances and total resistance (R_t) and the liver weight changes at 0.001–30 μM of norepinephrine (open circles) and at 1–1,000 μM of histamine (closed circles), as expressed by the percentage of the baseline in mouse livers. The values are given as mean ± SEM. n = 5–7. *P < 0.05 vs. the baseline.

new evidence that a similar response to norepinephrine was observed in isolated mouse livers. It is well known that norepinephrine causes a reduction in liver blood volume in cats [20], dogs [9, 21], rabbits [4, 19], guinea pigs [11], and rats [11]. In this respect, the present study showed that mouse livers also respond to norepinephrine with a reduction of liver weight, suggesting a decrease in liver blood volume. These findings suggest that norepinephrine, a mediator of the sympathetic nervous system, causes predominant presinusoidal constriction with a resultant decrease in liver blood volume beyond the species differences. The physiological significance of this finding is that the primitive response to life-threatening insults, which cause sympathoexcitation, may be similar among animals. In this respect, histamine, a mediator released from mast cells

in response to allergy or anaphylaxis, does not seem to be essential to life; therefore the hepatic responses may differ among animals.

In the present study, a decrease in *Wt* accompanied predominant presinusoidal vessel constriction, when norepinephrine or histamine was injected into mouse livers. The mechanism for this decrease cannot be currently clarified. However, it may be related to possible heterogeneous portal venule constriction. If heterogeneity existed in portal venule constriction among the hepatic lobules, that is, some vessels were closed and others open, the blood volume of sinusoids that was distal to the closed portal venules could be passively reduced because of a decrease in the distending pressure of the sinusoids. In contrast to this passive change in liver volume, another possibility exists that contractile elements exist in the walls of the hepatic sinusoids that may be stimulated by norepinephrine as well as endothelin [22–24]. Rothe and Maass-Moreno [24] infused norepinephrine into in vivo rabbit and found a decrease in liver volume, even though P_{pv} and hepatic venule pressure increased. This is clear proof of an active response and not a passive response to distending pressure.

As shown in Fig. 2, in response to the second bolus injection of histamine at 1 mM, hepatic venoconstriction was not observed, but the liver weight transiently decreased. The mechanism for this venoconstriction-independent decrease is unknown. We assumed that high osmolarity resulting from a bolus injection of 1 mM histamine might account for the decrease in liver weight: The hyperosmotic solution with 1 mM histamine might have caused osmosis and liver cell volume shrinkage, resulting in transient liver weight loss. Since the presence of structural pores of the sinusoidal endothelium enables free and rapid movement of drug and water molecules between the intravascular spaces and Disse's spaces, it is expected that an intravascular hyperosmolarity could easily cause osmosis at hepatocytes and at sinusoidal endothelial cells. Water derived from these cells might rapidly diffuse into the intravascular space through the endothelial pores and might be carried away extrahepatically via the blood stream. Indeed, we observed that a bolus injection of the solution with nonvasoactive sucrose at 1 mM, the volume and osmolarity of which are the same as those of the histamine solution, caused venoconstriction-independent liver weight loss in isolated perfused liver (data not shown).

There are limitations of the methods used in the present study. First, the livers were perfused via only the portal vein because of the technical difficulty to perfuse the hepatic artery. With the hepatic artery occluded, no clues were provided for the sensitivity of the hepatic arterioles to histamine and norepinephrine. Second, the livers were perfused with 5% bovine albumin-Krebs solution, but not with blood. There is a possibility that the oxygen sensitivity of the most metabolically active tissue may be limited. However, we confirmed previously that the bubbling with 95% oxygen of the albumin-Krebs perfusate produced the inflow perfusate PO_2, 300 mmHg [5]. We believe that the delivery of oxygen to the liver was adequate.

In conclusion, by measuring the hepatic sinusoidal pressure with the double occlusion method, we determined the basal vascular resistance distribution and the effects of histamine and norepinephrine on the segmental vascular resistances in isolated mouse livers perfused with blood-free albumin Krebs buffer. The presinusoidal and postsinusoidal resistances of mouse livers were similar in magnitude. In response to norepinephrine and histamine, presinusoidal vessels predominantly contract with a resultant decrease in hepatic vascular volume in mouse livers.

This work was supported by a Grant for Collaborative Research from Kanazawa Medical University (C2003-1, C2004-1, C2005-1) and a Grant-in-Aid for Scientific Research from the Ministry of Education, Culture, Sports, Sciences and Technology of Japan (No. 15591665).

REFERENCES

1. Maass-Moreno R and Rothe CF: Nonlinear resistances in hepatic microcirculation. Am J Physiol 269: H1922–H1930, 1995
2. Yamaguchi Y, Shibamoto T, Hayashi T, Saeki Y, and Tanaka S: Hepatic vascular response to anaphylaxis in isolated canine liver. Am J Physiol 267: R268–R274, 1994
3. Ruan Z, Shibamoto T, Shimo T, Tsuchida H, Koizumi T, and Nishio M: NO but not CO, attenuates anaphylaxis-induced postsinusoidal contraction and congestion in guinea pig liver. Am J Physiol Regul Integr Comp Physiol 286: R94–R100, 2004
4. Shibamoto T, Wang HG, Miyahara T, Tanaka S, Haniu H, and Koyama S: Presinusoidal vessels predominantly contract in response to norepinephrine, histamine, and KCl in rabbit liver. J Appl Physiol 87: 1404–1412, 1999
5. Wang HG, Shibamoto T, and Miyahara T: Endothelin-1 selectively contracts portal vein through ET_A- and ET_B-receptors in isolated rabbit liver. Am J Physiol 273: G1036–G1043, 1997
6. Wang HG, Shibamoto T, and Koyama S: The effect of platelet-activating factor on hepatic capillary pressure in isolated dog liver. Prostaglandins Leukot Essent Fatty Acids 57: 293–298, 1997
7. Bohlen HG, Maass-Moreno R, and Rothe CF: Hepatic venular pressures of rats, dogs, and rabbits. Am J Physiol 261: G539–G547, 1991
8. Ling YQ, Shibamoto T, Honda T, Kamikado C, Hironaka E, Hongo M, and Koyama S: Increased sinusoidal

pressure is associated with early liver weight gain in ischemia-reperfusion injury in isolated perfused rat liver. J Surg Res 88: 70–77, 2000
9. Shibamoto T, Wang HG, Tanaka S, and Koyama S: Hepatic capillary pressure is estimated using triple vascular occlusion method in isolated canine liver. Am J Physiol 271: R1130–R1141, 1996
10. Urayama H, Shibamoto T, Wang HG, and Koyama S: Thromboxane A_2 analogue contracts predominantly the hepatic veins in isolated canine liver. Prostaglandins 52: 483–495, 1996
11. Shibamoto T, Narushima M, Ling YQ, Shimo T, Tsuchida H, Kurata Y, and Ogura T: Different hepatic vascular response to noradrenaline and histamine between guinea pig and rat. Acta Physiol Scand 18: 255–263, 2004
12. Hansen CP, Man WK, Kirkegaad P, Jensen SL and Boesby S: Changes in plasma histamine during orthotopic liver transplantation in the pig. Agents Actions 23: 348–350, 1988
13. Maass-Moreno R and Rothe CF: Distribution of pressure gradients along hepatic vasculature. Am J Physiol 272: H2826–H2832, 1997
14. Lautt WW and Legare DJ: Effect of histamine, norepinephrine, and nerves on vascular pressures in dog liver. Am J Physiol 252: G472–G478, 1987
15. Mafhouz M and Geumei A: Pharmacodynamic of intrahepatic circulation in shock. Surgery 61, 755–762, 1967
16. Noguchi Y and Plaa GL: Effect of acetylcholine, serotonin and histamine on the hemodynamics on the isolated perfused rat liver. Arch int Pharmacodyn 188: 312–319, 1977
17. Cohen ML and Wiley KS: Comparison of arteries with longitudinal and circular venous muscle from the rat. Am J Physiol 232: H131–H139, 1977
18. Hogestatt ED, Hammarstrom LE, Andersson KE, and Holmin T: Contractile effects of various vasoactive agents in small rat portal veins and hepatic arteries and the influence of sympathetic denervation on the noradrenaline response. Acta Physiol Scand 128: 309–315, 1986
19. Rothe CF and Maass-Moreno R: Hepatic venular resistance responses to norepinephrine, isoproterenol, adenosine, histamine, and ACh in rabbits. Am J Physiol 274: H777–H785, 1998
20. Greenway CV and Lautt WW: Effects of infusions of catecholamines, angiotensin, vasopressin and histamine on hepatic blood volume in the anesthetized cat. Br J Pharmacol 44: 177–184, 1972
21. Bennett TD, Macanespie CL, and Rothe CF: Active hepatic capacitance responses to neural and humoral stimuli in dogs. Am J Physiol 242: H1000–H1009, 1982
22. Ito Y, Katori M, Majima M, and Kakita A: Constriction of mouse hepatic venules and sinusoids by endothelins through ETb receptor subtype. Int J Microcirc Clin Exp 16: 250–258, 1996
23. Kawada N, Tran-Thi T, Klein H, and Decker K: The contraction of hepatic stellate (Ito) cells stimulated with vasoactive substances. Possible involvement of endothelin 1 and nitric oxide in the regulation of the sinusoidal tonus. Eur J Biochem 213: 815–823, 1993
24. Rothe CF and Maass-Moreno R: Active and passive liver microvascular responses from angiotensin, endothelin, norepinephrine, and vasopressin. Am J Physiol 279: H1147–H1156, 2000

Am J Physiol Heart Circ Physiol 289: H1436–H1444, 2005.
First published May 27, 2005; doi:10.1152/ajpheart.00368.2005.

Hepatic venoconstriction is involved in anaphylactic hypotension in rats

Toshishige Shibamoto, Sen Cui, Zonghai Ruan, Wei Liu, Hiromichi Takano, and Yasutaka Kurata
Department of Physiology, Kanazawa Medical University, Uchinada Ishikawa 920-0293, Japan

Submitted 14 April 2005; accepted in final form 20 May 2005

Shibamoto, Toshishige, Sen Cui, Zonghai Ruan, Wei Liu, Hiromichi Takano, and Yasutaka Kurata. Hepatic venoconstriction is involved in anaphylactic hypotension in rats. *Am J Physiol Heart Circ Physiol* 289: H1436–H1444, 2005. First published May 27, 2005; doi:10.1152/ajpheart.00368.2005.—We determined the roles of liver and splanchnic vascular bed in anaphylactic hypotension in anesthetized rats and the effects of anaphylaxis on hepatic vascular resistances and liver weight in isolated perfused rat livers. In anesthetized rats sensitized with ovalbumin (1 mg), an intravenous injection of 0.6 mg ovalbumin caused not only a decrease in systemic arterial pressure from 120 ± 9 to 43 ± 10 mmHg but also an increase in portal venous pressure that persisted for 20 min after the antigen injection (the portal hypertension phase). The elimination of the splanchnic vascular beds, by the occlusions of the celiac and mesenteric arteries, combined with total hepatectomy attenuated anaphylactic hypotension during the portal hypertension phase. For the isolated perfused rat liver experiment, the livers derived from sensitized rats were hemoperfused via the portal vein at a constant flow. Using the double-occlusion technique to estimate the hepatic sinusoidal pressure, presinusoidal (R_{pre}) and postsinusoidal (R_{post}) resistances were calculated. An injection of antigen (0.015 mg) caused venoconstriction characterized by an almost selective increase in R_{pre} rather than R_{post} and liver weight loss. Taken together, these results suggest that liver and splanchnic vascular beds are involved in anaphylactic hypotension presumably because of anaphylactic presinusoidal contraction-induced portal hypertension, which induced splanchnic congestion resulting in a decrease in circulating blood volume and thus systemic arterial hypotension.

isolated perfused rat liver; anaphylaxis; hepatic circulation; portal hypertension; splanchnic congestion

ANAPHYLACTIC HYPOTENSION is primarily caused by alterations in the systemic circulation that decrease blood flow to the heart because left ventricular function is relatively well preserved during anaphylactic shock (4). Peripheral circulatory collapse is ascribed to hypovolemia, which results from a decrease in effective circulating blood volume. The latter could be because of vasodilation with the peripheral pooling and increased vascular permeability with a shift of intravascular fluid to the extravascular space (2).

In canine experimental models of anaphylactic shock, an increase in resistance to venous return is important in the pathogenesis of circulatory collapse (23); increased venous resistance decreases venous return with resultant decrease in stroke volume and systemic arterial pressure (P_{sa}). Indeed, eviscerated dogs did not develop anaphylactic shock (13). In addition, Enjeti et al. (5) reported that the severity of the anaphylactic shock could be decreased by occluding the descending aorta. In dogs, anaphylaxis-induced increase in venous resistance is partly caused by hepatic vasoconstriction, especially selective constriction of postsinusoidal hepatic veins in dogs (26). Indeed, anaphylaxis-induced hepatic venous constriction induces pooling of blood in liver itself, as well as in upstream splanchnic organs. However, in the rat, the roles of the splanchnic bed, and particularly the liver, are not known in the pathogenesis of anaphylactic hypotension, although, in the rat, portal venous pressure (P_{pv}) was increased during anaphylactic hypotension induced by ovalbumin (8). Thus the first purpose of the present study was to determine whether lesions of liver and splanchnic vascular bed contribute to anaphylactic hypotension in anesthetized rats. To resolve this question, P_{sa} changes were observed in sensitized rats with and without hepatic and splanchnic circulation after the antigen was intravenously administered.

In addition to canine livers (26), the guinea pig liver shows the anaphylactic response characterized by significant contraction of postsinusoidal vessel with resultant hepatic congestion (16). On the other hand, it is not known whether anaphylactic reaction in rats causes constriction of postsinusoidal hepatic veins, resulting in hepatic congestion, although anaphylactic venoconstriction is observed in isolated perfused livers of the sensitized rats (8). To clarify the anaphylactic disturbance of hepatic circulation, we herein established anaphylactic models of isolated portally perfused rat livers in which the sinusoidal pressure was measured by the double-occlusion method (20, 26). Thus the second purpose of the present study was to determine effects of anaphylaxis on hepatic vascular resistance distribution and liver weight in isolated perfused rat livers.

MATERIALS AND METHODS

Animals. Forty eight male Sprague-Dawley rats (Japan SLC, Shizuoka, Japan) weighing 372 ± 28 g were used in this study. Rats were maintained at 23°C under pathogen-free conditions on a 12:12-h dark-light cycle and allowed food and water ad libitum. The experiments conducted in the present study were approved by the Animal Research Committee of Kanazawa Medical University.

Sensitization. Rats were actively sensitized by the subcutaneous injection of an emulsion made by mixing equal volumes of complete Freund's adjuvant (0.5 ml) with 1 mg ovalbumin (grade V; Sigma) dissolved in physiological saline (0.5 ml). Nonsensitized rats were injected with complete Freund's adjuvant and ovalbumin-free saline. After injection (2 wk), the rats were used for the following in vivo or isolated perfused liver experiments.

In vivo experiment. After sensitization (2 wk), 35 rats were anesthetized with pentobarbital sodium (70 mg/kg ip) and placed on a thermostatically controlled heating pad (ATC-101B; Unique Medical) that maintained body temperature at 36–37°C throughout the experiment. The adequacy of anesthesia was monitored by the stability of blood pressure and respiration under control conditions and during a pinch of the hindpaw. Supplemental doses of anesthetic (10% of initial dose) were given as necessary. The left carotid artery was catheterized to measure P_{sa}. The right external jugular vein was

Address for reprint requests and other correspondence: T. Shibamoto, Dept. of Physiology, Kanazawa Medical Univ., Uchinada Ishikawa 920-0293, Japan (e-mail: shibamo@kanazawa-med.ac.jp).

The costs of publication of this article were defrayed in part by the payment of page charges. The article must therefore be hereby marked "*advertisement*" in accordance with 18 U.S.C. Section 1734 solely to indicate this fact.

catheterized, and the catheter tip was positioned at the confluence of the superior vena cava and the right atrium. This catheter was used for an intravenous injection of antigen and measurement of the central venous pressure (P_{cv}). Heart rate (HR) was measured by triggering the R wave of the electrocardiogram. The sensitized and nonsensitized animals were randomly divided into rats with gastrointestinal isolation and hepatectomy (GI-HptX) and intact rats. Thus the in vivo rats were randomly assigned to one of the following four groups: GI-HptX sensitized (n = 11), GI-HptX control (n = 7), intact sensitized (n = 10), and intact control (n = 7) groups. In the GI-HptX rats, through a 4-cm midline incision, ligation of the celiac artery and the mesenteric artery was followed by total hepatectomy, which consisted of resection of the median and left lateral lobe, the right lateral lobes, and the caudate lobes, as described by Gaub and Iversen (7). In the intact rats, after a midline incision, a catheter (0.47 mm ID, 0.67 mm OD) was inserted in the main portal vein without occlusion of the portal vein for continuous measurement of the P_{pv}. After closure of the abdomen, the baseline measurements were started.

The P_{sa}, P_{cv}, P_{pv}, and HR were continuously measured with pressure transducers (TP-400T; Nihon-Kohden) in the intact rats; P_{sa}, P_{cv}, and HR, but not P_{pv}, were measured in the GI-HptX rats. These pressures were continuously displayed on a thermal physiograph (RMP-6008; Nihon-Kohden). Outputs were also digitally recorded at 20 samples/s (PowerLab; ADInstruments). Hemodynamic parameters were observed for at least 20 min after surgery until a stable state was obtained. After the baseline measurements, 0.6 mg ovalbumin antigen was administered via the jugular vein catheter.

Isolated liver experiment. After sensitization (2 wk), these animals were anesthetized with pentobarbital sodium (70 mg/kg ip) and mechanically ventilated with room air. The basic methods for isolated perfused rat livers were described previously (18). In brief, a catheter was placed in the right carotid artery for later hemorrhage to obtain autologous blood for liver perfusion. After laparotomy, the hepatic artery was ligated, and the bile duct was cannulated with the polyethylene tube (0.5 mm ID, 0.8 mm OD). After intra-arterial heparinization (500 U/kg), 7–8 ml blood were withdrawn through the carotid arterial catheter. The intra-abdominal inferior vena cava (IVC) above the renal veins was ligated, and the portal vein was cannulated with a stainless cannula (1.3 mm ID, 2.1 mm OD) for portal perfusion. After thoracotomy, the supradiaphragmatic IVC was cannulated through a right atrium incision with a large-size stainless cannula (2.1 mm ID, 3.0 mm OD), and then portal perfusion was begun with the autologous blood diluted with 5% bovine albumin (Sigma-Aldrich, St. Louis, MO) in Krebs-Henseleit solution (in mM: 118 NaCl, 5.9 KCl, 1.2 $MgSO_4$, 2.5 $CaCl_2$, 1.2 NaH_2PO_4, 25.5 $NaHCO_3$, and 5.6 glucose) at Hct 8%. The liver was rapidly excised, suspended from an isometric transducer (TB-652T; Nihon-Kohden), and weighed continuously throughout the experimental period.

The livers were perfused at a constant flow rate in a recirculating manner via the portal vein with blood that was pumped using a Masterflex pump from the venous reservoir through a heat exchanger (37°C). The recirculating blood volume was 40 ml. The perfused blood was oxygenated in the venous reservoir by continuous bubbling with 95% O_2 and 5% CO_2. P_{pv} and hepatic venous pressure (P_{hv}) were measured with pressure transducers (TP-400T; Nihon-Kohden) attached by sidearm to the appropriate cannulas with the reference points at the hepatic hilus. To occlude inflow and outflow perfusion lines simultaneously for measurement of the double-occlusion pressure (P_{do}), two solenoid valves were placed in such a position that each sidearm cannula was between the corresponding solenoid valve and the liver. Portal blood flow rate (Q_{pv}) was measured with an electromagnetic flowmeter (MFV 1200; Nihon-Kohden), and the flow probe was positioned in the inflow line. Bile was collected drop by drop in a small tube suspended from the force transducer (SB-1T; Nihon-Kohden). One bile drop yielded 0.018 g, and the time between drops was measured for determination of the bile flow rate (11). The P_{pv}, P_{hv}, Q_{pv}, liver weight, and bile weight were monitored continuously and displayed through a thermal physiograph (RMP-6008; Nihon-Kohden). Outputs were also digitized by the analog-digital converter at a sampling rate of 100 Hz. These digitized values were displayed and recorded using a personal computer for later determination of P_{do}.

Hepatic hemodynamic parameters were observed for at least 20 min after the start of perfusion until an isogravimetric state (no weight gain or loss) was obtained by adjusting Q_{pv} and the height of the reservoir at a P_{hv} of 0–1 cmH_2O and at a Q_{pv} of 37 ± 6 $ml \cdot min^{-1} \cdot 10$ g liver wt^{-1}. After the baseline measurements, the perfused livers excised from the sensitized rats (anaphylaxis group, n = 7) and nonsensitized rats (control group, n = 6) were challenged with 0.015 mg ovalbumin injected in the reservoir.

The hepatic sinusoidal pressure was measured by the double-occlusion method (20, 26). Both the inflow and outflow lines were simultaneously and instantaneously occluded for 13 s using the solenoid valves, after which P_{pv} and P_{hv} rapidly equilibrated to a similar or identical pressure, which was P_{do}, using Liver software by Biomedical Science. In each experimental group, P_{do} was measured at baseline and at 3 and 6 min and then at 10-min intervals up to 30 min after antigen.

The total portal-hepatic venous (R_t) and presinusoidal (R_{pre}) and postsinusoidal (R_{post}) resistances were calculated as follows:

$$R_t = (P_{pv} - P_{hv})/Q_{pv} \quad (1)$$

$$R_{pre} = (P_{pv} - P_{do})/Q_{pv} \quad (2)$$

$$R_{post} = (P_{do} - P_{hv})/Q_{pv} \quad (3)$$

Statistics. All results are expressed as means ± SD. One-way ANOVA followed by Bonferroni's test was used to test for significant differences. Differences were considered as statistically significant at P values <0.05.

RESULTS

The response of the anesthetized rats to antigen. Figure 1*A* shows a representative example of the response to an intravenous injection of the ovalbumin antigen in an anesthetized intact rat sensitized with ovalbumin (the intact sensitized group). Figure 2 shows the summary data of time course changes in P_{pv} and P_{sa} of all four groups of anesthetized rats. After an antigen injection in the intact sensitized group, P_{sa} and P_{pv} simultaneously began to increase and decrease, respectively. P_{sa} rapidly decreased from the baseline of 120 ± 9 to 65 ± 11 mmHg at 1 min after the antigen and then continued to decrease progressively to the nadir of 43 ± 10 mmHg at 16 min, followed by a gradual recovery to 79 ± 18 mmHg at 60 min. P_{pv} increased from the baseline of 9.8 ± 0.9 cmH_2O to the peak of 24.3 ± 4.6 cmH_2O at 2.5 min after antigen and then gradually decreased to 10.9 ± 1.9 cmH_2O at 20 min. After that, P_{pv} remained at this level, which was not significantly different from the baseline. The postantigen period of up to 20 min during which P_{pv} remained elevated above the baseline (Fig. 2) was designated as the portal hypertension phase in the present study.

The surgical procedures of ligation of the celiac and the mesenteric arteries combined with total hepatectomy (GI-HptX) did not significantly affect the hemodynamic variables. Although P_{sa} transiently increased immediately after occlusion of the arteries, it returned to the pre-GI-HptX level during the baseline measurement after hepatectomy. Figure 1*B* shows a representative example in the GI-HptX sensitized group. The mean P_{sa} rapidly decreased from the baseline of 117 ± 12 to 80 ± 15 mmHg at 1 min. These levels were significantly

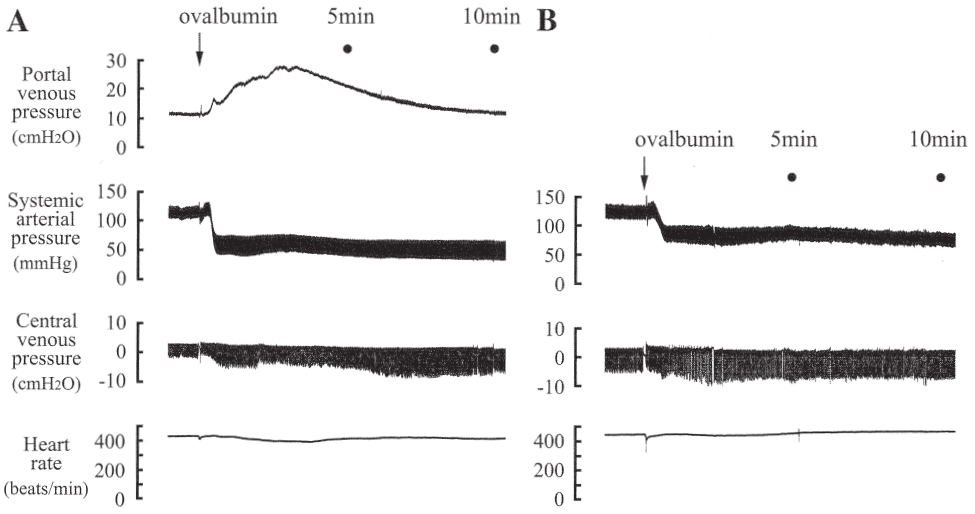

Fig. 1. Representative recording of the response to ovalbumin antigen (0.6 mg) in the intact sensitized group (*A*) and the gastrointestinal isolation and hepatectomy (GI-HptX) sensitized group (*B*). Portal venous pressure was not measured in the GI-HptX sensitized group because of no blood flow in the portal veins resulting from liver resection.

higher than the corresponding values of the intact sensitized group of 65 ± 11 mmHg. Thereafter, it did not further decrease but remained at this level throughout the experimental period, as shown in Fig. 2. Thus P_{sa} from 1 to 20 min after antigen in the GI-HptX sensitized group was significantly greater than that in the intact sensitized group. It should be noted that this period corresponded to the portal hypertension phase.

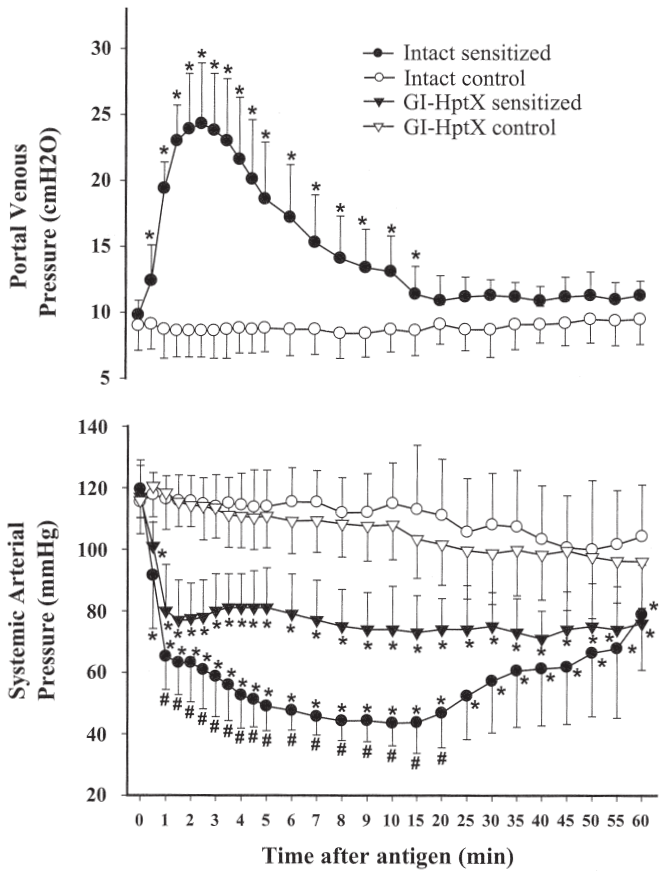

Fig. 2. Summary of changes in the systemic arterial pressure (P_{sa}) and portal venous pressure (P_{pv}) after antigen injection. Means ± SD; *$P < 0.05$ vs. baseline; #$P < 0.05$ vs. the intact sensitized group. P_{pv} was not measured in either the GI-HptX control or the GI-HptX sensitized group because the liver was excised.

At 10 min after antigen, P_{cv} in the intact sensitized group was significantly decreased from the baseline of 1.2 ± 0.3 to 0.1 ± 0.3 cmH_2O, whereas in the GI-HptX sensitized group, P_{cv} tended to decrease, but not significantly, from 0.8 ± 0.4 to 0.4 ± 0.8 cmH_2O. The changes in P_{cv} between the intact sensitized and GI-HptX sensitized groups at 10 min after antigen were significantly different (1.0 ± 0.3 vs. 0.4 ± 0.6 cmH_2O; $P < 0.05$). HR was not significantly changed after antigen in any groups studied, as shown in Fig. 1. Neither the P_{sa} nor the P_{pv} was significantly changed by the antigen in the control animals during the experimental periods of both the intact and GI-HptX groups (Fig. 2).

The response of the blood-perfused livers to antigen. The liver weight measured at the end of the perfusion experiment in the control and anaphylaxis groups was 9.3 ± 1.4 g ($n = 6$) and 9.0 ± 0.6 g ($n = 7$), respectively. The body weight in the control group was 0.288 ± 0.012 kg ($n = 6$), and that in the anaphylaxis group was 0.287 ± 0.021 kg ($n = 7$). There were no significant differences in the liver weight and body weight between the two groups. The liver weight-to-body weight ratio of all animals for the isolated perfusion study was 31.8 ± 3.1 g liver/kg body wt ($n = 13$).

An antigen injection caused hepatic venoconstriction, which was characterized by predominant presinusoidal constriction and liver weight loss, as shown in Fig. 3. Within 1 min after antigen, venoconstriction was evident by an increased P_{pv} that reached the peak value of 21.4 ± 4.9 cmH_2O from the baseline of 6.9 ± 0.1 cmH_2O (Fig. 4). The double-occlusion maneuver performed at 3 min after antigen revealed a P_{do} of 3.3 ± 0.3 cmH_2O that was significantly higher than that of the baseline of 2.3 ± 0.1 cmH_2O. Therefore, the P_{pv}-to-P_{do} gradient (in conjunction with the flow) defined the portal presinusoidal resistance (R_{pre}, *Eq. 2*). This resistance increased markedly from a baseline of 4.7 ± 0.2 to 18.1 ± 4.9 cmH_2O, whereas the P_{do}-to-P_{hv} gradient, the indicator of R_{post}, increased minimally, but significantly, from the baseline of 1.8 ± 0.1 to 2.8 ± 0.3 cmH_2O (Fig. 4). Thus R_{pre} increased by 250% the baseline from 0.13 ± 0.02 to 0.52 ± 0.19 $cmH_2O \cdot ml^{-1} \cdot min^{-1} \cdot 10$ g liver wt^{-1}, whereas R_{post} increased by only 67% from the baseline level of 0.05 ± 0.01 to 0.08 ± 0.01 $cmH_2O \cdot ml^{-1} \cdot min^{-1} \cdot 10$ g liver wt^{-1} (Fig. 4). This indicates that an injection of the antigen almost selectively increased R_{pre} rather than

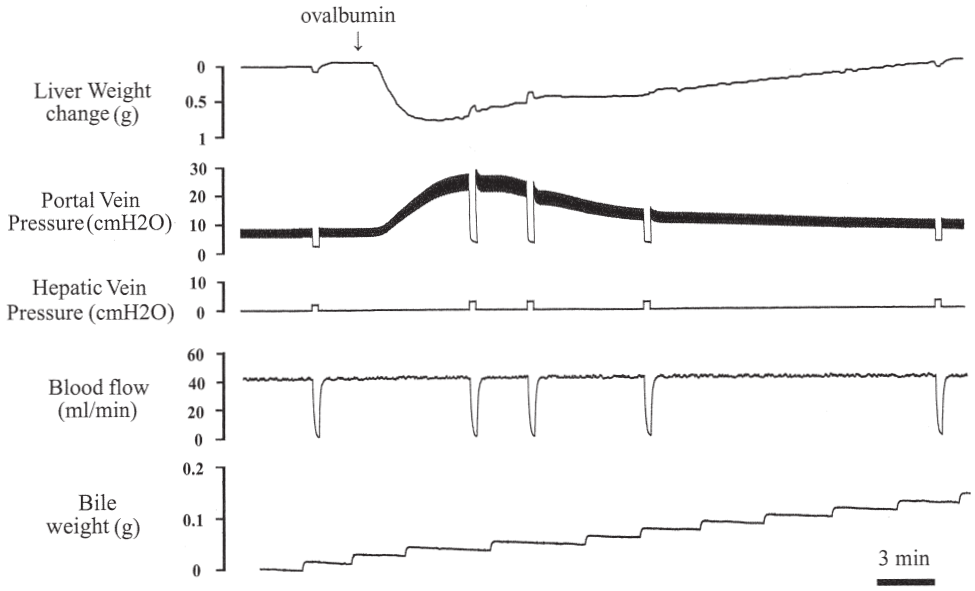

Fig. 3. Representative recording of the response to ovalbumin antigen (0.015 mg) in the blood-perfused liver isolated from a sensitized rat.

R_{post}, as reflected by a significant increase in the R_{pre}-to-R_t ratio from the baseline of 0.72 ± 0.01 to 0.86 ± 0.05. P_{pv}, and thus R_t, returned to the baseline at 30 min after antigen. Concomitant with venoconstriction, the liver weight showed a gradual decrease, reaching the nadir, −0.5 ± 0.4 g/10 g liver wt, at 3 min. Along with P_{pv}, the liver weight returned to the baseline at 30 min after antigen. The bile flow decreased to 67% of the baseline level of 0.01 ± 0.001 g·min^{-1}·10 g liver wt^{-1} during the maximal venoconstriction. In the control rat liver, no hemodynamic variables changed significantly after antigen (Fig. 4).

DISCUSSION

There are two major findings of the present study. The first finding (derived from the anesthetized rat experiments) is that elimination of the blood flow to the liver and splanchnic organs attenuated the antigen-induced decrease in P_{sa} during the portal hypertension phase. Another finding (derived from the isolated perfused rat liver experiments) is that hepatic anaphylactic venoconstriction is characterized by almost selective presinusoidal constriction and liver weight loss.

Hepatic anaphylactic postsinusoidal venoconstriction plays a crucial role in anaphylactic hypotension in dogs (6). In the present study, we have shown that immunological damage to the liver and splanchnic vascular beds also participated in the anaphylactic hypotension in rats. This is based on the finding that the elimination of hepatic and splanchnic circulation by ligation of the celiac and the mesenteric arteries combined with total hepatectomy attenuated the antigen-induced reduction of P_{sa} (Fig. 2). The mechanism for the beneficial effect of GI-

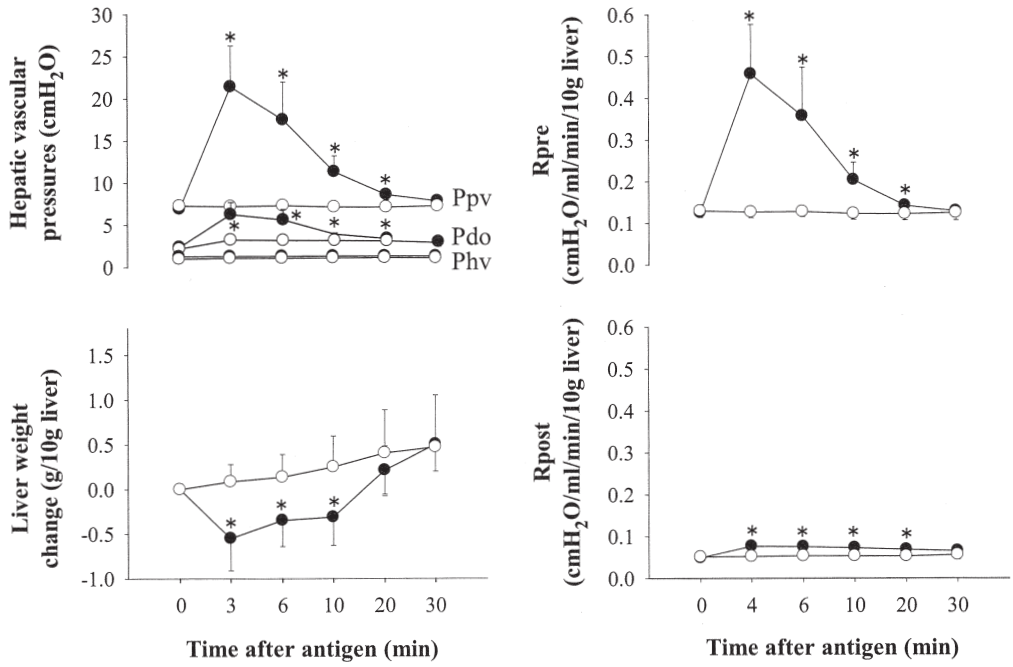

Fig. 4. Summary of changes in hepatic vascular pressures, liver weight changes, and pre (R_{pre})- and post (R_{post})-sinusoidal resistances after antigen injection in isolated perfused rat livers. Means ± SD; *P < 0.05 vs. baseline and the control group. P_{do}, double-occlusion pressure; P_{hv}, hepatic venous pressure; ●, anaphylaxis group; ○, control group.

HptX on the anaphylactic hypotension is not known. However, we assume that anaphylaxis-induced portal hypertension may account for the profound decrease in P_{sa} because the period during which attenuation of anaphylactic hypotension was observed corresponded to the portal hypertension phase during which the elevation of P_{pv} was sustained (Fig. 2). We speculate the following pathophysiological process: anaphylaxis causes hepatic venoconstriction, as observed in the isolated perfused sensitized liver, resulting in portal hypertension that then causes congestion of the upstream splanchnic organs, with resultant decrease in venous return and effective circulating blood volume, and finally augmentation of anaphylactic hypotension.

Another possible explanation may be related to the sources of mast cells that release vasoactive chemical mediators in response to antigens. Although mast cells occur throughout most tissues, they are more prevalent in gastrointestinal tract as well as the skin and lungs, the areas that come in contact with the external environment (14). A large number of mast cells in the gastrointestinal tract, including liver and intestines, may release substantial amounts of anaphylactic vasoactive substances in the systemic circulation. The elimination of these sources by the procedure of GI-HptX might have decreased the release of the anaphylaxis-related chemical mediators, resulting in a weak anaphylactic response.

Finally, there is a third possibility that anaphylaxis might be associated with significant splanchnic arterial vasodilation, as observed when platelet-activating factor (PAF), one of the mediators of anaphylaxis, was injected in the conscious rats (21). Splanchnic arterial dilation could contribute to both the reduced systemic pressure and increased P_{pv}. Moreover, splanchnic arterial ligation would attenuate these responses. However, there is currently no data that demonstrated splanchnic arterial vasodilation during anaphylactic hypotension in rats.

With respect to the mechanism for the early stage of anaphylactic hypotension in anesthetized rats, Bellou et al. (1) reported that histamine, serotonin, and nitric oxide are involved in the initial decrease in P_{sa} after ovalbumin antigen in the sensitized Brown Norway rats. Actually, either histamine or serotonin administered intravenously in the anesthetized rats causes a short-lasting decrease in P_{sa}, presumably because of dilatation of systemic arterioles (1). The initial arterial hypotension after antigen in the GI-HptX sensitized rats might be induced by the same mechanism proposed by Bellou et al. (1).

Anaphylactic hepatic venoconstriction, based on an increase in P_{pv}, was observed in rats (8), guinea pigs (16), and dogs (25, 26). However, a species difference between dog and guinea pig has been found in the hepatic vascular segments that preferentially contract during anaphylaxis: selective postsinusoidal constriction occurs in sensitized canine livers (26), whereas predominant presinusoidal but significant and substantial postsinusoidal constriction occurs in guinea pig livers (16). Using isolated, perfused, and sensitized rat livers, we have shown that anaphylactic hepatic venoconstriction in rats was different from that in dogs or guinea pigs and was characterized by a large presinusoidal contraction and only a minimal postsinusoidal contraction based on the double-occlusion method (20, 26) to estimate the sinusoidal pressure (P_{do}; see Figs. 3 and 4).

The mechanism for such a species-dependent response is not known. However, canine postsinusoidal hepatic veins anatomically contain smooth muscle sphincters in hepatic initial sublobular veins (4). Maass-Moreno and Rothe (12) also reported that major pressure gradients must lie upstream from the large (>2 mm) hepatic veins in dogs. Indeed, these postsinusoidal veins vigorously contract in response to various mediators of anaphylactic reaction, such as histamine (22), thromboxane A_2 (22), and PAF (24). In guinea pig livers, the anaphylactic presinusoidal constriction may be caused mainly by PAF, whereas the postsinusoidal constriction is caused by cysteinyl leukotrienes (19). Actually, PAF predominantly contracts presinusoidal vessels in guinea pig livers (17). However, effects of anaphylaxis-related vasoactive substances are not currently known on the segmental vascular resistances of rat livers. Further study is required to identify the chemical mediators responsible for the anaphylactic hepatic venoconstriction in rats.

In contrast to the liver weight gain response to the antigen of dogs (26) and guinea pigs (16), a liver weight loss was induced by marked anaphylactic presinusoidal constriction in isolated perfused rat livers. With the constant perfusion of the liver, the mechanism of the weight loss is unknown. This liver weight loss may be the result of hepatic vascular blood loss. Theoretically, the interstitial fluid volume loss also could contribute to a liver weight loss (10). Further study is required in this respect.

There are limitations of the present study. The first is related to the finding that the HR was high at baseline, as shown in Fig. 1, and that HR did not change in response to the marked drop in blood pressure during the anaphylactic shock. One of the reasons for high HR could be ascribed to the vagolytic property of pentobarbital sodium used in the present study (15). It is reported that pentobarbital decreases cardioinhibitory parasympathetic activity that dominates the control of HR (15). Indeed, in the pentobarbital-anesthetized rat study of others (3), the basal HR showed ~400 beats/min, as observed in the present study. With respect to the absence of the increase in HR in response to the antigen-induced marked drop in P_{sa}, that is, impairment of normal arterial baroreceptor reflex, Koyama et al. (9) demonstrated that systemic baroreceptor reflex control of HR and renal sympathetic nerve activity is reduced during anaphylactic hypotension in pentobarbital-anesthetized dogs. A similar impairment of arterial baroreceptor reflex might occur in the rat anaphylactic shock. Another shortcoming is the absence of hepatic arterial perfusion in the present isolated perfused livers. Hepatic arterial perfusion with normally oxygenated blood would improve the metabolic milieu of the liver. However, the perfusate was well oxygenated by bubbling with 95% O_2 and 5% CO_2, which provided perfusate oxygen tension of 290 ± 38 mmHg. Thus the isolated livers were perfused with hyperoxic blood, rather than hypoxic blood, and oxygenation was well done.

In summary, we determined the roles of splanchnic circulation in the anaphylactic hypotension in anesthetized rats sensitized with ovalbumin (1 mg). An intravenous injection of antigen (0.6 mg) caused not only a profound decrease in P_{sa} but also an increase in P_{pv}. The elimination of the splanchnic vascular beds, by the occlusions of the celiac and mesenteric arteries, combined with total hepatectomy attenuated anaphylactic hypotension during the portal hypertension phase. In addition, in isolated perfused sensitized rat livers, hepatic anaphylaxis caused almost selective presinusoidal constriction

and liver weight loss. Based on these findings, we conclude that liver and splanchnic vascular beds are partly involved in anaphylactic hypotension: anaphylactic presinusoidal contraction-induced portal hypertension and subsequent splanchnic congestion may cause a decrease in venous return and then hypotension.

ACKNOWLEDGMENTS

This study was supported by a Grant for Collaborative Research from Kanazawa Medical University (C2003–1, C2004–1, and C2005-1) and a Grant-in-Aid for Scientific Research from the Ministry of Education, Culture, Sports, Sciences, and Technology of Japan (No. 15591665).

REFERENCES

1. **Bellou A, Lambert H, Gillois P, Montemont C, Gerard P, Vauthier E, Sainte-Laudy J, Longrois D, Gueant JL, and Mallie JP.** Constitutive nitric oxide synthase inhibition combined with histamine and serotonin receptor blockade improves the initial ovalbumin-induced arterial hypotension but decreases the survival time in Brown Norway rats anaphylactic shock. *Shock* 19: 71–78, 2003.
2. **Brown AFT.** Anaphylactic shock: mechanism and treatment. *J Accid Emerg Med* 12: 89–100, 1995.
3. **Canyon SJ and Dobson GP.** Protection against ventricular arrhythmias and cardiac death using adenosine and lidocaine during regional ischemia in the in vivo rat. *Am J Physiol Heart Circ Physiol* 287: H1286–H1295, 2004.
4. **Ekataksin W and Kaneda K.** Liver microvascular architecture: an insight into the pathophysiology of portal hypertension. *Semin Liver Dis* 19: 359–382, 1999.
5. **Enjeti S, Bleecker ER, Smith PL, Rabson J, Permutt S, and Traystman RJ.** Hemodynamic mechanism in anaphylactic shock. *Circ Shock* 11: 297–309, 1983.
6. **Essex HE.** Anaphylactic and anaphylactoid reactions with special emphasis on the circulation. In: *Handbook of Physiology. Circulation*. Bethesda, MD: Am. Physiol. Soc., 1965, vol. III, chapt. 66, p. 2391–2408.
7. **Gaub J and Iversen J.** Rat liver regeneration after 90% partial hepatectomy. *Hepatology* 4: 902–904, 1984.
8. **Hines KL and Fisher RA.** Regulation of hepatic glycogenolysis and vasoconstriction during antigen-induced anaphylaxis. *Am J Physiol Gastrointest Liver Physiol* 262: G868–G877, 1992.
9. **Koyama S, Fujita T, Uematsu H, Shibamoto T, Aibiki M, and Kojima S.** Inhibitory effect of renal nerve activity during canine anaphylactic hypotension. *Am J Physiol Regul Integr Comp Physiol* 258: R383–R387, 1990.
10. **Lee JS, Lee LP, and Rothe CF.** Assessing microvascular volume change and filtration from venous hematocrit variation of canine liver and lung. *Ann Biomed Eng* 24: 25–36, 1996.
11. **Ling YQ, Shibamoto T, Honda T, Kamikado C, Hironaka E, Hongo M, and Koyama S.** Increased sinusoidal pressure is associated with early liver weight gain in ischemia-reperfusion injury in isolated perfused rat liver. *J Surg Res* 88: 70–77, 2000.
12. **Maass-Moreno R and Rothe CF.** Contribution of the large hepatic veins to postsinusoidal vascular resistance. *Am J Physiol Gastrointest Liver Physiol* 262: G14–G22, 1992.
13. **Manwaring WH.** The physiological mechanism of anaphylactic shock. *Bull Johns Hopkins Hosp* 21: 275–277, 1910.
14. **Metcalfe DD.** Mast cell mediators with emphasis on intestinal mast cells. *Ann Allergy* 53: 563–575, 1984.
15. **Murthy VS, Zagar ME, Vollmer RR, and Schmidt DH.** Pentobarbital-induced changes in vagal tone and reflex vagal activity in rabbits. *Eur J Pharmacol* 84: 41–50, 1982.
16. **Ruan Z, Shibamoto T, Shimo T, Tsuchida H, Koizumi T, and Nishio M.** NO, but not CO, attenuates anaphylaxis-induced postsinusoidal contraction and congestion in guinea pig liver. *Am J Physiol Regul Integr Comp Physiol* 286: R94–R100, 2004.
17. **Ruan Z, Shibamoto T, Shimo T, Koizumi T, Tsuchida H, Kurata Y, Ogura T, and Kubo K.** Effects of platelet-activating factor and thromboxane A_2 on isolated perfused-guinea pig liver. *Prostaglandins Other Lipid Mediat* 73: 73–85, 2004.
18. **Shibamoto T, Narushima M, Ling YQ, Shimo T, Tsuchida H, Kurata Y, and Ogura T.** Different hepatic vascular response to noradrenaline and histamine between guinea pig and rat. *Acta Physiol Scand* 180: 255–263, 2004.
19. **Shibamoto T and Ruan Z.** Chemical mediators responsible for hepatic vascular anaphylaxis in guinea pigs (Abstract). *Jpn J Physiol* 53: S167, 2003.
20. **Shibamoto T, Wang HG, Miyahara T, Tanaka S, Haniu H, and Koyama S.** Pre-sinusoidal vessels predominantly contract in response to norepinephrine, histamine, and KCl in rabbit liver. *J Appl Physiol* 87: 1404–1412, 1999.
21. **Siren AL and Feuerstein G.** Effects of PAF and BN 52021 on cardiac function and regional blood flow in conscious rats. *Am J Physiol Heart Circ Physiol* 257: H25–H32, 1989.
22. **Urayama H, Shibamoto T, Wang HG, and Koyama S.** Thromboxane A_2 analogue contracts predominantly the hepatic veins in isolated canine liver. *Prostaglandins* 52: 484–495, 1996.
23. **Wagner EM, Mitzner WA, and Bleecker ER.** Peripheral circulatory alterations in canine anaphylactic shock. *Am J Physiol Heart Circ Physiol* 251: H934–H940, 1986.
24. **Wang HG, Shibamoto T, and Koyama S.** Effect of platelet-activating factor on hepatic capillary pressure in isolated dog liver. *Prostaglandins Leukot Essent Fatty Acids* 57: 293–298, 1997.
25. **Weil R.** Studies in anaphylaxis. XXI. Anaphylaxis in dogs: a study of the liver in shock and peptone poisoning. *J Immunol* 2: 525–556, 1917.
26. **Yamaguchi Y, Shibamoto T, Hayashi T, Saeki Y, and Tanaka S.** Hepatic vascular response to anaphylaxis in isolated canine liver. *Am J Physiol Regul Integr Comp Physiol* 267: R268–R274, 1994.

１．研究課題名：肺癌の新しい機能的および形態的診断法の確立と分子標的治療法を指向した標的遺伝子の特定に関する研究（研究番号C2003-2）

２．キーワード：１）肺癌（lung cancer）
２）分子標的治療（molecular targeting therapy）
３）仮想気管支鏡（virtual bronchoscopy）
４）FDG PET（FDG PET）
５）furanonaphthoquinone誘導体（conductor of furanonaphthoquinone）

３．研究代表者：東　光太郎・医学部・教授・放射線診断治療学(放射線医学)
研究分担者：竹上　勉・総合医学研究所・教授・分子腫瘍学研究部門
上田善道・医学部・教授・病理病態学(病理学)
栂　博久・医学部・教授・呼吸機能治療学(呼吸器内科学)
佐川元保・医学部・助教授・呼吸機能治療学(呼吸器外科)
小林　健・金沢大学・医学部・講師・放射線科
松成一朗・先端医学薬学研究センター(主任研究員)
郭　建飛・中国医科大学・医学部・助手・放射線科

４．研究目的

平成１５年度の肺癌による死亡者は５６０００人と癌死の一位を占め、さらに増加傾向にある。肺癌の治療成績は不良で、再発をきたしやすい。肺癌の予後を改善するためには、新たな診断法および治療法の開発が不可欠である。本研究の目的は、以下の１）、２）、３）、４）により新たな診断法および治療法を開発し肺癌の予後改善に寄与することである。

１）非小細胞性肺癌の進展に関わる癌関連遺伝子群を明らかにし、新規の分子標的治療法を指向した標的分子・遺伝子を特定する。（担当：竹上、上田）

２）極細経の気管支鏡と multi detector CT を用いた仮想気管支鏡内視像を組み合わせることにより，末梢型微小肺癌の確実な組織採取法を確立する。（担当：佐川）

３）肺癌の生物学的特性を捉え、肺癌の新たな機能的画像診断法を開発・確立する。（担当：東、小林、松成、郭）

４）新しい肺癌治療薬としてfuranonaphthoquinone誘導体(J103)に注目し、furanonaphthoquinone誘導体(J103)の肺がん細胞に対する抗腫瘍効果を明らかにし、その機構を解明する。（担当：栂）

５．研究計画

１）非小細胞性肺癌の主として p53 関連遺伝子について遺伝子異常、発現変動を調べる。他方で肺腺癌細胞株A549における遺伝子発現の制御機構の解析を行う（担当：竹上）
laser-captured microdissection / real time RT-PCR法による肺癌新鮮凍結切片からのmRNA回収と定量的方法を確立する。また、TALPAT法を加えた微量 mRNA からの遺伝子発現プロファイリング法を確立する。さらに、非小細胞性肺癌のプログレッションに関わる遺伝子群のcDNAアレイ法による選別と組織レベルでの検証を行う。（担当：上田）

2）仮想気管支鏡の末梢微小陰影に関する画像再構成の至適条件を確立し，実際の症例で観察および組織採取を行う。仮想気管支鏡内視像に関して種々の画像再構成条件を試行し，末梢微小陰影に関する至適条件を検討する。（担当：佐川）

3）非小細胞性肺癌の増殖因子とくに血管新生因子（vascular endothelial growth factor、angiopoietin-2）の発現を測定し、FDG PETにより測定した糖代謝活性との関連を明らかにする。これにより、分子標的治療法とくに血管新生因子を標的とした阻害剤の適応を明らかにする。（担当：東、小林、松成、郭）

4）furanonaphthoquinone誘導体(J103)の肺がん細胞に対する抗腫瘍効果をin vitroの実験系で明らかにし、その機構を解明する。（担当：栂）

6．研究成果

1）p21 のプロモーター下流にルシフェラーゼ遺伝子を有するレポータープラスミド構築や人工mRNAを合成し、それらを細胞株A549に導入することによって、特異的な遺伝子発現制御の解析が可能になった。（担当：竹上）

cDNAアレイで選別した遺伝子発現を、real time RT-PCR法により検証できた。（担当：上田）

MMP-2, -3, -14, TIMP-1に関して、laser-captured microdissection / real time RT-PCRを応用し癌細胞・間質細胞別の遺伝子発現を解析した。（担当：上田）

肺腺癌の進展に関連する Aquaporin 遺伝子群の癌細胞特異的発現を laser-captured microdissection / real time RT-PCRにより明らかにした。（担当：上田）

2）仮想気管支鏡内視像に関して種々の画像再構成条件を試行し，末梢微小陰影に関する至適条件を検討した．実際の症例８例に行い，その結果を条件検討に反映させた（担当：佐川）。

3）肺癌の血管新生因子であるvascular endothelial growth factorやangiopoietin-2の発現の程度は肺癌の悪性度により異なり、特にangiopoietin-2の発現が強い肺癌は悪性度が高く予後が悪いこと明らかにした。また、FDG PETで測定した肺癌の糖代謝活性はangiopoietin-2の発現と相関していた。このことから、FDG PET によりangiopoietin-2を標的とした阻害薬の適応を決定できることが判明した。（担当：東、小林、松成、郭）

4）furanonaphthoquinone 誘導体(J103)はヒト肺腺癌由来培養細胞(A549)に対して抗腫瘍効果を示した。そのメカニズムは同細胞におけるFas(CD95/APO-1)受容体の発現増強によるものであり、Fas/Fas ligand システムを介するアポトーシスの増加があることを証明した。ヒト肺腺癌由来細胞(A549, LCSC#1)において、抗腫瘍薬エトポシドに抗生薬クラリスロマイシンを併用するとエトポシドの抗腫瘍効果は増強した。この作用はin vivoマウス腺癌でも同様に認められた。この効果はアポトーシス誘導の増加を伴っており、アポトーシス抑制関連のチトクロームc下流のXIAP抑制によることが示唆された。A549に分子標的治療薬であるepidermal growth factor receptor（EGFR）阻害薬を投与すると量依存性に腫瘍増殖抑制作用を示したが、同時にIL-8分泌が増加し、IL-8 mRNA発現も増強した。ステロイドはこのIL-8分泌を完全に抑制した。以上の薬剤は腫瘍免疫療法の新しい分野を切り開く可能性をもっていると考えられ、今後、作用メカニズムをさらに明らかにすることにより、臨床的応用が期待できる。（担当：栂）

7．研究の考察・反省

平成１５年度の成果として、まず細胞株A549を用いてp53関連遺伝子となるp21遺伝子発現へ

の影響を調べるアッセイ系を確立した。また、laser-microdissection / real time RT-PCR 法による浸潤部癌細胞と反応性間質細胞別の遺伝子発現解析法を確立した。これらは肺癌の進展に関わる癌関連遺伝子群の今後の解析に不可欠である。今後、これらの方法を用い数多くの癌関連遺伝子群を解析する予定である。

また、極細経の気管支鏡と multi detector CT を用いた仮想気管支鏡内視像を組み合わせることにより，一般的には困難とされる末梢型微小肺癌の組織採取が可能であることが今回明らかとなり、この方法が末梢型微小肺癌の診断能を向上させる可能性が示唆された。しかし症例数が少なく、今後さらに症例を増やし検討する必要がある。

肺癌の血管新生因子である angiopoietin-2 は肺癌の悪性度と強い関連があり、悪性度の高い肺癌の治療には angiopoietin-2 を標的とした分子標的治療が有望であることが示唆された。また、angiopoietin-2 の発現は肺癌の糖代謝とも相関があり、FDG PET 画像により angiopoietin-2 の発現を非侵襲的に評価できることも示唆された。しかし今回は angiopoietin-2 発現はタンパクレベルのみでの評価であり mRNA レベルでの評価が必要である。

さらに、furanonaphthoquinone 誘導体(JI03)の肺がん細胞に対する抗腫瘍効果が in vitro の実験系で明らかとなり、新しい肺癌治療薬として furanonaphthoquinone 誘導体(JI03)が有望であることが示唆された。しかし今回は in vitro のみの実験であり、動物実験での評価が必要である。今後作用メカニズムをさらに明らかにすることにより、臨床的応用が期待できる。

８．研 究 発 表

Higashi K, Ueda Y, Matsunari I, Kodama Y, Ikeda R, Miura K, Taki S, Higuchi T, Tonami H, Yamamoto I. ^{11}C-Acetate PET Imaging of Lung Cancer:Comparison with ^{18}F-FDG PET and ^{99m}Tc-MIBI SPET, Eur J Nucl Med Imaging 2004; 31: 13-21. (MLDB)

Guo J, Higashi K, Yokota H, Nagao Y, Ueda Y, Kodama Y, Oguchi M, Taki S,Tonami H, Yamamoto I. In vitro proton magnetic resonance spectroscopic lactate and choline measurements, F-18 FDG uptake, and prognosis in patients with lung adenocarcinoma. J Nucl Med 2004; 45: 1334-1339. (MLDB)

Higashi K, Ito K, Hiramatsu Y, Ishikawa T, Sakuma T, Matsunari I, Kuga G, Miura K, Higuchi T, Tonami H, Yamamoto I.^{18}F-FDG uptake by primary tumor as a predictor of intratumoral lymphatic vessel invasion and lymph node involvement in non-small cell lung cancer: analysis of a multicenter study, J Nucl Med 2005; 46: 267-273. (MLDB)

佐川元保，東光太郎，他，　すりガラス状陰影肺癌に対する仮想気管支鏡と極細径気管支鏡を用いたCTガイド下肺生検，　胸部外科　2004; 57: 1121-1125.

東　光太郎、松成一朗、上田善道、佐川元保、栂　博久、竹上　勉. FDG PETによる肺癌の診断と治療法の選択、日本老年医学会雑誌 2005; 42: 37-39.

^{11}C-acetate PET imaging of lung cancer: comparison with ^{18}F-FDG PET and ^{99m}Tc-MIBI SPET

Kotaro Higashi[1], Yoshimichi Ueda[2], Ichiro Matsunari[5], Yuko Kodama[1], Ryosuke Ikeda[3], Katsuyuki Miura[4], Suzuka Taki[1], Takahiro Higuchi[6], Hisao Tonami[1], Itaru Yamamoto[1]

[1] Department of Radiology, Kanazawa Medical University, Uchinada, Kahokugun, Ishikawa, Japan
[2] Department of Pathology, Kanazawa Medical University, Ishikawa, Japan
[3] Department of Urology, Kanazawa Medical University, Ishikawa, Japan
[4] Department of Public Health, Kanazawa Medical University, Ishikawa, Japan
[5] The Medical and Pharmacological Research Center Foundation, Hakui, Ishikawa, Japan
[6] Kanazawa Cardiovascular Hospital, Kanazawa, Ishikawa, Japan

Received: 13 June 2003 / Accepted: 4 August 2003 / Published online: 22 October 2003

Abstract. Recently carbon-11 acetate (AC) positron emission tomography (PET) has been reported to be of clinical value for the diagnosis of cancer that is negative on fluorine-18 fluorodeoxyglucoce (FDG) PET. We investigated the uptake of AC in lung cancer to determine whether this tracer is of potential value for tumour detection and characterisation, and to compare AC PET imaging with FDG PET and technetium-99m sestamibi (MIBI) single-photon emission tomography (SPET). Twenty-three patients with 25 lung cancers underwent AC and FDG PET. Twenty of 23 patients were also investigated with MIBI SPET. Dynamic images were acquired for 26 min after the injection of 555 MBq of AC. Standardised uptake values (SUVs) and/or tumour to non-tumour activity ratios (T/N) for each tumour were investigated at 10–20 min after AC administration, 40–60 min after administration of 185 MBq FDG and 15–45 min after administration of 555 MBq MIBI. Twenty lung cancers were resected surgically, and the degree of tracer uptake in the primary lesion was correlated with histopathological features (cell dedifferentiation and aggressiveness) and prognosis. Rapid uptake of AC followed by extremely slow clearance was observed. For the purpose of tumour identification, AC PET was inferior to FDG PET in 8 of 25 (32%) lung cancers, and the T/N of AC was lower than that of FDG. However, AC PET was superior to FDG PET in the identification of a slow-growing tumour (bronchiolo-alveolar carcinoma). There was a positive correlation between AC uptake (T/N) and MIBI uptake (T/N) (r=0.799, P<0.0001). A positive correlation was not observed between either AC or MIBI uptake and the degree of cell dedifferentiation in lung adenocarcinomas, whereas FDG uptake did correlate with the degree of cell dedifferentiation. In lung adenocarcinoma, there was a weak correlation between aggressiveness and FDG uptake, but no correlation was evident for AC and MIBI. In addition, a positive correlation was not observed between AC or MIBI uptake and postoperative recurrence in lung adenocarcinoma, whereas FDG uptake did correlate with postoperative recurrence. Thus, the greater the FDG uptake, the higher the malignant grade. In conclusion, for the purpose of tumour identification, AC PET was inferior to FDG PET but superior to MIBI SPET. Neither AC nor MIBI uptake reflects the malignant grade in lung adenocarcinoma, whereas FDG uptake does. AC PET is less diagnostically informative than FDG PET in patients with lung cancer. However, AC PET may play a complementary role in the identification of low-grade malignancies that are not FDG avid.

Keywords: Lung cancer – ^{11}C-acetate PET – ^{18}F-FDG PET – ^{99m}Tc-sestamibi SPET

Eur J Nucl Med Mol Imaging (2004) 31:13–21
DOI 10.1007/s00259-003-1326-7

Kotaro Higashi (✉)
Department of Radiology, Kanazawa Medical University,
1-1 Daigaku, 920-0293 Uchinada, Kahokugun, Ishikawa, Japan
e-mail: h550208@kanazawa-med.ac.jp
Tel.: +81-76-2862211, Fax: +81-76-2868096

Introduction

In tumour imaging using fluorine-18 fluorodeoxyglucose (FDG) positron emission tomography (PET), FDG is avidly taken up by tumour cells because cancer tissue consumes a large amount of glucose as an energy source [1]. FDG uptake has been found to reflect cell dedifferentiation [2, 3], proliferative potential [4], aggressiveness [5] and prognosis [6] in patients with lung cancer. Unfortu-

nately, some low-grade lung malignancies, such as bronchiolo-alveolar carcinomas [3] and carcinoid tumours [7], may not be reliably imaged using FDG PET. The poor performance of PET using FDG in this context is likely related to the low glucose metabolic rate of these relatively slow-growing tumours. The limitations of FDG warrant the development of better imaging radiopharmaceuticals.

Increased technetium-99m sestamibi (MIBI) concentration in lung tumours has been supported by several clinical studies [8, 9, 10]. Experimental observations have shown that the in vivo distribution of MIBI not a simple function of blood flow but rather represents a metabolic function. In particular, cellular uptake of MIBI is mainly related to its lipophilicity and membrane potentials, and MIBI is subsequently taken up into mitochondria [11, 12]. A significant advantage of MIBI as a tumour-seeking agent is its labelling with ^{99m}Tc, which renders it more suitable for radionuclide imaging compared with previously used tracers such as gallium-67 and thallium-201 [13].

Recently, carbon-11 acetate (AC) has been reported to show high uptake in tumour tissue [14, 15, 16, 17, 18, 19, 20, 21, 22]. Shreve et al. [15] reported that renal carcinomas demonstrate similar uptake of AC to normal and diseased non-neoplastic renal tissue but a substantially reduced rate of clearance, allowing for clear differentiation of renal carcinomas from non-neoplastic renal tissueon image frames acquired beyond 10 min after tracer administration. Oyama et al. [17] reported that AC showed marked uptake in prostate cancer that was negative on FDG PET. AC is more sensitive in the detection of prostate cancer than is FDG PET. Recently, Ho et al. [22] reported that AC has a high sensitivity and specificity as a radiotracer and is complementary to FDG in the PET imaging of hepatocellular carcinoma (HCC). They found that well-differentiated HCCs are detected by AC and poorly differentiated types are detected by FDG. AC may thus play a complementary role in the identification of tumours that are not FDG avid.

The purpose of this study was to investigate the feasibility of using AC for the detection and characterisation of lung cancers, and to compare AC PET with FDG PET and MIBI SPET.

Materials and methods

Patient preparation. After approval of our protocol by our institutional human use committee, 23 patients with 25 histologically confirmed lung cancers were studied. Tumour diameter varied between 1.2 and 7.0 cm. The 25 lung cancers consisted of 18 adenocarcinomas, five squamous cell carcinomas and two large cell carcinomas. Written informed consent was obtained from all patients. All patients were investigated with both AC PET and FDG PET. Twenty of the 23 patients were also investigated with MIBI SPET within 1 week.

Radiotracer preparation. ^{11}C was produced by proton bombardment of $^{14}N_2$. The resultant $^{11}CO_2$ was then reacted with methyl magnesium bromide. Radionuclide purity of AC was greater than 98%, and radiochemical purity determined by high-pressure liquid radiochromatography was consistently greater than 95%. ^{18}F was produced by ^{20}Ne (d, α) ^{18}F nuclear reaction, and FDG was synthesised by the acetyl hydrofluorite method.

Imaging protocol. PET scanning was performed with a dedicated PET camera (Headtome IV, Shimazu, Kyoto, Japan) with a 10-cm axial field of view. The Headtome IV has four detector rings with 768 bismuth germanate (BGO) crystals per ring. It uses direct and cross-plane coincidence detection to generate 14 slices per bed position. Reconstruction in a 128×128 matrix using a Hann filter (0.5 cut-off) yielded 5-mm intrinsic resolution at the centre. Transmission scans were obtained in all subjects for attenuation correction by using a germanium-68 ring source. A transmission scan was acquired for 10–20 min, depending on the specific radioactivity of the ring sources at the time of the study, for at least 2 million counts per slice. Immediately after the transmission scan, AC (555 MBq) was administered intravenously, with simultaneous initiation of 26 min of dynamic emission imaging. The image sequence included four 30-s imaging frame acquisitions followed by eight 60-s frames, and then eight 120-s frames.

FDG PET was performed within a week of AC PET study. All patients fasted for 6 h before scanning. Blood (1 ml) was drawn for baseline blood glucose estimation, and the data were recorded. Immediately after the transmission scan, FDG was administered intravenously. The average injection dose of FDG was 185 MBq. In this study, the body weight of the patients ranged from 37.0 kg to 78.6 kg, with a mean of 53.4 kg. The injection dose of FDG was reduced because of a low body weight. After a 40-min uptake period, an emission scan was acquired over a 20-min period.

MIBI SPET was also performed within a week of AC PET study. With the subject at rest, 555 MBq of MIBI was injected into a peripheral vein, and MIBI imaging was begun 15 min later. SPET was performed using a dual-headed rotating gamma camera system (PRISM 2000XP, Picker, Cleveland, OH) equipped with a high-resolution collimator, collecting 30 projection images for 40 s each over 360° by using a 128×128 matrix. The total acquisition time was approximately 30 min. The intrinsic resolution was 15 mm full-width at half-maximum at the centre. The slice thickness was 5.8 mm. A series of transverse slices was reconstructed with filtered back-projection using a Ramp Hanning filter with a cut-off frequency of 0.5 cycles/pixel. No attenuation correction was performed.

Data analysis. Attenuation- and decay-corrected images were reconstructed transaxially and displayed in a 128×128 matrix. We evaluated the images visually using a computer display of the transaxial reconstructions of the entire dynamic sequence. In all patients, correlative CT scans were available for comparison to aid in locating focal pathologies which were not tracer avid. For semiquantitative analysis of the AC and FDG uptake, regions of interest (ROIs) were manually defined on the transaxial tomograms that showed the lesion's highest uptake to be in the middle of the tumour. The ROIs placed on the lesions encompassed all pixels within that lesion that had uptake values of greater than 90% of the maximum uptake in that slice, and the average count rate in each ROI was calculated. In patients in whom no nodules were detectable by PET, the ROI was extrapolated from chest CT scans. After correction for radioactive decay, we analysed the ROIs by computing the standardised uptake values (SUVs), PET counts/

pixel/s × calibration factor/injected dose (MBq)/body weight, where the calibration factor = (MBq/ml)/(counts/pixel/s). We also calculated the tumour to non-tumour activity ratio (T/N). The SUVs and T/N of AC were calculated from the dynamic images at 10–20 min post injection of AC. To estimate the clearance of AC from lung cancer, we used a method based on the original report of Yeh et al. [19]. Using the time-activity curve, we calculated the clearance rate of AC from a lesion as $0.693/T_{1/2}$. We investigated the SUVs and T/N for each tumour for tracer activity at 40–60 min after FDG administration. For semiquantitative analysis of MIBI SPET, the radioactivity was measured for areas of the tumour showing the highest MIBI accumulation and the homologous contralateral normal lung to calculate the tumour to non-tumour activity ratio of the activity (T/N).

For visual inspection, we used a method based on the original report of Liu et al. [21]. The clearly visualised tumours with a T/N greater than 2.5 were defined as (+), and the visualised tumours with a T/N less than 2.5 were defined as (+/–). Non-visualised tumours were defined as (–).

Histopathological features. Twenty lung cancers were operated on. The surgically resected specimens were routinely fixed in 10% formalin and embedded in paraffin. All of the 5-mm sections were stained with haematoxylin-eosin and then examined by light microscopy. Fifteen of the 20 operated lung cancers were adenocarcinomas. Cell dedifferentiation and aggressiveness (i.e. pleural involvement, vascular invasion, lymphatic permeation and/or nodal involvement) were also estimated. Lung cancers with any one of these features were considered to be aggressive. The degree of tracer uptake in the primary lesion was correlated with these histopathological features in 15 lung adenocarcinomas.

Prognosis. Patients were monitored bimonthly at the outpatient clinic after surgery. Disease-free survival time was defined as the interval from the date of operation until recurrence or the last follow-up date.

Statistical analysis. Means of paired values among three groups were compared by two-way ANOVA, and multiple comparisons were made by Scheffe's method. Unpaired mean values between two groups were compared by the non-parametric Mann-Whitney test, because the power of Student's *t* test is inappropriate when the sample size is small. Pearson's correlation coefficients were calculated to look at simple correlations.

Results

Table 1 summarises the radionuclide and pathological findings for the 25 lung cancers studied.

AC PET imaging

A sample lung cancer time-activity curve is shown in Fig. 1. For comparison, the tissue time-activity curve of normal myocardium is included. There was rapid AC uptake followed by extremely slow clearance of AC from lung cancer, in contrast to rapid clearance from the myocardium. On dynamic AC PET, maximal tracer activity and optimal target to non-target activity were achieved rapidly within 10 min of tracer injection. The clearance of AC from lung cancer was extremely slow, and the mean clearance rate of lung cancer was 0.019±0.024. Lung cancer showed variable uptake of AC, with SUVs ranging from 0.14 to 5.50 at 10–20 min after AC administration.

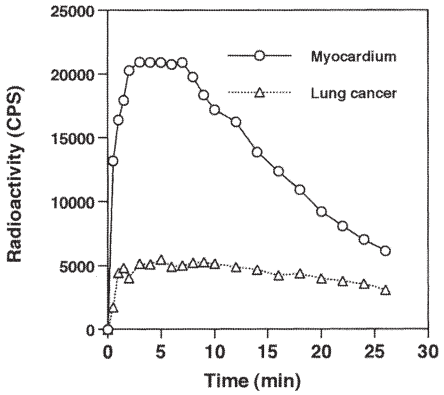

Fig. 1. Tissue time-activity curves of normal myocardium and lung cancer (patient no. 11) after administration of ^{11}C-acetate. Myocardium rapidly cleared the tracer, while lung cancer showed substantial relative retention of the tracer

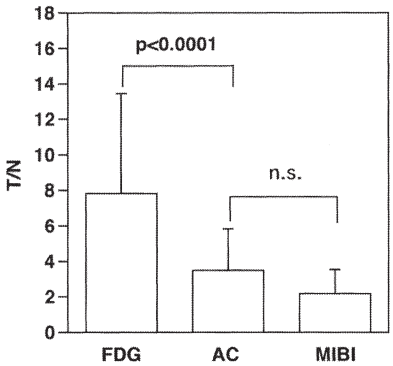

Fig. 2. Multiple comparisons among FDG, AC, and MIBI uptake (T/N) in lung cancers

Comparison of AC PET with FDG PET

Tables 2 and 3 show the results of visual inspection for the 25 lung cancers studied. For the purpose of tumour identification, AC PET was inferior to FDG PET in 8 of 25 (32%) lung cancers (Table 2), and the mean T/N ratio of AC (3.49±2.34) was significantly lower than that of FDG (7.84±5.61, $P<0.0001$) (Fig. 2). A representative case is shown in Fig. 3: this poorly differentiated adenocarcinoma with huge central necrosis (patient no. 15) showed weak AC uptake (SUV of 2.09 and T/N of 1.63) but was FDG avid (SUV of 5.97 and T/N of 10.2). However, AC PET was superior to FDG PET in the identification of a slow-growing tumour (bronchiolo-alveolar

Table 1. Patient characteristics and radionuclide imaging results

Patient no.[a]	Age (yr)	Sex	Histological type	Size (cm)	Operation	pStage	Aggressiveness			Postoperative recurrence	Interval (mo)[c]	AC				FDG			MIBI	
							P	V	L or N			SUV	T/N	Up-take	K_{mono}	SUV	T/N	Up-take	T/N	Up-take
1	67	M	BAC	2.6	T	IA	–	–	–	–	33	1.82	2.90	+	0.0129	0.93	1.00	–	1.85	+/–
2	73	F	BAC	2.8	T	IA	–	–	–	–	31	2.85	2.88	+	0.0065	2.31	4.22	+	2.16	+/–
3	65	F	Well-diff. AD	1.5	T	IA	–	–	–	–	18	2.03	4.32	+	0.0158	2.84	6.76	+	1.87	+/–
4	60	F	Well-diff. AD	1.6	T	IA	–	–	–	–	42	2.30	3.05	+	0.0132	1.85	3.19	+	1.78	+/–
5	70	F	Well-diff. AD	2.0	T	IA	–	–	+	–	4	2.26	3.63	+	0.0852	2.58	7.06	+	3.94	+
6	75	F	Well-diff. AD	2.0	WR		–	–	–	–	18	3.03	2.35	+/–	0.0053	2.81	2.90	+	1.77	+/–
7	65	F	Well-diff. AD	2.6	T	IA	–	–	–	–	35	1.92	2.17	+/–	0.0118	1.91	2.77	+	1.36	+/–
8	65	M	Well-diff. AD	2.8	T	IA	+	+	–	–	34	3.39	10.00	+	0.0101	1.79	5.39	+	3.99	+
9	80	M	Well-diff. AD	2.8	T	IA	–	–	–	–	18	4.41	2.60	+	0.0048	3.17	3.71	+	1.89	+/–
10	62	M	Well-diff. AD	3.0	OLB[b]	IIIB	+	–	–			2.63	2.39	+/–	0.0119	4.46	4.04	+	NA	NA
11	73	M	Mod. diff. AD	1.8	WR		–	–	–	–	22	1.76	5.97	+	0.0266	4.35	17.30	+	2.26	+/–
12	71	M	Mod. diff. AD	3.0	T	IIIA	–	–	+	–	7	2.59	2.65	+	0.0701	5.46	10.20	+	2.89	+
13	71	M	Poorly diff. AD	2.0	T	IIIA	+	+	+	–	7	2.24	2.14	+/–	0.0834	4.11	2.96	+	1.52	+/–
14	73	M	Poorly diff. AD	2.7	T	IIA	+	–	+	+	37	3.17	2.43	+/–	0.0091	8.05	13.20	+	1.88	+/–
15	59	M	Poorly diff. AD	5.5	T	IB	–	+	–	+	11	2.09	1.63	+/–	0.0032	5.97	10.20	+	1.00	–
16	55	F	AD	2.0								0.14	1.00	–	NA	0.88	1.00	–	1.46	+/–
17	72	F	AD	3.5								2.81	2.76	+	0.0036	3.22	5.51	+	NA	NA
18	73	F	AD	4.5								5.50	10.10	+	0.0175	5.79	21.70	+	7.04	+
19	73	M	Mod. diff. SCC	1.6	WR		–	–	–	–	22	1.42	3.48	+	0.0136	1.96	10.10	+	1.00	–
20	64	M	Mod. diff. SCC	2.0	OLB[b]	IIIB	+	–	+			1.73	2.55	+	0.0054	5.33	6.15	+	1.19	+/–
21	73	M	Mod. diff. SCC	2.7	T	IA	–	–	–	–	31	2.21	3.01	+	0.0081	4.19	12.70	+	2.06	+/–
22	72	M	Mod. diff. SCC	2.8	T	IA	–	+	+	–	6	1.62	2.51	+	0.0105	4.76	16.04	+	2.61	+
23	69	M	SCC	1.5								1.94	3.02	+	0.0101	0.63	4.37	+	1.59	+/–
24	72	M	LCC	7.0	T	IIB	+	–	–	–	29	3.66	2.31	+/–	0.0067	7.57	9.52	+	1.00	–
25	62	M	LCC	5.8								3.23	2.38	+/–	0.0098	3.89	6.54	+	NA	NA

BAC, Bronchioloalveolar carcinoma; diff., differentiated; AD, adenocarcinoma; Mod., moderately; SCC, squamous cell carcinoma; LCC, large cell carcinoma; T, thoracotomy; WR, wedge resection; OLB, open lung biopsy; pStage, pathological stage; P, pleural involvement; V, vascular involvement; L, lymphatic permeation; N, nodal involvement; AC, ^{11}C-acetate; NA, not available

[a] Numbers 11 and 19 represent the same patient; this is also the case for numbers 12 and 13

[b] Complete resection was not possible, due to pleural dissemination

[c] Interval from date of operation until recurrence or last follow-up

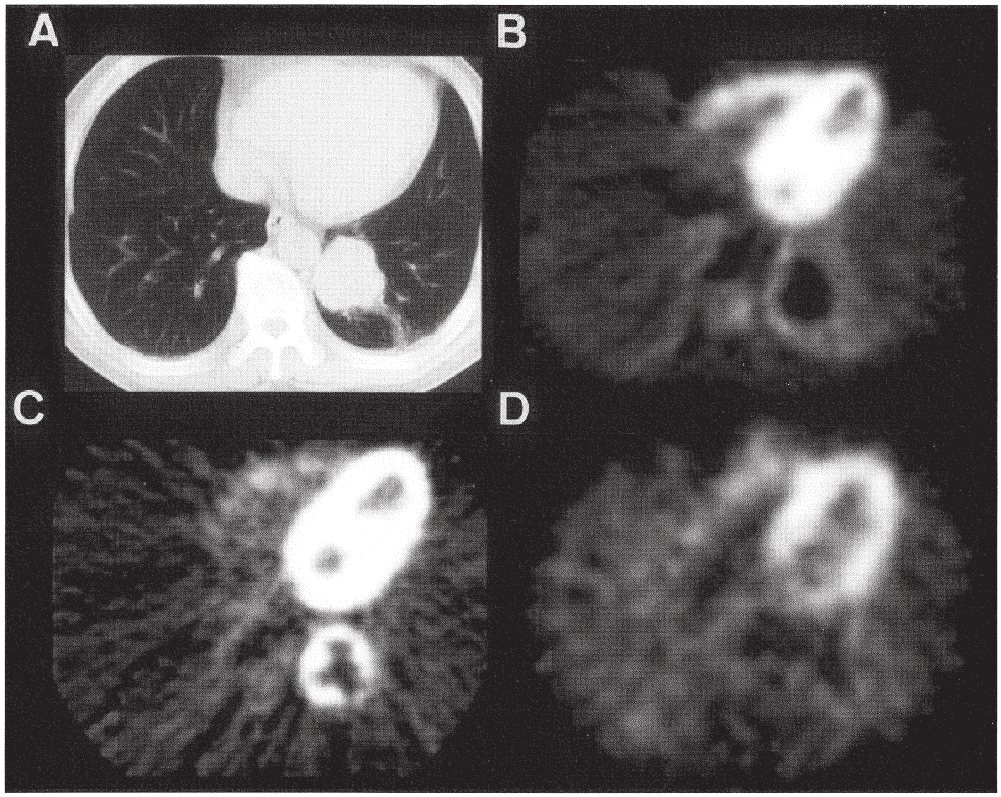

Fig. 3A–D. Patient 15: poorly differentiated adenocarcinoma with huge central necrosis, 5.5 cm in maximal diameter, pathological stage 1B (T2N0M0), aggressive lung cancer (vascular invasion +). **A** CT shows a large mass in the left lung. **B** AC PET shows weak accumulation (SUV, 2.09; TIN, 1.84). **C** FDG PET shows strong ring-like accumulation in the mass lesion (SUV, 5.97; T/N, 10.20). **D** MIBI SPET shows a negative result. The patient suffered a recurrence in the brain 11 months after surgery

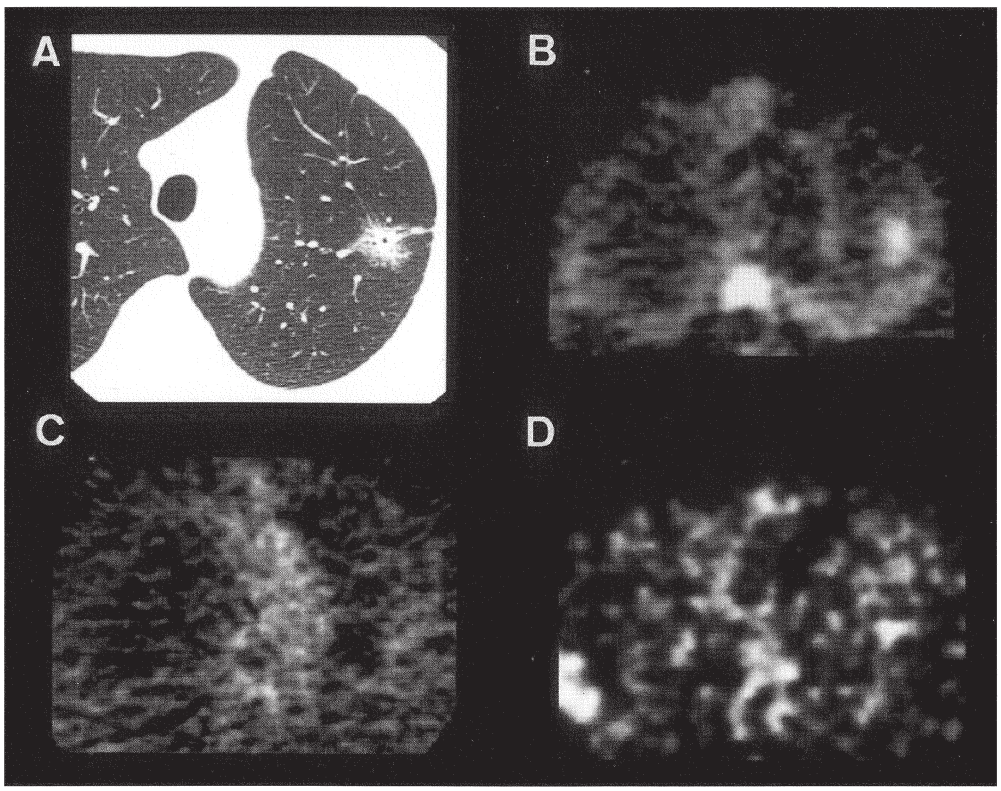

Fig. 4A–D. Patient 1: bronchiolo-alveolar carcinoma, 2.6 cm in maximal diameter, pathological stage 1A (T1N0M0), non-aggressive lung cancer. **A** CT shows a nodule in the left lung. **B** AC PET reveals good visualisation of the nodule (SUV, 1.82; T/N, 2.90). **C** FDG PET does not reveal any lesions (SUV, 0.93; T/N, 1.00). **D** MIBI SPET shows weak accumulation (T/N, 1.85) in the lung cancer. The patient suffered no recurrence, and was alive 33 months after surgery

Table 2. Results of visual inspection for the 25 lung cancers studied: comparison of AC PET and FDG PET

		FDG		
		+	+/–	–
AC	+	15	0	1[a]
	+/–	8	0	0
	–	0	0	1

[a] Bronchiolo-alveolar carcinoma

Table 3. Results of visual inspection for the 25 lung cancers studied: comparison of AC PET and MIBI SPET

		MIBI		
		+	+/–	–
AC	+	5	9	1
	+/–	0	4	2
	–	0	1	0

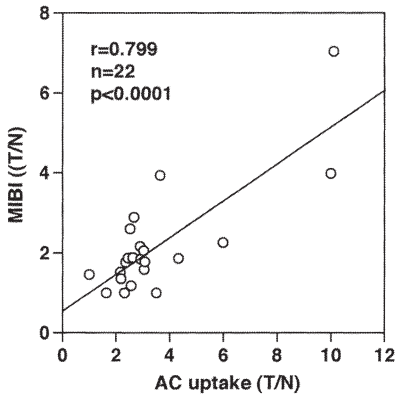

Fig. 5. Correlation between AC and MIBI uptake (T/N). The T/N ratio of AC was significantly correlated with that of MIBI (r=0.799, P<0.0001)

carcinoma) (Table 2). Figure 4 shows images of the patient (no. 1) with bronchiolo-alveolar carcinoma. FDG PET showed no uptake in the lung cancer, with an SUV of 0.93 and a T/N of 1.00, whereas AC PET showed higher uptake, with an SUV of 1.82 and a T/N of 2.90.

Comparison of AC PET with MIBI SPET

Table 3 shows the results of visual inspection for the 22 lung cancers studied. For the purpose of tumour identification, AC PET was superior to MIBI SPET in 12 of 22 (54.5%) lung cancers (Table 3), whereas the mean T/N ratio of AC (3.49±2.34) was not significantly higher than that of MIBI (2.19±1.35) (Fig. 2). The T/N ratio of AC was significantly correlated with that of MIBI (r=0.799, P<0.0001) (Fig. 5). Representative cases are shown in Figs. 3 and 4. In the FDG-avid, poorly differentiated adenocarcinoma shown in Fig. 3, both AC PET and MIBI SPET revealed weak uptake. Conversely, in the slow-growing bronchiolo-alveolar carcinoma shown in Fig. 4, both AC PET and MIBI SPET showed higher uptake than FDG PET. Thus, there was a positive correlation between AC and MIBI uptake.

Correlation between tracer uptake and histopathological features and prognosis

Ten of 15 operated lung adenocarcinomas were bronchiolo-alveolar carcinoma or well-differentiated adenocarcinoma, and five were moderately to poorly differentiated adenocarcinoma. A positive correlation was not observed between AC, MIBI uptake and the degree of cell dedifferentiation of lung adenocarcinoma (Fig. 6A, C). In contrast, mean FDG uptake (SUV) of moderately to poorly adenocarcinomas was significantly higher than that of bronchiolo-alveolar carcinomas and well-differentiated adenocarcinomas (Fig. 6B). Thus, FDG uptake correlated with the degree of cell dedifferentiation.

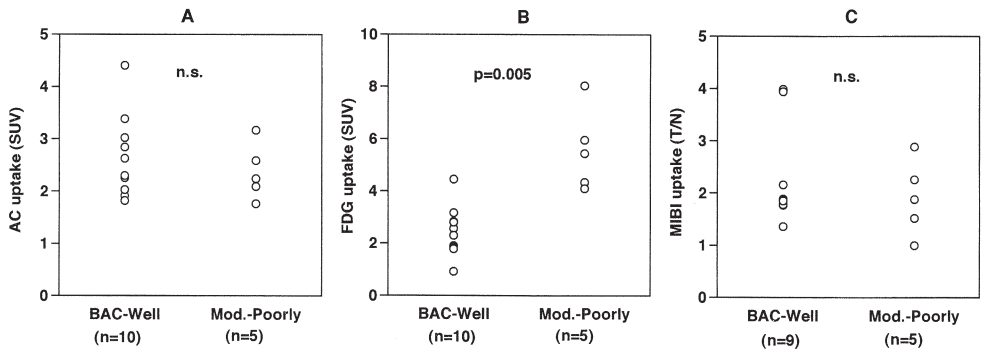

Fig. 6A–C. Correlation between cell dedifferentiation and tracer uptake in lung adenocarcinoma. No significant correlation was observed between AC (**A**) or MIBI (**C**) uptake and cell dedifferentiation. In contrast, FDG uptake by moderately to poorly differentiated adenocarcinomas (*Mod.-Poorly*) (5.59±1.58) was significantly higher than that by bronchiolo-alveolar carcinomas and well-differentiated carcinomas (*BAC-Well*) (2.4±0.959) (P=0.005) (**B**). All three lung adenocarcinomas with FDG SUV >5 were moderately to poorly differentiated

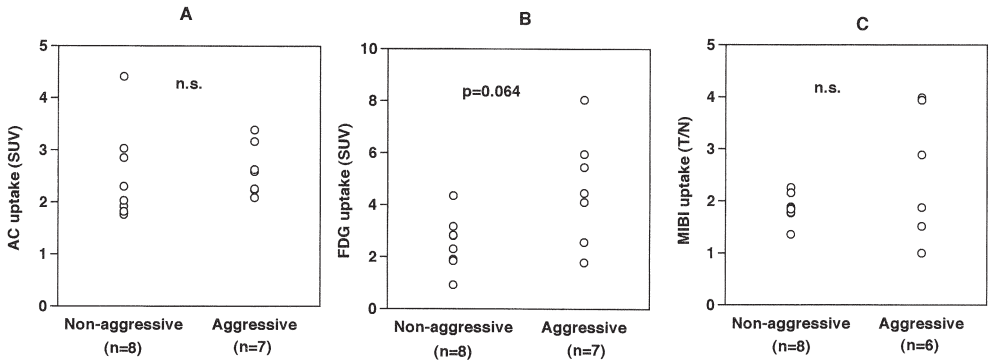

Fig. 7A–C. Correlation between aggressiveness (vascular invasion, pleural involvement, lymphatic permeation and/or nodal involvement) and tracer uptake in lung adenocarcinoma. No correlation was observed between AC (**A**) or MIBI (**C**) uptake and aggressiveness, whereas FDG uptake by aggressive lung adenocarcinomas (4.63±2.11) was slightly higher than that by non-aggressive ones (2.52±1.02) (*P*=0.064) (**B**). All three adenocarcinomas with FDG SUV >5 were aggressive

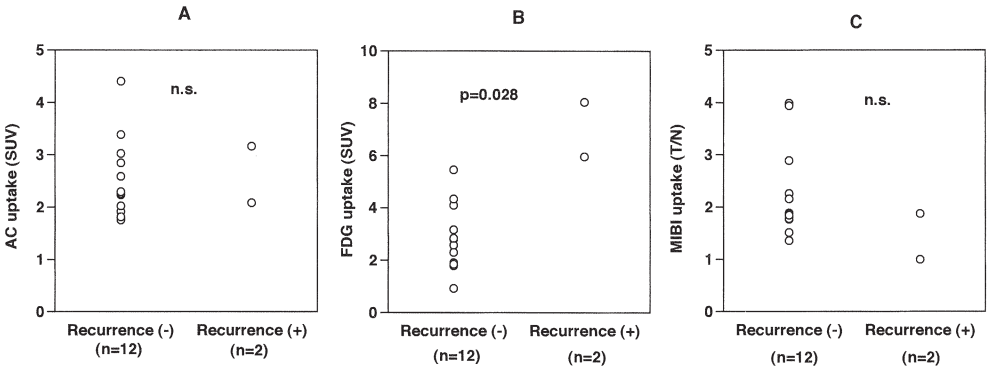

Fig. 8A–C. Correlation between postoperative recurrence and tracer uptake in lung adenocarcinoma. No correlation was observed between AC (**A**) or MIBI (**C**) uptake and postoperative recurrence. In contrast, FDG uptake by lung adenocarcinomas with postoperative recurrence (7.01±1.47) was significantly higher than that by lung adenocarcinomas without postoperative recurrence (2.84±1.27, *P*=0.028) (**B**)

Seven of 15 operated lung adenocarcinomas were aggressive, and eight were non-aggressive. There was no significant difference between aggressive and non-aggressive lung cancers with respect to AC (Fig. 7A) and MIBI (Fig. 7C) uptake. However, mean FDG uptake (SUV) of aggressive lung cancers was slightly higher than that of non-aggressive lung cancers (Fig. 7B), though the difference was not significant (*P*=0.064).

Postoperative recurrence was observed in 2 of 14 patients with surgically resected lung adenocarcinoma (nos. 14 and 15). AC (Fig. 8A) and MIBI (Fig. 8C) uptake did not differ significantly between lung cancer with recurrence and lung cancer without recurrence after surgery. Mean FDG uptake (SUV) of lung cancers with recurrence after surgery was significantly higher than that of lung cancers without recurrence (Fig. 8B).

Thus, in lung adenocarcinoma, the greater the FDG uptake, the higher the malignant grade, whereas neither AC nor MIBI uptake reflects the malignant grade in lung adenocarcinoma.

Discussion

The principal findings of this study are that for the purpose of tumour identification, AC PET was inferior to FDG PET but superior to MIBI SPET, and that neither AC nor MIBI uptake reflects the malignant grade in lung adenocarcinoma, whereas FDG uptake does. AC PET is less diagnostically informative than FDG PET in patients with lung cancer. However, AC PET may play a complementary role in the identification of low-grade malignancies that are not FDG avid.

AC has been known as a positron-emitting tracer for measurement of oxidative metabolism in the myocardium. As soon as the myocardium takes up AC, it is converted to acetyl-coenzyme A in the mitochondria, followed by rapid clearance as carbon dioxide through the citric acid cycle. The mechanism of high AC accumulation in tumour tissue cells, although as yet unknown, is thought to be different from that of myocardial uptake. In an in vitro study, it was reported that AC uptake in tumour cells is caused by enhanced lipid synthesis, and suggested that AC may be an important probe of the ana-

bolic pathway of metabolism in cancer tissue [23]. However, some controversy surrounds this finding. In patients with prostate cancer, Oyama et al. [17] observed no relationship between the accumulation of AC and clinical parameters such as clinical stage and serum PSA value, whereas they did find a positive correlation between clinical stage and FDG uptake. These findings indicate that FDG uptake but not AC uptake is associated with progression of prostate cancer. In an animal study, Oyama et al. [24] also investigated whether AC and FDG PET imaging could evaluate early metabolic changes in prostate tumours following androgen ablation therapy. They found insensitivity of AC for measurement of metabolic changes in prostate tumours following treatment, whereas FDG PET imaging could evaluate early metabolic changes. Ho et al. [22] reported that poorly differentiated hepatocellular carcinomas (HCCs) had lower AC but higher FDG uptake than did well-differentiated HCCs. Thus, there was a negative correlation between AC uptake and malignant potential in HCC. There was, however, a positive correlation between FDG uptake and malignant potential. These results cannot be explained only by the enhanced lipid metabolism that is associated with the cell membrane because of tumour growth. In the current study, in one slow-growing tumour (a bronchiolo-alveolar carcinoma) FDG PET showed lower uptake than did AC PET (Fig. 4). In contrast, a poorly differentiated adenocarcinoma was FDG avid but showed weak uptake on AC PET (Fig. 3). These results are concordant with those of Oyama et al. [17, 24] and Ho. et al. [22]. In addition to further basic studies, a clinical study with a larger number of patients is needed to clarify the mechanism of AC uptake in lung cancer.

In the current study, there was a positive correlation between AC and MIBI uptake in lung cancer (Fig. 5), and no positive correlation was observed between AC or MIBI uptake and cell dedifferentiation, aggressiveness or postoperative recurrence . Tracer kinetic analysis yields parameters associated with both blood flow and metabolism [15]. However, in lung cancer, AC was initially rapidly distributed into tissue via the bloodstream, and there was rapid uptake followed by extremely slow clearance from lung cancer, in contrast to the rapid clearance from the myocardium (Fig. 1). MIBI is also rapidly distributed into lung cancer [25], the peak level being reached within first minute. These phenomena may suggest that both AC uptake and MIBI uptake in lung cancer are parameters mainly associated with blood flow, rather than malignant grade.

This study has limitations. First, the study population was too small for useful comparison of squamous and large cell carcinomas. Second, the study included only cases of histologically proven lung cancer. Therefore, although the true-positive rate could be calculated, the true-negative rate could not be evaluated. In this respect, a prospective analysis of patients with suspected lung cancer may be warranted to compare the diagnostic accuracy of these techniques.

In conclusion, for the purpose of tumour identification, AC PET was inferior to FDG PET but superior to MIBI SPET. AC and MIBI uptake do not reflect malignant grade in lung adenocarcinoma, whereas FDG uptake does. AC PET is less diagnostically informative than FDG PET in patients with lung cancer. However, AC PET may play a complementary role in the identification of low-grade malignancies that are not FDG avid. Further studies using AC PET with a larger number of patients are needed to determine its ultimate clinical utility.

Acknowledgements. We thank Dr. Hiroyasu Seki for his great assistance. This work was supported by a Grant for Collaborative Research from Kanazawa Medical University (C2003-2), by a Grant-in Aid for Cancer Research (12-4) from the Ministry of Health and Welfare, Japan, and by a Grant-in Aid for Scientific Research (13670192) from the Ministry of Education, Science and Culture, Japan.

References

1. Strauss LG, Conti PS. The application of PET in clinical oncology. *J Nucl Med* 1991; 32:623–648.
2. Higashi K, Ueda Y, Sakurai A, et al. Correlation of Glut-1 glucose transporter expression with F-18 FDG uptake in non-small cell carcinoma. *Eur J Nucl Med* 2000; 27:1778–1785.
3. Higashi K, Ueda Y, Seki H, et al. Fluorine-18-FDG PET imaging is negative in bronchioloalveolar lung carcinoma. *J Nucl Med* 1998; 39:1016–1020.
4. Higashi K, Ueda Y, Yagishita M, et al. FDG PET measurement of the proliferative potential of non-small cell lung cancer. *J Nucl Med* 2000; 41:85–92.
5. Higashi K, Ueda Y, Ayabe K, et al. FDG PET in the evaluation of the aggressiveness of pulmonary adenocarcinoma: correlation with histopathological features. *Nucl Med Commun* 2000; 21:707–714.
6. Higashi K, Ueda Y, Arisaka Y, et al. F-18 FDG uptake as a biologic prognostic factor for recurrence in patients with surgically resected non-small cell lung cancer. *J Nucl Med* 2002; 43:39–45.
7. Erasmus JJ, McAdams HP, Patz EF, et al. Evaluation of primary pulmonary carcinoid tumours using FDG PET. *Am J Roentgenol* 1998; 170:1369–1373.
8. Kao CH, Wang SJ, Lin WY, et al. Differentiation of single solid lesions in the lungs by means of single-photon emission tomography with technetium-99m methoxyisobutylisonitrile. *Eur J Nucl Med* 1993; 20:249–254.
9. Komori T, Narabayashi I, Matsui R, et al. Evaluation of uptake and release of technetium-99m MIBI SPET of pulmonary and mediastinal lesions. *Ann Nucl Med* 1997; 11:227–232.
10. Wang H, Maura S, Mainolfi C, et al. Tc-99m MIBI scintigraphy in patients with lung cancer comparison with CT and fluorine-18 FDG PET imaging. *Clin Nucl Med* 1997; 22:243–249.
11. Chiu MI, Kronauge JF, Piwnica-Worms D. Effect of mitochondrial and plasma membrane potentials on accumulation of hexakis (2-methoxyisobutysonitrile) technetium (I) in cultured mouse fibroblasts. *J Nucl Med* 1990; 31:1646–1653.

12. Crane P, Laliberte R, Heminway S, et al. Effect of mitochondrial viability and metabolism on technetium-99m-sestamibi myocardial retention. *Eur J Nucl Med* 1993; 20:20–25.
13. Abdel-Dayem HM, Scott A, Macapinlac H, et al. Tracer imaging in lung cancer. *Eur J Nucl Med* 1994; 21:57–81.
14. Liu RS. Clinical application of C-11 acetate PET. *Clin Positron Imaging* 2000; 3:185.
15. Shreve P, Chiao PC, Humes HD, et al. Carbon-11-acetate PET imaging in renal disease. *J Nucl Med* 1995; 36:1595–1601.
16. Shreve PD, Gross MD. Imaging of the pancreas and related diseases with PET carbon-11-acetate. *J Nucl Med* 1997; 38: 1305–1310.
17. Oyama N, Akino H, Kanamaru H, et al. C-11 acetate PET imaging of prostate cancer. *J Nucl Med* 2002; 43:181–186.
18. Shreve PD. Carbon-11 acetate PET imaging of prostatic cancer [abstract]. *J Nucl Med* 1999; 40 (Suppl):60P.
19. Yeh SH, Liu RS, Wu LC, et al. ^{11}C-acetate clearance in nasopharyngeal carcinoma. *Nucl Med Commun* 1999; 20:131–134.
20. Liu RS, Chu YK, Chu LS, et al. C-11 acetate PET imaging in detection and characterization of lung cancer [abstract]. *J Nucl Med* 2001; 43(Suppl):7P.
21. Liu RS, Shei HR, Feng CF, et al. Combined F-18 FDG and C-11 Acetate PET imaging in pulmonary carcinoma [abstract]. *J Nucl Med* 2002; 43(Suppl):127P.
22. Ho C, Yeung DW. C-11 acetate PET imaging in hepatocellular carcinoma and other liver masses. *J Nucl Med* 2003; 44:213–221.
23. Yoshimoto M, Waki A, Yonekura Y, et al. Characterization of acetate metabolism in tumour cells in relation to cell proliferation: acetate metabolism in tumour cells. *Nucl Med Biol* 2001; 28:117–122.
24. Oyama N, Kim J, Jones LA, et al. MicroPET assessment of androgenic control of glucose and acetate uptake in the rat prostate and prostate cancer tumour model. *Nucl Med Biol* 2002; 29:783–790.
25. Hassan IM, Sahweil A, Constantinides C, et al. Uptake and kinetics of Tc-99m hexakis 2-methoxy isobutyl isonitrile in benign and malignant lesions in the lungs. *Clin Nucl Med* 1989; 14:333–340.

In Vitro Proton Magnetic Resonance Spectroscopic Lactate and Choline Measurements, ^{18}F-FDG Uptake, and Prognosis in Patients with Lung Adenocarcinoma

JianFei Guo, MD[1]; Kotaro Higashi, MD[1]; Hajime Yokota, MD[1]; Yosinobu Nagao, PhD[2,3]; Yoshimichi Ueda, MD[4]; Yuko Kodama, MD[1]; Manabu Oguchi, MD[1]; Suzuka Taki, MD[1]; Hisao Tonami, MD[1]; and Itaru Yamamoto, MD[1]

[1]Department of Radiology, Kanazawa Medical University, Ishikawa, Japan; [2]Division of Advanced Medicine, Medical Research Institute, Kanazawa Medical University, Ishikawa, Japan; [3]Department of Biochemistry, Kanazawa Medical University, Ishikawa, Japan; and [4]Department of Pathology, Kanazawa Medical University, Ishikawa, Japan

It has been reported that ^{18}F-FDG uptake, lactate concentration, and choline concentration are good indicators of malignant grade in several different kinds of tumors. In this study, we investigated the correlation between ^{18}F-FDG uptake in ^{18}F-FDG PET imaging, lactate concentration and choline concentration measured by in vitro ^{1}H magnetic resonance spectroscopy (MRS), and survival probabilities in human lung adenocarcinoma. **Methods:** Nineteen patients with lung adenocarcinoma underwent ^{18}F-FDG PET before surgery. The ^{1}H MRS spectra were obtained in vitro from methanol–chloroform–water extracts of lung adenocarcinomas and normal lungs. The ratios of the lactate (R_{lac}) or choline (R_{cho}) concentration of lung adenocarcinoma to normal lung from the same patient were correlated with the mean standardized uptake value (SUV). The Kaplan–Meier life table method was used to analyze the relationship between ^{18}F-FDG uptake, R_{lac}, R_{cho}, and patient survival probabilities. **Results:** There was no significant correlation between mean SUV and R_{lac} or R_{cho} in patients with lung adenocarcinoma. An SUV > 5 means poorer survival probabilities in patients with lung adenocarcinoma ($P = 0.004$). A higher R_{lac} probably indicates a trend for patients with lung adenocarcinoma to have poorer survival probabilities; however, R_{cho} is not an indicator of survival probability. ^{18}F-FDG uptake significantly correlated with cell differentiation ($P = 0.007$), whereas R_{lac} and R_{cho} had no correlation with it. **Conclusion:** No significant correlation was found between SUV and R_{lac} or R_{cho} in patients with lung adenocarcinoma. Compared with R_{lac} and R_{cho} measured by in vitro MRS, ^{18}F-FDG uptake is a better indicator of prognosis in patients with lung adenocarcinoma.

Key Words: ^{18}F-FDG; lung adenocarcinoma; magnetic resonance spectroscopy; lactate; choline; prognosis

J Nucl Med 2004; 45:1334–1339

Received Nov. 6, 2003; revision accepted Jan. 29, 2004.

For correspondence or reprints contact: Kotaro Higashi, MD, Department of Radiology, Kanazawa Medical University, 1-1, Daigaku, Uchinada, Kahoku-gun, Ishikawa, 920-0293, Japan.

E-mail: h550208@kanazawa-med.ac.jp

Warburg first discovered that tumors are characterized by abnormally increased glucose metabolism, with increased production of lactate (caused by glycolysis) (*1*). This finding has subsequently been used to clinical and research advantage.

After ^{18}F-FDG was introduced in clinical settings, PET with ^{18}F-FDG provided a means for the noninvasive quantitative assessment of tumor glucose metabolism in vivo (*2*). Recently, accumulative evidence has shown that ^{18}F-FDG uptake can serve not only as a good diagnostic tool for tumors but also as a good indicator of proliferative ability and prognosis in some tumors (*3,4*), particularly in lung cancer (*5–10*).

Lactate, as the end product of anaerobic glycolysis, may reflect tumor glucose metabolism by another aspect and can be detected noninvasively by magnetic resonance spectroscopy (MRS). It has been expected that hot spots on ^{18}F-FDG images could be matched by hot spots on lactate-concentration MRS images (*11*). Although, until now, there have been no conclusive results about the relationship between lactate concentration determined by MRS and tumor malignancy, some researchers have found that lactate concentration has prognostic value in patients with gliomas or cervical cancers (*12,13*).

Lung cancer has become the leading cause of cancer death in Japan and most Western counties. Therefore, the early and precise prediction of survival probabilities will facilitate more appropriate therapeutic planning for patients with lung cancer. Considering that increased glucose metabolism is an outstanding biochemical characteristic of cancer tissue, we tried to compare the prognostic significance of ^{18}F-FDG uptake by ^{18}F-FDG PET imaging (reflecting glucose metabolism) and lactate concentration by in vitro MRS (reflecting the end product of glycolysis) in this study. In addition, some reports found that choline concentration can indicate proliferative ability and prognosis in

some tumors (*14,15*), and choline PET has become a useful diagnostic tool (*16–19*) clinically. Therefore, we also compared the correlation between choline concentration and prognosis in patients with lung adenocarcinoma.

MATERIALS AND METHODS

Patients

Nineteen patients (8 male, 11 female; age range, 48–78 y; mean age, 64 y) participated in the study. All patients underwent a thoracotomy within 4 wk after their ^{18}F-FDG PET study. Final diagnoses were established histologically (via a thoracotomy) in all patients. The sizes of the tumors were determined from the resected specimens and ranged in diameter from 1.6 to 5.2 cm. None of the patients had insulin-dependent diabetes, and the serum glucose levels of all patients just before ^{18}F-FDG injection were less than 120 mg/dL. Informed consent was obtained from all patients participating in the study.

^{18}F-FDG PET

^{18}F-FDG PET was performed using a PET camera (Headtome IV; Shimazu) with a 10-cm axial field of view. The Headtome IV has 4 detector rings with 768 bismuth germanate crystals per ring. It uses direct and cross-plane coincidence detection to generate 14 slices per bed position. For the thorax, 2 bed positions (28 slices at 6.5-mm intervals) were obtained. Reconstruction in a 128 × 128 matrix using a Hann filter (0.5 cutoff) yielded 5-mm intrinsic resolution at the center. Transmission scans of all subjects were obtained before ^{18}F-FDG administration for attenuation correction using a ^{68}Ge ring source. A transmission scan was acquired for 10–20 min at each bed position, depending on the specific radioactivity of the ring sources at the time of the study, for at least 2 million counts per slice. Blood (1 mL) was drawn for the baseline blood glucose estimation, and the data were recorded. Immediately after the transmission scan, ^{18}F-FDG was administered intravenously. The average injected dose of ^{18}F-FDG was 185 MBq. After a 40-min uptake period, the patient was repositioned in the scanner. An emission scan was acquired for 10 min at each bed position, and the process took a total of 20 min.

For semiquantitative analysis of the ^{18}F-FDG uptake, regions of interest (ROIs) were manually defined on the transaxial tomograms that showed the highest uptake to be in the middle of the tumor. The ROIs placed on the lesions encompassed all pixels within that lesion that had uptake values of greater than 90% of the maximum uptake in that slice, and the average counted rate in each ROI was calculated. In patients in whom no nodules were detectable by PET, the ROI was extrapolated from chest CT scans. After correction for radioactive decay, we analyzed the ROIs by computing the standardized uptake values (SUVs) and PET counts/pixel/s × calibration factor/injected dose (MBq)/body weight, where the calibration factor = (MBq/mL)/(counts/pixel/s).

In Vitro ^{1}H MRS

Human lung cancer specimens were obtained from 19 patients undergoing scheduled surgical procedures. Noninvolved lung tissue was obtained from all patients at the same time. The surgically dissected lung tissue was immediately stored in 10% dimethyl sulfoxide solution at −20°C until use. Specimens ranged in weight from 20 to 230 mg.

The methanol–chloroform–water extracts were prepared according to previously described procedures (*20*), with some modification. Reagent-grade methanol and chloroform (4°C) in a ratio of 2:1 (v/v; 20 mL/g tissue) were added to the frozen, ground tissue. The tissue/solvent mixture was allowed to thaw before being transferred to polypropylene conical tubes. After approximately 15 min of contact with the first solvents, chloroform and distilled water were added to the samples in a ratio of 1:2 (6 mL/g of tissue) to form an emulsion. The samples were then centrifuged at 13,000 rpm for 20 min. The upper phase (methanol and water) was separated from the lower (organic) phase using a glass syringe. The residue from the first tissue extraction was then reextracted and pooled with the original extracted fractions. The total upper fractions were centrifuged at 3,000 rpm for 10 min, and 0.2 mL of a 1 mmol/L concentration of 3-(trimethylsily)propionic acid (TSP) was added as an external standard. The supernatant was then collected and lyophilized for 48 h.

After lyophilization, the dried extract samples were redissolved with 0.5 mL of D_2O in a 5-mm sample tube before the MRS analysis. The spectra were recorded with a 6.34-T spectrometer (JNM-EX270; JEOL) at 270.05 MHz for protons. The 1-dimensional proton spectra were acquired after 300 repetitions with acquisition of 16,000 data points. Quantification was performed by comparing the integrated TSP signal with the signal of the lactate and choline in the specimen spectrum after baseline correction. After the relative concentrations of lactate and choline were determined by spectra analysis, R_{lac} and R_{cho}—the ratios of the lactate or choline concentration of lung cancer to normal lung from the same patient—were calculated.

Statistical Analysis

All values are expressed as mean ± SD. The differences in ^{18}F-FDG uptake, R_{lac}, and R_{cho} between patients with different cell differentiation were determined using the independent 2-tailed Student *t* test. Probability values of less than 0.05 were considered statistically significant. Correlation was analyzed using the Pearson product moment test. Disease-free and overall survival probabilities were calculated with the Kaplan–Meier life table method. Differences between survival probabilities were analyzed using the log-rank test.

RESULTS

For the 19 patients evaluated in this study, the following data were measured and are summarized in Table 1: clinical, imaging, and follow-up.

A pair of typical spectra of the methanol–chloroform–water extracts from a poorly differentiated adenocarcinoma (PDA) and normal lung tissue (patient 17) are shown in Figure 1. Relative to the external standard TSP (0 ppm), the lactate peak and choline peak were located at 1.33 ppm and 3.22 ppm, respectively.

There was no correlation between SUV and R_{lac} in the 19 patients with lung adenocarcinoma (r = 0.16, not statistically significant) (Fig. 2A). There was also no correlation between R_{cho} and SUV (Fig. 2B).

The 19 patients were classified into 2 groups. Group A included bronchioloalveolar carcinoma (BAC) and well-differentiated adenocarcinoma (WDA), and group B included moderately differentiated adenocarcinoma (MDA) and PDA. For ^{18}F-FDG uptake, the mean value of group A (1.9 ± 0.7) was significantly lower than that of group B

TABLE 1
Clinical, Imaging, and Follow-up Patient Data

Patient no.	Age (y)	Sex	Histologic type	pStage	Size (cm)	MRS		^{18}F-FDG (SUV)	Postoperative recurrence	Survival interval (mo)		Status
						R_{lac}	R_{cho}			Disease-free	Overall	
1	60	F	BAC	IA	1.6	1.6	1.3	1.85	−	45	45	Alive
2	66	M	BAC	IB	4.0	1.1	1.0	2.14	−	34	34	Alive
3	59	F	BAC	IA	2.2	0.9	0.9	1.20	−	48	48	Alive
4	69	F	BAC	IB	3.8	1.2	2.6	2.78	−	37	37	Alive
5	76	F	BAC	IA	2.0	3.3	4.0	1.32	−	50	50	Alive
6	73	F	BAC	IA	2.8	1.1	2.0	2.31	−	31	31	Alive
7	61	F	WDA	IA	2.0	1.5	1.9	1.24	−	18	18	Alive
8	65	M	WDA	IA	2.8	0.5	1.9	1.79	−	34	34	Alive
9	48	F	WDA	IA	2.0	3.3	2.9	1.78	−	31	31	Alive
10	78	F	WDA	IA	2.0	2.1	3.0	1.21	−	23	23	Alive
11	65	F	WDA	IA	2.6	3.2	6.1	1.91	−	35	35	Alive
12	64	F	WDA	IA	3.0	0.6	2.4	3.25	−	2	2	Alive
13	74	M	MDA	IA	1.8	0.4	0.6	2.52	+	2	4	Deceased
14	64	M	MDA	IIIB	3.6	2.0	2.5	5.94	+	21	36	Deceased
15	69	M	MDA	IIIA	3.8	1.9	1.8	4.87	+	8	10	Deceased
16	60	F	MDA	IIIA	3.5	2.6	4.4	7.06	+	14	19	Deceased
17	50	M	PDA	IB	5.2	1.0	1.8	5.02	+	30	46	Deceased
18	54	M	PDA	IIIA	4.0	3.5	4.0	8.29	+	4	5	Deceased
19	73	M	PDA	IIA	2.7	1.1	3.0	8.05	+	38	45	Alive

pStage = pathologic stage; disease-free = time from date of operation until recurrence or the last follow-up date; overall = time from date of operation until death or the last follow-up date; BAC = bronchioloalveolar carcinoma; WDA = well-differentiated adenocarcinoma; MDA = moderately differentiated adenocarcinoma; PDA = poorly differentiated adenocarcinoma.

(6.0 ± 2.0, $P = 0.007$) (Fig. 3A). There were no differences in R_{lac} and R_{cho} between groups A and B (Figs. 3B and 3C).

The Kaplan–Meier life table method was used to further analyze the relationship between ^{18}F-FDG uptake, R_{lac}, R_{cho}, and patient survival probabilities. According to the previous report (*8*), the patients were classified into 2 groups: a high-SUV group (SUV > 5) and a low-SUV group (SUV ≤ 5). The mean lactate and choline concentration ratios of all tumors were grouped into a high- and a low-lactate class or a high- and a low-choline class, compared with the median value of the overall data. A significant difference ($P = 0.004$) in survival probabilities between the high-SUV group and the low-SUV group in the disease-free survival analysis is shown in Figure 4A, and a marginally significant difference ($P = 0.058$) in the overall survival analysis is shown in Figure 4D. As shown in Figures 4B and 4E, there was a tendency toward a negative correlation between lactate concentration ratio and survival probabilities for patients with lung adenocarcinoma; however, neither of the results reached statistical significance in the disease-free or overall survival analysis ($P = 0.281$ and 0.178, respectively). No significant differences were found in either the disease-free or the overall survival probabilities in this study by choline concentration ratio grouping (Figs. 4C and 4F).

DISCUSSION

^{18}F-FDG PET imaging has been shown to be of value in the prognostic evaluation of some tumors (*3,4*). In lung cancer, prior studies have shown the importance of ^{18}F-FDG PET imaging in the assessment of aggressiveness, proliferative potential, grade of malignancy, and prognosis (*21,22,5–10*). A previous study even found that ^{18}F-FDG uptake is superior to pathologic stage in predicting relapses in patients with non–small cell lung cancer (*8*). The higher the SUV of the tumor, the worse the survival probabilities of the patients. In the present study we classified the patients into a high-SUV group and a low-SUV group, according to the former report (*8*). Compared with the low-SUV group, the high-SUV group had a worse outcome in this study, especially in the disease-free survival analysis ($P = 0.004$). In addition, the subgroup study showed that ^{18}F-FDG uptake is significantly different between patients with BAC or WDA and patients with MDA or PDA ($P = 0.007$). That finding demonstrates that ^{18}F-FDG uptake is of value in the prediction of malignancy in lung adenocarcinoma.

As the end product of anaerobic glycolysis, lactate is expected to reflect the glucose metabolism of the tumors. Because the lactate concentration can be detected in the MRS study, there are expected associations between the ^{18}F-FDG PET study and the MRS study, with the linkage being the detection of glycolysis (*11*). Recently, an in vivo MRS investigation of brain tumors found that the ratio of lactate concentration to *N*-acetyl aspartate was the strongest prognostic factor in that study. That ratio is a better indicator of survival than are tumor grade and patient age (*12*). This report is also in accordance with that of Walenta et al.

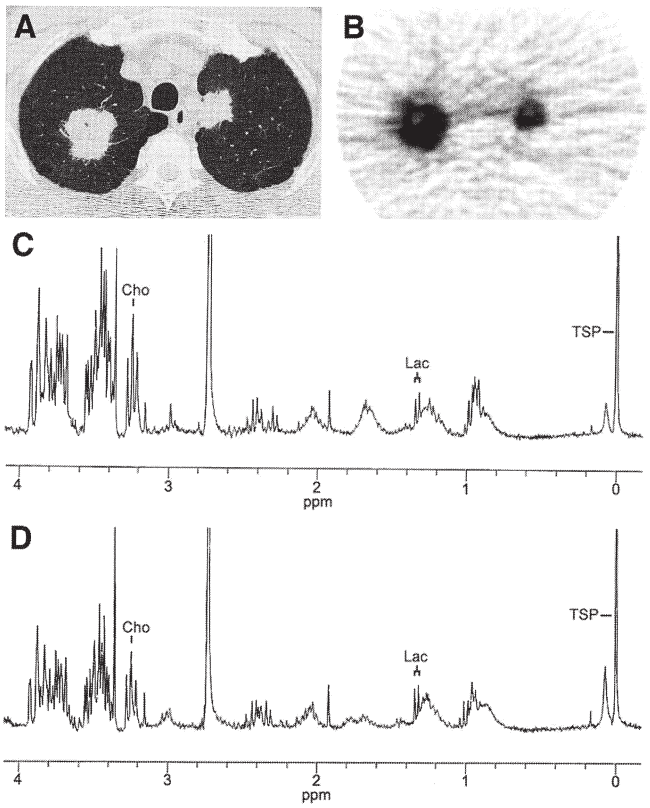

FIGURE 1. A 50-y-old man (patient 17) with PDA in both lungs. (A) CT shows that one tumor is in the right pulmonary apex and one is in the left pulmonary apex. (B) ^{18}F-FDG PET shows radioactive accumulation in the tumors. SUV is 5.02 (high-SUV group) for the lesion in the right lung. (C and D) MRS spectra for the lesion in the right lung (C) and for normal lung tissue from the same patient (D). The final calculated values were 1.0 (median, 1.9) for R_{lac} and 1.8 (median, 2.5) for R_{cho}. Lac = lactate; Cho = choline.

(*13,23,24*), who found that a higher lactate concentration means poorer survival probabilities in human cervical cancers and a higher incidence of metastasis in head and neck tumors. In the present study, although the survival analysis showed that survival was generally longer for patients with a lower R_{lac}, the difference did not reach statistical significance either in the disease-free or the overall survival analysis. Therefore, compared with the significant correlation between ^{18}F-FDG uptake and disease-free survival probabilities (P = 0.004), these results demonstrated that R_{lac} is not a good indicator of prognosis in patients with lung adenocarcinoma. In addition, no significant correlation was found between R_{lac} and ^{18}F-FDG uptake in this study. This discordance has various possible reasons. On the one hand, although lactate production is known to be higher in proliferating cells than in quiescent cells (*25*), some reports have suggested that ^{18}F-FDG uptake may not necessarily correlate with lactate production (*26*), because increased glucose use may be due to increased activity of the pentose phosphate shunt for increased DNA synthesis (*27*). On the other hand, because previous studies have shown that glucose transporter activity is the major rate-limiting step of ^{18}F-FDG uptake in some tumors (*28,29*), including non–small cell lung cancer (*30*), those previous findings may partially account for our current result of no correlation between ^{18}F-FDG uptake and lactate concentration. However, the underlying mechanism of this discordance still needs further investigation.

Choline-containing compounds are involved in both the synthesis and the degradation of cellular membranes. Because choline is characteristically elevated in some malignant tumors, its concentration as measured by MRS has been expected to be an indicator of grade of malignancy (*14*) and prognosis (*15*). However, there have been some conflicting reports regarding the relationship between the two. Tamiya et al. found that choline concentration can reflect proliferative ability in astrocytomas but cannot predict the survival probabilities of the patients (*31*). Another multicenter study also concluded that choline concentration cannot differentiate types of gliomas (*32*). In the present study, we found that R_{cho} was not associated with prognosis or with any of the other parameters tested, including ^{18}F-FDG uptake and cell differentiation.

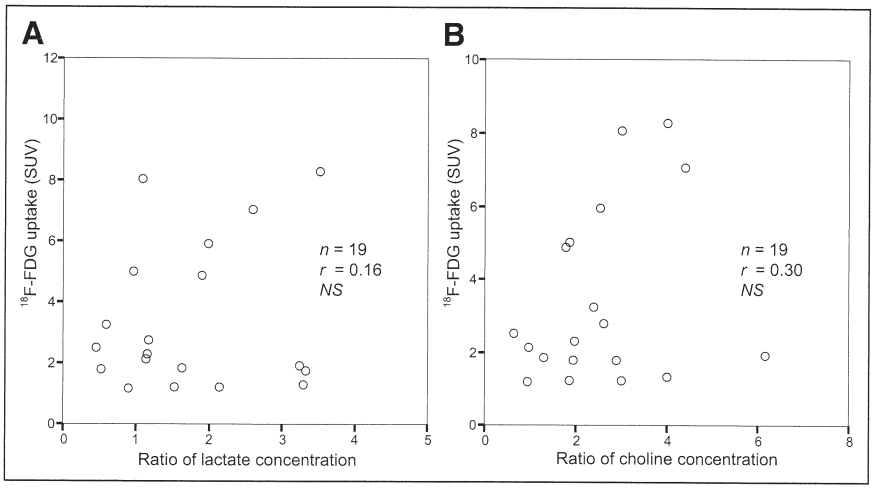

FIGURE 2. Relationship between ^{18}F-FDG uptake and R_{lac} (A) or R_{cho} (B) in lung adenocarcinoma. ^{18}F-FDG uptake showed no significant correlation with R_{lac} or R_{cho} in lung adenocarcinoma. NS = not statistically significant.

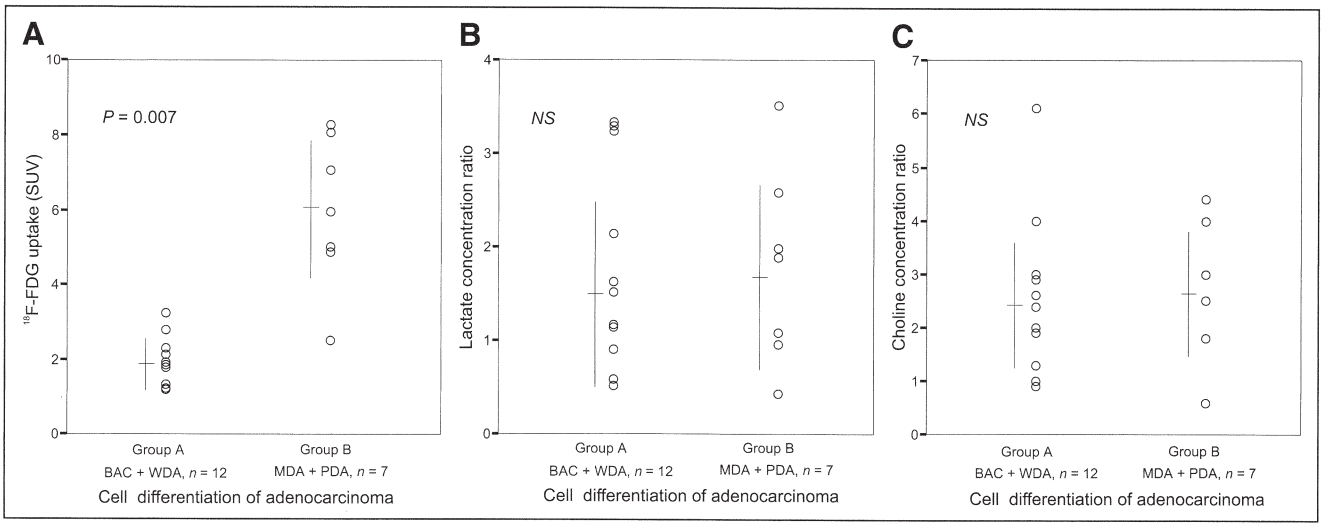

FIGURE 3. Relationship between cell differentiation and ^{18}F-FDG uptake, R_{lac}, and R_{cho} in lung adenocarcinoma. The mean SUV of group A (BAC + WDA) was significantly lower than that of group B (MDA + PDA) (A), whereas the mean R_{lac} (B) and R_{cho} (C) were not significantly different between the 2 groups. NS = not statistically significant.

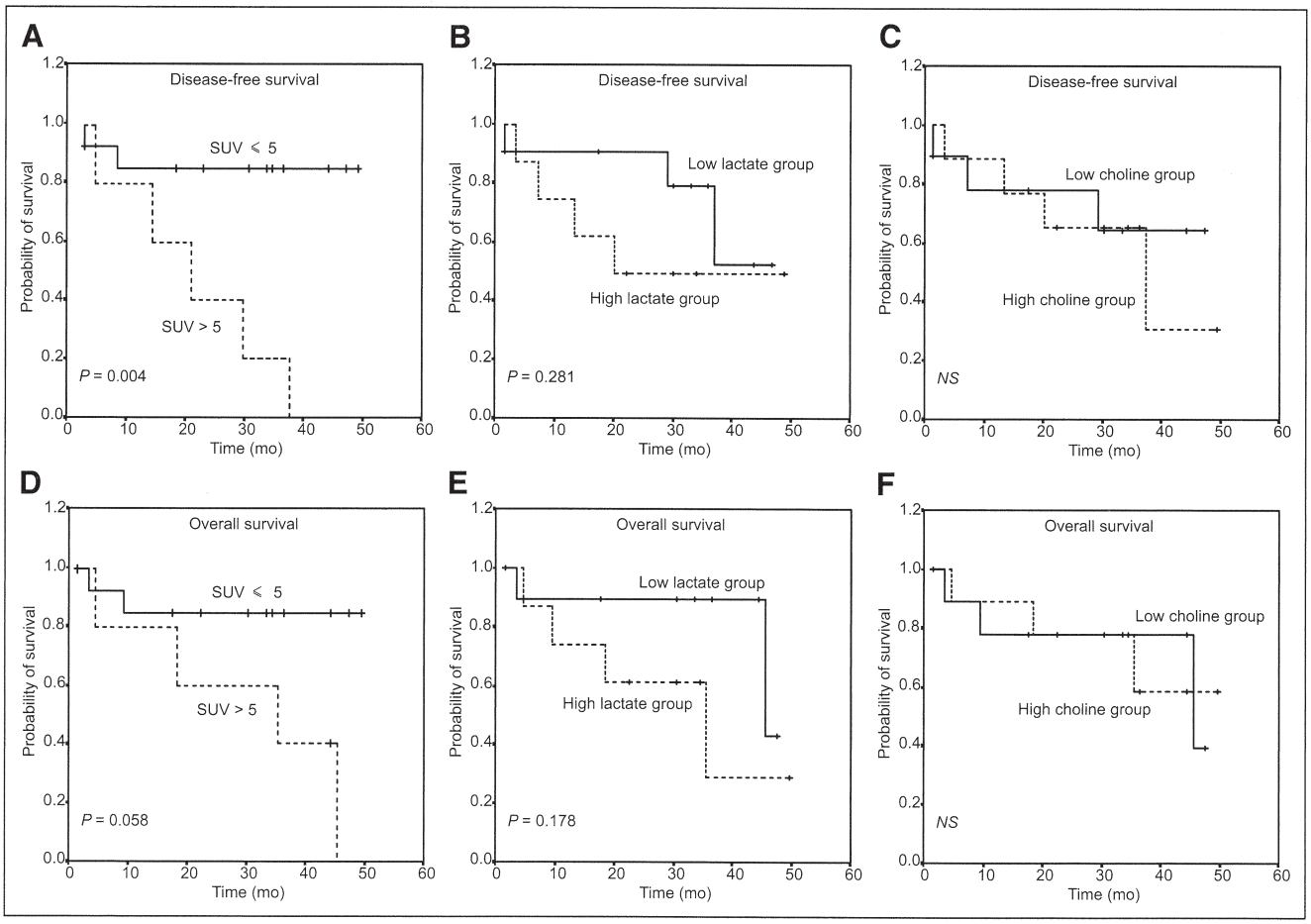

FIGURE 4. Kaplan–Meier plots showing disease-free (A–C) and overall (D–F) survival probabilities of patients with high or low SUV (A and D), high or low R_{lac} (B and E), and high or low R_{cho} (C and F). An SUV of 5 was used as cutoff value for ^{18}F-FDG uptake, and median levels were used as cutoff values for R_{lac} and R_{cho}. NS = not statistically significant.

On the whole, our results show that ^{18}F-FDG uptake is a better indicator of prognosis in patients with lung adenocarcinoma than are R_{lac} and R_{cho} measured by in vitro MRS. The results also show that ^{18}F-FDG uptake correlates significantly with cell differentiation ($P = 0.007$), whereas R_{lac} and R_{cho} have no correlation with it. To the best of our knowledge, there have been no previous reports on the relationship between lactate concentration, choline concentration, and prognosis in lung adenocarcinoma. Therefore, although the predictive value in lung adenocarcinoma is still obscure, lactate concentration still deserves attention, considering the importance of energy metabolism in tumor cells.

We realize that this study was limited by its small sample size—only 19 patients. Therefore, it was difficult to conclude whether R_{lac} can predict the outcome of lung adenocarcinoma in a larger number of patients. However, the preliminary results show that, compared with ^{18}F-FDG uptake, R_{lac} and R_{cho} are not good indicators of survival probability in lung adenocarcinoma. This study also did not include other types of lung cancer. Because different results have been obtained for some types of squamous cell carcinoma, further studies including patients with squamous cell carcinoma are needed.

CONCLUSION

Our results showed no significant correlation between SUV and R_{lac} or R_{cho} in patients with lung adenocarcinoma. Compared with the lactate and choline concentration ratios measured by in vitro MRS, ^{18}F-FDG uptake is a better indicator of prognosis in patients with lung adenocarcinoma.

ACKNOWLEDGMENTS

This work was supported by a Grant of Collaborative Research from Kanazawa Medical University (C2003-2) and by a Grand-in-Aid for Cancer Research (12-4) from the Ministry of Health and Welfare, Japan.

REFERENCES

1. Warburg O. *The Metabolism of Tumors.* New York, NY: Richard Smith; 1931: 129–169.
2. Strauss LG, Conti PS. The applications of PET in clinical oncology. *J Nucl Med.* 1991;32:623–648.
3. Miller TR, Pinkus E, Dehdashti F, Grigsby PW. Improved prognostic value of ^{18}F-FDG PET using a simple visual analysis of tumor characteristics in patients with cervical cancer. *J Nucl Med.* 2003;44:192–197.
4. Franzius C, Bielack S, Flege S, Sciuk J, Jurgens H, Schober O. Prognostic significance of (18)F-FDG and (99m)Tc-methylene diphosphonate uptake in primary osteosarcoma. *J Nucl Med.* 2002;43:1012–1017.
5. Vesselle H, Schmidt RA, Pugsley JM, et al. Lung cancer proliferation correlates with [F-18]fluorodeoxyglucose uptake by positron emission tomography. *Clin Cancer Res.* 2000;6:3837–3844.
6. Higashi K, Ueda Y, Yagishita M, et al. FDG PET measurement of the proliferative potential of non-small cell lung cancer. *J Nucl Med.* 2000;41:85–92.
7. Pandit N, Gonen M, Krug L, Larson SM. Prognostic value of [^{18}F] FDG-PET imaging in small cell lung cancer. *Eur J Nucl Med Mol Imaging.* 2003;30:78–84.
8. Higashi K, Ueda Y, Arisaka Y, et al. ^{18}F-FDG uptake as a biologic prognostic factor for recurrence in patients with surgically resected non-small cell lung cancer. *J Nucl Med.* 2002;43:39–45.
9. Hicks RJ, Kalff V, MacManus MP, et al. (18)F-FDG PET provides high-impact and powerful prognostic stratification in staging newly diagnosed non-small cell lung cancer. *J Nucl Med.* 2001;42:1596–1604.
10. Dhital K, Saunders CA, Seed PT, O'Doherty MJ, Dussek J. [(18)F]Fluorodeoxyglucose positron emission tomography and its prognostic value in lung cancer. *Eur J Cardiothorac Surg.* 2000;18:425–428.
11. Lear JL. Glycolysis: link between PET and proton MR spectroscopic studies of the brain. *Radiology.* 1990;174:328–330.
12. Tarnawski R, Sokol M, Pieniazek P, et al. ^{1}H-MRS in vivo predicts the early treatment outcome of postoperative radiotherapy for malignant gliomas. *Int J Radiat Oncol Biol Phys.* 2002;52:1271–1276.
13. Walenta S, Wetterling M, Lehrke M, et al. High lactate levels predict likelihood of metastases, tumor recurrence, and restricted patient survival in human cervical cancers. *Cancer Res.* 2000;60:916–921.
14. Herminghaus S, Pilatus U, Moller-Hartmann W, et al. Increased choline levels coincide with enhanced proliferative activity of human neuroepithelial brain tumors. *NMR Biomed.* 2002;15:385–392.
15. Girard N, Wang ZJ, Erbetta A, et al. Prognostic value of proton MR spectroscopy of cerebral hemisphere tumors in children. *Neuroradiology.* 1998;40:121–125.
16. Hara T, Inagaki K, Kosaka N, Morita T. Sensitive detection of mediastinal lymph node metastasis of lung cancer with ^{11}C-choline PET. *J Nucl Med.* 2000;41:1507–1513.
17. Pieterman RM, Que TH, Elsinga PH, et al. Comparison of (11)C-choline and (18)F-FDG PET in primary diagnosis and staging of patients with thoracic cancer. *J Nucl Med.* 2002;43:167–172.
18. Khan N, Oriuchi N, Zhang H, et al. A comparative study of ^{11}C-choline PET and [^{18}F]fluorodeoxyglucose PET in the evaluation of lung cancer. *Nucl Med Commun.* 2003;24:359–366.
19. Utriainen M, Komu M, Vuorinen V, et al. Evaluation of brain tumor metabolism with [^{11}C]choline PET and ^{1}H-MRS. *J Neurooncol.* 2003;62:329–338.
20. Le Belle JE, Harris NG, Williams SR, Bhakoo KK. A comparison of cell and tissue extraction techniques using high-resolution ^{1}H-NMR spectroscopy. *NMR Biomed.* 2002;15:37–44.
21. Higashi K, Matsunari I, Ueda Y, et al. Value of whole-body FDG PET in management of lung cancer. *Ann Nucl Med.* 2003;17:1–14.
22. Higashi K, Ueda Y, Ayabe K, et al. FDG PET in the evaluation of the aggressiveness of pulmonary adenocarcinoma: correlation with histopathological features. *Nucl Med Commun.* 2000;21:707–714.
23. Schwickert G, Walenta S, Sundfor K, Rofstad E, Mueller-Klieser W. Correlation of high lactate levels in human cervical cancer with incidence of metastasis. *Cancer Res.* 1995;55:4757–4759.
24. Walenta S, Salameh A, Lyng H, et al. Correlation of high lactate levels in head and neck tumors with incidence of metastasis. *Am J Pathol.* 1997;150:409–415.
25. Burk D, Woods M, Hunter J. On the significance of glucolysis for cancer growth, with special reference to Morris rat hepatomas. *J Natl Cancer Inst.* 1967;38:839–863.
26. Terpstra M, High WB, Luo Y, de Graaf RA, Merkle H, Garwood M. Relationships among lactate concentration, blood flow and histopathologic profiles in rat C6 glioma. *NMR Biomed.* 1996;9:185–194.
27. Ikezaki K, Black KL, Conklin SG, Becker DP. Histochemical evaluation of energy metabolism in rat glioma. *Neurol Res.* 1992;14:289–293.
28. Waki A, Kato H, Yano R, et al. The importance of glucose transport activity as the rate-limiting step of 2-deoxyglucose uptake in tumor cells in vitro. *Nucl Med Biol.* 1998;25:593–597.
29. Higashi T, Tamaki N, Honda T, et al. Expression of glucose transporters in human pancreatic tumors compared with increased FDG accumulation in PET study. *J Nucl Med.* 1997;38:1337–1344.
30. Higashi K, Ueda Y, Sakurai A, et al. Correlation of Glut-1 glucose transporter expression with [^{18}F]FDG uptake in non-small cell lung cancer. *Eur J Nucl Med.* 2000;27:1778–1785.
31. Tamiya T, Kinoshita K, Ono Y, Matsumoto K, Furuta T, Ohmoto T. Proton magnetic resonance spectroscopy reflects cellular proliferative activity in astrocytomas. *Neuroradiology.* 2000;42:333–338.
32. Negendank WG, Sauter R, Brown TR, et al. Proton magnetic resonance spectroscopy in patients with glial tumors: a multicenter study. *J Neurosurg.* 1996; 84:449–458.

^{18}F-FDG Uptake by Primary Tumor as a Predictor of Intratumoral Lymphatic Vessel Invasion and Lymph Node Involvement in Non-Small Cell Lung Cancer: Analysis of a Multicenter Study

Kotaro Higashi, MD[1]; Kengo Ito, MD[2]; Yoshinori Hiramatsu, MD[3]; Tsutomu Ishikawa, MD[4]; Tsutomu Sakuma, MD[5]; Ichiro Matsunari, MD[6]; Gencho Kuga, MD[1]; Katsuyuki Miura, MD[7]; Takahiro Higuchi[8], MD; Hisao Tonami, MD[1]; and Itaru Yamamoto, MD[1]

[1]Department of Radiology, Kanazawa Medical University, Ishikawa, Japan; [2]Department of Biofunctional Research, National Institute for Longevity Sciences, Aichi, Japan; [3]Department of Thoracic Surgery, National Institute for Longevity Sciences, Aichi, Japan; [4]Department of Image Diagnosis, Tochigi Prefectural Cancer Center, Tochigi, Japan; [5]Department of Respiratory Surgery, Kanazawa Medical University, Ishikawa, Japan; [6]The Medical and Pharmacological Research Center Foundation, Ishikawa, Japan; [7]Department of Public Health, Kanazawa Medical University, Ishikawa, Japan; and [8]Department of Radiology, Kanazawa Cardiovascular Hospital, Ishikawa, Japan

Intratumoral lymphatic vessel invasion and lymph node involvement are important factors in the planning of therapeutic strategies, particularly limited surgical resection in patients with non-small cell lung cancer. ^{18}F-FDG uptake within the primary lesion correlates with aggressiveness on PET studies. The more metabolically active the tumor, the more aggressive are the findings. The aim of this multicenter study was to determine whether ^{18}F-FDG uptake of the primary tumor is a predictor of intratumoral lymphatic vessel invasion and lymph node metastasis in patients with non-small cell lung cancer. **Methods:** One hundred thirty-two patients with lung cancer were studied. All patients underwent a thoracotomy within 4 wk of the ^{18}F-FDG PET study. A 3-point visual scoring system (low, moderate, or high grade in comparison with mediastinal activity) was used to interpret ^{18}F-FDG uptake within the primary lesions. The degree of ^{18}F-FDG uptake in the primary tumor was correlated with the incidence of intratumoral lymphatic vessel invasion and lymph node involvement. Multivariate analysis was performed with logistic multivariate analysis to assess the joint effects and interactions of the variables (age, sex, tumor size, histology, and ^{18}F-FDG uptake) on intratumoral lymphatic vessel invasion and lymph node involvement. **Results:** Intratumoral lymphatic vessel invasion and lymph node involvement were found in 7.1% and 5.9%, respectively, of the patients classified in the low-grade group, and in 14.3% and 10.0%, respectively, of the patients classified in the moderate-grade group. In contrast, of the patients classified in the group with high ^{18}F-FDG uptake, intratumoral lymphatic vessel invasion and lymph node involvement were found in 39.7% and 38.9%, respectively. Multivariate analysis showed that only ^{18}F-FDG uptake was a significant factor for intratumoral lymphatic vessel invasion and that tumor size and ^{18}F-FDG uptake were significant factors for lymph node involvement. Of the patients in the high-grade group whose tumors were classified as ≥3 cm in size, lymph node involvement was found in 51.5%. In contrast, of the patients in the low- to moderate-grade group whose tumors were classified as <3 cm in size, lymph node involvement was found in only 9.1% ($P < 0.0001$). **Conclusion:** Patients with a low to moderate ^{18}F-FDG uptake in the primary lesion had a significantly lower risk of concurrent intratumoral lymphatic vessel invasion and nodal involvement than did patients with a high ^{18}F-FDG uptake. In patients with non-small cell lung cancer, ^{18}F-FDG uptake by the primary tumor is a strong predictor of intratumoral lymphatic vessel invasion and lymph node metastasis.

Key Words: lung cancer; ^{18}F-FDG PET; nodal involvement

J Nucl Med 2005; 46:267–273

Lymph node involvement is an important prognostic factor in lung cancer without distant metastases (*1*). Patients without metastatic lymph nodes, or with only intrapulmonary or hilar lymph nodes, are generally considered candidates for straightforward resection. Intratumoral lymphatic vessel invasion is also important in the evaluation of lung cancer, because intratumoral lymphatic vessel invasion reflects tumor aggressiveness and is directly associated with lymph node involvement. Patients with intratumoral lymphatic vessel invasion had recurrence of the disease, and died earlier, than did those without (*2*). Thus, intratumoral

Received Apr. 5, 2004; revision accepted Sep. 17, 2004.

For correspondence or reprints contact: Kotaro Higashi, MD, Department of Radiology, Kanazawa Medical University, 1-1, Daigaku, Uchinada, Kahoku-gun, Ishikawa, 920-0293, Japan.

E-mail: h550208@kanazawa-med.ac.jp

lymphatic vessel invasion was also associated with a poor prognosis (*3,4*).

Both intratumoral lymphatic vessel invasion and lymph node involvement are important factors in the planning of therapeutic strategies, particularly limited surgical resection in patients with non-small cell lung cancer (*5*). Ichinose et al. (*5*) reported that 44% of tumors showed lymphatic vessel invasion in patients with resected non-small cell lung cancer classified as pathologic stage I located at the periphery of the lung. If we could select patients with tumors without intratumoral lymphatic vessel invasion and lymph node involvement, limited resection might successfully be performed without local recurrence (*5*).

Matsuguma et al. (*6*) reported that the area of ground-glass opacity on thin-section CT scans is a strong predictor of intratumoral lymphatic vessel invasion and lymph node metastasis in patients with clinical T1 N0 M0 adenocarcinoma and thus could be a useful index for planning a limited surgical resection for these patients. This excellent strategy is, however, applicable only to patients with lung adenocarcinoma.

^{18}F-FDG uptake within the primary lesion has been shown to correlate with aggressiveness (*7*) and survival (*8*) on PET studies of patients with non-small cell lung cancer. The more metabolically active the tumor, the more aggressive it is, and the worse the outcome. Recently, Vesselle et al. (*9*) reported that the metabolic activity of the primary tumor and tumor size are important variables in ^{18}F-FDG PET interpretation for non-small cell lung cancer, as they affect the likelihood of malignant involvement in nodes. However, the relationship between the metabolic activity of the primary tumor and intratumoral lymphatic vessel invasion is unknown.

The aim of this study was to determine whether a correlation exists among the incidence of intratumoral lymphatic vessel invasion, nodal involvement, and ^{18}F-FDG uptake in primary lung cancer and to determine whether ^{18}F-FDG uptake by primary tumor is a predictor of intratumoral lymphatic vessel invasion and lymph node metastasis in patients with non-small cell lung cancer. We conducted a multicenter study to increase the sample size and to decrease bias.

MATERIALS AND METHODS

Patient Preparation

In this retrospective study, we included 132 patients who were referred for PET for preoperative staging of their suspected or proven lung cancer. None of the patients had received prior treatment. All patients underwent CT of the chest within 4 wk of the PET study for the staging of lung cancer. All 132 patients were considered to be potential candidates for surgical resection. Seventy-six men and 56 women (age range, 42–84 y) were enrolled in this study. All patients underwent sampling of multiple mediastinal lymph nodes on thoracotomy within 4 wk after the PET study. Written informed consent was obtained from all patients.

Imaging Protocol

In this multicenter study, PET was performed with 3 types of dedicated PET camera, either the Headtome IV (Shimazu) (n = 62), at Kanazawa Cardiovascular Hospital; the Advance (General Electric Medical Systems) (n = 56), at the Medical and Pharmacologic Research Center Foundation; or the ECAT HR (Siemens/CTI) (n = 14), at the National Institute for Longevity Sciences. All patients fasted for 6 h before the scanning. Blood (1 mL) was drawn for estimation of baseline blood glucose levels, and the data were recorded. ^{18}F-FDG was administered intravenously. The average injected dose of ^{18}F-FDG was 370 MBq. After a 40- to 50-min uptake period, an emission scan was acquired. Two-dimensional acquisition was used at 2 of the PET centers (Kanazawa Cardiovascular Hospital and the Medical and Pharmacologic Research Center Foundation), and 3-dimensional acquisition was used at the third PET center (National Institute for Longevity Sciences). Transmission scans of all subjects were obtained for attenuation correction. At 2 of the PET centers (Kanazawa Cardiovascular Hospital and National Institute for Longevity Sciences), filtered backprojection with measured attenuation correction was used for reconstruction. At the third PET center (the Medical and Pharmacologic Research Center Foundation), iterative reconstruction with segmented attenuation correction was used, applying the expectation maximization algorithm with ordered subsets (28 subsets and 2 iterations).

Data Analysis

^{18}F-FDG accumulation within the primary lung tumor on the attenuation- and decay-corrected images was graded independently. A 3-point visual scoring system (low, moderate, or high grade) was used to interpret the ^{18}F-FDG uptake within the primary lesions: low grade = less than mediastinal blood-pool activity, moderate grade = equal to mediastinal blood-pool activity, and high grade = much greater than mediastinal blood-pool activity. This is a modified method of Lowe et al. (*10*) and Vansteenkiste et al. (*1*).

Histologic Study

The nodal status was determined for each patient on the basis of the thoracotomy findings. Ipsilateral hilar and mediastinal sampling was performed during the thoracotomy. The surgically resected specimens were routinely fixed in 10% formalin and embedded in paraffin. All 5-mm sections were stained with hematoxylin–eosin and then examined by light microscopy for histology. The histologic sections of the primary tumor were also studied for evidence of intratumoral lymphatic vessel invasion using hematoxylin–eosin staining. To distinguish intratumoral lymphatic vessel invasion from blood vessel invasion, an elastica van Gieson's stain was also used. In 96 patients, the existence of intratumoral lymphatic vessel invasion in the primary tumor was confirmed histopathologically.

The degree of tracer uptake in the primary lesion was correlated with the existence of pathologic intratumoral lymphatic vessel invasion and nodal staging.

Statistical Analysis

Statistical analysis was performed using the SPSS software system (version 10.0; SPSS Inc.) for Windows (Microsoft). Univariate analysis was used to analyze the associations among the pathologic variables and age (≤60 y or >60 y), sex, tumor size (≤3 cm or >3 cm), histology (adenocarcinoma or nonadenocarci-

TABLE 1
Patient and Tumor Characteristics

Variable	*n*	%
Age		
≤60 y	34	25.8
>60 y	98	74.2
Sex		
Male	76	57.6
Female	56	42.4
Tumor size		
<3 cm	77	58.3
≥3 cm	55	41.7
Histology		
Adenocarcinoma	103	78.0
Squamous cell carcinoma	21	15.9
Adenosquamous cell carcinoma	5	3.8
Large cell carcinoma	2	1.5
Carcinoid	1	0.8
Pathologic N stage		
pN0	92	69.7
pN1	14	10.6
pN2	26	19.7
Pathologic stage		
IA	64	48.5
IB	24	18.2
IIA	3	2.3
IIB	10	7.6
IIIA	26	19.7
IIIB	5	3.8
Intratumoral lymphatic vessel invasion		
Negative	66	68.8
Positive	30	31.2
^{18}F-FDG uptake		
Low	17	12.9
Moderate	20	15.1
High	95	72.0

noma), and ^{18}F-FDG uptake by the primary tumor (low to moderate grade or high grade). Multivariate analysis was performed with logistic multivariate analysis to assess the joint effects and interactions of the variables on intratumoral lymphatic vessel invasion and lymph node involvement. Cox proportional-hazards regression was used to calculate the multivariate-adjusted relative risks of incidence and the corresponding 95% confidence intervals for baseline ^{18}F-FDG uptake categories. The multivariate-adjusted relative risks were adjusted for sex, age, lesion size, and histology.

RESULTS

In the diagnosis of the N stage, the sensitivity, specificity, accuracy, positive predictive value, and negative predictive value for ^{18}F-FDG PET were 76.9%, 89.1%, 85.5%, 75.0%, and 90.1%, respectively.

Tumor characteristics are shown in Table 1. The tumor size was measured pathologically. The diameters of the primary lung tumors ranged from 0.8 to 12.0 cm. Fifty-five (41.7%) of the lung tumors were ≥3 cm in diameter (Table 1). Of the remaining 77 lung tumors (58.3%), 48 (36.4%) were 2.0–2.9 cm and 29 (21.9%) were <2 cm. Regarding the degree of ^{18}F-FDG uptake in the primary lesions, 17 tumors (12.9%) were classified as low grade, 20 (15.1%) as moderate grade, and 95 (72.0%) as high grade (Table 1).

Intratumoral lymphatic vessel invasion and lymph node involvement were found in 7.1% and 5.9%, respectively, of the patients classified in the low-grade group and in 14.3% and 10.0%, respectively, of the patients classified in the moderate-grade group (Table 2). In the patients classified in the low- and moderate-grade groups, the lymph node involvement was microscopic. In contrast, of the patients classified in the group with high ^{18}F-FDG uptake, intratumoral lymphatic vessel invasion and lymph node involvement were found in 39.7% and 38.9%, respectively (Table 2). Thus, patients with a low ^{18}F-FDG uptake in the primary lesion had a significantly decreased risk of concurrent intratumoral lymphatic vessel invasion and lymph node metastasis than did patients with a high ^{18}F-FDG uptake (P = 0.028 and P = 0.010, respectively) (Table 2).

In univariate analysis, sex and ^{18}F-FDG uptake (low- to moderate-grade group or high-grade group) were factors significantly associated with intratumoral lymphatic vessel invasion (Table 3). However, in multivariate analysis, only ^{18}F-FDG uptake was significantly associated with intratumoral lymphatic vessel invasion (Table 3).

In univariate analysis, sex, tumor size (≤3 cm or >3 cm), histology (adenocarcinoma or nonadenocarcinoma), and ^{18}F-FDG uptake (low- to moderate-grade group or high-grade group) were factors significantly associated with lymph node involvement (Table 4). However, in multivariate analysis, tumor size and ^{18}F-FDG uptake were factors significantly associated with lymph node involvement (Ta-

TABLE 2
Risk for Intratumoral Lymphatic Vessel Invasion and Lymph Node Involvement Based on ^{18}F-FDG Uptake

Uptake	Intratumoral lymphatic vessel invasion			Significance (vs. low)	Lymph node involvement			Significance (vs. low)
	−	+	%		−	+	%	
Low	13	1	7.1		16	1	5.9	
Moderate	12	2	14.3	NS	18	2	10.0	NS
High	41	27	39.7	P = 0.028	58	37	38.9	P = 0.010

− = negative; + = positive; NS = not statistically significant.

TABLE 3
Univariate and Multivariate Analysis of Factors Associated with Intratumoral Lymphatic Vessel Invasion

Variable	Intratumoral lymphatic vessel invasion			Univariate		Multivariate	
	−	+	%	RR (95% CI)	Significance	RR (95% CI)	Significance
Age							
≤60 y	15	9	37.5	0.69 (0.26–1.81)	NS	0.32 (0.08–1.23)	NS
>60 y	51	21	29.2				
Sex							
Male	28	21	42.9	3.17 (1.26–7.95)	$P = 0.014$	2.40 (0.86–6.71)	NS
Female	38	9	19.1				
Tumor size							
<3 cm	42	13	26.3	2.29 (0.95–5.51)	NS	1.39 (0.49–3.98)	NS
≥3 cm	24	17	41.5				
Histology							
Adenocarcinoma	52	24	31.6	1.08 (0.37–3.14)	NS	1.79 (0.52–6.13)	NS
Nonadenocarcinoma	14	6	30.0				
^{18}F-FDG uptake							
Low–moderate	25	3	10.7	5.49 (1.51–20.0)	$P = 0.010$	7.43 (1.51–36.5)	$P = 0.014$
High	41	27	39.7				

− = negative; + = positive; RR = relative risk; CI = confidence interval; NS = not statistically significant.

ble 4). Of the patients in the high-grade group whose tumors were classified as ≥3 cm in size, lymph node involvement was found in 51.5% (Table 5). In contrast, of the patients in the low- to moderate-grade group whose tumors were classified as <3 cm in size, lymph node involvement was found in only 9.1% ($P < 0.0001$) (Table 5).

The multivariate-adjusted relative risks for the incidence of intratumoral lymphatic vessel invasion and lymph node metastases were 7.43 and 4.46 for the low- to moderate-grade group and high-grade group, respectively (Tables 3 and 4).

Thus, a significant correlation exists among the incidence of intratumoral lymphatic vessel invasion, nodal involvement, and ^{18}F-FDG uptake in primary lung cancer. Patients with a low to moderate ^{18}F-FDG uptake in the primary lesion had a significantly decreased risk of concurrent intratumoral lymphatic vessel invasion and lymph node metastasis than did patients with high ^{18}F-FDG uptake.

TABLE 4
Univariate and Multivariate Analysis of Factors Associated with Lymph Node Involvement

Variable	Lymph node involvement			Univariate		Multivariate	
	−	+	%	RR (95% CI)	Significance	RR (95% CI)	Significance
Age							
≤60 y	25	9	26.5	1.28 (0.54–3.08)	NS	0.55 (0.19–1.60)	NS
>60 y	67	31	31.6				
Sex							
Male	47	29	38.2	2.52 (1.13–5.65)	$P = 0.024$	1.42 (0.57–3.49)	NS
Female	45	11	19.6				
Tumor size							
<3 cm	63	14	18.2	4.03 (1.84–8.84)	$P < 0.0001$	2.51 (1.05–5.99)	$P = 0.037$
≥3 cm	29	26	47.3				
Histology							
Adenocarcinoma	78	26	25.0	0.33 (0.14–0.79)	$P = 0.013$	0.49 (0.18–1.32)	NS
Nonadenocarcinoma	14	14	50.0				
^{18}F-FDG uptake							
Low–moderate	34	3	8.1	7.23 (2.07–25.2)	$P = 0.002$	4.46 (1.14–17.5)	$P = 0.032$
High	58	37	38.9				

− = negative; + = positive; RR = relative risk; CI = confidence interval; NS = not statistically significant.

TABLE 5
Risk for Lymph Node Involvement Based on Tumor Size and ^{18}F-FDG Uptake

Group	Tumor size		^{18}F-FDG uptake	Lymph node involvement			Significance (vs. a)
				−	+	%	
a	≥3 cm	and	High	25	26	51.5	
b	≥3 cm	and	Low–moderate	4	0	0	NS
c	<3 cm	and	High	33	11	25.0	0.012
d	<3 cm	and	Low–moderate	30	3	9.1	$P < 0.0001$

− = negative; + = positive; NS = not statistically significant.
c vs. d: $P = 0.084$.

DISCUSSION

The principal finding of this study is that a significant correlation exists among the incidence of intratumoral lymphatic vessel invasion, nodal involvement, and ^{18}F-FDG uptake by the primary tumor. This study indicated that low to moderate ^{18}F-FDG uptake by the primary tumor led to a significantly and independently decreased risk of intratumoral lymphatic vessel invasion and lymph node metastases. Patients whose lung cancer showed high ^{18}F-FDG uptake had a 4.46- to 7.43-fold higher risk of intratumoral lymphatic vessel invasion and lymph node metastases after multivariate adjustment than did patients whose lung cancer showed low to moderate ^{18}F-FDG uptake. These phenomena can be explained by the fact that the greater the ^{18}F-FDG uptake is, the higher is the malignant grade. ^{18}F-FDG is avidly taken up by tumor cells because cancer tissue consumes a large amount of glucose as an energy source. ^{18}F-FDG uptake reflected cell dedifferentiation (*11*), proliferative potential (*12*), aggressiveness (*7*), and prognosis (*8*) in patients with lung adenocarcinoma.

The Lung Cancer Study Group reported the results of a prospective randomized trial comparing limited resection with lobectomy for the management of patients with T1 N0 (*13*). A total of 247 patients were eligible for analysis. The limited-resection group had a significantly higher local recurrence rate than did the lobectomy group. The Lung Cancer Study Group therefore concluded that limited resection should not be recommended as the resection of choice for patients with T1 N0 disease. Ichinose et al. (*5*) reported that 44% of tumors showed intratumoral lymphatic vessel invasion in patients with resected non-small cell lung tumors classified as pathologic stage I located at the periphery of the lung. They speculated that this was the main reason that the limited-resection group had a higher local recurrence rate in the Lung Cancer Study Group trial. Others reported that intratumoral lymphatic vessel invasion correlated with a poor prognosis in patients with non-small cell lung cancer (*2–4*). This finding suggested that intratumoral lymphatic vessel invasion reflected tumor aggressiveness. Therefore, if we could select patients with tumors without lymphatic invasion, limited resection might successfully be performed without local recurrence. In our series, tumors with a low to moderate ^{18}F-FDG uptake had a low incidence of intratumoral lymphatic vessel invasion, and multivariate analysis showed that only ^{18}F-FDG uptake was a significant factor for intratumoral lymphatic vessel invasion. Among patients with non-small cell lung cancer, ^{18}F-FDG uptake by lung cancer was related to the aggressiveness of the tumor, independent of tumor size. This finding suggests that ^{18}F-FDG uptake is an important factor in the planning of appropriate surgical treatment, especially less invasive surgical intervention. Limited resection might successfully be performed without recurrence on patients whose lung cancer shows low ^{18}F-FDG uptake.

Several studies have shown that ^{18}F-FDG PET is superior to CT in the staging of mediastinal disease, with a reported sensitivity and specificity of 67%–91% and 82%–96%, respectively (*14*). Although ^{18}F-FDG PET may accurately establish lymph node staging in lung cancer patients, there are drawbacks to PET staging. ^{18}F-FDG PET staging of the mediastinum remains challenging because of the decreased specificity caused by ^{18}F-FDG accumulation in inflamed lymph nodes and silicotic nodes, which can lead to a false-positive interpretation (*15*). Conversely, the lack of sufficient ^{18}F-FDG in lymph nodes with minimal metabolic involvement can result in a false-negative interpretation. Gupta et al. (*16*) reported that the false-negative rate was 8% and the false-positive rate was 13%. Vansteenkiste et al. (*1*) demonstrated that the range of ^{18}F-FDG uptake overlaps significantly for both inflammatory and malignant nodes. Therefore, mediastinoscopy is still used for decisions on resectability status, as it depends on the presence of N2/N3 disease.

Recently, Vesselle et al. (*9*) reported that ^{18}F-FDG uptake by the primary tumor and tumor size are important variables in ^{18}F-FDG PET interpretation for non-small cell lung cancer, as they affect the likelihood of malignant involvement in hypermetabolic nodes. The size of a non-small cell lung tumor significantly influenced the incidence of malignant mediastinal adenopathy, with larger tumors being more likely to have nodal involvement than smaller tumors (*9*). These data appear to agree with many previous studies that generally showed a higher risk with increased T stage (*17,18*). The larger the primary tumor, the greater is the

likelihood that it has spread to the lymph nodes (*17,18*). ^{18}F-FDG uptake of the primary tumor is a variable that depends on the aggressiveness of lung adenocarcinoma (*7*). In our current study, ^{18}F-FDG uptake and tumor size were found to be significant factors for lymph node involvement in both univariate and multivariate analyses. Of the patients in the high-grade group whose tumors were classified as ≥3 cm in size, lymph node involvement was found in 51.5%; in contrast, of the patients in the low- to moderate-grade group whose tumors were classified as <3 cm, lymph node involvement was found in only 9.1% ($P < 0.0001$). These phenomena support the results of Vesselle et al. (*9*) and suggest that a small lesion with a low ^{18}F-FDG uptake may obviate mediastinoscopy.

This study had several limitations. First, a visual grading system was used to interpret ^{18}F-FDG uptake within the primary lesions, and the SUV threshold was not used. We selected a multicenter study to increase the sample size and to decrease bias, but the disadvantage of this strategy was the difficulty of obtaining unity in methodology. This was the main reason that the data were not analyzed using SUV threshold in the current study. SUV measurements are affected by the applied methods for both image reconstruction and attenuation correction (*19,20*). Iterative reconstruction with segmented attenuation correction resulted in significantly higher mean SUVs and maximum SUVs than those resulting from filtered backprojection with measured attenuation correction (*19,20*). This finding should be considered when serial PET studies are performed on cancer patients. Moreover, if SUV is used for tissue characterization, different cutoff values should be applied, depending on the chosen method of acquisition, image reconstruction, and attenuation correction. In the current multicenter study, filtered backprojection with measured attenuation correction was used for reconstruction at 2 of the PET centers. However, iterative reconstruction with segmented attenuation correction was used at the third PET center. In addition, the use of 3-dimensional acquisition rather than 2-dimensional acquisition also could potentially influence the accuracy of SUV measurements (*20*). In the current multicenter study, 2-dimensional acquisition was used at 2 of the PET centers, and 3-dimensional acquisition was used at the third PET center. Finally, it is uncertain whether and to what degree the geometry and specifications of different PET tomographs from different manufacturers might affect the accuracy and reproducibility of SUV measurements (*20*). In the current multicenter study, PET was performed with 3 types of dedicated PET cameras. Therefore, the SUV threshold was not adequate in the current multicenter study, and the data were analyzed using a visual grading system. Lowe et al. (*10*) reported that SUV and visual evaluations are equally accurate methods of ^{18}F-FDG PET data analysis in the differentiation of malignant from benign focal pulmonary abnormalities. This study showed that ^{18}F-FDG uptake in the mediastinum can be used as an accurate reference for visual interpretation. The researchers evaluated lesion uptake relative to mediastinal uptake to provide a distinct reference for assessment. Lesion uptake greater than mediastinal uptake most likely represents a malignant process. In the current study, a modified method of Lowe et al. was used to interpret the ^{18}F-FDG uptake within the primary lesions. Vansteenkiste et al. (*1*) also reported that a visual scale is as accurate as the use of an SUV threshold in distinguishing between benign and malignant lymph nodes. Therefore, in this multicenter study, a visual scale was found to be more adequate than the SUV threshold.

Second, the area of ground-glass opacity on thin-section CT scans was reported to be a strong predictor of intratumoral lymphatic vessel invasion and lymph node metastasis in patients with clinical T1 N0 M0 adenocarcinoma (*6*) and thus could be a useful index for planning a limited surgical resection for these patients. It is necessary to compare the ^{18}F-FDG uptake of primary tumors on PET with the area of ground-glass opacity in the primary tumor on CT as predictors of intratumoral lymphatic vessel invasion and lymph node metastasis.

In our series, tumors with a low to moderate ^{18}F-FDG uptake had a low incidence of intratumoral lymphatic vessel invasion, and small lesions (<3 cm) with a low to moderate ^{18}F-FDG uptake had a low incidence of lymph node involvement. These results suggest that limited resection might successfully be performed without recurrence in patients whose lung cancer shows low ^{18}F-FDG uptake and that a small lesion with a low ^{18}F-FDG uptake may obviate mediastinoscopy. Further studies will be necessary to clarify this issue.

CONCLUSION

A significant correlation exists among the incidence of intratumoral lymphatic vessel invasion, nodal involvement, and ^{18}F-FDG uptake by the primary tumor in patients with non-small cell lung cancer. Patients with a low to moderate ^{18}F-FDG uptake in the primary lesion had a significantly decreased risk of concurrent intratumoral lymphatic vessel invasion and lymph node metastasis than did those with a high ^{18}F-FDG uptake. In patients with non-small cell lung cancer, ^{18}F-FDG uptake by the primary tumor is a strong predictor of intratumoral lymphatic vessel invasion and lymph node metastasis.

ACKNOWLEDGMENTS

This work was supported by a grant for collaborative research from Kanazawa Medical University (C2003-2); by a grant-in-aid for cancer research (12-4,16-5) from the Ministry of Health and Welfare, Japan; and by a grant-in-aid (50189750) for scientific research from the Ministry of Education.

REFERENCES

1. Vansteenkiste JF, Stroobants SG, De Leyn PR, et al. Lymph node staging in non-small-cell lung cancer with FDG-PET scan: a prospective study on 690 lymph node stations from 68 patients. *J Clin Oncol.* 1998;16:2142–2149.

2. Roberts TE, Hasleton PS, Musgrove C, et al. Vascular invasion in non-small cell lung carcinoma. *J Clin Pathol.* 1992;45:591–593.
3. Sayar A, Turna A, Solak O, et al. Nonanatomic prognostic factors in resected nonsmall cell lung carcinoma: the importance of perineural invasion as a new prognostic marker. *Ann Thorac Surg.* 2004;77:421–425.
4. Fu XL, Zhu XZ, Shi DR, et al. Study of prognostic predictors for non-small cell lung cancer. *Lung Cancer.* 1999;23:143–152.
5. Ichinose Y, Yano T, Yokoyama H, Inoue T, Asoh H, Katsuda Y. The correlation between tumor size and lymphatic vessel invasion in resected peripheral stage I non-small cell lung cancer: a potential risk of limited resection. *J Thorac Cardiovasc Surg.* 1994;108:684–686.
6. Matsuguma H, Yokoi K, Anraku M, et al. Proportion of ground-glass opacity on high-resolution computed tomography in clinical T1 N0 M0 adenocarcinoma of the lung: a predictor of lymph node metastasis. *J Thorac Cardiovasc Surg.* 2002;124:278–284.
7. Higashi K, Ueda Y, Ayabe K, et al. FDG PET in the evaluation of the aggressiveness of pulmonary adenocarcinoma: correlation with histopathological features. *Nucl Med Commun.* 2000;21:707–714.
8. Higashi K, Ueda Y, Arisaka Y, et al. F-18 FDG uptake as a biologic prognostic factor for recurrence in patients with surgically resected non-small cell lung cancer. *J Nucl Med.* 2002;43:39–45.
9. Vesselle H, Turcotte E, Linda W, Haynor D. Application of a neural network to improve nodal staging accuracy with F-18 FDG PET in non-small cell lung cancer. *J Nucl Med.* 2003;44:1918–1926.
10. Lowe VJ, Hoffman JM, DeLong DM, et al. Semiquantitative and visual analysis of FDG-PET images in pulmonary abnormalities. *J Nucl Med.* 1994;35:1771–1776.
11. Higashi K, Ueda Y, Seki H, et al. Fluorine-18-FDG PET imaging is negative in bronchioloalveolar lung carcinoma. *J Nucl Med.* 1998;39:1016–1020.
12. Higashi K, Ueda Y, Yagishita M, et al. FDG PET measurement of the proliferative potential of non-small cell lung cancer. *J Nucl Med.* 2000;41:85–92.
13. Ginsberg RJ, Rubinstein LV. Randomized trial of lobectomy versus limited resection for T1 N0 non-small cell lung cancer. Lung Cancer Study Group. *Ann Thorac Surg.* 1995;60:615–622.
14. Gould MK, Kuschner WG, Rydzak CE, et al. Test performance of positron emission tomography and computed tomography for mediastinal staging in patients with non-small-cell lung cancer: a meta-analysis. *Ann Intern Med.* 2003;139:879–892.
15. Konishi J, Yamazaki K, Tsukamoto E, et al. Mediastinal lymph node staging by FDG-PET in patients with non-small cell lung cancer: analysis of false-positive FDG-PET finding. *Respiration.* 2003;70:500–506.
16. Gupta NC, Tamim WJ, Graeber GG, Bishop HA, Hobbs GR. Mediastinal lymph node sampling following positron emission tomography with fluorodeoxyglucose imaging in lung cancer staging. *Chest.* 2001;120:521–527.
17. Takamochi K, Nagai K, Suzuki K, Yoshida J, Ohde Y, Nishiwaki Y. Clinical predictions of N2 disease in non-small cell lung cancer. *Chest.* 2000;117:1577–1582.
18. Ohta Y, Oda M, Wu J, et al. Can tumor size be a guide for limited surgical intervention in patients with peripheral non-small cell lung cancer? Assessment from the point of view of nodal micrometastasis. *J Thorac Cardiovasc Surg.* 2001;122:900–906.
19. Ramos CD, Erdi YE, Gonen M, et al. FDG-PET standardized uptake values in normal anatomical structures using iterative reconstruction segmented attenuation correction and filtered back-projection. *Eur J Nucl Med Mol Imaging.* 2001;28:155–164.
20. Schoder H, Erdi YE, Chao K, et al. Clinical implications of different image reconstruction parameters for interpretation of whole-body PET studies in cancer patients. *J Nucl Med.* 2004;45:559–566.

１．研究課題：悪性神経膠腫の分化誘導と遺伝子治療に関する研究（研究番号 C2003-3）

２．キーワード：１）悪性神経膠腫（glioblastoma）
２）分化誘導（induction of differentiation）
３）遺伝子治療（gene therapy）
４）HMGI-C

３．研究代表者：飯塚秀明・医学部・教授・脳脊髄神経治療学（脳神経外科学）
研究分担者：伊達孝保・医学部・教授・ゲノム医科学（生化学）
野島孝之・医学部・教授・病態診断医学（臨床病理学）
栗原孝行・総合医学研究所・講師・共同利用部門

４．研究目的

中枢神経に原発する腫瘍のなかで、悪性神経膠腫の治療成績は未だ不良である。現在、摘出手術・放射線・化学療法が治療の主体であるが、5 生率は 20%以下であり新たな治療法の開発が望まれる分野である。なかでも膠芽腫は、他の分化型神経膠腫と比べ最も予後が悪く、また分化型神経膠腫が膠芽腫へ悪性転化することも稀ならず経験される。腫瘍発生に関わる遺伝子発現の機構には、①特定の配列に結合する転写因子によるものと、②転写活性ドメインはなく、DNA に結合してその framework を変化させて転写複合体を形成し、その結果転写活性の亢進を生ずる architectural factor によるものがある。Architectural factor のひとつに HMGI-C 蛋白が知られているが、間葉系腫瘍ではすでに *HMGI-C* 遺伝子の転位が確認されており、この因子が細胞の分化および腫瘍発生やその分化度に関与している可能性が考えられている。

膠芽腫は、星細胞が起源とされているが、いわゆる脱分化が著しく、細胞起源を特定できる形態学的特徴は失われ、著しい多型性を呈し、細胞の分化に破綻をきたした状態であることは知られている。即ち、HMGI-C 蛋白・遺伝子などの細胞分化に関与する architectural factor の異常が生じていることが予想され、逆に、膠芽腫細胞に HMGI-C 蛋白を発現させ分化した星細胞へと誘導することによる治療の可能性が期待できる。本研究は、星細胞腫などの分化型神経膠腫と膠芽腫における HMGI-C 蛋白・遺伝子の発現の差異を検討し、膠芽腫の遺伝子治療への臨床応用の可能性について検討することを目的とする。

５．研究計画

＜全体計画＞

申請者らは、preliminary study として原発性脳腫瘍の摘出生検組織での HMGI－C 蛋白・遺伝子発現を検討した結果、分化型星細胞腫では HMGI－C 蛋白が過剰発現しているのに対し、膠芽腫ではその発現がほとんどみられず、また、*HMGI－C* 遺伝子の発現も同様であることを観察している。また、２例の悪性転化した膠芽腫では、HMGI－C 蛋白・遺伝子の発現が消失していることを確認している。

以上の結果をもとに、本研究では以下のように計画している。

①臨床生検および剖検摘出組織で、さらに多数例での HMGI－C 蛋白・遺伝子発現の差異を検討し、その発現の差異による細胞分化の意義を明らかにする、②培養膠芽腫細胞への *HMGI－C* 遺伝子導入の試み、③*HMGI－C* 遺伝子を導入した膠芽腫細胞の細胞生物学的特徴の in vitro/in vivo での検討、④臨牀応用へ向けた *HMGI－C* 遺伝子導入の in vivo での検討、⑤臨床での遺伝子治療。

＜平成 15 年度計画＞

1．摘出生検および剖検脳からの腫瘍組織（分化型神経膠腫から悪性転化した膠芽腫例を含む）における HMGI－C 蛋白・遺伝子発現の検討

（1）分化型神経膠腫（星細胞腫・上衣腫・乏突起膠腫）と膠芽腫における HMGI－C 蛋白の発現の差異を、免疫組織化学および Western blot により解析する。

（2）遺伝子発現の差異の検討

摘出組織より total RNA および DNA を抽出し、*HMGI－C* 遺伝子の exon 1 と exon 3 に対するプライマーを用いた nested RT-PCR により遺伝子発現の差異を解析する。

2．培養膠芽腫細胞への *HMGI－C* 遺伝子導入

（1）培養膠芽腫細胞における *HMGI－C* 遺伝子発現の有無を nested RT-PCR で予め確認する。

（2）培養膠芽腫細胞への *HMGI－C* 遺伝子導入の試み

HMGI－C cDNA と ligation した plasmid vector を E.coli 内で増幅、精製し、培養膠芽腫細胞に transfection させる。

6．研究成果

HMGI-C に対する特異性の高い抗体を作成するために、HMGI-C とグルタチオン-S-トランスフェラーゼ（GST）の融合蛋白質を大腸菌で発現させ、GST とグルタチオンとの結合を利用して GST-HMGI-C 融合蛋白質を精製した。GST-HMGI-C 融合蛋白質をウサギに免疫し、GST-HMGI-C 融合蛋白質に対する抗血清を作成した。この抗血清は、ウェスタンブロット法で GST-HMGI-C 融合蛋白質、および動物細胞内の HMGI-C を検出したが、免疫染色法では、バックグラウンドが高く、動物細胞内の HMGI-C を検出することができなかった。

HMGI-C の発現を欠いた膠芽腫細胞株 T98G に、HMGI-C 発現プラスミドを導入し、テトラサイクリン濃度依存性に HMGI-C を発現する細胞株、T98GHMGI-C、を樹立した。上記の抗 HMGI-C 抗血清は、T98GHMGI-C 細胞の HMGI-C を、ウェスタンブロット法で検出することができたが、免疫染色法では検出することができなかった。光学顕微鏡による観察では、T98GHMGI-C 細胞と親細胞 T98G の間で明らかな形態の差は認められなかった。また細胞の増殖速度にも大きな差が認められなかった。

７．研究の考察・反省

HMGI-C を発現する膠芽腫細胞株 T98GHMGI-C を樹立した。T98GHMGI-C 細胞と親細胞 T98G の間で明らかな増殖速度の差が認められなかったことより、HMCI-C は細胞増殖抑制効果をもたないことが分かった。また、光学顕微鏡レベルでは、両細胞株の間で明らかな形態の差は認められなかった。しかし、HMCI-C と細胞分化の関係については、電子顕微鏡による形態観察や膠芽腫細胞の分化抗原の発現検討などを待たないと、はっきりした結論は出せないと考える。今後、両細胞株をそれぞれヌードマウスの脳内に移植し、両細胞株の腫瘍形成能の差を調べたい。

今回作成した抗 HMGI-C 抗血清は、ウェスタンブロット法では細胞内の HMGI-C を検出できたが、免疫染色法では検出できなかった。これが、摘出生検組織での HMGI-C 蛋白発現の実験を遅らせている原因である。今後、抗 HMGI-C 抗血清から、抗 HMGI-C 抗体を精製し、より特異的で高力価の抗体を用いて実験する予定である。

８．研 究 発 表

Akai T, Ueda Y, Sasagawa Y, Hamada T, Date T, Katsuda S, Iizuka H, Okada Y, Chada K. High mobility group I-C protein in astrocytoma and glioblastoma. Pathol Res Pract 2004 ; 200 : 619-624. (MLDB)

Available online at www.sciencedirect.com
SCIENCE DIRECT®
ELSEVIER
Pathology – Research and Practice 200 (2004) 619–624
PATHOLOGY
RESEARCH AND PRACTICE
www.elsevier.de/prp

ORIGINAL ARTICLE

High mobility Group I-C protein in astrocytoma and glioblastoma

Takuya Akai[a], Yoshimichi Ueda[b,*], Yasuo Sasagawa[a], Tomio Hamada[c], Takayasu Date[c], Shogo Katsuda[b], Hideaki Iizuka[a], Yasunori Okada[d], Kiran Chada[e]

[a]*Department of Neurosurgery, Kanazawa Medical University, Japan*
[b]*Department of Pathology, Kanazawa Medical University, 1-1 Daigaku, Uchinada-machi, Kahoku-gun, Ishikawa, 920-0293, Japan*
[c]*Department of Biochemistry, Kanazawa Medical University, Japan*
[d]*Department of Pathology, Keio University, Japan*
[e]*Department of Biochemistry, UMDNJ-Robert Wood Johnson Medical School, USA*

Abstract

High mobility group I-C (HMGI-C) protein is a non-histone DNA-binding factor that organizes active chromatin. This protein is expressed during the limited phase of embryonic development and may regulate the expression of genes critical for embryonic cell growth and differentiation. As embryonic mechanisms are also known to play a role in the development of some neoplasms, we investigated human brain tumors for the expression of HMGI-C to determine its role in the differentiation of glial cell tumors. Immunohistochemical analysis revealed HMGI-C in all of the low-grade astrocytomas, in 2 of 3 anaplastic astrocytomas (grade 3), but in only one of 8 glioblastomas. The results were confirmed at the mRNA level by nested reverse-transcription polymerase chain reaction analyses. Loss of HMGI-C was also demonstrated in a case of glioblastoma transformed from the low-grade astrocytoma strongly expressing HMGI-C protein. These results suggest that HMGI-C may be involved in the differentiation of glial tumor cells, and that loss of HMGI-C expression may contribute to the transformation of low-grade astrocytoma into glioblastoma.

Keywords: HMGI-C; Astrocytoma; Glioblastoma

Introduction

High mobility group (HMG) proteins are heterogeneous non-histone DNA-binding factors that organize active chromatin [10,11,30]. HMGI-C is a member of the HMGI family of HMG proteins and consists of 109 amino acids residues [21]. The HMGI-C gene is located on chromosome 12 [14]. HMGI-C is responsible for the correct three-dimensional configuration of protein–DNA complexes and plays a key role in DNA transcription [32]. Through protein–protein and protein–DNA interactions, HMGI-C organizes the framework of the nucleoprotein–DNA transcriptional complex. As this protein can change the conformation of DNA, HMGI-C has been referred to as an architectural factor [32]. Present in embryonic adrenal glands, HMGI-C levels diminish during development and are completely absent in the adult gland [10,34]. In murine studies, inactivation of HMGI-C resulted in a pygmy phenotype [33]. These reports suggest that HMGI-C regulates the expression of one or more genes that control embryonic cell growth and differentiation [35].

HMGI-C may also affect the expression of oncogenes and/or tumor suppressor genes. Investigators have reported the expression of HMGI-C in benign tumors,

*Corresponding author.
E-mail address: z-ueda@kanazawa-med.ac.jp (Y. Ueda).

0344-0338/$ - see front matter © 2004 Elsevier GmbH. All rights reserved.
doi:10.1016/j.prp.2004.06.008

such as lipoma [1] and leiomyoma [19,29], and in malignant tumors, such as breast cancer [26] and neuroblastoma [9].

Glial cell tumors range from the differentiated relatively slow-growing astrocytomas, whose histologic structure is homogeneous, to the highly invasive, rapidly growing glioblastomas, whose cell structure is poorly differentiated. Glioblastomas represent the most aggressive type of glial brain tumors. Treatment is rarely successful, and prognosis for patients is very poor, while patients with astrocytomas have better prognoses and longer survival [20].

To determine the role of HMGI-C in the differentiation of gliomas, we assayed human glioma tissue for the expression of HMGI-C gene at both the protein and the mRNA levels.

Materials and methods

Histology and immunohistochemical analysis

Tumor samples were surgically obtained from 19 patients with 20 primary brain tumors. Tissues were fixed with 4% paraformaldehyde for 16 h at 4 °C and prepared for paraffin-embedded sections. Sections of each tissue sample were stained with hematoxylin and eosin (H&E) and were evaluated under a standard light-microscope. An independent neuropathologist confirmed the tumor diagnoses.

Tumor tissue samples were prepared for immunohistochemical analysis according to the method of Hsu et al. [13]. Briefly, the tissue sections of low-grade astrocytomas (WHO grade 2; $n=9$), anaplastic astrocytomas (WHO grade; $n=3$), and glioblastomas (WHO grade; $n=8$) were subjected to 0.3% H_2O_2/methanol to inhibit internal peroxidase reactions, washed with phosphate-buffered saline (PBS), and heated in a microwave for 15 min at 500 W in citrate buffer. After washing in PBS, sections were incubated in 10% normal goat serum for 10 min at room temperature and then incubated with rabbit anti-HMGI-C polyclonal antibody at 4 °C overnight [34]. After washes in PBS, the sections were incubated with biotinylated goat anti-rabbit antibody for 1 h at room temperature. After washes in PBS, they were incubated with avidin for 30 min and developed with a peroxidase, 3,3′-diaminobenzidine. We also analyzed mouse fetal tissues, including brain, of various developmental stages ranging from postovulatory day 7 to day 13.

Nested RT-PCR analysis

RNA was prepared for RT-PCR according to the method of Nakamura et al. [18]. Total RNA was isolated from four surgical specimens (2 glioblastomas and 2 astrocytomas) by ISOGEN (Nippon Gene, Toyama, Japan). Each specimen was homogenized in ISOGEN and left for 5 min at room temperature. Chloroform that was equal to one-fifth volume of ISOGEN was added to the samples, and these were centrifuged at 12,000 rpm for 15 min at 4 °C. The RNA-containing supernatant was collected. The same amount of isopropyl alcohol was added to the samples, and these were left for 5 min at room temperature. This solution was centrifuged at 15,000 rpm for 15 min at 4 °C. The supernatant was removed, and 75% ethanol was added to the RNA pellet. After centrifugation at 3,000 rpm for 5 min at 4 °C, the pellet was dried in a vacuum. The dried pellet was then dissolved in RNase-free water, and the optical density of the solution at 260 nm was measured with a spectrophotometer to determine concentration.

The extracted RNA was treated with DNase to eliminate DNA contamination. The RNA extract was mixed with DNase buffer, RNasin, and RQ1Dnase (Promega, WI, USA), and incubated for 1 h at 37 °C and for 5 min at 90 °C. The volume was determined, and 2 M sodium acetic acid, phenol, and chloroform were added. The volume of 2 M sodium acetic acid added was equal to one-tenth of the sample's volume, and the volumes of phenol and chloroform were equal to one-half of the sample's volume. This RNA extract solution was left on ice for 5 min and centrifuged at 15,000 rpm for 15 min at 4 °C. The RNA-containing supernatant was collected, added to the same amount of isopropyl alcohol, and left for 5 min at room temperature. This procedure was repeated as above to measure the optical density of the RNA solution.

Nested RT-PCR was performed according to Geurts et al. [8]. cDNAs were prepared from 5 μg of total RNA by reverse transcriptase with a primer specific for exon 5 of HMGI-C gene (primer 95C3362, 5′-TAC AGC AGT TTT TCA CTA-3′). The cDNAs were amplified by the first PCR using primers specific for human HMGI-C gene (primer 31970-004, 5′-CCC AGC CCT ATC ACC TCA-3′; primer 32627-001, 5′-AAG ACC ATG GCA ATA CAG-3′). The products were amplified by the second PCR using primer 31970-005 (5′-CTC ATC TCC CGA AAG GTG-3′) and primer 3267-001. The conditions for the first PCR were as follows: 40 cycles at 94 °C for 1 min, 55 °C for 1 min, 72 °C for 1 min, followed by incubation at 72 °C for 5 min, and those for the second PCR were 30 cycles at 94 °C for 1 min, 60 °C for 1 min, 72 °C for 1 min, followed by incubation at 72 °C for 5 min. The products were electrophoresed on 2% agarose gels. The gels were incubated with ethidium bromide in a bath at room temperature for 15 min and observed in the dark for fluorescence. Sequences of the products were confirmed by direct sequencing using ABI-PRISM (Perkin–Elmer applied biosystems, CA,

USA). In all the samples examined, the quality of total RNA was evaluated by RT-PCR for G3PDH as described in detail by Nakamura et al. [18].

Results

Immunohistochemical analysis

All of the 8 astrocytoma speicmens showed positive reactions for HMGI-C intranuclearly. Most nuclei of the astrocytomas very strongly expressed HMGI-C. Two of 3 specimens of anaplastic astrocytoma also showed diffuse and strong expression of HMGI-C. By contrast, glioblastoma cells were negative for HMGI-C, although one of the 8 glioblastomas showed weak expression of HMGI-C focally (Fig. 1). No positive reaction was detected in non-neoplastic cells of the brain, including reactive astrocytes. In mouse fetuses between the 9th and 11th gestational day, mesenchymal cells in the subcutis and mesentery strongly expressed HMGI-C intranuclearly. Mouse fetal glial cells of the same gestational stage also expressed HMGI-C.

RT-PCR analysis

HMGI-C mRNA was detected at 380 base pairs (bps) in the astrocytoma tissues, but was not seen in the glioblastoma ones (Fig. 2). The direct sequence of the PCR product was confirmed to be the same as that reported in Gene Bank accession No. X92518.

HMGI-C expressions at different stages of astrocytoma in one and the same patient

We had an opportunity to study the expression of HMGI-C mRNA at different stages of astrocytoma in one and the same patient. On the first operation, the resected specimen was histologically diagnosed as astrocytoma, WHO grade 2. Two years later, the tumor recurred in this patient. A second operation was performed, and the histologic examination of the

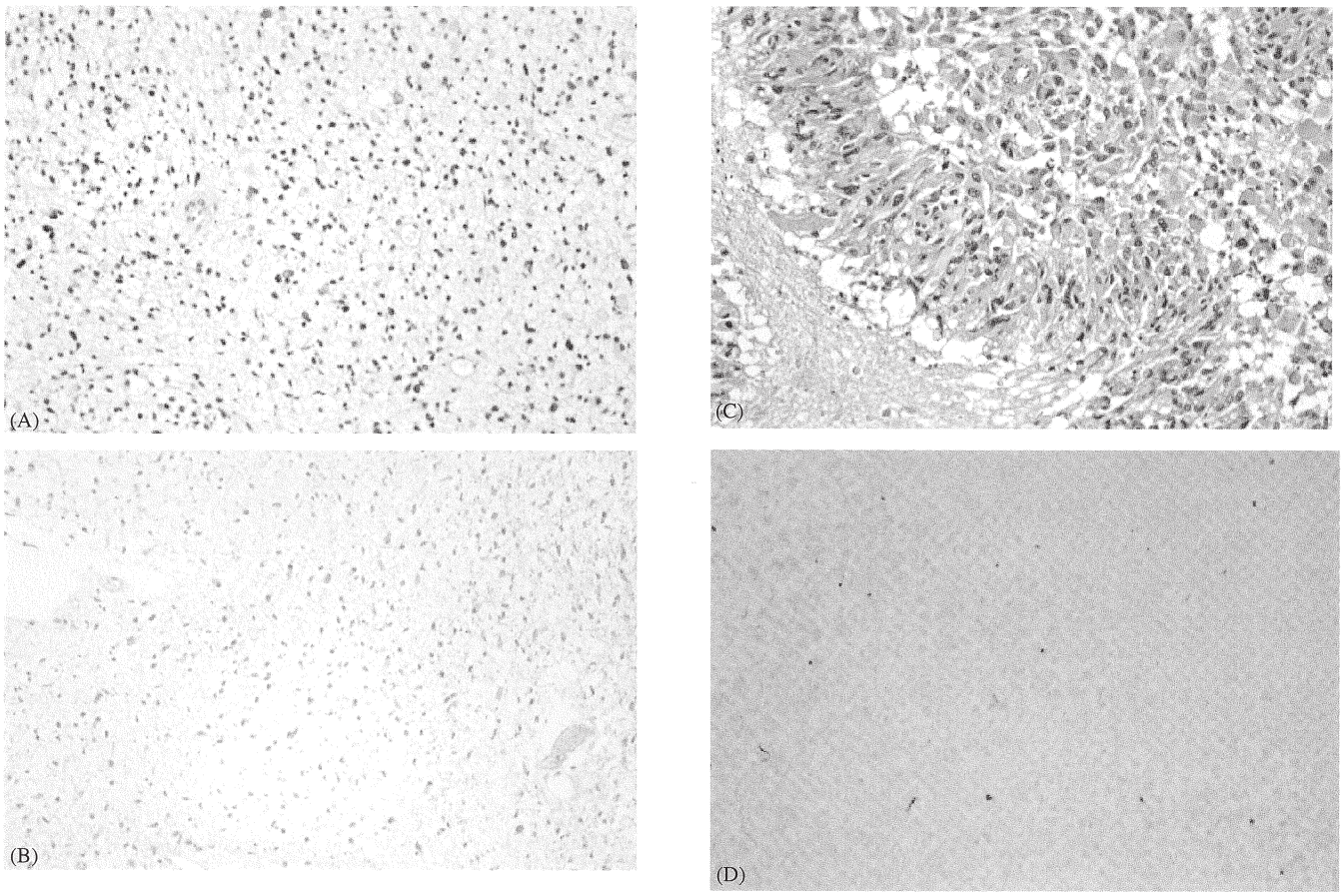

Fig. 1. Immunolocalization of HMGI-C in astrocytoma and glioblastoma tissues. Paraffin sections were immunostained with antibody against HMGI-C as described in Materials and methods. Staining the nuclei of astrocytoma cells reveals the presence of HMGI-C (B), whereas there was no staining in glioblastoma tissue (D). Astrocytoma cells (A) and glioblastoma cells (C) stained with hematoxylin and eosin.

recurrence revealed glioblastoma, WHO grade 4. RT-PCR disclosed expression of HMGI-C mRNA only in the astrocyoma (first operation), but not in the glioblastoma (second operation, Fig. 3).

Discussion

This study is the first to report on HMGI-C expression in brain astrocytic neoplasms. Our results showed that HMGI-C was expressed exclusively in the nuclei of the astrocytoma, not in those of the glioblastoma, and the sequential observation may suggest that expression of HMGI-C may get lost during the transformation into glioblastoma.

Expression of high mobility group HMGI (Y) protein, which is another member of non-histone chromatin-associated proteins, was reported in several human cancer cells [4,6]. However, HMGI-C has mostly been reported to be expressed in benign tumors, such as lipoma, uterine leiomyoma, fibroadenoma, salivary pleomorphic adenoma and pulmonary hamartoma, or in low grade malignant tumors, such as well-differentiated liposarcoma [1,12,19,27,29]. As high grade human malignant tumors, only neuroblastoma was disclosed to express HMGI-C [9]. Neuroblastoma sometimes occurs congenitally with other congenital abnormalities, and small neuroblastomas in infants less than 3 months of age undergo maturation and regress spontaneously. These findings suggest developmental abnormality-like features of neuroblastomas [24]. This may explain the positive expression of HMGI-C in neuroblastoma cells. Expression of elevated HMGI-C mRNA was noted in peripheral blood of human metastatic breast cancer [16,23,26], but was not confirmed in breast cancer cells. There are a few reports that animal cancer cell lines, such as mouse Lewig lung carcinoma and rat thyroid cancer cell line, require elevated HMGI-C expression during the course of malignant transformation [3,17,31].

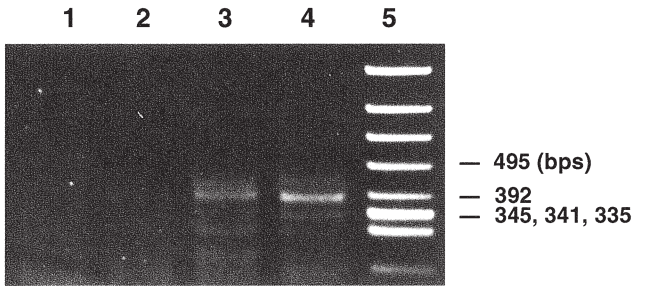

Fig. 2. mRNA expression of HMGI-C in astrocytoma and glioblastoma. Total RNA was extracted from glioblastoma and astrocytoma specimens, reverse transcribed into cDNA, and amplified by PCR reaction. A band corresponding to HMGI-C mRNA was detected at 380 bps in astrocytoma (lane 3 and 4), but not in glioblastoma (lane 1 and 2). Lane 5 is the marker.

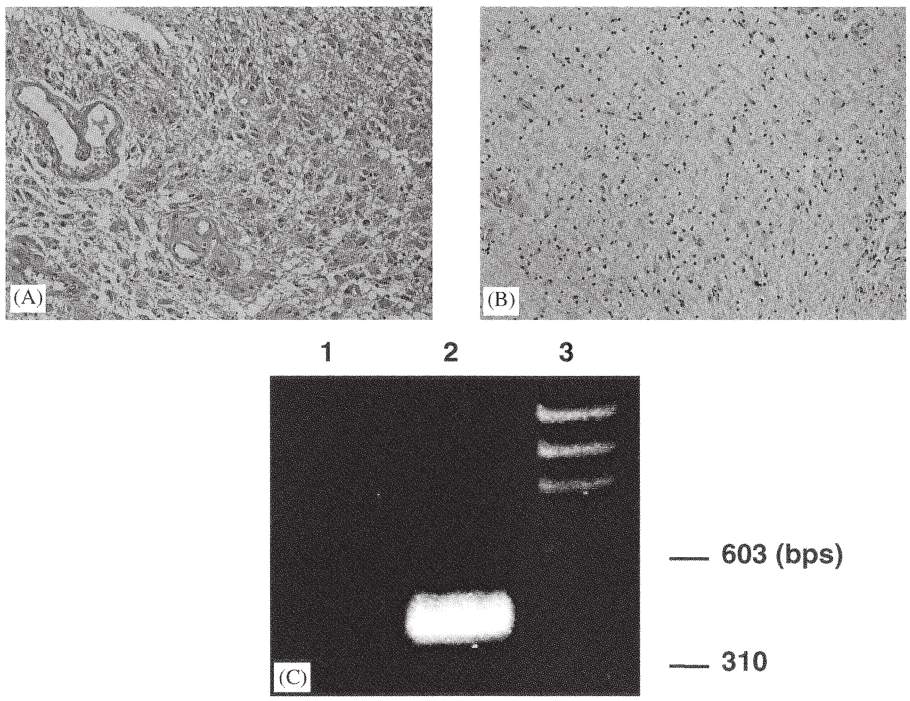

Fig. 3. mRNA expression of HMGI-C in astrocytoma and glioblastoma in one and the same patient from the different operation. Glioblastoma cells (A) from the second operation and astrocytoma cells (B) from the first operation stained with hematoxylin and eosin. RT-PCR (C) showed a band corresponding to HMGI-C in astrocytoma (lane 2), but not in glioblastoma (lane 1). Lane 3 is the marker.

Fusco's group also has demonstrated previously that HMGI proteins are necessary for the rat thyroid cells to undergo malignant transformation [3,31]. In their recent study, however, they reported that HMGI-C gene expression is not required for in vivo thyroid cell malignant transformation [25]. There is no convincing evidence that expression of HMGI-C protein is elevated in a fully malignant human cell line.

Hess proposed that the HMGI-C translocations are remarkable for their low risk of progressing to malignancy, because HMGI-C expression is common in benign mesenchymal tumors [12]. The present data of HMGI-C in glial tumors support this concept. HMGI protein may simultaneously activate the expression of differentiation-promoting and tumor suppressor genes preventing malignant transformation.

HMGI-C gene is located on chromosome 12q. Tallini et al. found that the expression of HMGI-C is a common occurrence in mesenchymal benign tumors, such as lipomas, pulmonary chondroid hamartomas, leiomyomas, and that it correlates with 12q chromosomal alterations [28,29]. This chromosomal change may result in rearrangement of HMGI-C gene and in deregulated expression of HMGI-C [2,7,8,29]. Alterations of chromosome 10 and 19 related to tumor suppressor genes expression have been reported for astrocytoma and glioblastoma [5,15]. For chromosome 12, frequent associations of breakage with deletion have been reported in malignant gliomas [22]. Further studies are necessary to investigate the activation mechanism of HMGI-C gene in astrocytoma and that of glioblastoma with the use of new modalities such as 5′-RACE and FISH.

Acknowledgements

This work was supported in part by the Project Research Grant of Kanazawa Medical University p 99-4 and Grant for Collaboration Research from Kanazawa Medical University C2003-3.

References

[1] H.R. Ashar, F. Schoenberg, A. Tkachenko, X. Zhou, J.A. Fletcher, S. Weremowicz, C.C. Morton, K. Chada, Disruption of the architectural factor HMGI-C: DNA-binding AT hook motifs fused in lipomas to distinct transcriptional regulatory domains, Cell 82 (1995) 57–65.

[2] S. Battista, V. Fidanza, M. Fedele, A.J. Klein-Szanto, E. Outwater, H. Brunner, M. Santoro, C.M. Croce, A. Fusco, The expression of a truncated HMGI-C gene induces gigantism associated with lipomatosis, Cancer Res. 59 (1999) 4793–4797.

[3] M.T. Berlingieri, G. Manfioletti, M. Santoro, A. Bandiera, R. Visconti, V. Giancotti, A. Fusco, Inhibition of HMGI-C protein synthesis suppresses retrovirally induced neoplastic transformation of rat thyroid cells, Mol. Cell Biol. 15 (1995) 1545–1553.

[4] G. Chiappetta, A. Bandiera, M.T. Berlingieri, R. Visconti, G. Manfioletti, S. Battista, F.J. Martinez-Tello, M. Santoro, V. Giancotti, A. Fusco, The expression of the high mobility group HMGI(Y) proteins correlates with the malignant phenotype of human thyroid neoplasias, Oncogene 10 (1995) 1307–1314.

[5] A. Von Deimling, J. Nagel, B. Bender, D. Lenartz, J. Schramm, D.N. Louis, O.D. Wiestler, Deletion mapping of chromosome 19 in human gliomas, Int. J. Cancer 57 (1994) 676–680.

[6] M. Fedele, A. Bandiera, G. Chiappetta, S. Battista, G. Viglietto, G. Manfioletti, A. Casamassimi, M. Sanantoro, V. Giancotti, A. Fusco, Human colorectal carcinomas express high levels of high mobility group HMGI(Y) proteins, Cancer Res. 56 (1996) 1896–1901.

[7] M. Fedele, M.T. Berlingieri, S. Scala, L. Chiariotti, G. Viglietto, V. Rippel, J. Bullerdiek, M. Santoro, A. Fusco, Truncated and chimeric HMGI-C genes induce neoplastic transformation of NIH3T3 murine fibroblasts, Oncogene 17 (1998) 413–418.

[8] J.M. Geurts, E.F. Schoenmakers, E. Roijer, G. Stenman, W.J. de Ven, Expression of reciprocal hybrid transcripts of HMGIC and FHIT in a pleomorphic adenoma of the parotid gland, Cancer Res. 57 (1997) 13–17.

[9] G. Giannini, L.D. Marcotullio, E. Ristori, M. Zani, M. Crescenzi, S. Scarpa, G. Piaggio, A. Vacca, F.A. Peverali, F. Diana, I. Screpanti, L. Frati, A. Gulino, HMGI(Y) and HMGI-C genes are expressed in neuroblastoma cell lines and tumors and affect retinoic acid responsiveness, Cancer Res. 59 (1999) 2484–2492.

[10] G. Goodwin, The high mobility group protein, HMGI-C, Int. J. Biochem. Cell Bio. 30 (1998) 761–766.

[11] R. Grosschedl, K. Giese, R.J. Pagel, HMG domain proteins: architectural elements in the assembly of nucleoprotein structures, Trends Genet. 10 (1994) 94–100.

[12] J.L. Hess, Chromosomal translocations in benign tumors: the HMGI proteins, Am. J. Clin. Pathol. 109 (1998) 251–261.

[13] S.M. Hsu, L. Raine, H. Fanger, Use of avidin-biotin-peroxidase cmplex (ABC) in immunoperoxidase techniques: a comparison between ABC and unlabeled antibody (PAP) procedures, J. Histochem. Cytochem. 29 (1981) 577–580.

[14] M.J. Justice, L.D. Siracusa, D.J. Gilbert, N. Heisterkamp, J. Groffen, K. Chada, C. Silan, N. Copeland, N.A. Jenkins, A genetic linkage map of mouse chromosome 10: localization of eighteen molecular markers using a single interspecific backcross, Genetics 125 (1990) 855–866.

[15] F.F. Lang, D.C. Miller, M. Koslow, E.W. Newcomb, Pathways leading to glioblastoma multiforme: a molecular analysis of genetic alterations in 65 astrocytic tumors, J. Neurosurg. 81 (1994) 427–436.

[16] C. Langelotz, P. Schmid, C. Jakob, U. Heiber, K.D. Wernecke, K. Possinger, O. Sezer, Expression of high-mobility-group-protein HMGI-C mRNA in the peripheral blood is an independent poor prognostic indicator for

survival in metastatic breast cancer, Br. J. Cancer 88 (2003) 1406–1410.
[17] G. Manfioletti, V. Giancotti, A. Bandiera, E. Buratti, P. Sautiera, P. Cary, C. Crane-Robinson, B. Coles, G.H. Goodwin, cDNA cloning of the HMGI-C phosphoprotein, a nuclear protein associated with neoplastic and undifferentiated phenotypes, Nucleic Acids Res. 19 (1991) 6793–6797.
[18] T. Nakamura, Y. Ueda, Y. Juan, S. Katsuda, H. Takahashi, E. Koh, Fas-mediated apoptosis in adriamycin-induced cardiomyopathy in rats. In vivo study, Circulation 102 (2000) 572–578.
[19] M. Nilbert, S. Heim, Uterine leiomyoma cytogenetics, Genes Chromosome Cancer 2 (1990) 3–13.
[20] K. Nomura, Special report of brain tumor registry of Japan, Neurol. Med. Chir. (Tokyo) 39 (1999) 59–107.
[21] U.A. Patel, A. Bandiera, G. Manfiioletti, V. Giancotti, K.Y. Chau, C. Crane-Robinson, Expression and cDNA cloning of human HMGI-C phosphoprotein, Biochem. Biophy. Res. Comm. 201 (1994) 63–70.
[22] G. Reifenberger, J. Reifenberger, K. Ichimura, V.P. Collins, Amplification at 12q13-14 in human malignant gliomas is frequently accompanied by loss of heterozygosity at loci proximal and distal to the amplification site, Cancer Res. 55 (1995) 731–734.
[23] P. Rogalla, K. Drechsler, B. Kazmierczak, V. Rippe, U. Bonk, J. Bullerdiek, Expression of HMGI-C, member of the high mobility group protein family, in a subset of breast cancers: relationship to histologic grade, Mol. Carcinog. 19 (1997) 153–156.
[24] J. Rosai, Surgical pathology, Ninth Ed., Mosby, New York, 2004.
[25] S. Scala, G. Portella, D. Vitagliano, C. Ledent, G. Chiappetta, V. Giancotti, J. Dumont, A. Fusco, HMGI-C gene expression is not required for in vivo thyroid cell transformation, Carcinogenesis 22 (2001) 251–256.
[26] O. Sezer, C. Langelotz, J.-U. Blohmer, P. Schmid, K. Akrivakis, K. Possinger, Detection of HMGI-C in the peripheral blood of breast cancer patients, Eur. J. Cancer 36 (2000) 1944–1948.
[27] G. Tallini, P. Cin Dal, K.J. Rhoden, G. Chiapetta, G. Manfioletti, V. Giancotti, A. Fusco, H. Van den Berghe, R. Sciot, Expression of HMGI-C and HMGI(Y) in ordinary lipoma and atypical lipomatous tumors: immunohistochemical reactivity correlates with karyotypic alterations, Am. J. Pathol. 151 (1997) 37–43.
[28] G. Tallini, P.D. Cin, HMGI(Y) and HMGI-C dysregulation: a common occurrence in human tumors, Adv. Anat. Pathol. 6 (1999) 237–246.
[29] G. Tallini, R. Vanni, G. Manfioletti, B. Kazmierczak, G. Faa, P. Pauwels, J. Bullerdiek, V. Giancotti, H. Van den Berghe, P. Dal Cin, HMGI-C and HMGI(Y) immunoreactivity correlates with cytogenetic abnormalities in lipomas, pulmonary chondroid hamartomas, endometrial polyps, and uterine leiomyomas and is compatible with rearrangement of the HMGI-C and HMGI(Y) genes, Lab. Invest. 80 (2000) 359–369.
[30] D. Thanos, T. Maniatis, The high mobility group protein HMGI(Y) is required for NF-kB-dependent virus induction of the human IFN-beta gene, Cell 71 (1992) 777–789.
[31] D. Vallone, S. Battista, G.M. Pierantoni, M. Fedele, L. Casalino, M. Santoro, G. Viglietto, A. Fusco, P. Verde, Neoplastic transformation of rat thyroid cells requires the junB and fra-1 gene induction which is dependent on the HMGI-C gene product, EMBO J. 16 (1997) 5310–5321.
[32] A. Wolffe, Architectural factors, Science 264 (1994) 1100–1101.
[33] X. Zhou, K.F. Benson, H.R. Ashar, K. Chada, Mutation responsible for the mouse pygmy phenotype in the developmentally regulated factor HMGI-C, Nature 376 (1995) 771–774.
[34] X. Zhou, K.F. Benson, K. Przybysz, J. Liu, Y. Hou, L. Cherath, K. Chada, Genomic structure and expression of the murine Hmgi-c gene, Nucleic Acids Res. 24 (1996) 4071–4077.
[35] X. Zouh, K. Chada, HMGI family proteins: Architectural transcription factors in mammalian development and cancer, Keio J. Med. 47 (1998) 73–77.

2003　平成15年度金沢医科大学共同研究成果報告書

平成17年12月発行

編　集　　研究推進評価特別委員会

発行所　　金沢医科大学出版局

石川県河北郡内灘町大学 1丁目1番地